Forschungszentrum Jülich
IBG-2: Institute for Bio- and Geosciences – Plant Sciences

Proline mediated drought tolerance of selected barley (*Hordeum vulgare* L.) introgression lines and characterization of *in vivo* spike development

Dissertation

zur Erlangung des Grades

Doktor der Agrarwissenschaften (Dr. agr.)

der Landwirtschaftlichen Fakultät

der Rheinischen Friedrich-Wilhelms-Universität Bonn

vorgelegt von:

FELIX FRIMPONG

aus

Bechem, Ghana

Bonn 2022

Angefertigt mit Genehmigung der Landwirtschaftlichen Fakultät der Universität Bonn

Referent: Prof. Dr. Uwe Rascher
Koreferent: Prof. Dr. Michael Frei
Fachnahes Mitglied: Prof. Dr. Gabriel Schaaf
Prüfungsvorsitz: Prof. Dr. Jens Léon
Tag der mündlichen Prüfung: 11. 08. 2022

SUMMARY

The potential yield of barley is likely to decrease in the future due to the prevalence of drought stress in many world regions. In our study, drought stress affected phenology, biomass and other growth traits, and seed yield-related traits. We observed that drought stress in barley causes alterations in critical physiological parameters, including leaf water status, net CO_2 assimilation rate, stomatal conductance, transpiration rate, water use efficiency, floret fertility, and seed filling. The drought in our study generally decreased our barley types' shoot and root growth by at least 70%.

Different barley introgressions and elite varieties of varying genetic makeup were investigated under well-watered and water stress treatments. The mechanistic responses of these lines to water stress, specifically, how they accumulate proline in their shoots and roots relating to stress tolerance, were analyzed and discussed. We found that a wild allele of *Pyrroline-5-carboxylate synthase1* (*P5cs1*) led to proline accumulation in the spikes and leaves of barley introgression lines, contributing to improved performance under reduced water availability. We found that water stress applied at the seedling stage induces increased shoot and root proline accumulation in a more homogenous near-isogenic barley line *NIL 143*, which harbours the wild allele at the *P5cs1* locus, and that this effect was associated with increased lateral root growth. We conclude that proline, functioning as an osmoprotectant, promotes drought tolerance mainly by helping maintain whole-plant water status. Our results suggest that proline accumulation at the reproductive stage contributes to the maintenance of grain formation under water shortage (Frimpong et al., 2021a). Increased shoot and root proline accumulation in the *NIL 143* barley was associated with increased lateral root growth. Future studies on the *P5cs1*-introgressions should focus on validating presented physiological variation in field conditions and the effect of elevated proline on grain quality traits. We recommend further studies to explore the variations in root-shoot growth observed for *NIL 143* in the field to test their performance under a water-limited environment. In addition, further studies will be required to explore how proline accumulation promotes barley root water uptake under water stress.

Furthermore, we explored the use of MRI to visualize barley grain development as a tool to detect internal florets, seed initiation and seed abortion, seed structures, spike architecture, and temporal growth of the grain on intact spikes of two-row spring barley genotypes. We found that MRI visualized differential genotypic seed initiation, seed growth and development, or abortion. MRI highlighted genotypic variations in a-synchronicity of floret initiation, seed set, and filling along the different spike axis. Also, MRI distinguished barley spike morphology and seed abortion as affected by water stress treatment compared to well-watered plants in our barley types. We recommend that future MRI studies of the spike could integrate algorithmic tools, and machine learning models to explore different functional seed traits and physiological behaviour beyond our photographing. Finally, using six multiplexed NMR sensors, we monitored and quantified non-destructively the dynamics of seed loading in terms of fresh weight, water and dry matter content during barley grain filling. Based on the acquired non-invasive data, peak seed filling rate, the diurnal rate of change in accumulation rate (fresh weight, dry matter content and water influx), and the variations in genotypes on live barley spikes were determined and discussed. We found that the grain yield of all our barley genotypes from our destructive harvest was consistent with the non-destructive multiplexed NMR sensor measurements.

KURZFASSUNG

Das Ertragspotenzial von Gerste wird in Zukunft wahrscheinlich abnehmen, da in vielen Regionen der Welt Trockenstress vorherrscht. In unserer Studie wirkte sich der Trockenstress auf die Phänologie, die Biomasse und andere Wachstumsmerkmale sowie auf Merkmale, die mit dem Samenertrag zusammenhängen, aus. Wir stellten fest, dass Trockenstress bei Gerste zu Veränderungen bei kritischen physiologischen Parametern führt, darunter der Wasserstatus der Blätter, die Netto-CO_2-Assimilationsrate, die stomatäre Leitfähigkeit, die Transpirationsrate, die Wassernutzungseffizienz, die Fruchtbarkeit der Blüten und die Samenfüllung. In unserer Studie verringerte die Trockenheit das Spross- und Wurzelwachstum unserer Gerstensorten generell um mindestens 70 %.

Verschiedene Gersten-Introgressionen und Elitesorten mit unterschiedlichem Erbgut wurden bei guter Bewässerung und unter Wasserstressbedingungen untersucht. Die mechanistischen Reaktionen dieser Linien auf Wasserstress, insbesondere die Art und Weise, wie sie Prolin in ihren Sprossen und Wurzeln im Zusammenhang mit der Stresstoleranz anreichern, wurden analysiert und diskutiert. Wir fanden heraus, dass ein Wild-Allel der *Pyrrolin-5-Carboxylat-Synthase1 (P5cs1)* zu einer Prolin-Akkumulation in den Ähren und Blättern der Gersten-Introgressionslinien führte, was zu einer verbesserten Leistung bei reduzierter Wasserverfügbarkeit beitrug. Wir fanden heraus, dass Wasserstress im Keimlingsstadium zu einer erhöhten Prolin-Akkumulation in Spross und Wurzel in einer homogeneren, fast isogenen Gerstenlinie *NIL 143* führt, die das Wild-Allel am *P5cs1*-Locus trägt, und dass dieser Effekt mit einem erhöhten Seitenwurzelwachstum verbunden ist. Wir kommen zu dem Schluss, dass Prolin als Osmoprotektivum die Trockentoleranz vor allem dadurch fördert, dass es zur Aufrechterhaltung des Wasserstatus der gesamten Pflanze beiträgt. Unsere Ergebnisse deuten darauf hin, dass die Prolin-Akkumulation im Reproduktionsstadium zur Aufrechterhaltung der Kornbildung bei Wasserknappheit beiträgt. Die erhöhte Prolin-Akkumulation in Spross und Wurzel der *NIL 143* Gerste war mit einem verstärkten Wachstum der Seitenwurzeln verbunden. Zukünftige Studien zu den *P5cs1*-Introgressionen sollten sich auf die Validierung der vorgestellten physiologischen Variationen unter Feldbedingungen und die Auswirkungen von erhöhtem Prolin auf die Kornqualitätsmerkmale konzentrieren. Wir empfehlen weitere Studien, um die bei *NIL 143* im Feld beobachteten Variationen im Wurzel-Spross -Wachstum zu erforschen und ihre Leistung in einer wasserarmen Umgebung zu testen. Darüber hinaus sind weitere Studien erforderlich, um zu untersuchen, wie die Prolin-Akkumulation die Wasseraufnahme der Gerstenwurzel unter Wasserstress fördert.

Darüber hinaus untersuchten wir den Einsatz von MRI zur Visualisierung der Gerstenkornentwicklung als Instrument zur Erkennung von inneren Blüten, Sameninitiierung und Samenabbruch, Samenstrukturen, Ährenarchitektur und zeitlichem Wachstum des Korns an intakten Ähren von zweizeiligen Sommergerstengenotypen. Wir fanden heraus, dass MRI unterschiedliche genotypische Sameninitiierung, Samenwachstum und -entwicklung oder Abbruch sichtbar macht. MRI zeigte genotypische Variationen in der Asynchronität von Blühbeginn, Samenansatz und Füllung entlang der verschiedenen Ährenachsen auf. Außerdem konnte mit MRI die Morphologie der Gerstenähre und den Samenabbruch im Vergleich zu gut bewässerten Pflanzen bei unseren Gerstentypen durch Wasserstress unterschieden werden. Wir empfehlen, dass künftige MRT-Studien der Ähre Algorithmen und machine learning einbeziehen, um verschiedene funktionelle Samenmerkmale und physiologisches Verhalten über unsere Bildgebung hinaus zu untersuchen. Schließlich haben wir mit sechs Multiplex-NMR-Sensoren die Dynamik der Saatgutbeladung in Bezug auf Frischgewicht, Wasser- und Trockenmassegehalt während der Gerstenkornfüllung nicht-destruktiv überwacht und quantifiziert. Auf der Grundlage der gewonnenen, nicht-invasiven Daten wurden die

Spitzenrate der Samenfüllung, die tägliche Änderungsrate der Akkumulationsrate (Frischgewicht, Trockensubstanzgehalt und Wasserzufluss) und die Variationen der Genotypen an lebenden Gerstenähren bestimmt und diskutiert. Wir stellten fest, dass der Kornertrag aller unserer Gerstengenotypen aus unserer destruktiven Ernte mit den nicht-destruktiven NMR-Multiplexsensormessungen übereinstimmte.

LIST OF ABBREVIATIONS

- A- CO_2 assimilation rate
- B-Booting
- CPMG- Carr-Purcell-Meiboom-Gill
- DAWS- Days after water stress
- DLI- Daily light integral
- DSI-Drought susceptibility index
- DW- Dry weight
- E- Transpiration rate
- ETR- Electron transport rate
- FID- Free induction decay
- FW- Fresh weight
- Fv/Fm – Quantum efficiency of Photosystem II
- FW- Fresh weight
- GF-Grain filling
- gsw- stomatal conductance
- HD-Heading
- iWUE – intrinsic water use efficiency
- J- Regeneration of ribulose-1, 5-biphosphate
- LCP- Light compensation point
- MRI- Magnetic resonance imaging
- NMR- Nuclear Magnetic Resonance
- NIL– Near isogenic line
- PPFD- Photosynthetic photon flux density
- *P5cs1- Pyrroline-5-carboxylate synthase1*
- *P5CS2- Pyrroline-5-carboxylate synthase2*
- *P5CR- Pyrroline-5-carboxylate reductase*
- *P5C- Pyrroline-5-carboxylate*
- *ProDH1-Proline dehydrogenase1*
- RFW – Root fresh weight
- RDW – Root dry weight
- RWC – % Relative leaf water content
- SFW – Shoot fresh weight
- SWC – Soil water content
- TPU- Triose phosphate utilisation
- Vcmax- Maximum rate of rubisco carboxylation activity
- VPDleaf- Vapor pressure deficit in the leaf
- WC- Water content
- WS-Water stress
- WW-Well-watered
- WUEplant–whole-plant water use efficiency
- Ψplant – Plant water potential
- Ψsoil – Soil water potential

ACKNOWLEDGMENTS

I want to express my sincere gratitude to my IBG-2 supervision committee, Dr. Fabio Fiorani, Dr. W. Carel Windt, and Dr. Dagmar van Dusschoten for the opportunity they gave to work under their supervision and direction throughout the doctoral research. I am grateful to Prof. Dr. Uwe Rascher, my Doktor Vater, for his immense motivation and support to make this Ph.D. a reality. I am also thankful to Prof. Dr. Michael Frei and PD. Dr. Ali Ahmad Naz, my advisors, helped conceptualized and share breeder's barley seeds for research work in Jülich and co-authored manuscripts for this thesis. I want to thank Prof. Dr. Ingar Janzik of IBG-2, PhD coordination, who shared her molecular laboratory for proline analysis and also supported in diverse ways my welfare as a doctoral researcher at IBG-2. I would also like to thank Dr. Daniel Pflugfelder for assisting me in analyzing the MRI of the barley spikes and the immense personal motivation he offered whenever I reached out to him.

I want to thank Dr. Robert Koller and the Enabling Technologies / JPPC groups, and the rest of the team to share facilities (laboratories, workshop, and MRI) and support my work at IBG-2. Special appreciation goes to Johannes Kochs of IBG-2 for various electrical support during the experiments. My sincere gratitude goes to Dr. Abdulai Issaka (Uni. Göttingen, Germany) and Dr. Yoshiaki Ueda (JICA, Japan) for reading and advising during the manuscript write up. My sincere applause goes to Michael Anokye (Uni. TUM/HHU), who conducted his master thesis on the roots at the seedlings stage using the isogenic line as part of this project for his hard work and significant contribution to this doctoral research. Thanks to Kelvin Acebron, who supported the gas exchange photosynthetic measurements at the greenhouse of IBG-2.

I would also like to thank my colleagues Dr. Fang He, Norman Wilke, Lu Gao, Phillip Norf, Yannick Muellers, Archis Pandya, Dr. Eric Owusu Danquah, Khadija B., Xinyu G., Simone Junker and Dr. Shree Pariyar for their immense support during the Ph.D. work at IBG-2, Jülich. To Silvia Braun, Birgit Bleise, Anna Galinski, Jonas Lentz, Esther Breuer, Andrea Neuwohner, Sabine Preiskowski, Daniel Kingsley Cudjoe, Beate Uhlig, and Katharina Wolter-Heinen, I say thank you for the technical support during the greenhouse rhizotrons experiment and proline lab analysis, I say vielen Dank. Finally, a remarkable depth of gratitude goes to Mr Francis Wilson Owusu and his entire family, my parents (Mrs Salomey Opoku and Mr Nsiah Frimpong), brothers and sisters; Bright, Theophilus, Louisa, Gifty and finally to my wife and children; Esther, Adelyn, Ava, Jeremiah, for their love and encouragement throughout my studies. This work would not have been possible without these beautiful people. I hope our paths cross again in this life or the next. Yet, I am not afraid. You have taught me well with your intelligence, care, courage and have brightened my world. My heart is filled with hope.

To God be the Glory.
Thank you all.

TABLE OF CONTENT

LIST OF FIGURES

LIST OF TABLES

LIST OF APPENDICES

This PhD thesis consists of seven (7) chapters. It starts with a general introduction, a description of the methods used, four experimental studies (Chapters 3 to 6), and finally, a general discussion. Each experimental study focuses on specific aims and objectives stated under sections 1.7 and 1.8. These four studies form the most important parts of this thesis. They have been published as peer-reviewed journal articles (Frimpong et al., 2021a: Frontiers in plant sci.: doi.org/10.3389/fpls.2021.633448, Frimpong et al., 2021b: Plants: https://doi.org/10.3390/plants10102177), or are in preparation to be submitted for publication. My contributions to each paper are specified and listed under the publications section of this thesis.

CHAPTER 1

1. INTRODUCTION

Humanity faces a critical moment, as it will be required to feed an ever-growing population that is estimated to reach more than 9.6 billion by 2050 in a world of drought-prone environments and dwindling arable land resources (FAO, 2017). In most regions of the world, yield variations due to drought pose significant anomalies, affecting the food market and security. For example, in 2018, drought detrimentally affected productivity and functioning in European agriculture (Ahmed et al., 2021). The 2003 widespread drought, as reported by Ciais et al. (2005), significantly reduced European gross primary production by about 20%. For cereal crops such as maize, rice, barley, or wheat, a 20-50% yield loss due to drought has been projected (Daryanto et al., 2016; Fahad et al., 2017). Since 1976, unprecedented large-scale drought was recorded in 2018 across the whole soil column of Germany according to statistics from the drought monitor (www.ufz.de), indicating dwindling water resources for crop production (Figure 1.1).

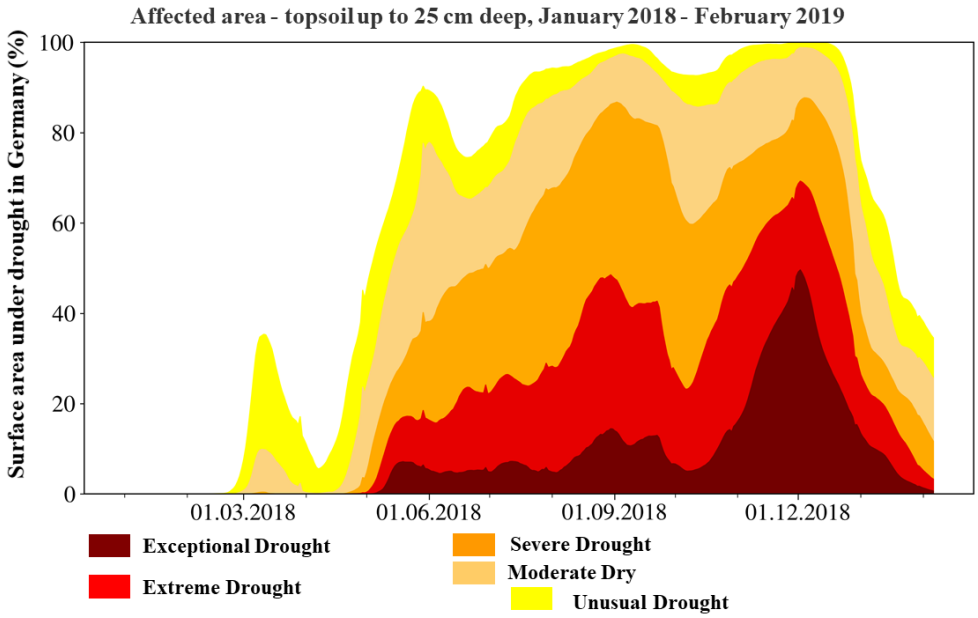

Figure 1.1 Large scale drought recorded for Germany in 2018 showing dwindling water resources for crop production. The figure was retrieved from www.ufz.de (9th September 2021, 12.00 CET).

It is estimated that droughts have caused 1820 million tons of cereal yield loss during the past four decades globally (Leng & Hall, 2019). One approach to decrease this loss of yield is to breed for crop varieties that can adjust their osmotic potential to tolerate drought with a reduced final yield penalty. The development of cultivars with drought tolerance is a daunting task because complex plant genetics and metabolic pathways are involved in plants response to water stress. This may include differential expression of alternative alleles of major genes in quantitative trait loci (QTL) under stress and non-stress conditions (Kebede et al., 2019). The identification of genes that may lead to drought tolerance is extremely important and can be achieved by genotyping and phenotyping progenies including from wild introgressions (Honsdorf et al., 2014). Drought-tolerant plants often show less reduction in water content, improved membrane stability, and maintain higher photosynthetic activity when exposed to drought (Sallam et al., 2019). The tolerant plants may also accumulate soluble sugars, proline, amino acids, chlorophyll content, and display increased enzymatic and non-enzymatic antioxidant activities (Abid et al., 2016). In barley genotypes having a high degree of drought tolerance were produced through crosses from promising drought-tolerant genotypes and selecting among their progeny (Sallam et al., 2019). Therefore, phenotyping, physiological characterization, and analysis of superior lines under controlled and field conditions under water stress scenarios are necessary to select and potentially release cereal crop varieties, including barley.

1.1 Ancestry, cultivation, use, and economic value of barley

Barley (*Hordeum vulgare* L.) is an old crop, originating from the Middle East (Fertile Crescent) more than ten thousand years ago, as a descendant from its wild relative *Hordeum spontaneum* C. Koch. (Badr et al., 2000; Grando et al., 2005). Morphologically, cultivated barley is closely related to the wild type but has broader leaves, shorter stems and awns, tough ear rachis, shorter and thicker spikes, and bigger seed size (Badr et al., 2000). Depending on the use or location, a specific barley type may be chosen. There are three growth habits in barley, i.e. winter, alternative/facultative and spring types (Berkeley International, 2021). It is known that many genes control barley growth habits. In terms of crop physiology, vernalization sensitivity, photoperiodism, and cold tolerance define barley growth habits (Muñoz-Amatriaín et al., 2020). Winter and alternate barley types are more cold-tolerant than the spring types. Concerning the inflorescence, it can be classified in a six or two-rowed ear type (Verstegen et al., 2014). Two-row barley has 2-rows of seed on each spike and six-row barley has 6-rows of seed on each spike.

Botanically speaking, a 2-row has one fertile floret per rachis node, and a 6-row has three fertile florets per rachis node (Berkeley International, 2021).

Cultivated barley is the fourth most important cereal in terms of production and consumption, with more than 150 million tons, 55 million ha, and 2.4 t/ha yield in the world since 2007 (Kelly, 2019). Presently, barley is cultivated on 48 million ha in moderate, continental, and subtropical environmental conditions (Verstegen et al., 2014). The Russian Federation, Germany, France, UK, Spain, Turkey, and Ukraine are among the ten leading barley countries in Europe and Eurasia (Taner et al., 2004). Australia, the USA, and Canada are also among the list of major barley producers (Taner et al., 2004). In Europe, around 12 million ha of barley is cultivated annually (Lovarelli et al., 2020). However, its production is detrimentally affected by seasonal climate variability, including erratic rainfall (too much or too little precipitation) and strong winds. Presently, Germany has the highest yield level (6.4 t/ha and 5.9 t/ha), while the Russian Federation and Ukraine have the lowest (1.4t/ha and 1.8 t/ha http://www.fao.org/worldfoodsituation/csdb/en/). In terms of applications, grain barley can be used as food in stews, soups, and bread. The whole barley plant (leaf, stalk, grains, and root) may be harvested for hay or as fodder to feed animals (Kelly, 2019). In industry, barley is used as a source of malt for alcoholic beverages such as spirits, beer, but also in products such as spices, raw organic food, natural collagen boosters (Zhou, 2010).

1.2 Above and below-ground traits of plants under drought

Drought has been defined in many ways. The most common definition refers to drought as an extended period (a season, a year, or several years) of low water availability compared to the long term mean, leading to water shortage for some activity, group, or environmental sector (Blum, 2005; Kebede et al., 2019). In simple terms, drought may mean water is unavailable or available in insufficient amounts. Drought negatively affects plant developmental processes, such as growth, nutrient and water relations, photosynthesis, assimilate partitioning, and ultimately yield (Sallam et al., 2019; Avramova et al., 2016).

Several phenotypic responses can be distinguished in above-ground and below-ground plant traits. However, interactions between the root and shoot growth were also observed. For instance, drought significantly reduced wheat or barley shoot height, biomass, root length, root surface area, root volume, and shoot/root dry weight, but it did not significantly affect root/shoot ratio and water use efficiency (Becker et al., 2016; Mohamed et al., 2014; Rani & Chaudhary,

2018). Lozano et al. (2020) showed that grasses exhibit decreased shoot mass, specific leaf area, and leaf number under drought relative to the control treatment. On above-ground plant traits, Abid et al. (2016) and Ugarte et al. (2007) reported progressive decline in the leaf water potential, membrane stability index, photosynthesis, chlorophyll fluorescence, the efficiency of photosystem II. Accelerated grain filling rate with shortened grain filling duration at post-anthesis and reduced grain yields during drought stress imposed at the vegetative stage was reported for selected wheat cultivars (Rekowski et al., 2021). Drought stress imposed at the beginning of the reproductive stage can disrupt floral meristem differentiation and reduce the number of spikelets formed, and thus, the number of grains per spike (Honsdorf et al., 2017). The gametogenesis process of florets within each initiated spikelet appears to be sensitive to drought stress and can lead to abortion and severely decreased seed set (Dolferus et al., 2011).

Generally, to elucidate plant responses to drought events at seed set and filling stages, four key physiological factors must be considered; (a) daytime flowering to escape the stress; (b) photosynthetic health of the crop; (c) source-sink relations of water-soluble carbohydrates and (d) seasonal yield-related parameters and estimates (Hein et al., 2021). During grain filling of rice and wheat, drought scenarios led to 28% and 29% yield reductions, respectively, as was concluded on the basis of a meta-analysis of more than 100 independent experiments (Zhang et al., 2018). A similar account was given by Sehgal et al. (2018), demonstrating that drought and heat stress at the grain filling stage of cereals reproductive development is the most susceptible growth period with substantial yield penalties. These findings emphasize that the effect of heat and drought scenarios at the reproductive developmental period on cereals need to be adequately understood, researched and new solutions provided to accelerate the breeding of stress-tolerant cereal genotypes.

Root responses to drought are even more complex than the shoot responses and may differ strongly among species (Lozano et al., 2020). In barley roots perform vital roles for adaptation and productivity under drought, even though their trait-specific functions may be poorly understood (Oyiga et al., 2020). To guide breeding efforts, we need to understand the phenotypic responses in root traits better. For example, drought induces considerable alterations in the nodal root traits of spring barley (Jia et al., 2019). Drought reduced the growth of barley nodal roots and total root convex hull area, whereas the tiller nodal roots and root xylem density increased, and suberization of large cortical aerenchyma cells was observed to take place (Oyiga et al., 2020).

Features of an optimal maize root ideotype for water and nitrogen acquisition under drought have been suggested (Lynch, 2013). Some of the features suggested included bigger primary root with few but long laterals (to promote tolerance in cold soil temperatures), having more seminal roots with shallow growth angles, smaller root diameter and possession of several but longer lateral roots and hairs that might improve heat or water stress tolerance (Lynch, 2013). In a broader sense, these specific features of an ideotype may contribute to rooting depth, which enables the plant to reach or tap water available from deeper soil layers upon abiotic stress (Maeght et al., 2013). Large cortical cell size might also improve drought tolerance in maize through a decrease in the metabolic cost for water uptake from deeper soil layers, promoting growth and yield (Chimungu et al., 2014). It was suggested by Chimungu et al. (2014) that cortical cell size in maize breeding should be targeted in further research due to the large genetic diversity and variations that exist and their potential relevance for drought tolerance. Experiment-wise, the intriguing question begging for answers is whether barley roots and other cereals can also be optimized following these ideotypes.

Therefore, studies into barley below-ground root traits suggested fine root diameter, specific root length, specific root area, root angle, and root length density as valuable indicators of drought-tolerant cultivars (Wasaya et al., 2018). Additional traits include a comparatively higher root hair density, root volume and an increased number of nodal roots per tiller. These traits may increase the ability to access water present in deep soil horizons thereby improving the plant acquisition of water under water scarcity (Comas et al., 2013; Naz et al., 2014).

1.3 Proline-mediated drought tolerance during osmotic stress

A change in the concentrations of solutes in and around plant cells due to water stress, salinity, etc., leads to osmotic stress (Feng et al., 2016). Plants have evolved various physical, chemical, cellular, and molecular mechanisms to tolerate osmotic stress, including osmotic stress resulting from drought. Higher plants can achieve drought resistance by means of four basic mechanisms: (i) avoidance, (ii) tolerance, (iii) escape, and (iv) recovery (Fang & Xiong, 2015). A plant can be drought tolerant when it can maintain its physiological activity through regulating and adjusting networks of genes and various metabolic pathways to minimize damage (Shanmugavadivel et al., 2019). Osmotic adjustment or the accumulation of compatible solutes have been extensively reported to have a vital role in plant adaptation during reduced water availability through cell turgor maintenance, stability of membrane integrity and the protection of

cellular functions by certain solutes such as glycine betaine, mannitol, sugars and others (Blum, 2017). Generally, a plant's drought responses can be characterized into two types of physiological processes, i.e., Abscisic acid (ABA) -dependent or ABA -independent pathways (Nakashima et al., 2009). Proline is one of many compatible solutes linked to the ABA-dependent pathway of plants responses to drought (Takahashi et al., 2020).

Specifically, proline is a compatible solute discovered decades ago, which accumulates in various plants experiencing water limitations and other stresses (Heuer, 2016). Proline is one of the essential amino acids involved in signalling, homeostasis and defence of plants response to drought, very low and high temperatures, heavy metal contamination of soils, and salinity stress (Kavi Kishor & Sreenivasulu, 2014). Under these conditions, it has been linked to improved growth, productivity and anatomy of several crops' species (Hayat et al., 2012; Rady et al., 2016). Proline has been shown to allow plants to increase cellular osmolarity during water shortage (Verslues & Sharma, 2010). Likewise, proline scavenges for hydroxyl radicals and reduce cell acidity levels or protect large molecules from denaturation as a compatible solute (Lee et al., 2009).

Metabolite profiling studies showed accumulation of proline and hexoses in the flag leaves of drought-adapted Mediterranean and German elite barley lines three days after stress establishment compared to control. Proline synthesis, either a primary or secondary response to stress, is linked via a signal transduction pathway to osmosensing or changes in metabolism as a plant defense mechanism (Delauney & Verma, 1993; Templer et al., 2017; Trovato et al., 2019). Drought was reported to significantly increase leaf proline content in all wheat cultivars in a panel of ten (Mickky et al., 2019). However, this accumulation was more pronounced in the drought-tolerant cultivars than in their drought-sensitive relatives. An ancestral allele *pyrroline-5-carboxylate synthase 1* (*P5CS1*) promoted proline accumulation and drought adaptation in cultivated barley (Muzammil et al., 2018). The *P5CS1* (*AT2G39800*) gene expression pattern showed that proline synthesis is highly induced in shoot tissues that are photosynthetically active at a low water potential (Sharma et al., 2011). *Pyrroline-5-carboxylate synthetase* (*P5CS*) is an intermediate product for proline metabolism and catabolism in higher plants (Bhaskara et al., 2015; Muzammil et al., 2018). Recent evidence indicates that proline-*P5C* gene expression is tightly regulated in plants, especially during pathogen infection and exposure to abiotic stress (Bhaskara et al., 2015; Qamar et al., 2015). Efforts to enhance osmo-tolerance by increasing proline should

be focused on this gene (Delauney & Verma, 1993) because the encoded enzyme it is arguably the most limiting step in proline biosynthesis.

1.4 Pathways, signalling and transport of proline

The proline biosynthetic pathway was discovered more than 40 years ago in *Escherichia coli* (Hayat et al., 2012). In plants, proline is confined to the chloroplast, cytosol and other cellular compartments where it serves to protect the cells upon injury (Meena et al., 2019). Proline is synthesized from either glutamine or ornithine (Chiang & Dandekar, 1995). The glutamine pathway is mainly engaged under osmotic stress conditions such as drought, salinity or cold stress (Figure 1.2a, Deng et al., 2013; Szabados & Savouré, 2010). Plant proline synthesis begins with glutamate as the precursor reduced to glutamate-semialdehyde (*GSA*) by the action of *pyrroline-5-carboxylate synthetase* (*P5CS*) enzyme and an intermediate form *pyrroline-5-carboxylate* (*P5C*, Szabados & Savouré, 2010). Synthesis continues where *P5C* reductase (*P5CR*) further reduces the *P5C* intermediate to proline (Szabados & Savouré, 2010). In most plant species, two genes encode *P5CS* and only one for *P5CR* (Szabados & Savouré, 2010). During catabolism (Figure 1.2a), proline is converted back to glutamate in the mitochondria by the sequential action of proline dehydrogenase (*PDH*) and *P5C* dehydrogenase (*P5CDH*, Furlan et al., 2020). In Arabidopsis and tobacco (Nicotiana tabacum) two genes have been shown to encode *PDH*, whereas a single gene encodes *P5CDH* (Furlan et al., 2020). *PDH* transcription is activated by rehydration but repressed by dehydration, preventing proline degradation during exposure to abiotic stress (Hayat et al., 2012).

1.5 Functions of proline in plants under drought

Proline accumulation is one of the most significant metabolic responses to water shortage (Sharma et al., 2011). The fact that proline is strongly compartmentalized implies that extensive intracellular proline transport occurs between the cytosol, chloroplasts and mitochondria (Figure 1.2a, Sharma et al., 2011; Verslues & Sharma, 2010). Several studies have shown that proline catabolism occurs in the mitochondria, whereas proline synthesis is cytoplasmic (Figure 1.2a, Kishor et al., 2014; Verslues & Sharp, 1999). Physiological data suggest that proline uptake into mitochondria is an active process, indicating the existence of specific amino acid transporters (Szabados & Savouré, 2010). Under low water potential, proline acts as an osmolyte and osmoprotectant, helping plants maintain cell turgor (Figure 1.2b, Trovato et al., 2019). In addition, proline protects protein integrity, redox buffering and energy transfer (Verslues & Sharma, 2010)

and improves the plant's antioxidant system defense (Rady et al., 2016). Verslues & Sharp (1999) reported that proline concentration increased considerably in the root tips of maize (*Zea mays* L.) at low water potential, largely due to an increased net rate of proline deposition. Lee et al. (2009a) highlighted that increased proline accumulation/transport decreases water potential in cells of the root tip. These authors further indicated that proline is transported from the leaf chloroplasts (source) to the roots (sink) through the phloem, as illustrated in Figure 1.2a.

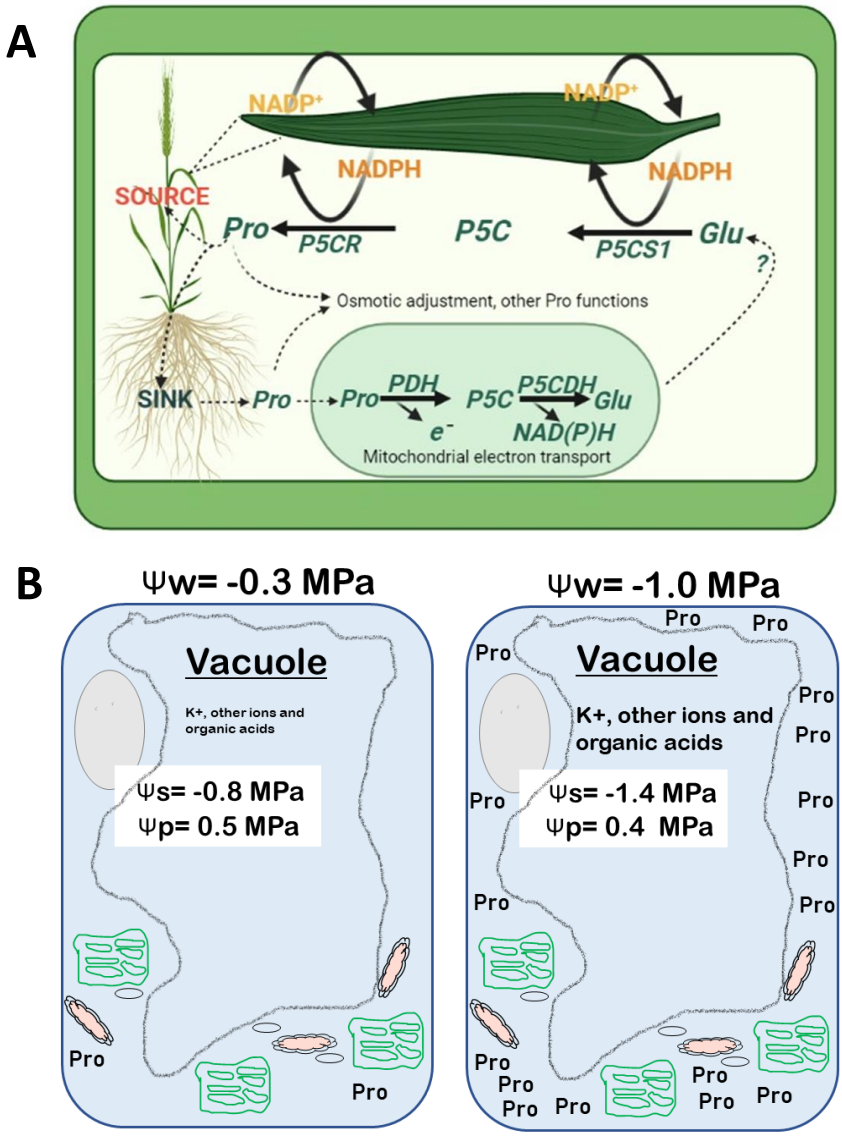

Figure 1.2 Diagrams of proline biosynthetic pathway, signaling and transport (A), adapted from Sharma et al. (2011). Proline accumulation in the plant cell during osmotic stress in higher plants is shown in panel (B), adapted from Szabados & Savouré (2010). In panel (A), proline is transported to the roots and shoots of the plant after production in photosynthetic source structures. The process results in by-products of energy in the form of NADPH. Panel (B) depicts two plant cells in a stressed (right, Ψw=-1MPa) scenario and unstressed (left, Ψw=-0.3MPa) condition. In the unstressed cell (left), proline production is produced only for general housekeeping functions. On the other hand, in the stressed cell (right), a cascade of proline is shown in the cytosol and subcellular structures to maintain osmolarity and turgor. The green structures are chloroplast, mitochondria are coloured in pink, and the peroxisomes are the small grey oval shapes. The two figures were created with BioRender.com but adapted from their original sources above. [Abbreviations: *Pro: proline, Glu: glutamate, P5C: pyrroline-5-carboxylate synthase, P5CS1: pyrroline-5-carboxylate synthase 1, P5CSR: pyrroline-5-carboxylate synthase reductase, PDH: proline dehydrogenase, P5CDH: pyrroline-5-carboxylate dehydrogenase, Ψw: water potential, Ψs: osmotic potential, Ψp: turgor potential, K^+: potassium ions, NADPH: reduced form of nicotinamide adenine dinucleotide phosphate, $NADP^+$: nicotinamide adenine dinucleotide phosphate ions, e^-: electrons*].

1.6 Imaging cereal seed set and filling under drought

Diagnosing and interpreting how cereals develop and interact with their surroundings would demand tools able to dissect their internal spatial and temporal resolution (Borisjuk et al., 2012). A variety of new high-throughput, non-destructive imaging techniques are now available to assess plant performance and screen relevant plant traits under abiotic stress studies (Munns et al., 2010). Originally, most of these imaging tools, magnetic resonance imaging (MRI), X-ray microcomputed tomography-μCT, etc. were developed for medical diagnostics as non-invasive imaging techniques based on differential signal attenuation due to material composition and density (X-ray tomography), or in the case of MRI, differences in signal strength and tissue-dependent signal relaxation behaviour (Hughes et al., 2019). They can provide an accurate two-dimensional (2D) and three-dimensional (3D) representation and quantification of internal structures non-invasively or non-destructively. In the plant sciences, MRI has been used for a variety of purposes as well. It has been used to visualize root growth development, caryopsis development, monitored water and dry matter content in leaves and grains of cereals in different environments (Windt et al., 2021). Such approaches aid the *in vivo* characterization of functional plant traits on live plants and enable phenotyping of individual plants and plant organs with high temporal resolution (Rascher et al., 2011).

For example, non-destructive MRI successfully evaluated drought induced rust in potatoes (Hajjar et al., 2021), estimated specific internal wheat and barley traits (Borisjuk et al., 2012), revealed postharvest browning disease in pear (Hernández-Sánchez et al., 2007), evaluated barley pericarp growth dynamics as mediated by hormones (Pielot et al., 2015), easily identified seedless vs seeds of the citrus fruit, Mandarins (Hernández-Sánchez et al., 2006). In order to elucidate water stress effect on seed abortion and filling early in the reproductive development phase (before grain maturation of barley, Frimpong et al. (2021a), this thesis) used MRI to scan immature spikes at the BBCH- scale, 83, i.e., at the soft milky dough stage. Recently, Hughes et al., 2017; Strange et al., 2015 showed that using μCT scanning of ripe wheat spikes, combined with an image analysis pipeline (Hughes et al., 2019), can accurately extract and measure grain and spike parameters such as length, width, depth, volume and other information that, combined, can provide a complete description of grain size and shape variations.

1.7 Study aims

1. Few studies have so far addressed the role of proline in the reproductive organs under water stress. In this study, we addressed this knowledge gap by measuring spike and leaf proline content, changes in photosynthetic performance and assessed barley seed abortion and grain filling under water stress using Magnetic Resonance Imaging (MRI) at the reproductive stages (***Chapter 3*** of this thesis; Frimpong et al. 2021a). In this chapter, we tested the hypothesis that drought-induced proline accumulation in the spikes of barley genotypes harbouring the wild variant of *P5cs1* improves drought tolerance as measured by seed number and final yield in a greenhouse experiment.

2. Drought inducible proline accumulation in the root apex contributes about 50% of the osmotic adjustment in this tissue (Sharp et al., 1990; Voetberg & Sharp, 1991). Many researchers estimate the plant tissue water status on the basis of relative water content. Higher relative water content under water deficit typically indicates osmotic adjustment in the stressed tissue (Shrestha, 2020). We indirectly tested the osmotic adjustment capacity of the high proline accumulating isogenic line, *NIL-143*, through RWC measurements. Shrestha, 2020 demonstrated that the recovery rate in the progeny *NIL-143* was superior to the parental line, *Scarlett*. We investigated whether proline accumulation contributes to barley root growth under water stress **(*Chapter 4*)**.

3. Drought can cause a large percentage of seeds to abort during early spike development, strongly reducing yield. Monitoring the number of florets or seeds that abort or develop under the influence of abiotic stresses thus is of great interest but can be laborious and time-intensive because of the need to dissect large numbers of spikes and florets. In this study, we tested if it was possible to use non-invasive MRI to rapidly visualize seed development or abortion and apply this methodology to phenotyping studies of cereals subjected to drought stress. **(*Chapter 5*)**.

4. Seed loading of photosynthates into the developing ear is thought to be strongly affected by abiotic factors such as drought and heat. The temporal and diurnal dynamics of grain filling, particularly as it is affected by abiotic stress factors, therefore would be interesting to characterize in an objective fashion. A recently developed mobile NMR sensor has made it possible to study the diurnal dynamics of barley grain filling non-destructively (Windt et

al., 2021). In this study, we test how an improved, multiplexed version of the NMR sensor can be used to characterize seed filling in barley. Windt et al. (2021) observed strong diurnal fluctuations in seed loading in wheat grain filling and observed that most dry matter was deposited in wheat grains during the night. We tested if the night-time deposition of solids could be observed during barley grain development and if variations in the diurnal loading pattern existed between the different genotypes. Previous studies on rice, wheat, and barley grain filling used destructive methods to compute the mean grain filling rate, peak grain filling, and grain filling duration (Briarty et al., 1979; Emes et al., 2003; ZHANG et al., 2021; Zhong et al., 2003). In this work, we established how the same traits of peak influx, peak filling rate, and grain filling rate could be obtained, from seed initiation until the fully ripe stage, measuring spikes of a limited number of individuals of two-row spring barley elite varieties continuously and non-destructively. (***Chapter 6***).

1.8 Study objectives

1. Characterize a panel of contrasting elite genotypes and *P5cs1*-introgression lines and monitor morpho-physiological responses after water withdrawal during reproductive development.

2. Characterize root placement (2D root positioning within the substrate profile) under water-stressed and well-watered control conditions in barley genotypes, including the breeding line which harbours the wild allele at the *P5cs1* locus originating from *H. spontaneum*. Assess whether proline accumulation differs between roots and the shoots of the contrasting barley genotypes and if that leads to changes in net CO_2 assimilation rate, transpiration rate, plant water potential, leaf chlorophyll content, root and shoot morphology.

3. Determine the extent to which MRI can be used to image reproductive development of intact spikes rapidly. Specifically, analyze MRI scans of floral developmental stages of whole spikes of barley to reveal the temporal growth of seed development.

4. Determine how a multiplexed NMR sensor can be utilized to quantify the rate of change (peak influx, fresh weight, and dry matter content) of barley grain filling non-invasively, simultaneously on a panel of up to six live spikes of different two-row genotypes. Further, determine and recommend appropriate metrics for future drought stress studies based on the characterization of barley spikes.

CHAPTER 2

This chapter is adapted from Frimpong et al., 2021a & b of this thesis with modifications.

2 METHODS

2.1 Plant cultivation and root phenotyping

All our experiments were carried out in the greenhouse or growth chamber at the Institute of Bio and Geosciences, IBG-2, Plant Sciences, Forschungszentrum Jülich, Germany; 50°55'17.36 "N, 6°21'45.61 "E (Figure 2.1A). Plants were cultivated under long-day conditions (16h/8h day/night). Extra illumination (SON-T AGRO 400, Philips, Amsterdam, The Netherlands) was automatically supplied when the ambient light intensity inside the greenhouse was <400 µmol m^{-2} s^{-1}, between 06:00 and 22:00 h. Day/night minimum and maximum temperature of the greenhouse was ~ 20 ± 4 and 30 ± 4 °C during the day and ~ 16 ± 2 and 20 ± 2 °C during the night, respectively. Three tablets of 5 g Osmocote Exact slow-release fertilizer (14-8-11; N - P_2O_5 - K_2O + 2 MgO + trace elements) were applied per plant in three aliquots starting two weeks after transplanting. Pests and diseases were controlled chemically according to established greenhouse practices. Water was administered with the help of an automated drip irrigation setup at the greenhouse (Netafilm, Adelaide, Australia), watering the pots twice daily. Rhizoboxes (Figure 2.2C) outer dimensions: 60 × 30 × 3 cm, were filled with soil and used for root phenotyping later presented in this thesis.

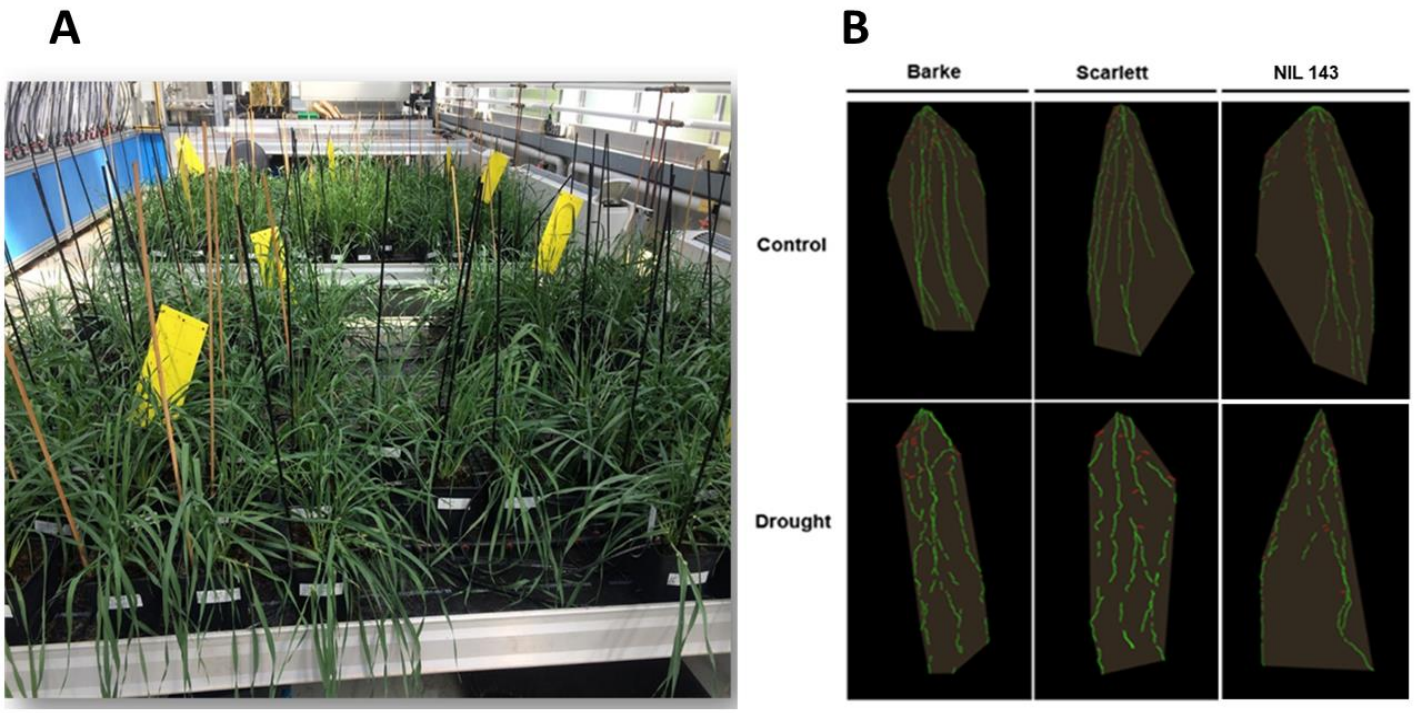

Figure 2.1 Potted barley plants growing in the greenhouse (A) and images of seedling roots drawn by means of PaintRhizo (B). Root drawings of seedlings of barley genotypes *Barke*, *Scarlett*, *NIL 143* were acquired after the rhizoboxes experiment, 17 days after sowing under drought or control conditions.

A self-developed PaintRhizo software (version 2.0.6, copyright: IBG-2), previously described by (Nagel et al., 2009), was used to draw the roots (Figure 2.1B) after imaging in a mobile dark box imaging station fitted with a Canon camera EOS 70D (Canon Inc. China, Figure 2.2 A and B).

Figure 2.2 Mobile imaging box and rhizoboxes at the IBG-2 Plant sciences greenhouse, Forschungszentrum Jülich GmbH, Germany. In panel (A) the black mobile imaging box is shown; in panel (B) the camera that was fitted in it for taking pictures of the rhizoboxes. In panel (C) rhizoboxes are shown, sets of 6 arranged in a big blue box inclined at 45˚ angle to force rooting towards the transparent viewing window. Note that the marked-white area in panel (A) indicates the side of the rhizoboxes which was placed for imaging from a transparent plate oriented towards the camera.

2.2 Proline determination

Fresh tissue plant samples were quickly placed in small labelled rubber vials, closed and submerged in liquid nitrogen, and later stored in a -80°C freezer for later use. The stored leaf, stem, and root tissue samples were manually crushed into a fine powder using a ceramic mortar and pestle in liquid nitrogen. The extraction of proline from each tissue was performed by adopting the colourimetric proline determination method described by Bates and Waldren 1973 with modifications. Acid-ninhydrin was first prepared by warming 2.5 g ninhydrin in 60 mL glacial acetic acid and 40 mL 6 M phosphoric acid, with vigorous agitation using a magnetic stirrer until it was completely dissolved. The solution was covered with aluminium foil to avoid exposure to light and stored in a 4ºC refrigerator for 24 hours before use. 100 mg of the crushed tissue samples were then weighed into chilled 2 mL Eppendorf tubes and homogenized in 1.5 mL of 3 % sulfosalicylic acid by vortexing. The mixture was centrifuged at 12000 rpm for 10 mins. After centrifugation, 500 µL of sample extract (supernatant) was mixed with 500 µl of glacial acetic acid and 500 µL of ninhydrin reagent in glass tubes (fitted with lids). The mixture was then vigorously vortexed, incubated at 95-100ºC for 45-60 minutes in an HB-1000 Hybridizer oven (UVP, Inc., Cambridge, UK). The reaction was terminated quickly with ice. The reaction mixture was extracted with 1.5 mL toluene, mixed vigorously by vortexing. The solution was left at room temperature for 30 mins to settle until the two phases separated. 100 µL of the chromophore (upper phase) was then carefully pipetted into 96 well plates and read with a microplate reader (Synergy™ 2 Multi-Mode, BioTek, Winooski, Vermont, USA). A dark purple colouration shows a stronger proline concentration (Figure 2.3A). An empirical calibration curve based on eight points of proline standard concentrations (0, 10, 20, 30, 50, 70, 90, and 100 µg/g) yielded a linear regression, r^2=0.99 between proline concentration and the measured absorbance at 520 nm, which was used to determine the proline concentrations in the samples (Figure 2.3B).

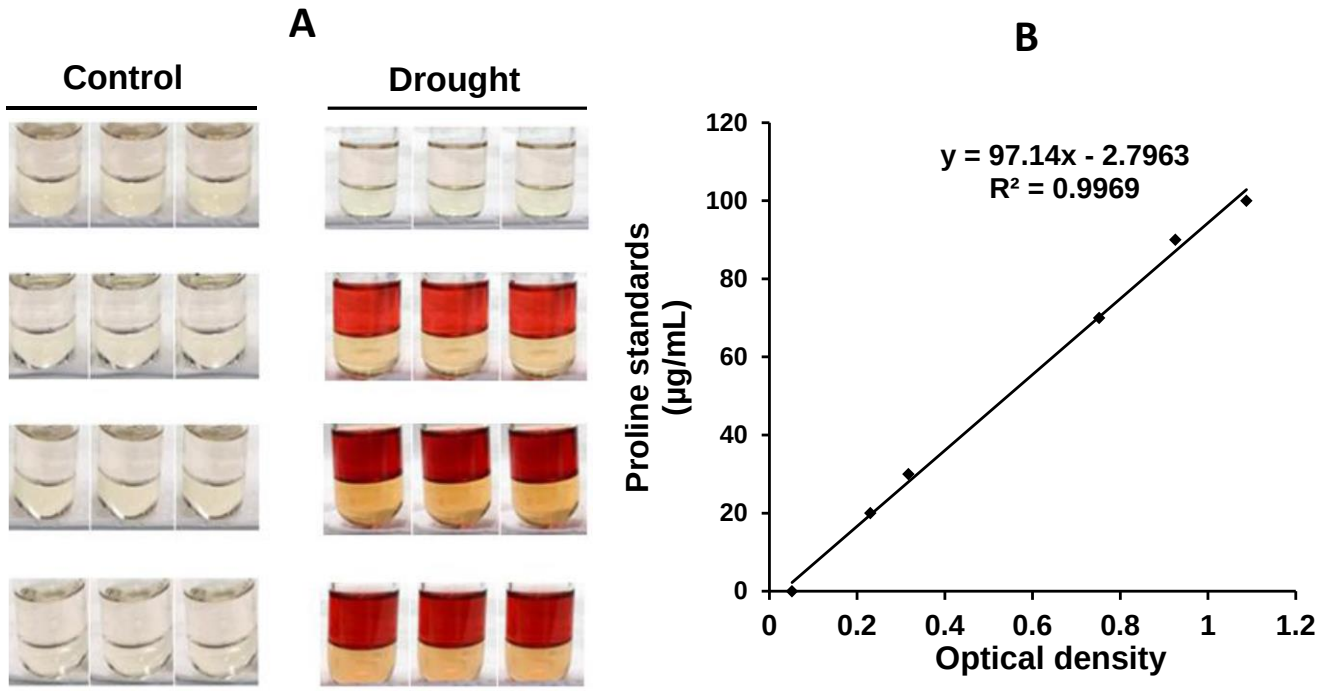

Figure 2.3 Proline as concentrated in test tubes from well-watered (control) or water stress (drought) treated plant samples (A), and the standard proline curve (B). No coloration is visible for the well-watered treatment, whereas dark purple-red coloration signifies higher proline concentration in the drought treated plant samples. The regression plot in panel B is used for the standard proline calculations.

2.3 Leaf-level gas exchange measurements

Instantaneous photosynthesis and stomatal conductance were measured after steady-state gas exchange conditions inside the cuvette were reached (using portable infrared gas analyzers, LI-6800 (LI-COR Inc., Lincoln, NE, USA) with fluorometer head MPF-551065 or MPF-831744). Measurements were completed between 10:00 am and 3:00 pm during the day for all barley plants by following the randomization order of the experimental layout to account for the possible effects of time of day on the measurements, which could spuriously bias genotypic values and variability estimation as well.

2.4 Magnetic resonance imaging

Magnetic resonance imaging (MRI) measurements were performed using two imagers, the first based on a 4.7 Tesla (T) and the second on a 1.5 T magnet (Figures 2.4 A and B). Detailed descriptions of the magnets were previously reported (Pflugfelder et al., 2017; van Dusschoten et al., 2016). The spike scans from the 1.5 T were non-invasive and continuous from the same tiller, while 4.7 T were cut at specific time points from different plant's main spikes. Regarding the 4.7 T measurements, developing spike images were acquired in their natural vertical orientation. The system was equipped with a quadrature to transmit/receive coil with an inner diameter of 100 mm and a 300 mT/m gradient system. A robotic system (MiniLiner 3.0, Geiger Handling GmbH and Co. Kg, Jülich, Germany) was used to carefully lower and centre the specimen into the MRI scanner. Two-dimensional images of developing spikes were acquired using a multi-spin- echo sequence with an in-plane spatial resolution of 0.3750 and 0.1875 mm. The following set routines; 32 echoes, 1.5 s repetition time, echo time of n × 8 ms, two averages, 512 × 256 image matrix, a field of view of 100 (read direction) by 50 mm (phase direction), at a slice thickness of 50 mm were used. The acquired datasets presented show amplitude images of water content per pixel. Each spike was imaged for 12 mins. An additional 10 mins of preparation and setting the sample to the centre of the magnet were required. For all spikes, the MRI images presented are amplitude parameter maps of a single echo image in grey values in their sagittal orientation after analyzing using image reconstruction set scripts from Spyder software, scientific programming in Python 3.6.

Regarding the 1.5 T, we used an rf-coil with an inner diameter of 25 mm and a length of 50 mm for the spike image acquisition. Spike images were acquired with a field of view of 45 mm. Spikes in their sagittal orientation were scanned for 3D images, the sequence "ge3d" with a resolution of 130 μm isotropic, eight averages were used at a scan time of approximately 60 mins. The raw data files were later analyzed with the medical image processing and visualization software "MeVisLab" (https://www.mevislab.de/) version 3.0.2 with installed packages "PhenoVein", "Spike_analyses" and "ImageViewer" were used to process for the 3D images.

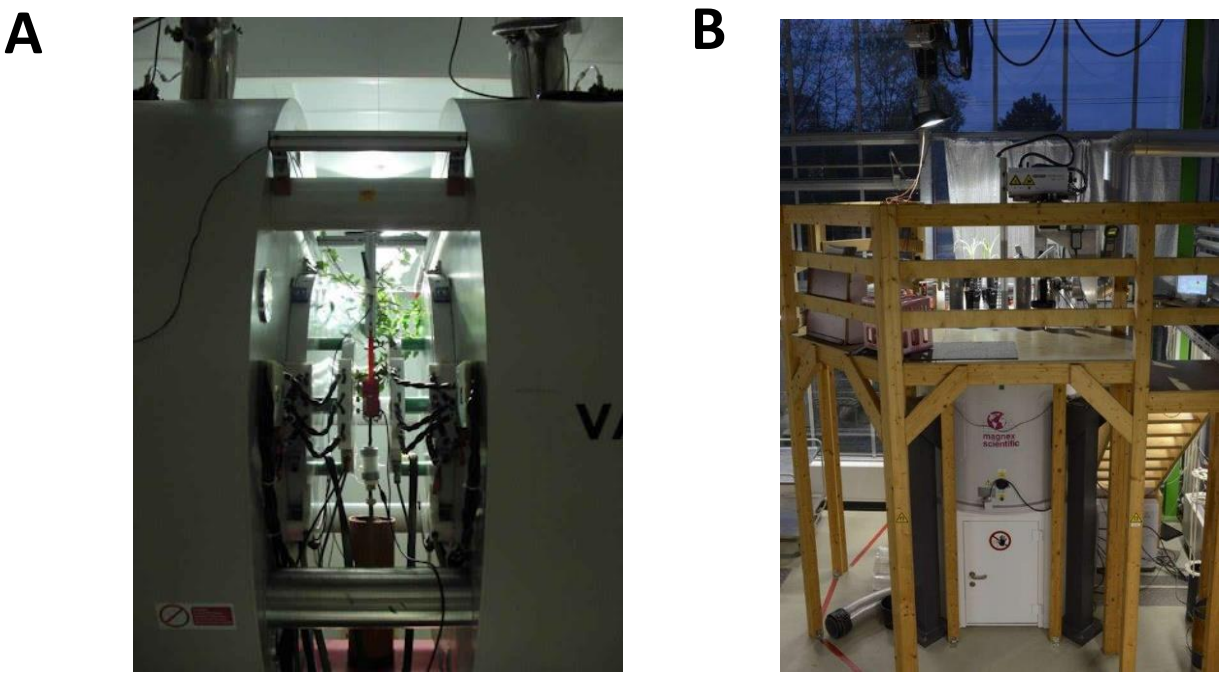

Figure 2.4 Pictures of the eco MRI machines at the IBG-2 Forschungzentrum Jülich, Germany, used for scanning in *vivo* barley spike development. In the panel, (A): 1.5 T, and (B): 4.7 T MRI.

2.5 Setup of the Nuclear Magnetic Resonance Multiplexed sensor

The Nuclear Magnetic Resonance (NMR) multiplexed sensor setup is an upgrade of the single mobile NMR Sensor (Windt et al. 2021). The multiplexed NMR sensor comprised six C-shaped movable NMR magnetic sensors (remanence (Br) 1.42T; MCE, Bedfordshire, United Kingdom) and a spectrometer in a climate-controlled housing (Figure 2.5). All the NMR sensor heads were fitted with solenoidal radio frequency (rf) coils (25 mm long, Ø20 mm wide), wound onto glass formers, allowing light penetration and easy spike inspection. The C-shaped magnets enabled access from the sides providing easy spike insertion and height adjustment. We measured the lower-mid section of the spike (20 mm long as allowed by the rf coil size) for all our genotypes. We included only data from spikes of all genotypes with no abortive seed at this specific lower-mid section area during the measurement to avoid biases. At any given time, six spikelets or later grains were counted (three on each side of our two-row spikes) inside the coil during the measurements. Prospa, Magritek, New Zealand, a spectrometer proprietary software, was used for the NMR signal measurements. Amplitude proton densities of the developing spikes were generated by the mono-exponentially fitting of a particular part of the echo train stated below (Figure 2.5) based on the equation (1):

$$\boldsymbol{A = A_0 e^{-t/T2}} \quad \text{..... (1)},$$

where; A_0 is the signal amplitude directly after excitation and is a direct measure of the number of spins under observation in the detector coil, T2 is the spin-spin relaxation time. Two NMR methods (sequences) were combined to acquire the NMR signal, free induction decay (FID) and Carr-Purcell-Meiboom-Gill (CPMG, Windt et al., 2021). The FID sequence is used to acquire the signal of all protons in the sample, including that of the fast decaying protons in the solids, and provides an estimate of the total proton density (Windt et al., 2021). Total proton density was measured by acquiring the FID of the sample. FID data points between 0 and 75 µs were fitted with a single exponential to obtain these values. The proton density of the liquid fraction was approximated based on a CPMG sequence (Windt et al., 2021). The CPMG curve data points between 0 and 25 ms of the echo train were averaged.

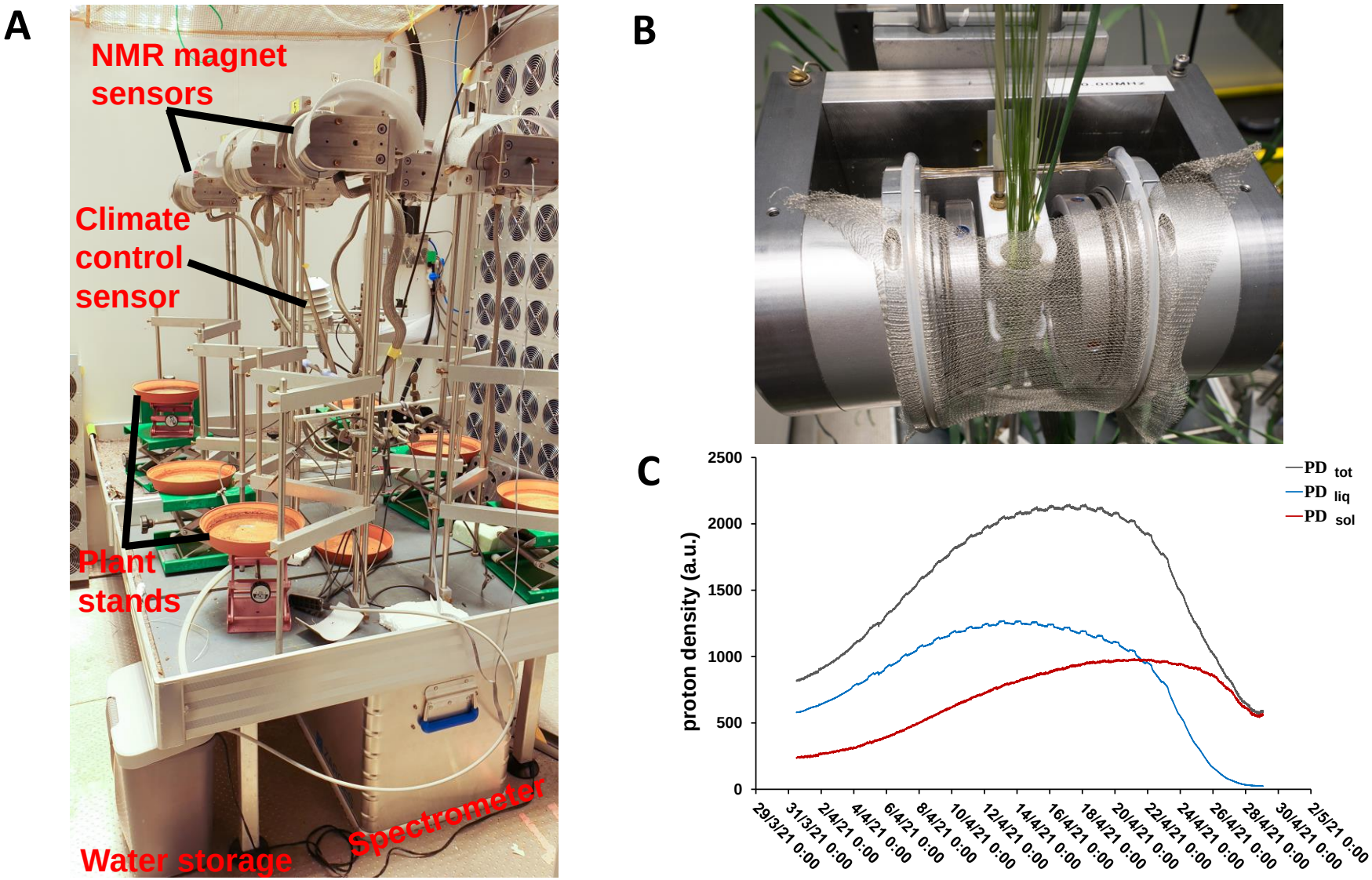

Figure 2.5 The multiplexed NMR setup (A) comprises six NMR sensors and is placed in a growth chamber with automated control of temperature and light. In the close-up view of the NMR sensor head (B) a barley spike at grain filling stage can be seen, inserted into the rf-coil of the NMR sensor. Using the NMR sensor the total proton density (PD_{tot}; grey line), liquid proton density (PD_{liq}; blue line), and solid proton density-PD_{sol}; red line) of the developing spike can be measured, continuously and non-invasively.

2.6 Floral transition and barley spike development

To study florets and spike development (Figure 2.6), we scored the plants (according to the Zadoks decimal growth scale, Zadoks et al., 1974) after dissection under a stereomicroscope (Leica MZ12 stereo microscope, Germany) equipped with the 1.0× planochromatic objective and with 10× eyepieces, a numerical aperture of 0.125, and a resolution of 375 line pairs/mm (Frimpong et al., 2021a). The working distance of 0.8× Plano objective of 112 mm was used to acquire all images. The spike early floral development begins from the maximum number of primordia where spikelet initiation is complete (Kirby, E. J. M., Appleyard, 1984). Floral development (Figure 2.6) continues to the active growth stage of the spike at the booting stage (flag leaf sheath extended and swollen). The spike further develops to the heading stage, i.e. the last stage of pre-anthesis development, where the spike is pushed out of the flag leaf sheath. It then progresses to the anthesis stage, often characterized by spikelets having more than 50% matured anthers. Later spike developmental stages involve grain filling (flowering already completed and first grains reached half their final size) and physiological maturity stages before ripening (Feng et al., 2017; Ochagavía et al., 2018; Zadoks et al., 1974).

Figure 2.6 Barley phenological growth stages according to (Kirby, 1988; Zadoks et al., 1974). Shown are images of developing ears, ordered left to right according to developmental stage. Below the images, final grain yield is depicted as a function of both genotypic and environmental factors. Note that the images are not to scale and were taken from different plants. [Abbreviation/symbol: *DC-Digital code, PM-Physiological maturity, GN-grain number, FP-fertile primordia, MNP-maximum number of primordia, ⋈- function of]*.

2.7 Light Microscopy

Scoring of floret developmental stages of harvested barley spikes (six main tillers/plants per developmental stage) was done using three regions along the spike axis (20 mm relative to the axis length per section, Steinfort et al., 2017), i.e. apical (top), central (mid), and basal (bottom) sections and dissected under a stereomicroscope (Leica MZ12 stereo microscope, Germany, Figure 2.7) equipped with the 1.0 × planochromatic objective and with 10 × eyepieces, a numerical aperture of 0.125, and a resolution of 375-line pairs / mm (Frimpong et al., 2021). The working distance of 0.8 × Plano objective of 112 mm was adjusted to acquire all microscopic images.

Figure 2.7 Author using the stereomicroscope (Leica MZ12 stereo microscope, Germany) to take barley floret images. The microscope is equipped with a built-in camera to capture images which are saved to a computer.

2.8 Statistics and measurement time points for the experiments

We used a factorial in randomized complete block design or a simple, completely randomized design in all our experiments as specified in each experiment later in this thesis. Again, all the data were subjected to normality (Shapiro Wilk test) and variance homogeneity tests (Levene's test) before analysis of variance (ANOVA) using the "Agricolae" package of 'R' statistical software, version 3.6.1. or latest (R Core Team, 2019 & 2020). "Tukey's HSD (Honest Significant Difference test) and estimated marginal means (adjusted using "bonferroni" method) was used to determine significant differences between treatment, genotype and tissue-type means within plant traits. Spearman correlation coefficients for pair-wise comparisons for selected traits were computed. Power transformation (Box and Cox, 1964) and square root was performed when normality or homogeneity conditions were not met. We used the generalized linear model for three-way (type III), two-way and one-way ANOVA (equations 2, 3, 4, respectively):

$$\boldsymbol{\mu_{ijkt} = \mu + \alpha_i + \beta_j + \gamma_k + (\alpha\beta_{ij}) + (\alpha\gamma_{ik}) + (\beta\gamma_{jk}) + (\beta\gamma_{ijk}) + \varepsilon_{ijkt}} \text{ ..... (2),}$$

where:

μ = grand mean

$\alpha_i, \beta_j \; and \; \gamma_k$ = main effects of water stress treatment and genotypes of the ith , jth and *kth* levels

the $(\alpha\gamma\beta_{ijk})$ represents the interaction effect

the ε_{ijkt} is the error term.

$$\boldsymbol{\mu_{ijk} = \mu + \alpha_i + \beta_j + (\alpha\beta_{ij}) + \varepsilon_{ijk}} \text{..... (3),}$$

where:

μ = grand mean

$\alpha_i \; and \; \beta_j$ = main effects of water stress treatment and genotypes of the ith and jth levels

the $(\alpha\beta_{ij})$ represents the interaction effect

the ε_{ijk} is the error term.

and one-way ANOVA (4):

$\boldsymbol{\mu} = \boldsymbol{\mu} + \boldsymbol{\alpha} + \boldsymbol{\varepsilon_k}$..... (4),

Where:

μ = grand mean

α = main treatment effects

the ε_k is the error term.

Please note that further details are given in each experimental section (Chapters 3-6 of this thesis). An illustration at what developmental stage the measurements of various experiments were done is given in Figure 2.8.

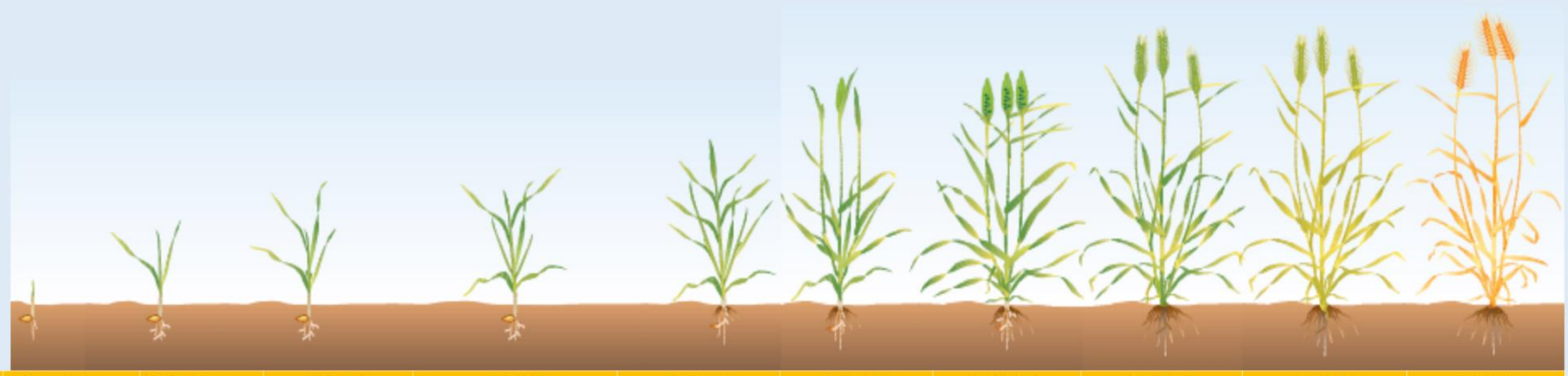

Zadoks Digital code	DC 00-09	DC10-19	DC20-29	DC30-39	DC40-49	DC50-59	DC60-69	DC70-79	DC80-89	DC90-99
Development phase	Germination	Seedling growth	Tillering	Stem elongation	Booting	Ear Emergence	Flowering	Milk Development (grain filling period)	Dough development (grain filling period)	Ripe
Measurement time point for each study										
Study I					A wild allele of *Pyrroline-5-carboxylate synthase1* leads to proline accumulation in spikes and leaves of barley, contributing to improved performance under reduced water availability					
Study II	Proline mediated drought tolerance in the barley (*Hordeum vulgare* L.) isogenic line is associated with lateral root growth at the early seedlings stage									
Study III				*In vivo* visualization of barley (*Hordeum vulgare* L.) grain development by MRI						
Study IV					Quantifying spike filling rate, dry matter and water content of two-row barley genotypes with the non-invasive NMR multiplexed sensor					

Figure 2.8 Schematic illustrating the developmental stage at which the various experiments (chapters 3 to 6) were done. The figure was adapted from (Poole, 2005).

CHAPTER 3

A wild allele of *Pyrroline-5-carboxylate synthase1* leads to proline accumulation in spikes and leaves of barley, contributing to improved performance under reduced water availability

(This chapter is based on Frimpong et al., 2021a: Frontiers in plant sci: doi.org/10.3389/fpls.2021.633448, with the exception that spike proline data were reanalyzed and selected samples excluded because of concerns on measurement quality. Reanalyzed data are presented in Fig. 3.3 B. Accordingly, minor modifications of the text were necessary compared with the published article.)

Felix Frimpong[1, 2], Carel W. Windt[1], Dagmar van Dusschoten[1], Ali A. Naz[2], Michael Frei[2, 3], Fabio Fiorani[1*]

[1] IBG-2: Plant Sciences, Institute of Bio- and Geosciences, Forschungszentrum Jülich GmbH, 52425 Jülich, Germany

[2]Institute of Crop Science and Resource Conservation, University of Bonn, 53115 Bonn, Germany

[3]Institute of Agronomy and Plant Breeding, Justus-Liebig-Universität Gießen, 35392 Gießen, Germany

[*]**Correspondence:** Fabio Fiorani**,** f.fiorani@fz-juelich.de

Abstract

Water stress during spike development strongly affects final grain yield in cereals. Proline, an osmoprotectant amino acid, may contribute to alleviating the effects of cell and tissue dehydration. We studied five spring barley genotypes contrasting in their drought response, including two introgression lines, *S42IL-143* and *S42IL-141*, harbouring a *Pyrroline-5-carboxylate synthase1-P5cs1* allele originating from the wild barley accession *ISR42-8*. We tested the hypothesis that barley genotypes harbouring a wild allele at the *P5cs1* locus are comparatively more drought-tolerant at the reproductive stage by inducing proline accumulation in their immature spikes. At the booting stage, we subjected plants to well-watered and water stress treatments until physiological maturity. Several morpho-physiological traits had significant genotype by treatment interaction and reduction under water stress. Varying levels of genotypic proline accumulation and differences in water stress tolerance were observed. Spike proline accumulation was higher than leaf proline accumulation for all genotypes under water stress. Also, introgression lines carrying a wild allele at *P5cs1* locus had a markedly higher spike and leaf proline content compared with the other genotypes. These introgression lines showed milder drought symptoms compared with elite genotypes, remained photosynthetically active under water stress, and maintained their intrinsic water use efficiency. These combined responses contributed to the achievement of higher final seed productivity. Magnetic resonance imaging of whole spikes at the soft dough stage showed an increase in seed abortion among the elite genotypes compared with the introgression lines 15 days after water stress treatment. Our results suggest that proline accumulation at the reproductive stage contributes to the maintenance of grain formation under water shortage.

Keywords: barley, introgression lines, seed yield, proline accumulation, pyrroline-5-carboxylate synthase1, water stress

3.1 Background

The ability of crops to withstand water stress is a critical aspect of the potential impact of climate change on crop productivity in agricultural systems (Ferguson, 2019; Gupta et al., 2020). Plants use different strategies to cope with water shortage: avoidance, escape, or tolerance. The escape strategy is an adaptive mechanism that involves rapid plant development to enable the completion of the full life-cycle before a drought event can occur (Shavrukov et al., 2017). In cereals, drought escape is associated with a short vegetative stage and early flowering time. The avoidance strategy involves minimization of water loss and optimization of water uptake, which comprises physiological responses that improve photosynthetic water use efficiency, such as stomatal closure (Basu et al., 2016; Blum, 2005; Fahad et al., 2017; Rodrigues et al., 2019), stay green (Sallam et al., 2019; Tardieu et al., 2018; Wasaya et al., 2018), deeper rooting (Arai-Sanoh et al., 2014; Kebede et al., 2019; Lynch & Wojciechowski, 2015), or the accumulation of osmolytes and osmoprotectants (Bandurska et al., 2017).

Drought is known to profoundly affect plant metabolism (Templer et al., 2017). The accumulation of compatible solutes such as sugars, proline, fructans, glycine betaine, and polyamines is associated with increased drought tolerance in plants (Templer et al., 2017; Trovato et al., 2019). Drought stress increased proline concentration about 10-fold in the leaves of monocotyledons such as rice (*Oryza sativa*) and dicotyledons species such as *Brassica oleracea* seedlings (Dien et al., 2019; Podda et al., 2019).

Proline is synthesized from glutamate by the action of three enzyme coding genes, pyrroline-5 carboxylate synthase (*P5CS*), pyrroline-5-carboxylate synthase-2 (*P5CS2*), and pyrroline-5-carboxylate reductase (*P5CR*) (Bhaskara et al., 2015; Trovato et al., 2019). Several reports investigated the proline biosynthetic pathway and the corresponding key enzymes *P5CS* and *P5CR* have been well characterized (Abdel-Ghani et al., 2019; Choudhury et al., 2017; Forlani et al., 2015; Kamal et al., 2019). The most rate-limiting enzyme for proline synthesis in higher plants is pyrroline-5-carboxylate synthase (Trovato et al., 2019). Proline biosynthesis occurs under non-limiting and limiting growth conditions (Cattivelli et al., 2011; Nieves-Cordones et al., 2019). Under non-limiting growth conditions, proline is used in protein biosynthesis to maintain the housekeeping function of the cell (Hoffmann et al., 2017). Proline accumulation under water stress precedes the increased expression of *P5cs1* (Muzammil et al., 2018). The expression of both *P5cs1* and *P5CR* is increased in leaves when barley is exposed to drought, resulting in enhanced proline

synthesis in the chloroplast, whereas *P5CS2* is primarily linked to proline synthesis in the cytosol (Sayed et al., 2012).

In barley, introgression lines carrying naturally occurring alleles (cross between *Scarlett* and wild type *ISR42-8*) associated with proline accumulation and leaf wilting under drought stress conditions were reported previously (Honsdorf et al., 2014, 2017; Naz et al., 2014; Sayed et al., 2012). To test the hypothesis that the allelic variant of *P5cs1* controls the drought-inducible QTL (*QPro.S42-1H*) in the donor parental line and progenies, Muzammil et al. (2018) performed a series of phenotypic evaluations. They demonstrated that the progeny introgression lines maintained leaf water content and photosynthetic activity longer compared with those of the cultivated parents under drought conditions. Nonetheless, to understand the integrative networks of plant metabolites and signalling molecules, their biosynthesis and action sites must be clarified (Kuromori et al., 2018). Understanding the specific target sites regulating seed filling events in leaves and seeds and how they are affected by abiotic stresses is imperative to enhance seed quality (Sehgal et al., 2018). Knowledge of the physiological, biochemical, and genetic mechanisms which govern seed filling under stressful environments helps to devise strategies to improve stress tolerance (Abdelrahman et al., 2020; Sehgal et al., 2018). Little attention has been paid to the role of proline in the reproductive organs (Heuer, 2016), especially spikes or seeds, and the changes in its concentration in different plant organs under water stress. In this study, we addressed this knowledge gap by measuring spike and leaf proline content, changes in photosynthetic performance, and assessing barley seed abortion and grain filling under water stress using Magnetic Resonance Imaging (MRI) at the reproductive stages.

We tested the hypothesis that drought-induced proline accumulation in spikes of barley genotypes harbouring the wild variant of *P5cs1* improves drought tolerance as measured by seed number and final yield in greenhouse experiments. To this end, we characterized a panel of contrasting elite genotypes and *P5cs1*-introgression lines and monitored morpho-physiological responses after water withdrawal during reproductive development.

3.2 Materials and methods

3.2.1 Plant material

Four two-row and one six-row spring barley genotypes *S42IL-141*, *S42IL-143*, *Scarlett*, *Barke*, and *HOR10151* were chosen for this study based on their genetic background, breeding history, agronomical importance, and previously reported yield under drought stress conditions. *S42IL-141*, *S42IL-143* carried chromosomal introgressions at the *P5cs1* locus from wild barley accession *ISR42-8* (Muzammil et al., 2018). *Barke* and Scarlett are elite German cultivars. *HOR10151* is a six-row traditional landrace known to escape drought when grown at high elevations of the Libyan region where it originated.

3.2.2 Growth conditions and water stress treatment

Two experiments were conducted in a greenhouse in two consecutive years, June - October 2018 and 2019. Cumulative growing degree days were calculated assuming a base temperature of 0°C (Hecht et al., 2019; Miller et al., 2001) from the time of emergence until the ripening stage. These were 2155 and 2059 degree days in 2018 and 2019, respectively. The average minimum and maximum greenhouse daily light integral (DLI, mol m^{-2} day^{-1}) were 6 and 13 in 2018 and 3 and 12 in 2019 (Appendix 3.1). Pre-germinated seeds of five genotypes were transplanted into 1.5 L pots upon reaching the three leaves stage. Peat soil (Einheitserde, "null type") was used for both experiments arranged in a 5×2 factorial randomized complete block design with six and fifteen replicates per genotype and treatment in 2018 and 2019, respectively.

Starting from the booting stage (BBCH-scale 41, Meier, 2001), all genotypes were subjected to two irrigation regimes. The treatments were well-watered (WW) and water stress (WS). We applied WS by first withholding water for the selected plants for 48 hours and then adjusted the irrigation volume three times per week to maintain target soil moisture per treatment. WW plants were irrigated daily (400 mL per plant) approximately to 50% g/g gravimetric soil water content in two aliquots per day; WS plants were irrigated daily (120 mL per plant) approximately to 20% g/g gravimetric soil water content in two aliquots per day (Appendix 3.2). Soil water content was monitored with the aid of a three-pin time-domain-reflectometry soil moisture Theta ML2 probe (Delta-T Devices Ltd, UK), after calibration (R^2=0.94) from volumetric to gravimetric soil water

content. The corresponding soil water potential (Ψ soil) values of WW and WS were -0.001 and -1.5 MPa, respectively. These soil water potential values were estimated using eight-point water retention curves that were fitted with the van Genuchten model (van Genuchten, 1980).

3.2.3 Morphometric and physiological measurements

Twice a week, two plants of each genotype were dissected under a stereomicroscope to observe spike developmental stages and characterize treatment effects. The stereomicroscope (Leica MZ12 stereo microscope, Germany) was equipped with a 1.0× planochromatic objective and with 10× eyepieces, a numerical aperture of 0.125, and a resolution of 375 line pairs / mm. The number of days to reach each stage of development was counted for both WW, and WS treated plants. Plant height and tiller number were determined at harvest. At harvest (20 days after water stress), yield traits such as spike number, spike length (cm), spike weight (g), total grain weight (g), grain number, shoot fresh weight (g), shoot dry weight (g) were determined on a per plant basis. A drought susceptibility index (DSI) for dry grain yield (g) per plant was calculated using the formula (5) according to (Haddadin, 2015):

$$DSI = \frac{1-\frac{YD}{YP}}{1-\frac{WD}{WP}} \text{ ..... (5),}$$

where

YD = mean yield of individual genotype under the WS condition.
YP = mean yield of individual genotype under the WW condition.
WD = mean of all genotypes under the WS condition.
WP = mean of all genotypes under the WW condition.

Fresh and dry weight per plant (g) were determined for shoot and root (after washing) biomass at harvest. Percentage relative leaf water content (6) of fully expanded leaves was calculated:

$$\%\, relative\ leaf\ water\ content\ (RWC) = \frac{\text{(fresh leaf weight} - \text{dry leaf weight)}}{\text{(turgid leaf weight} - \text{dry leaf weight)}} \times 100 \text{ ..... (6),}$$

leaf water content (RWC)=,(fresh leaf weight-dry leaf weight)-(turgid leaf weight-dry leaf weight).×100 (6),

according to Barrs & Weatherley (1962), fifteen days after the WS application.

WS treated leaves were scored for wilting one-time forenoon, fifteen days after the onset of treatment using a scale from 0 to 9. A score of 0 indicated no wilting, and 9 was fully wilted (De Datta et al., 1988; Sallam et al., 2019). Gas exchange parameters (net CO_2 assimilation - *A*, µmol CO_2 m^{-2} s^{-1}, stomatal conductance - *gsw*, mmol H_2O m^{-2} s^{-1}, transpiration rate - *E*, mol H_2O m^{-2} s^{-1}, intrinsic water use efficiency (*A/ gsw)* –iWUE, µmol CO_2 $mmol^{-1}$ H_2O) were measured on the youngest leaf directly below the flag leaf on the main stem at a one-time point during the experiment of 2018 (15 days after WS). The flag leaf of the main stem was used for the gas exchange measurements in 2019 at 3, 9, and 15 days after WS application. Fifteen and six plants per genotype per treatment in 2019 and 2018, respectively, were used for the gas exchange measurements. Leaves were clamped in the MultiPhase Flash ^{TM} fluorometer chamber (551065), 10% blue light, 6 cm^2 LiCOR cuvette, and exposed to PPFD of 1500 µmol $m^{-2}s^{-1}$, Airflow (500 mmol s^{-1}), block temperature of 25°C, 400 ppm of CO_2, humidity (RH) ranging between 50-65% using a LiCor 6800 (LiCOR Inc., Lincoln, NE, United States).

3.2.4 Magnetic Resonance Imaging

The magnetic resonance imaging (MRI) scans were carried out using a custom-built, vertical bore 4.7 T MRI scanner, driven by a Varian console VNMRS, vertical wide-bore MRI system (Varian Inc., http://www.varianinc.com). The system was equipped with a quadrature to transmit/receive coil with an inner diameter of 100 mm and a 300 mT/m gradient system. The main spikes at the dough stage (BBCH-scale, 83) were collected together with a section of the stalk (>20 mm). The cut spikes were placed in a vial with tap water directly after excision. A robotic system (MiniLiner 3.0, Geiger Handling GmbH and Co. Kg, Jülich, Germany) was used to carefully lower and centre the specimen into the MRI scanner. 2D images of developing spikes were acquired with an in-plane spatial resolution of 0.3750 · 0.1875 mm, using a multi-spin-echo sequence based on the following set routines; 32 echoes, 1.5 seconds repetition time, echo time of n×8 ms, two averages, 512×256 image matrix, a field of view of 100 (read direction) by 50 mm (phase direction), at a slice thickness of 50 mm. The acquired datasets show amplitude images of water content per pixel (Edzes et al., 1998). Each spike was imaged for 12 minutes. An additional 10 minutes of preparation and setting the sample to the centre of the magnet were required. For all spikes, the MRI images presented are amplitude parameter maps of a single echo image in grey values in their sagittal orientation after analyzing using image reconstruction set scripts from Spyder, scientific programming in Python 3.6.

3.2.5 Proline determination in barley leaves and spikes

Proline concentrations were determined based on Bates et al. (1973) protocol, as earlier described in section 2.2 of this thesis. Six replicates of each flag leaf and immature spike samples were collected from both treatments and genotypes.

3.2.6 Statistics

All data were subjected to normality (Shapiro Wilk test) and variance homogeneity tests (Levene's test). Power transformations (Box & Cox, 1964) and square root was performed for the gas exchange and proline measurements, respectively because normality or homogeneity conditions were not met. The main effects of genotypes and WS treatments and their corresponding interactions were tested using a two-way analysis of variance, except for spike tissue type analysis (results section 3.3.3 of this thesis) where three-way analysis of variance, type III error was used. Six replicates were used for all data analysis except for proline spike-tissue type data analysis where there were random missingness due to spike damage (at least four replicates were used but corrected using ANOVA type III error of unequal replications, Appendix 3.3). Two-way ANOVA was used as following step for proline tissue type spike data to test simple simple comparisons-tissue_type effect in genotype. We used the generalized linear models; (see equations 2, 3 and 4 stated under section 2.8 above), built-in the "Agricolae" package of "R" statistical software, version 3.6.1 (R Core Team, 2020). Tukey's HSD (Honest Significant Difference test) and estimated marginal means (adjusted using "bonferroni" method) was used to determine significant differences between treatments,genotypes and spike tissue-type means within plant traits. Spearman correlation coefficients for pairwise comparisons for selected traits were computed.

3.3 Results

3.3.1 Effects of water stress on barley morphology and physiology

Pronounced leaf wilting was observed under WS for all the genotypes and treatments (Figure 1). However, the two introgression lines *S42IL-143* and *S42IL-141,* showed milder wilting symptoms (-40%) than the elite barley types *Barke, Scarlett,* and *HOR10151* (Tables 3.1 and 3.2). The six-row barley type, *HOR10151,* showed higher susceptibility to wilting than the introgression lines, with more than 50% of its leaves drying 15 days after stress application (Tables 3.2 and Figure 3.1). Averagely, WS *S42IL-143* and *S42IL-141* had a wilting score of 2 or less while the elite lines were 3 and above (Table 3.2). None of the WW plants showed any wilting symptoms (Table 3.1). Results from both 2018 and 2019 experiments showed that introgression lines *S42IL-143* and *S42IL-141* maintained their RWC (>70%) under WS and WW conditions Table 2. Differently from the WW conditions, elite cultivars showed smaller variations in RWC under WS. (Tables 3.1 and 3.2). In 2019, *Barke* and *HOR10151* had the lowest RWC (~35%, Tables 3.1 and 3.2) under WS.

The spike developmental stages from booting, heading, and anthesis up to the onset of grain filling were delayed by at least one day under WS treatment for all genotypes (Appendix 3.4). Barley genotype *HOR10151* had the most considerable delay (three days difference between WS and WW plants, Appendix 3.4). Plant performance for all genotypes was significantly reduced for both experimental years (Tables 3.1 and Appendix 3.5). Relative to WW conditions, we observed a percentage reduction (%) of average plant height (18, 27), tiller number (19, 47), spike number (45, 38), grain number (30, 58), spike length (18, 22), grain weight (76, 76), RWC (15, 35), net CO_2 assimilation (56, 72), stomatal conductance (74, 77), transpiration rate (63,76), and electron transport rate (31, 28) (Appendix 3.5) in 2018 and 2019, respectively.

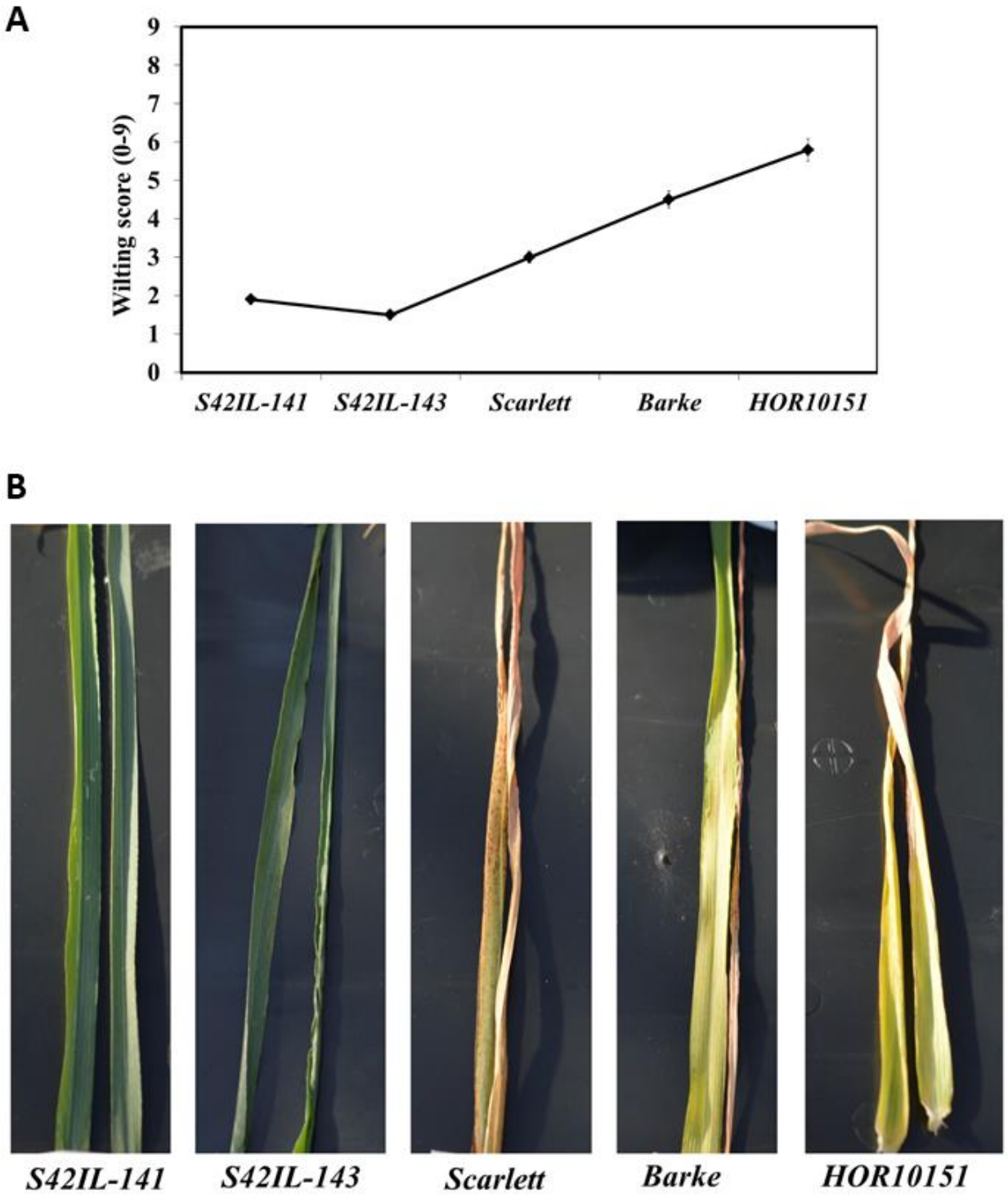

Figure 3.1 Wilting severity by the different genotypes recorded forenoon, 15 days after onset of water stress, scored following the method by De Datta et al., 1988 (A). Drought symptoms of representative leaves (leaf 5 and 6 fully expanded) of the different genotypes are shown in panel (B). The figure was taken from Frimpong et al., 2021a.

Prolonged WS of fifteen days led to several leaves drying and reduced net CO_2 assimilation by at least 50% (Figure 3.2A and Figure 3.1). Net CO_2 assimilation, stomatal conductance, transpiration rate, and electron transport rate were significantly reduced due to WS (Table 3.1). Significant genotypic variations were observed in the gas exchange parameters under WW conditions (Figure 3.2A-D). For instance, net CO_2 assimilation in fully turgid leaves was between 22 and 24 µmol m^{-2} s^{-1} throughout the experiment period (Figure 3.2A). *Scarlett* had the lowest and *HOR10151* the highest net CO_2 assimilation under WW (Figure 3.2A). On the other hand, the WS plants had a net CO_2 assimilation rate between 2.5 and 10.7 µmol m^{-2} s^{-1} throughout the stress period (Figure 3.2A). *Barke* had the lowest value for net CO_2 assimilation (2.5 µmol m^{-2} s^{-1}), while the highest net CO_2 assimilation rate was by *S42IL-141*and *S42IL-143* (10.7 and 12.5 µmol m^{-2} s^{-1}) under WS, respectively (Figure 3.2A).

Transpiration rate was between 0.43×10^{-2} and 0.66×10^{-2} mol $m^{-2}s^{-1}$ under WW conditions, compared with 0.52×10^{-3} and 0.27×10^{-2} mol $m^{-2}s^{-1}$ under WS throughout the stress period (Figure 3.2B). *HOR10151* had the lowest transpiration rate, 0.52×10^{-3} mol $m^{-2}s^{-1}$ while *S42IL-143* transpired the most, 0.27×10^{-2} mol $m^{-2}s^{-1}$, 15 days after WS (Figure 3.2B). Stomatal conductance of fully turgid leaves was between 0.2 and 0.4 mol m^{-2} s^{-1} compared with WS leaves of 0.03 and 0.1 mol m^{-2} s^{-1} from booting to the onset of grain filling stages (Figure 3.2C). Introgression lines *S42IL-143* and *S42IL-141* maintained their photosynthetic activities by not only photosynthesizing at a higher rate several days after imposing WS but were also able to keep transpiring with low to moderate stomatal opening, ranging from 0.130 and 0.097 mol m^{-2} s^{-1} when the grain started filling (Figure 3.2C). These values were higher than those measured for *Barke, Scarlett,* and *HOR10151,* which were between 0.025 – 0.055 mol m^{-2} s^{-1} under WS (Figure 3.2C). Under WW conditions, intrinsic water use efficiency (iWUE) ranged between 59 and 105 μmol^{-1} CO_2 H_2O^{-1} (Figure 3.2D). iWUE of fully turgid flag leaves of *S42IL-141* was the lowest, while *S42IL-143* was the highest across developmental stages. iWUE of the flag leaves of WS plants ranged between 65 and 122 $\mu mol^{-1}CO_2$ H_2O^{-1}. On average, *Barke and Scarlett* had the lowest values at heading and onset of grain filling, respectively. *S42IL-141* had the highest iWUE under WS at booting and heading (Figure 3.2D). Interestingly, the iWUE of WS leaves of *S42IL-141*and *S42IL-143* increased by more than 20% compared with *Barke, Scarlett,* and *HOR10151* relative to their WW conditions (Figure 3.2D). iWUE of *Barke, Scarlet,* and *HOR10151* also increased marginally by 7% under

WS on average. On average, elite genotypes *Barke, Scarlett,* and *HOR10151* had a lower increment of iWUE (7%) under WS than under WW conditions (Figure 3.2D).

Table 3.1 Two-way analysis of variance of the plant traits in 2018 and 2019 under control, drought, genotypes, and genotype × treatment interaction, at the end of water stress or control treatment.

Traits	2018					2019				
	Control	Drought	Treatment	Genotype	G×T	Control	Drought	Treatment	Genotype	G×T
Plant height (cm)	92.9	75.9	***	NS	NS	93.3	67.8	***	***	NS
Tiller number	17.50	13.97	***	NS	NS	21.40	11.39	***	*	NS
Wilting/drought score	0.00	2.85	***	***	NA	0.07	3.36	***	***	NA
Relative leaf water content (%)	87.5	74.4	***	***	***	85.9	55.7	***	***	***
Spike number	18.35	10.00	***	***	*	26.40	16.39	***	***	***
Grain weight/plant (g)	12.57	2.91	***	***	***	14.22	4.37	***	***	***
Grain number per the main tiller	25.27	18	***	***	NS	28.84	11.05	***	***	***
Length of the main spike (cm)	10.61	8.68	***	***	NS	10.01	7.82	***	***	***
Shoot fresh weight (g)	59.01	46.13	***	***	**	35.8	19.9	***	***	NS
Shoot dry weight (g)	27.63	23.56	***	***	**	18.22	12.15	***	***	*
Root dry weight (g)	4.99	3.91	***	***	NS	3.99	2.91	***	***	NS
Root/shoot ratio (g)	0.18	0.17	NS	NS	NS	0.22	0.24	NS	NS	NS
A (µmol m^{-2} s^{-1})	28.83	13.13	***	***	***	21.51	6.08	***	***	***
E (mol m^{-2} s^{-1})	$9.9E^{-3}$	$3.6E^{-3}$	***	***	***	$9E^{-3}$	$2E^{-3}$	***	***	***
Ci (µmol mol^{-1})	260.86	176.54	***	***	***	239	216	*	NS	NS
VPDleaf	2.34	3.19	***	***	***	2.22	2.32	***	NS	NS
gsw (mol m^{-2} s^{-1})	0.43	0.11	***	***	***	0.28	0.063	***	***	***
iWUE (µmol CO_2 $mmol^{-1}$ H_2O)	68	118	***	NS	*	81	95	***	***	***
ETR (µmol m^{-2} s^{-1})	163	99	***	***	***	139	100	***	***	***
Leaf proline (µg/g FW)	63	325	***	***	***	43	299	***	***	***
Spike Proline (µg/g FW)	-	-	-	-	-	120	580	***	***	***

", **, ***" - Follows the standard probability values (P≤0.05, P≤0.01or P≤0.001). Means of A, E, Ci, VPDleaf, gsw, iWUE, ETR, and proline was back-transformed to original values after transformation. A-Net CO_2 assimilation, E- transpiration, gsw-stomatal conductance, VPDleaf- Vapor pressure deficit of the leaf, iWUE-intrinsic water use efficiency-A/gsw, ETR-electron transport rate, FW-Fresh weight, NA-not analyzed, NS-not significant. The table was taken from Frimpong et al., 2021a.*

Table 3.2 Differential biochemical and yield traits in response to water stress among the genotypes and drought treatments.

Year	Genotype	Well-watered				Water stress				
		% Relative leaf water content	Grain weight/plant (g)	Grain number per the main tiller	Length of the main spike (cm)	% Relative leaf water content	Wilting score	Grain weight/plant (g)	Grain number per the main tiller	Length of the main spike (cm)
2018	*Barke*	89.4±1.07ab	13.7±0.33ab	20.5±1.77a	10.6±0.11bc	56.5±1.07c	3.3±0.18b	1.4±0.33f	6.3±1.77b	8.3±0.11d
	HOR10151	86.4±0.88ab	9.8±1.39c	27.33±3.50a	6.2±0.26e	57.2±0.88c	4.9±0.14a	2.8±1.39ef	17.33±3.50ab	4.9±0.26e
	Scarlett	90.9±1.64a	14.0±0.90a	25.7±2.02a	11.7±2.06ab	86.1±1.64ab	2.9±0.15bc	2.3±0.90ef	18.2±2.02a	9.2±2.06cd
	IL141	87.4±0.69ab	11.3±0.72bc	26.5±1.65a	12.7±1.65a	85.3±0.69ab	1.9±0.15cd	5.3±0.72de	23.7±1.65a	10.7±1.65bc
	IL143	85.6±0.95ab	14±0.52a	26.3±1.41a	11.8±1.40ab	84.6±0.95b	1.2±0.16de	6.7±2.54d	24.2±0.52a	10.4±1.40bc
2019	*Barke*	87.5±2.04a	14.0±0.38a	23.6±0.75b	10.0±0.21bc	27.1±1.99d	4.5±0.11b	0.5±0.24e	2.3±0.63e	7.27±0.29e
	HOR10151	84.6±1.77a	10.6±0.36b	43.2±1.85a	6.5±0.19e	28.6±1.85d	5.8±0.15a	1.1±0.20de	4.0±0.70de	4.5±0.16f
	Scarlett	82.4±1.42a	13.5±0.51a	27.1±1.05b	11.1±0.22ab	56.9±1.22c	3.0±0.12c	2.7±0.43d	9.5±1.66d	8.47±0.20d
	IL141	84.2±1.19a	13.6±0.58a	24.4±1.22b	11.1±0.32ab	73.6±0.73b	1.9±0.10d	4.9±0.30c	22.1±1.32bc	10.1±0.26bc
	IL143	86.2±2.11a	13.3±0.38a	25.9±1.12b	11.27±0.23a	84.7±1.01a	1.5±0.12d	6.7±0.24c	17.3±1.23c	9.23±0.23cd

Different letters indicate significant differences among treatments and genotypes based on Tukey's HSD test ($P \leq 0.05$) within a trait.
Values are least-square means ± standard errors of 6 replicate for 2018 and 15 replicates for 2019.
Control plants showed no wilting and therefore scored zero and were not analyzed. The figure was taken from Frimpong et al., 2021a.

Generally, barley plants exposed to WS reduced their photosynthetic capacity, transpired less by closing their stomata with an overall leaves dehydration compared with their counterparts under sufficient water supply. Under WS, we observed two groups of genotypes for net CO_2 assimilation, stomatal conductance, and transpiration rate, with the two introgression lines as one and the three elite materials as the other group (Figure 3.2A-C). Under WW conditions, the electron transport rate (ETR) ranged from 74.49 to 179.51 µmol m-2 s-1 (Appendix 3.6). *Barke* had the lowest ETR, while *S42IL-141* had the highest ETR under WW conditions. ETR was between 51.59 and 160.09 µmol m^{-2} s^{-1} under WS conditions (Appendix 3.6). Again, *Barke* had the least ETR, while *S42IL-143* had the highest ETR under WS (Appendix 3.6). In terms of trait relationships (Appendix 3.7), the percentage relative leaf water content was significantly ($P \leq 0.05$) and negatively correlated with wilting score (r =-0.74), iWUE (r=-0.29) and leaf proline (r=-0.26). The percentage relative leaf water content significantly ($P \leq 0.05$) and positively correlated with net CO_2 assimilation (r=0.73), stomatal conductance (r=0.718), transpiration rate (r= 0.71), electron transport rate (r=0.62), grain weight (r= 0.61), grain number (r=0.66), plant height (r=0.61) and shoot biomass (r=0.36). The leaves' susceptibility to drying, *i.e.*, the wilting score was significant ($P \leq 0.05$) under WS and correlated negatively with reductions in net CO_2 assimilation rate (r = -0.88), stomatal conductance (r=-0.87), and transpiration rate (r=-0.88). However, leaf wilting correlated positively with leaf proline content (r=0.48). The reduction in net CO_2 assimilation rate under WS was significant ($P \leq 0.05$) and correlated positively with reductions in stomatal conductance (r =0.96), transpiration rate (r=0.97), and grain weight (r=0.85).

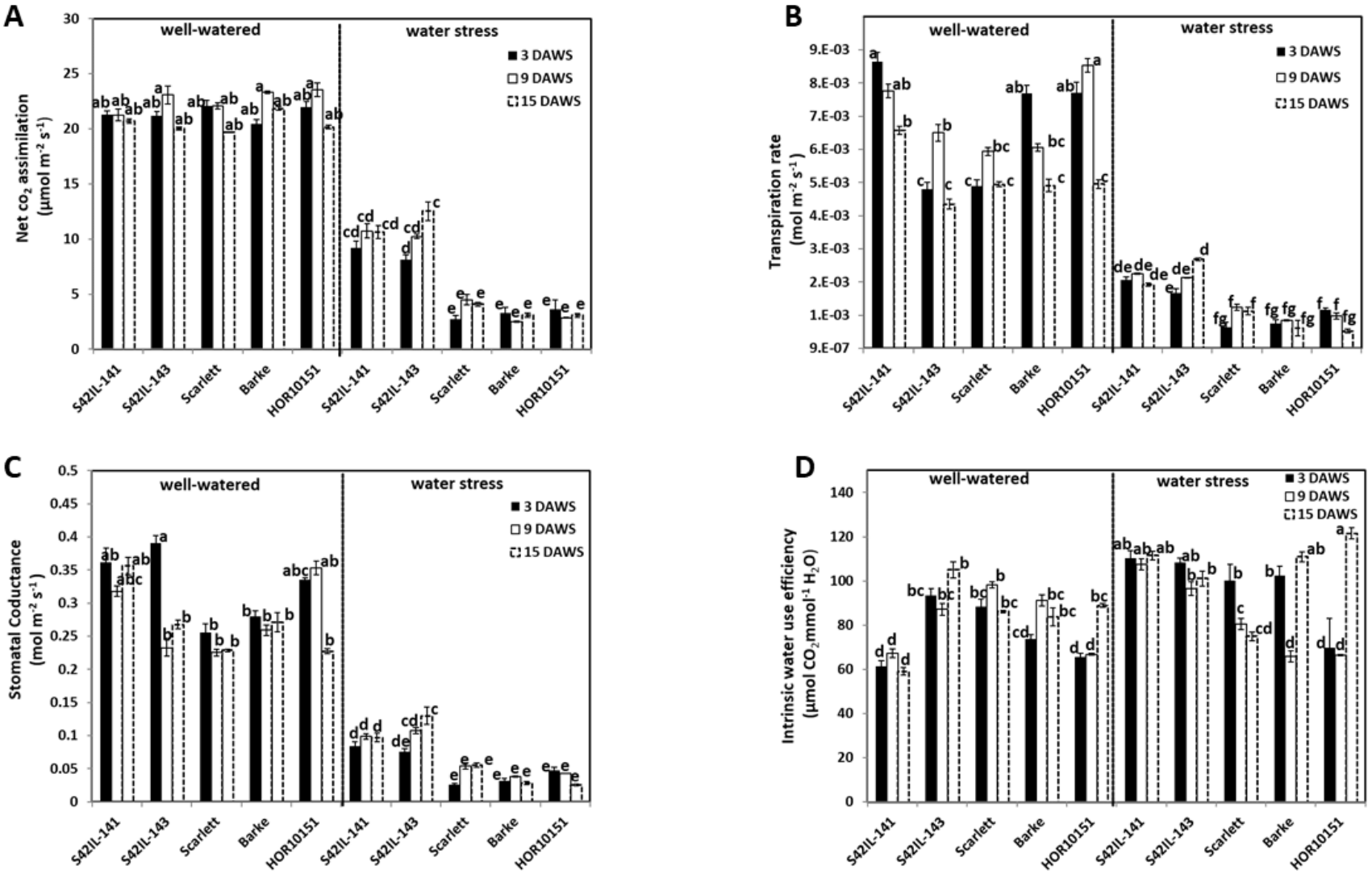

Figure 3.2 Gas exchange measurements of the different barley genotypes under well-watered and water stress treatment. Measurements were taken at 3, 9, and 15 days after water stress (DAWS), at booting, heading, and the onset of grain filling stages of spike development, respectively. Means and standard error bars are shown. The different letters indicate significant differences in treatment means based on Tukey's (HSD) test (n = 15). (A) The net CO_2 assimilation. (B) Transpiration rate. (C) Stomatal conductance. (D) Intrinsic water use efficiency. The figure was taken from Frimpong et al., 2021a.

3.3.2 Barley yield traits under water stress

Grain number per the main tiller had a significant genotypic, treatment, and genotype × treatment interaction effect in the 2019 experiment (Table 3.1). In 2018, we observed a significant ($P \leq 0.001$) treatment effect and a genotypic effect, but no genotype × treatment interaction (Table 3.1). Grain number per the main tiller ranged from 20 to 43 and from 2 to 24 for WW and WS treated plants, respectively (Table 3.2). The six-row barley, *HOR10151,* had the highest number of grains per main tiller (27, 43) under WW conditions in 2018 and 2019, respectively. *S42IL-141*and *S42IL-143* had the highest grain number per the main tiller (24, 24, and 22, 17) under WS conditions in 2018 and 2019, respectively (Table 3.2). *Barke* had the lowest grain number per the main tiller (20, 6, and 24, 2) in 2018 and 2019 under WW and WS conditions, respectively (Table 3.2). For all genotypes, we observed at least a 30% reduction in the grain number per the main tiller under WS for the 2018 and 2019 experimental years (Appendix 3.8).

WS plants showed significant variations in total grain weight per plant in both the 2018 and 2019 experimental years (Table 3.1). We observed at least a 76% reduction in grain weight for all the genotypes investigated (Appendix 3.8). Grain weight ranged from 9.8 to 14.0 g under WW and from 0.5 to 7 g under WS conditions (Table 3.2). WW *Barke* had the highest grain weight of 14 g in 2018 and 2019 (Table 3.2). *S42IL-141*and *S42IL-143* had the highest grain weight of 5 and 7 g under WS conditions in 2018 and 2019 (Table 3.2). *S42IL-141*and *S42IL-143* had more than 40% grain weight compared with *Barke, Scarlet,* and *HOR10151* under WS (Table 3.2). Grain weight correlated positively with grain number per main tiller (r=0.7), shoot fresh weight (r=0.55), plant height (r=0.76), transpiration (r= 0.83), stomatal conductance (r= 0.84), electron transport rate (r= 0.42). These correlations were significant ($P \leq 0.05$; Appendix 3.7). Grain weight correlated negatively with proline (r= -0.49) and iWUE (r= -0.41). These correlations were significant ($P \leq 0.05$; Appendix 3.7). WS plants had reductions of at least 38%, 30%, 18%, and 16% in spike number, grain number, shoot fresh weight, and shoot dry weight, respectively (Table 3.1 and Appendix 3.8).

Average DSI values based on the grain weight per plant ranged from 0.2 to 1.2 in 2018 and from 0.4 to 0.7 in 2019 in response to prolonged WS of 15 days, respectively (Appendix 3.9). *Barke* had the highest DSI in 2018 and 2019, which meant it was the most WS susceptible genotype (Appendix 3.9). *P5cs1*-introgression line *S42IL-143,* on the other hand, had the least DSI in both

2018 and 2019 (Appendix 3.9). Spike length had a significant genotype and genotype × treatment interaction effect in 2019 (Table 3.1). However, in 2018, a significant ($P \leq 0.01$) treatment effect and a genotypic effect were observed, with no interaction effect for spike length (Table 3.1). Spike length ranged from 4.5 to 10.7 cm and 6.2 to 12.7 cm under WS and WW conditions, respectively, across genotypes for both experimental years (Table 3.2). The spikes of the introgression lines *S42IL-143* and *S42IL-141* were the longest, both under WW and WS (Table 3.2). The six-row barley, *HOR10151,* had the shortest spike length, both under WW conditions and WS (Table 3.2). Generally, WS plants had spikes that were shorter by at least 18% (Appendix 3.8). Spearman correlation coefficient resulted in significant ($P \leq 0.001$) and positive correlations between spike length and grain weight (r=0.69), grain number (r=0.54), and plant height (r=0.36; Appendix 3.7). These data indicate that these reductions in spike length are associated with significant reductions in grain number and grain weight. Root dry weight had a significant ($P \leq 0.01$) treatment effect and a genotypic effect, with no interaction effect for both experimental years (Table 3.1). The average WW root dry weight (g) was 3.9 in 2019 compared with 4.9 in 2018. The average WS root dry weight (g) was 2.9 in 2019 compared with 3.9 in 2018 (Table 3.1). In 2019, *Barke* had the highest root dry weight (g) of 5.75 and 5.1 under WW and WS conditions, respectively. *Scarlett* and *S42IL-141* had the lowest root dry weight (g) of 2.9 and 4.1 under WW and WS, respectively. We found no significant differences in treatment effect, genotypic, and interaction effect in root/shoot ratio (dry weight) under WW and WS in the 2018 and 2019 experiments (Table 3.1).

3.3.3 Proline accumulation in barley leaves and immature spikes

WW spike proline content ranged from 48 to 198 µg/g FW (Figure 3.3A). WW *Barke* and *HOR10151* had the lowest and highest spike proline, respectively. WS spike proline ranged from 319 to 884 µg/g FW (Figure 3.3A). Again, *Barke* had the lowest while *S42IL-141* had the highest spike proline under WS (Figure 3.3A). WW leaf proline ranged from 42 to 117 µg/g FW and 23 to 60 µg/g FW in 2018 and 2019, respectively (Figure 3.3A and Appendix 3.10). *S42IL-143, HOR10151,* and *Scarlett* had the lowest leaf proline under WW (Figure 3.3A and Appendix 3.10). *S42IL-141*and *Barke* had the and highest leaf proline under WW (Figure 3.3A and Appendix 3.10). Proline accumulated markedly both in the immature spikes and the leaves of barley, fifteen days after WS onset, particularly among the introgression lines (Figure 3.3A and Appendix 3.10). WS leaf proline ranged from 79 to 680 µg/g FW and 99 to 696 µg/g FW in 2018 and 2019, respectively (Figure 3.3A and Appendix 3.10). *Scarlett, Barke and HOR10151* had the lowest leaf proline under

WS (Figure 3.3A and Appendix 3.10). *S42IL-143* and *S42IL-143* had the highest leaf proline under WS (Figure 3.3A and Appendix 3.10). In detail, the immature spikes of WS introgression lines *S42IL-141*and *S42IL-143* had the highest mean proline concentrations (884 and 803 µg/g FW, respectively; Figure 3.3A). In contrast, immature spikes of the elite genotypes *Barke, Scarlett*, and *HOR10151* had the lowest mean proline concentrations (319, 341, and 552 µg/g FW, respectively) under WS (Figure 3.3A). *HOR10151* and *Scarlett*, compared with the other three genotypes, exhibited an increase of about 198 µg/g FW of spike proline under WW (Figure 3.3A). Leaf proline concentrations in the genotypes expressed per unit dry weight (DW) showed significant ($P \leq 0.001$) differences as well (Appendix 3.2), which followed a similar trend to the proline concentrations measured per unit FW (Figure 3.3A and Appendix 3.2). Leaf proline per dry biomass ranged from 5 - 14 µmol/g under WW and 5 – 55 µmol/g under WS (Appendix 3.2). The introgression line *S42IL-143* had the highest proline concentration on a dry biomass basis, and the elite genotype, *Scarlett, was* the lowest (Appendix 3.2).

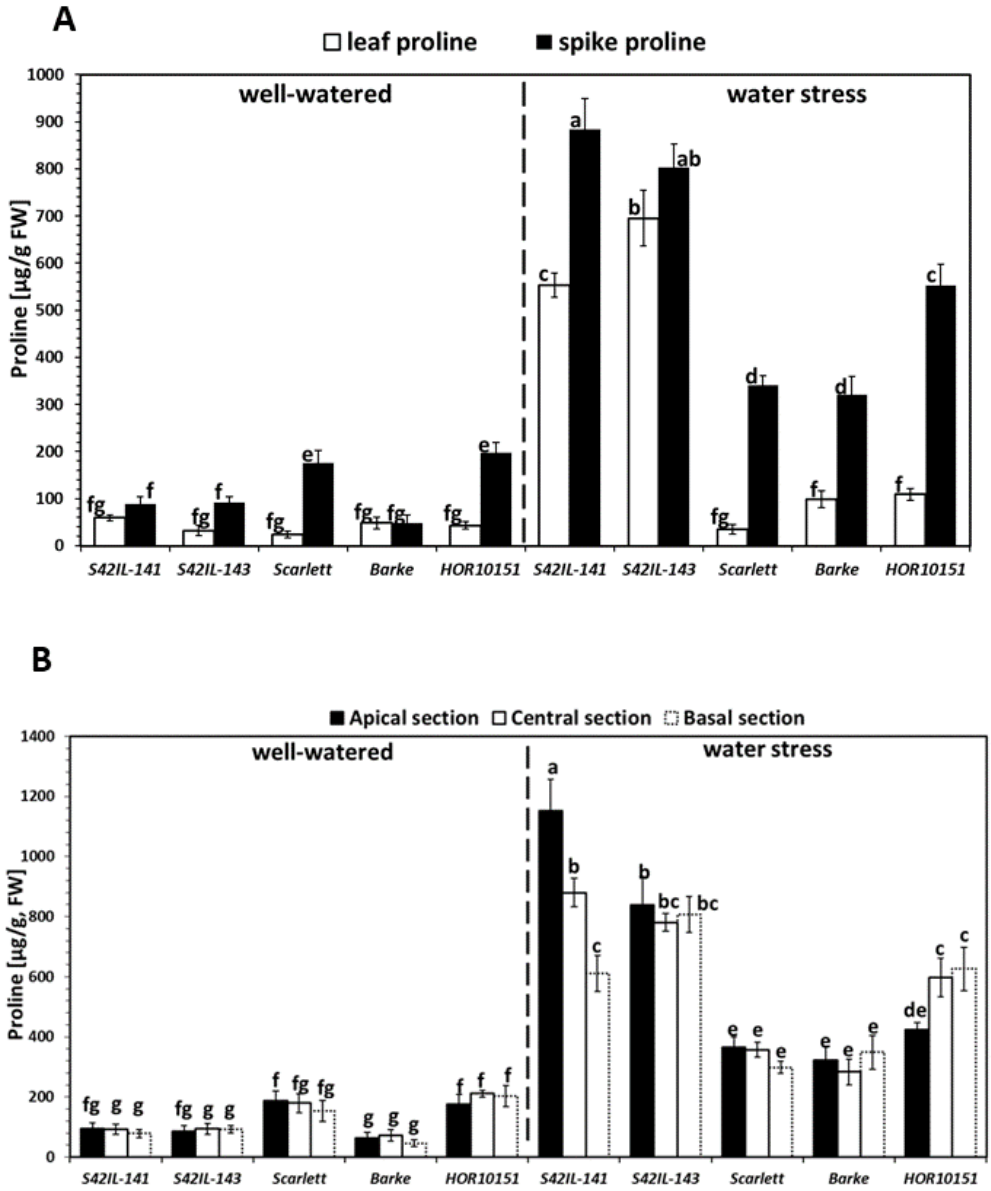

Figure 3.3 Proline accumulation to the spikes and leaves among the five barley genotypes 15 days after water stress. Different letters on the bars denote significant differences ($P \leq 0.05$) according to Tukey's HSD test (n = 6 for 3.3A, n ≥ 4 ⊁ 6 for 3.3B, as explained under section 3.2.6). (A) Proline concentration to the spike and leaf measurements for 2019 under well-watered and water stress conditions. (B) Spike proline concentrations along the axis of the different spike sections for the 2019 experiment under well-watered and water stress conditions. The figure was adapted from Frimpong et al., 2021a.

In the experiment of 2019, proline from the basal, central, and apical sections of the immature spikes showed significant differences among the genotypes, treatments, tissue type and their interactions (Figure 3.3B and Appendix 3). WW spike proline from the apical, central, and basal sections ranged from 63, 72, 45 to 186, 211, 202 µg/g FW, respectively (Figure 3.3B). WW spike proline of *Barke* (63, 72, 45 µg/g FW) from the apical, central, and basal sections, respectively, was the lowest (Figure 3.3B). The spike proline of the apical section of *Scarlett* (186 µg/g FW) was the highest among all the five genotypes under WW conditions. Spike proline from the central and basal sections of *HOR10151* (211, 202 µg/g FW) was the highest under WW conditions (Figure 3.3B). WS spike proline from the apical, central, and basal sections ranged from 322, 283, 299 to 1151, 879, 806 µg/g FW, respectively (Figure 3.3B). WS spike proline of *Barke* (322, 283 µg/g FW) from the apical and central sections, respectively, were the lowest while *Scarlett* was the lowest for the basal section (Figure 3.3B). Spike proline from the apical and central sections of *S42IL-141* (1151, 879 µg/g FW) was the highest under WS conditions (Figure 3.3B). WS spike proline from the basal section of *S42IL-143* (806 µg/g FW) was highest among all five genotypes (Figure 3.3B).

We found an increase of at least 40% in proline among the apical and central spike sections of *S42IL-141* (1151, 879 µg/g FW) compared with *HOR10151* (424, 597 µg/g FW), respectively (Figure 3.3B). This increase under WS did not follow a clear position-dependent gradient along the spike, although the introgression lines generally had at least a 10% higher spike proline (Figure 3.3B). There were no differences in proline content in the basal spike section of *S42IL-141* (612 µg/g FW) to the basal and central section of *HOR10151* (626, 597 µg/g FW) under WS (Figure 3.3B). In summary, section-specific differences existed considering the apical, central, and basal spike proline of *S42IL-141* and *HOR10151* individually under WS. Analysis of spike and leaf revealed a higher increase in proline concentration in the spikes than in the leaves for all genotypes under WS (Figure 3.3A-B). *P5cs1*-introgression lines had a significantly higher proline concentration in their developing spikes than the leaves under WS conditions, exhibiting an average difference of 30% (Figure 3.3A). Similarly, elite genotypes *Barke, Scarlett,* and *HOR10151* also had markedly more proline in their immature spikes than in the leaves under WS conditions (average difference of 134%, Figure 3.3A). However, in absolute terms, the introgression lines had higher spike proline content than the elite lines under WS (Figure 3.3A-B).3.3.4 Imaging of water-stressed spikes with MRI

To examine the effect of WS on seed abortion and filling early in the reproductive development phase (before grain maturation) of barley, we used MRI to scan immature spikes at the BBCH-scale, 83, *i.e.*, at the soft milky dough stage (Figure 3.4A-B and Appendix 3.11). We acquired amplitude images of 2D projections of barley spikes and evaluated them for the presence of initiated, developing, fully developed, sterile, or aborted seeds (Figure 3.4A-B, and Appendix 3.11). We did MRI scans of intact spikes at the early dough stage. Seed abortion was more prevalent among the elite genotypes (*Barke*, *Scarlett*, and *HOR10151*) than in the introgression lines (*S42IL-143* and *S42IL-141*) after prolonged 15 days of WS treatment (Figure 3.4A-B). Poor seed yield performance among the elite lines compared with the introgression lines under WS (Tables 3.1 and 3.2), were additionally revealed by several of our phenotypic traits (spike length, grain number, grain weight) similar to the MRI observations (Figure 3.4A-B). MRI scans (Figure 3.4A) of WW spikes of all genotypes showed a lower seed abortion rate, or no abortion at all, for all our barley types (Figure 3.4A). MRI scans of whole spikes grown under prolonged WS treatment, however, showed increased seed abortion (and in some cases complete spike abortion) among the elite genotypes, *Scarlett*, *Barke,* and *HOR10151*, much more so than the introgression lines, *S42IL-143* and *S42IL-141* (Figure 3.4B). For all genotypes, WS-treated main spikes were found to contain shrivelled or small developing grains (Figure 3.4B). Conversely, none of the spikes from WW plants showed shrunken seeds (Figure 3.4A).

Grain filling under water stress thus was reduced more among the elite genotypes than in the introgression lines (Figure 3.4B and Table 3.2). Also, under WS, the grain number in *Scarlett*, *Barke*, and *HOR10151* was reduced more than in *S42IL-143* and *S42IL-141* (Figure 3.4B). These results were confirmed by the 2019 seed count (Table 3.2). At harvest, under WS, the grain numbers of the main spike of *S42IL-143* and *S42IL-141* were 17 and 22, respectively; significantly higher than for the elite genotypes of *Scarlett*, *Barke,* and *HOR10151* (9.5, 2, and 4, respectively, Table 2). Again, similar to what we observed in the MRI projections (Figure 3.4A-B), phenotypic spike lengths of *S42IL-143* and *S42IL-141* were significantly longer than *Scarlett*, *Barke,* and *HOR10151* under WS (Tables 3.1 and 3.2). In summary, both MRI and phenotypic data confirmed that the introgression lines performed better in terms of seed yield than the elite lines under WS.

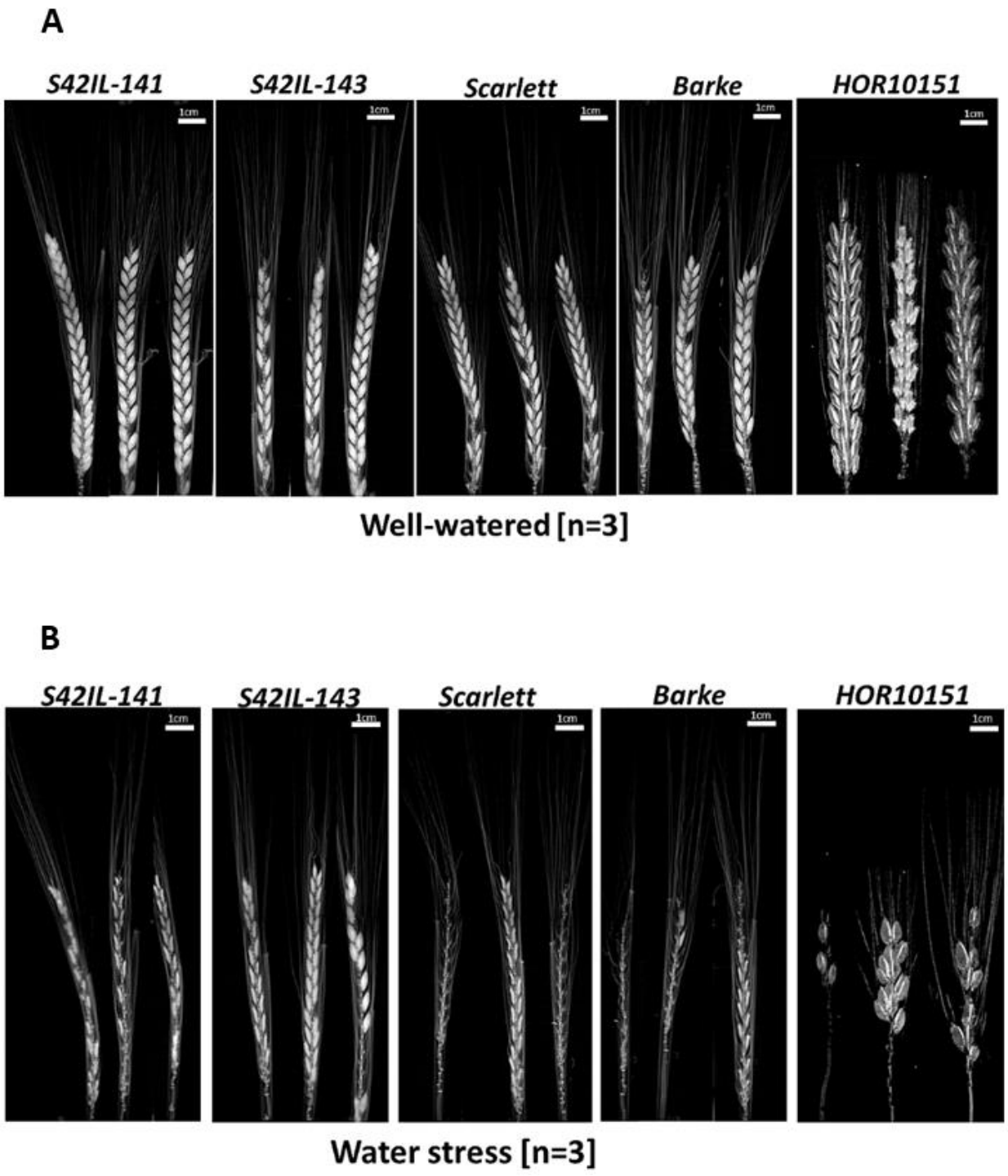

Figure 3.4 MRI amplitude images of barley main spikes at BBCH-scale 83, 15 days after stress application. Shown in panel A are main spikes of *S42IL-141*, *S42IL-143*, *Scarlett*, *Barke* and *HOR10151* grown under well-watered conditions; in panel B are shown spikes from plants grown under water stress (n=3, scale = 1). The figure was taken from Frimpong et al., 2021a.

3.4 Discussion

We characterized barley *P5cs1*-introgression lines and their physiological responses to reduced water availability. To consolidate our findings, we conducted two experiments in a greenhouse with a genotype panel including the same introgression lines and elite cultivars and with the same type of WS treatment applied at pre-flowering stages and kept as constant as possible throughout spike and seed development. Calculation of thermal sums for the whole duration of the two experiments shows that there was a difference of only about 5% in cumulated degree-days between the experiments of 2018 and 2019 (see Materials and Methods of this chapter). However, average daily temperatures were generally lower (i.e., below 25^{o}C) during and after flowering time in 2019 compared with 2018. DLI maximum values were very similar in both experimental years, whereas the minimum values were generally lower in 2018 compared with 2019 (Appendix 3.1). Overall, we obtained very similar results under WW conditions in the two subsequent experimental years (Appendix 3.5). We note that the average grain weight per plant at harvest under WW conditions was somewhat higher in 2019 compared with 2018, which might be linked to the lower daily temperatures during grain filling. Imposing WS conditions at booting stages resulted in overall more severe effects in 2019 compared with 2018, in particular leading to a more pronounced decrease in tiller numbers and shoot weight at harvest on average, considering all genotypes (Appendix 3.5). In addition, relative water content and net assimilation rates measured three days after the onset of the drought treatment were also lower in 2019 compared with 2018. Because these effects cannot be simply explained by temperature and DLI differences between the two years, we conclude that the first few days after the onset of WS led to a more pronounced decrease in soil water content values in 2019, as we can observe by comparing the time profile of pot soil moisture measured by time-domain-reflectance sensors (Appendix 3.2).

Drought is a complex trait and may lead to several morpho-physiological alterations within a plant. As an adaptation to drought stress, plants adjust their transpiration, photosynthesis, and thus WUE to prevent water loss and tissue damage while preserving the capacity for CO_2 assimilation (Belko et al., 2012; Li et al., 2017). Naz et al. (2014) and Muzammil et al. (2018) reported earlier on the same introgression lines, *S42IL-143* and *S42IL-141*, that they maintained 70% percentage relative leaf water content and displayed less severe wilting under WS. These findings were confirmed in our study. *S42IL-143* and *S42IL-141* maintained relative leaf water content of more than 70% even under WS (Table 3.2). On average, iWUE of the introgression and

elite lines under WS increased by 20% and 7%, respectively. The two introgression lines often had very similar responses in terms of net CO_2 assimilation, stomatal conductance, and transpiration rate under WS (Figure 3.2A-C). Yang et al. (2019) reported similar increases in iWUE (39% and 37%) for their contrasting rice hybrid cultivars under drought. WS caused an increase in the duration of spike development of all our barley genotypes. Earlier studies (Matin et al., 1989; Rani & Chaudhary, 2018) reported a prolonged duration in spike development due to WS at grain filling. The impact of WS on plant floral development generally might either cause a shortened or prolonged life cycle taking into account genotype specificity leading to an overall reduction in productivity (Boussora et al., 2019; Dolferus, 2014). Similarly, Li et al. (2017) reported wide variations in gas exchange parameters of drought-treated flag leaves compared with control conditions at the heading stages of drought-susceptible wheat cultivars compared with tolerant genotypes.

Water shortage during the post-anthesis period has been shown to significantly reduce harvest index and grain yield (Vadez et al., 2014). Due to the dehydrating effect of the WS treatment, 15 days after stress, the seeds of all genotypes became smaller (Figure 3.4B). All spikes showed strong reductions in spike length, seed size and number under WS conditions (Figure 3.4B). Consequently, there was a significant loss of 76% in total grain weight (all genotypes averaged; Table 3.1). The elite genotypes *HOR10151* or *Scarlett* and *Barke* showed pronounced leaf wilting symptoms, leaf dehydration, and significant seed abortion over time under WS (Table 3.2 and Figure 3.1, 3.4A-B). *IL143* and *IL141,* on the other hand, showed fewer wilting symptoms and less leaf dehydration (Figure 3.1). These effects were also reflected in the spikes values. Grain number and size of the introgression lines were also severely affected by WS but performed better than the elite genotypes (Figure 3.4A-B). These results are similar to studies obtained with computed tomography of wheat grains under WS or heat treatment, which showed shrivelled seeds in 3D projections (Schmidt et al., 2020; Tracy et al., 2017). These findings confirm that low water use during the post-anthesis period significantly reduces harvest index and grain yield (Vadez et al., 2014) and further highlights the critical importance of maintaining plant water status before and during the grain-filling period.

Prior studies have noted the importance of proline accumulation in many plant species as one of the most prominent changes in plant metabolism during drought and low soil water potential (Shinde et al., 2016). Contrary to proline accumulation in reproductive organs, proline

accumulation in leaves and roots has been extensively researched in earlier work (Verbruggen & Hermans, 2008). Proline accumulation in different plant organs is time-dependent and different concentrations have been reported for different plant species even under apparently similar stress scenarios. Proline accumulates rapidly and is degraded as the plant recovers (Dar et al., 2016; Heuer, 2016). Mickky et al. (2019) reported an increase in leaf proline content in ten wheat cultivars under drought conditions. They observed that proline accumulation was more pronounced in the drought-tolerant cultivars than in the sensitive ones. Similarly, in our investigation, we identified a more than 5-fold increase in leaf proline under WS in the tolerant introgression lines *S42IL-143* and *S42IL-141*, much higher than in the susceptible elite genotypes *Barke*, *Scarlett*, and *HOR10151* (Figure 3.3A-B). In a similar study, Templer et al. (2017) found a more than 5-fold increase for leaf proline content under drought and heat stress in their tolerant barley genotypes, as compared with control.

In the current study, we report higher proline contents in the reproductive structures of the WS immature spikes than in the leaves for all our barley genotypes. Accumulation of proline in undeveloped seeds of *Vicia faba* indicated that proline might play an essential role in the development of generative organs (Venekamp & Koot, 1984). Numerous studies reported high-proline contents in Arabidopsis seeds developing under water stress (Chiang & Dandekar, 1995; Schmidt et al., 2007), although data on proline accumulation in seeds of other species are more scarce (Dar et al., 2016). In our study, *P5cs1*-introgression lines accumulated the highest proline amounts (+30%) in their developing spike compared with leaves of elite genotypes (Figure 3.3A). These elite genotypes under WS had more than double the proline content in their immature spikes than in their leaves (Figure 3.3B).

Proline accumulation is a common physiological response to various stresses but is also part of the developmental program in generative tissues (Heuer, 2016). Proline may act as an osmoprotectant to protect the actively growing cellular and subcellular structures of the spike from dehydration under WS (Chiang & Dandekar, 1995). Further evidence suggests that proline is also involved in flowering and development both as a metabolite and possibly as a signal molecule (Dar et al., 2016). In our introgression lines, higher proline content was associated with higher relative leaf water content and a reduced wilting score (Table 3.1). As a protective mechanism to water stress, barley and wheat are known to allocate proline to actively growing vegetative tissues in shoots and roots. This is associated with reduced dehydration and wilting under water stress

(Bandurska et al., 2017; Delauney & Verma, 1993; Koenigshofer & Loeppert, 2019; Lee et al., 2009). In barley, Cai et al. (2020) reported that genotypes that show less leaf wilting under stress were able to osmotically adjust and better tolerate water shortage. In our study, *P5cs1*-introgression lines showed less severe leaf wilting (-40%) under WS compared with elite counterparts, which indicates reduced susceptibility to soil drying conditions.

We found a higher electron transport rate in the drought-tolerant introgression *S42IL-143* under WS than in the elite lines. As Shinde et al. (2016) emphasized, proline metabolism regenerates $NADP^+$ to provide a continued supply of electron acceptors for chloroplast electron transport. However, most drought susceptible genotypes like *Scarlett* fail to accumulate and use proline because of early leaf wilting and leaf death, resulting in proline reduction under drought conditions (Sayed et al., 2012). We found a higher net CO_2 assimilation rate, reduced transpiration, stomatal opening, intrinsic water use efficiency, and an active electron transport rate several days after WS in *P5cs1-S42IL-143* and *S42IL-141*compared with *Barke*, *Scarlett*, and *HOR10151* under WS (Figure 3.2A-D and Appendix 3.6). The net CO_2 assimilation rate of *S42IL-143* and *S42IL-141*was more than double the rate of *Barke*, *Scarlett*, and *HOR10151* under WS. *S42IL-143* and *S42IL-141*had a marginally (5%) higher stomatal conductance compared with the elite lines *Barke*, *Scarlett*, and *HOR10151* under WS. A contributing factor to the higher stomatal conductance and overall photosynthetic rate of the introgression lines under WS is their wild allele *P5cs1*. It has been shown to enhance the drought protective mechanism of proline biosynthesis (Allahverdiyev, 2015; Qamar et al., 2015; Sucre & Suárez, 2011; Szabados & Savouré, 2010). Several reports have already established that drought-tolerant barley genotypes accumulate proline to maintain stomatal conductance and active photosynthesis, even under dehydrating conditions, while drought-sensitive genotypes immediately reduce the stomatal aperture (Deng et al., 2013; Haddadin, 2015; Marok et al., 2013; Naz et al., 2014).

In the current study, our introgression lines achieved approximately double the grain weight of the elite lines under WS. Similar results were reported by Templer et al. (2017), who under drought conditions found a decrease of 65% in the harvest index in drought susceptible German cultivars, whereas drought-tolerant Mediterranean cultivars decreased not more than 14%. Based on a drought susceptibility index (DSI) which we calculated from the grain weight per plant, the most tolerant genotype was *S42IL-143* with the least DSI of 0.2, 0.4 in 2018, and 2019, respectively after fifteen days of WS (Appendix 3.9). Haddadin (2015) reported a DSI of >1 for

susceptible spring barley and <0.5 for tolerant types. A possible explanation for the higher grain yield under WS by *S42IL-143* and *S42IL-141*is the enhanced proline accumulation (Sayed et al., 2012). The observed proline increases due to WS also had significant correlations with reduced grain number, grain yield, plant height, and shoot biomass (Appendix 3.7). Sallam et al. (2018) previously reported an increase in grain proline and reduction in starch content due to heat stress, with significant reductions in yield per plot, grain yield per spike and 1000-kernel weight. Several studies reported a negative correlation between shoot proline concentration, growth and yield traits (Bandurska et al., 2017; Boussora et al., 2019). However, this negative correlation might be interpreted as an indication that the plants experienced water stress and do not necessarily reflect a causal relation between proline accumulation and reduced plant growth and yield. On the contrary, in our study, we found drought-induced proline accumulation in the spikes of barley genotypes harbouring the wild variant of *P5cs1* to be associated with improved drought tolerance, as expressed in their photosynthetic capacity, seed number and final yield under water stress.

Proline is likely associated with the energy demand of young dividing cells during resumed growth following stress relief (Verslues and Sharma, 2010). This possibility is also corroborated by findings at the transcriptional level in which *P5CS2*, *P5CR* (encoding *P5C* reductase), and *ProDH1* are upregulated in meristematic tissues such as root tips, shoot apices, lateral buds, and the inflorescence (Sharma et al., 2011). Young spike tissues of all our genotypes at their early grain development of the soft milky dough stages had accumulated more proline. Most root and leaf cells that are actively dividing, elongating and developing tend to accumulate more proline under drought (Dar et al., 2016), which contributes to coping with drought stress during reproductive development and to increasing proline sink strength in those tissues (Kishor & Sreenivasulu, 2014). The question of where proline synthesis primarily occurs in plants upon imposition of stress still remains unclear. Proline metabolism varies among organs and tissues, and transport of proline within the plant is likely to occur (Koenigshofer and Loeppert 2019).

3.5 Conclusion

Prolonged water stress at the booting stage caused a significant reduction of 76% of barley grain weight per plant. We found drought-inducible proline accumulation to be not exclusive to the leaves, rather proline significantly accumulates in barley spikes, and it may contribute to the maintenance of seed initiation and grain filling processes by preventing excessive water loss. Spike proline content under water stress increased by more than 30% compared with leaf proline content in all our barley genotypes. *P5cs1*-introgression lines harbouring a wild barley allele involved in the proline biosynthetic pathway had higher leaf and spike proline contents as well as a higher grain yield under water stress conditions. Generally, the elite lines were much more affected by water stress than the introgression lines on several morpho-physiological traits. *S42IL-143* and *S42IL-141* carrying the *P5cs1* allele from wild barley showed an increased water stress tolerance associated with a reduced seed abortion rate and a higher spike proline concentration compared with Scarlett, *Barke,* and *HOR10151*. Our results suggest that proline accumulation in spikes of barley under water stress plays a major role in the maintenance of final seed yield.

CHAPTER 4

Proline mediated drought tolerance in barley (*Hordeum vulgare* L.) isogenic line is associated with lateral root growth at the seedlings stage

(*This chapter is based on Frimpong et al., 2021b: Plants, https://doi.org/10.3390/plants10102177 with minor modifications to the text in general to improve clarity*).

Felix Frimpong[12*], Michael Anokye[3], Carel W. Windt[1], Ali A. Naz[4], Michael Frei[5], Dagmar van Dusschoten[1] and Fabio Fiorani[1]

[1] IBG-2 Plant Sciences, Institute for Bio- and Geosciences, Forschungszentrum Jülich GmbH, 52425 Jülich, Germany
[2] CSIR-Crops Research Institute of Ghana, P. O. Box 3785, Kumasi
[3] Technische Universität München, Center of Life and Food Sciences Weihenstephan, Germany
[4] University of Bonn, Institute of Crop Science and Resource Conservation, 53115 Bonn, Germany
[5] Institute of Agronomy and Plant Breeding, Justus-Liebig-Universität Gießen, 35390, Germany

***Correspondence:** Felix Frimpong: f.frimpong@fz-juelich.de

Abstract

A vigorous root system in barley promotes water uptake from the soil under water-limited conditions. We investigated three spring barley genotypes with varying water stress responses using rhizoboxes at the seedlings stage. The genotypes comprised two elite German cultivars, *Barke* and *Scarlett*, and a near-isogenic line, *NIL 143*. The isogenic line harbors the wild allele *pyrroline-5-carboxylate synthase1-P5cs1*. Root growth in rhizoboxes under reduced water availability conditions caused a significant reduction in total root length, rooting depth, root maximum width, and root length density. On average, root growth was reduced by more than 20% due to water stress. Differences in organ proline concentrations were observed for all genotypes, with shoots grown under water stress exhibiting at least 30% higher concentration than the roots. Drought induced higher leaf and root proline concentrations in *NIL 143* compared with any of the other genotypes. Under reduced water availability conditions, *NIL 143* showed less severe symptoms of drought, higher lateral root length, rooting depth, maximum root width, root length density, and convex hull area compared with *Barke* and *Scarlett*. Within the same comparison, under water stress, *NIL 143* had a higher proportion of lateral roots (+30%), which were also placed at deeper substrate horizons. *NIL 143* had a less negative plant water potential and higher relative leaf water content and stomatal conductance compared with the other genotypes under water stress. Under these conditions, this genotype also maintained an enhanced net photosynthetic rate and exhibited considerable fine root growth (diameter class 0.05-0.35 mm). These results show that water stress induces increased shoot and root proline accumulation in the *NIL 143* barley genotype at the seedlings stage and that this effect is associated with increased lateral root growth.

Keywords: Drought, Fine roots, lateral roots placement, near-isogenic barley lines, proline, root system architecture

4.1 Background

Climate variability and ever more frequent drought events negatively affect cereal production (Jiménez-Donaire et al., 2020; Liu & Basso, 2020; Ochieng et al., 2016). Therefore, developing adapted cultivars that maintain yields under reduced water availability is essential (Challinor et al., 2014). Crop adaptation requires that cultivars adjust their above and below-ground morphology, physiology, and biochemical traits to the stress scenario (Calleja-Cabrera et al., 2020; Raza et al., 2019). As a critical below-ground trait, the ability to develop deep roots enable the entire plant to adjust to or avoid reduced water availability (Uga et al., 2013; Arai-Sanoh et al., 2014; Lynch & Wojciechowski, 2015). Changes in root growth and root architecture to short- and long-term drought scenarios are considered possible adaptation strategies that may help stabilize leaf water potential under stress (Tardieu et al., 2018). Essential root traits associated with maintaining plant productivity under drought include small fine root diameters Yamauchi et al. (2021), long specific root length, root area, root angle, and considerable root length density, especially within deep soil horizons containing available water (Comas et al., 2013; Ostonen et al., 2007; Weemstra et al., 2020).

Under drought conditions, proline plays a role in stabilizing cell membranes, maintaining cell osmotic balance, preventing electrolyte leakage. Moreover, proline functions as an antioxidant regulating the levels of reactive oxygen species for continual plant growth and development (Guan et al., 2020). Biancucci et al. (2015) showed that proline affects the size of the root meristematic zone in Arabidopsis, indicating that proline in this location could modulate and control cell division and differentiation. Proline is known to act as an osmoprotectant in barley, and its accumulation is known to stabilize whole-plant photosynthetic health, growth, metabolism and grain yield under water deficit (Ghaffari et al., 2019; Rady et al., 2016; Teixeira et al., 2020). Plant proline homeostasis is determined by its biosynthesis, catabolism, and transport. Proline is generally synthesized through the glutamate pathway during osmotic stress. In the glutamate pathway, proline is produced from glutamate by *pyrroline-5-carboxylate* synthetase (*P5CS*) and *pyrroline-5-carboxylate* reductase 1 (*P5CR1*) enzymes (Guan et al., 2020). In modern barley (*Hordeum vulgare* ssp. Vulgare), breeding efforts to widen the limited genetic diversity successfully used wild relatives (*Hordeum vulgare* ssp. Spontaneum) as donors of exotic germplasm to enhance cultivated varieties (Schmalenbach et al., 2008). For instance, through repeated backcrossing of wild barley to recurrent parent *Scarlett*, followed by rounds of selfing and marker-assisted

selection, alleles from wild barley, *ISR42-8,* have been introduced into *Scarlett* (Naz et al., 2014; Honsdorf et al., 2014). Muzammil et al. (2018) found that the ancestral allele of *pyrroline-5-carboxylate synthase1* promotes proline accumulation and drought adaptation in cultivated *Scarlett* barley.

Naz et al. (2014) studied barley introgression lines and detected quantitative trait loci (QTLs) which underpin root traits such as root dry weight, root length, and root volume, all of which promote improved fitness under drought stress. They showed that beneficial alleles underlying the measured root traits originated from wild barley, suggesting the role of specific introgressions in cultivated barley from the wild progenitor. The introgression lines bear the wild allele at *pyrroline-5-carboxylate synthase1* (*P5cs1*) locus (Schmalenbach et al., 2008), which enhances proline accumulation in leaves leading to a comparatively higher yield under drought (Muzammil et al., 2018). However, the introgression lines' purity can be improved as they may possess a significant fraction of the wild barley donor genome (Honsdorf et al., 2017). Further breeding efforts advanced such introgressions into a more homogeneous near-isogenic type (Hernandez et al., 2020). Our present work studied the near-isogenic barley line *NIL 143,* which was generated from several backcrossing between the drought-tolerant introgression line *S42IL-143* and the cultivar *Scarlett* followed by selfing and aided by marker-assisted selection (Shrestha, 2020).

So far, few abiotic stress studies have explicitly focused on the contribution of proline to root development in domesticated crops. Drought-inducible proline accumulation in the root apex contributes to 50% osmotic adjustment in the region (Sharp et al., 1990; Voetberg & Sharp, 1991). Through repeated experiments, Shrestha, 2020 demonstrated that the drought recovery rate in *NIL 143* was superior to *Scarlett*. Therefore, we assume that more proline in *NIL 143* would translate to more energy generation for root growth. We investigated whether proline accumulation contributes to barley lateral root growth under water stress.

For these reasons, our current study investigated the hypothesis that proline accumulation contributes to barley root growth under water stress. We evaluated the root-specific traits of contrasting barley genotypes for proline accumulation in different plant organs and their coping strategies under reduced water availability. To this end, we used a non-invasive root phenotyping tool, soil-filled rhizoboxes, and combined it with root imaging and scanning (Nagel

et al., 2012; Wasson et al., 2020). Soil-filled rhizoboxes make it feasible to evaluate the overall differences among crop varieties and further diagnose specific key below-ground traits that might underlie such variations. Using rhizoboxes, Avramova et al. (2016) demonstrated that phenotypic differences between maize genotypes differing in drought tolerance under field conditions could already be identified at the seedling stage by measurements of root length and shoot biomass. We characterized root architectural traits and root placement (roots positioning within the substrate profile) under water stress and control conditions in barley genotypes, including a breeding line which harbours the wild allele at the *P5cs1* locus. We further assessed whether proline accumulation differs between roots and the shoots of the contrasting barley genotypes and if that led to changes in net CO_2 assimilation rate, transpiration rate, plant water potential, leaf chlorophyll content, roots, and shoots morphology.

4.2 Materials and Methods

4.2.1 Plant growth condition

All plants were grown in a greenhouse at the Institute of Biosciences and Geosciences, IBG-2, Plant Sciences, Forschungszentrum Jülich GmbH, Germany, August 2020. In the present study, we used two elite German cultivars of malting spring barley (*Hordeum vulgare* L.), '*Scarlett'* and '*Barke'* and a near-isogenic line, *NIL 143*, carrying the wild barley introgression at the *P5cs1* locus derived from the *S42IL-143* genotype (Shrestha, 2020). *Barke* was also selected as a negative control with an independent genomic background compared with *Scarlett* and the progeny. Plants were grown under day/night minimum and maximum temperatures of ~ 20 ± 2 and 30 ± 2 °C, 16 h during the day and ~ 19 ± 2 and 20 ± 2 °C 8 h during the night, respectively at an air humidity of 65 ± 5 %. The average vapour pressure deficit inside the greenhouse was approximately 4.7 kPa. Barley seeds for each genotype were pre-germinated on filter paper inside a closed petri dish (between two filter papers imbibed with 1.25 mL of water). Germinated seeds with roots of about 1 cm at one day after sowing were transplanted into rhizoboxes (outer dimensions: 60 × 30 × 3 cm), manually filled with approximately 6L of loose sieved black peat soil (Graberde; Plantaflor Humus, Vechta, Germany; containing N, 120 mg L^{-1}; P_2O_5, 20 mg L^{-1}, and K_2O, 170 mg L^{-1}). A two centimetres space was left at the upper open surface of the rhizoboxes

to allow subsequent watering. The greenhouse's daily light integral ranged between a minimum and maximum of 9 and 19 (mol m^{-2} day^{-1}), respectively.

4.2.2 Experimental design

The experiment was a 2×3 factorial, randomized complete block design with six replications. There were three genotypes (*Barke, Scarlett,* and *NIL 143*) and two watering regimes (well-watered and water stress) as fixed factors. Soil water content (SWC) of well-watered (WW) was maintained at 70% (g/g). After pre-drying the substrate, SWC of water stress (WS) at the start of the experiment was 40% (g/g) and was further reduced to 6% (g/g) after 17 days. The SWC of both treatments was measured with the aid of a weighing scale, KERN-DBS60-3 (Kern & Sohn GmbH, Balingen, Germany). The estimated soil water potential (Ψ_{soil}) of WW and WS treatments after 17 days were -0.032 and less than -1.513 MPa, respectively. Ψ_{soil} values were estimated using an eight-point water retention curve fitted with the van Genuchten model (van Genuchten, 1980). Before transplanting seedlings to the rhizoboxes, both WW and WS treatments were supplied with 500 mL and 200 mL of water, respectively, to enable stand establishment. Subsequently, 60 mL of water was provided three times a week for the WW treated plants. The WS treated plants received a one-time watering of 60 mL (BBCH=12), after which no further watering was given until the experiment was terminated 17 days after sowing. The rhizoboxes upper open surface was covered with a one-centimetre layer of white plastic beads to prevent water evaporation from the substrate in both treatments. The rhizoboxes were arranged in containers. They were inclined by approximately 45° towards the horizontal plane, with seedlings planted close to the rhizoboxes transparent plexiglass view pane, such as root growth could be visualized. A black plastic sheet was used to cover the transparent side plate of the rhizoboxes to prevent light from reaching roots at all times. The black sheet was only removed briefly for acquiring images (Appendix 4.1).

4.2.3 Root and shoot measurements

Shoot height, leaf length, and leaf width were manually measured with a ruler at harvest (17 days after the start of WS treatment). The number of leaves was manually counted at harvest. Leaf area at harvest was determined destructively using an LI-3100C area meter (LI-COR, Lincoln, NE, USA). At harvest, shoot and root fresh and dry weights (g) of plants were determined using a weighing scale XS4002S (Mettler Toledo, Switzerland). Dry weights were measured after samples had been oven-dried at 65ºC for 72 h. Leaf turgid weight was determined after storing fresh leaves

overnight in deionized water. The leaf turgid, fresh, and dry weight measurements were used to calculate the percentage relative leaf water content (RWC, (Tahara et al., 1990). A detailed description of measured plant traits and the units is shown below (Appendix 4.2).

Root measurements were performed using a mobile imaging box for rhizoboxes described by Nagel et al. (2009). Images of every plant's root system were manually captured twice every week, starting two days after transplanting. Subsequent photos of the roots were taken until harvest (17 days after sowing). The resulting image sequences were analyzed using the PaintRHIZO software version 3.1 for root growth image analysis by following the protocol developed by (Nagel et al., 2009). The software allows extraction of visible root traits, such as total visible root lengths, seminal root lengths, lateral root lengths, root system depth and width, root surface coverage area, root length density, and root homogeneity distribution along the vertical axis of the rhizoboxes. At harvest, roots were manually washed under running tap water to remove substrate debris. Washed roots were stored in a cold room (10 °C) in Falcon tubes containing 50% ethanol and subsequently scanned at 300 dpi with Epson Expression 12000XL 6.2, Regent Instruments INC., Québec Country, Canada, calibrated for image analysis. The scanned total root system was then analyzed with Regent instrument WinRHIZO^{TM} software, version 2017. Main root traits extracted from the analysis included were total root length (cm), root length distribution per diameter classes (cm^{-1}), root volume (cm^3), root length density (total root length/root volume, cm cm^{-3}), average root diameter (mm), seminal root number, and root distribution homogeneity ratio (convex hull area/root volume, cm^{-1}).

4.2.3.1 Gas exchange and chlorophyll fluorescence

We measured six plants per genotype and per treatment, 15 days after WS, using two portable infrared gas analyzers, LI-6800 (LI-COR Inc., Lincoln, NE, USA) with fluorometer MPF-551065 and MPF-831744, respectively. Measurements were made on fully expanded leaf number four. Light-adapted values included net CO_2 assimilation (*A*) and stomatal conductance (*gsw*). Measurements were performed with CO_2 concentration and temperature in the leaf chamber maintained at 400 µmol mol^{-1} and 25ºC, respectively. Photosynthetic photon flux density was kept at 1500 µmol $m^{-2}s^{-1}$ by a red light-emitting diode (LED) light source and at ambient relative humidity 55% ± 5. All light-adapted parameters were measured between 10:00 am and 12:00 noon to lessen possible variation in parameter values due to diurnal light intensity fluctuations. Intrinsic

water use efficiency (iWUE; *A/gsw*) was calculated as the ratio between net CO_2 assimilation and stomatal conductance. Chlorophyll fluorescence parameter, Fv/Fm, a measurement of the quantum yield of PSII, was performed on fully expanded leaf number four after dark-adaption in a dark room for 45 minutes. The measurement took place between 20:00 and 21:00. Dark-adapted measurements were performed with the control mode of the LI-6800 set off while the measuring beam was turned on. Multiphase flash was set up as follows; the red target was kept at 8000 µmol $m^{-2}s^{-1}$, phases 1 to 3 maintained at 300 ms with a 25 % ramp. The output rate and margin were set to 500 Hz and 5 points, respectively.

4.2.3.2 Plant water potential

Plant water potential was determined on fully expanded leaf number four, using the Scholander pressure bomb method (Scholander et al., 1964). Measurement of plant water potential was performed between 12:00 noon and 2:00 pm, when water potential variation is expected to change slowly due to comparatively higher light intensity. Six plants per genotype per treatment were measured 17 days after WS (BBCH = 15, Meier, 2001). Leaves were covered with opaque aluminium foil for about 30 minutes, typically recommended Scholander et al. (1964), before excision to stop leaf transpiration, allowing the leaf water potential to come into equilibrium with the plant water potential. The entire leaf wrapped in aluminium foil was sealed inside the pressure chamber (Model 1000 Pressure Chamber, PMS Instrument Company, Albany, SE, USA) but leaving the cut end exposed outside the chamber. Water expulsion at the cut surface of the leaf was viewed using a stereomicroscope stereo microscope.

4.2.3.3 Proline content determination

Leaf-blades (leaf), leaf sheaths (stem), and root tissues were separated after harvest for proline analysis using six replicates. Samples were quickly placed in small labelled rubber vials, closed and submerged in liquid nitrogen, and later stored in a -80 °C freezer for later use. The stored leaf, stem, and root tissue samples were manually crushed into a fine powder using a ceramic mortar and pestle in liquid nitrogen. The extraction of proline from each tissue was performed by adopting the colourimetric proline determination method described by Bates and Waldren 1973 and Frimpong et al. (2021) with slight modifications. Acid-ninhydrin was first prepared by warming 2.5 g ninhydrin in 60 mL glacial acetic acid and 40 mL 6 M phosphoric acid, with vigorous agitation using a magnetic stirrer until completely dissolved. The solution was covered

with aluminium foil to avoid exposure to light and stored at a 4ºC refrigerator for 24 hours before use. 100 mg of the crushed tissue samples were then weighed into chilled 2 mL Eppendorf tubes and homogenized in 1.5 mL of 3 % sulfosalicylic acid by vortexing. The mixture was centrifuged at 12000 rpm for 10 mins. After centrifugation, 500 µL of sample extract (supernatant) was mixed with 500 µL of glacial acetic acid and 500 µL of ninhydrin reagent in glass tubes (fitted with lids). The mixture was then vigorously vortexed, incubated at 95-100ºC for 45-60 minutes in an HB-1000 Hybridizer oven (UVP, Inc., Cambridge, UK). The reaction was terminated quickly with ice. The reaction mixture was extracted with 1.5 mL toluene, mixed vigorously by vortexing. The solution was left at room temperature for 30 mins to settle until the two phases separated. 100 µL of the chromophore (upper phase) was then carefully pipetted into 96 well plates and read with a microplate reader (Synergy™ 2 Multi-Mode, BioTek, Winooski, Vermont, USA). An empirical calibration curve based on eight points of proline standard concentrations (0, 10, 20, 30, 50, 70, 90, and 100 µg/g) yielded a linear regression, r^2=0.99 between proline concentration and the measured absorbance at 520 nm, which was used to determine the proline concentrations in the samples (Frimpong et al., 2021a).

4.2.3.4 Chlorophyll determination

Chlorophyll-a was determined after harvesting six replicates of whole leaves of fully expanded leaf number four of each genotype between 9:00 am and 10:00 am CET using the protocol by Markwell et al. (1986) with slight modifications. 40 mg of the crushed leaf tissues were weighed into 2 mL Eppendorf tubes with two metal balls pre-cooled in liquid nitrogen. From here, the reaction was cooled on ice, 1 mL of 95% ethanol (EtOH) plus 0.5 g of $CaCO_3$ was added, and the samples were extracted by milling and homogenizing twice (1 min intervals) in pre-cooled Eppendorf-racks using Retsch tissue lyser MM400 (Retsch GmbH, 42781, Haan, Germany, www.retsch.com). Samples were then centrifuged for 15 min at 4°C at 12000 rpm. After centrifugation, the supernatant was carefully transferred into new 2 mL Eppendorf tubes on ice. The extraction was repeated by adding 1 mL EtOH+$CaCO_3$ to the pellet, milled twice in the pre-cooled racks, centrifuged, and supernatants combined. 200 µL of supernatant was diluted with 800 µL EtOH+$CaCO_3$ and mixed by inverting. Three portions of 150 µL of each sample and a blank (EtOH+$CaCO_3$) were pipetted into a 96-well plate on ice and absorbance measured at 470, 649, and 664 nm using the microplate reader (Synergy™ 2 Multi-Mode, BioTek, Winooski, Vermont,

USA). The calculation for chlorophyll a was done using the equation (7) according to (Porra et al., 1989):

Chlorophyll-*a* [µg/mL]: $\frac{\mathbf{13{,}36 \times A664 - 5{,}19 \times A649}}{\boldsymbol{weight\ of\ sample} \times \mathbf{10} \times \mathbf{1/0.45}}$ ……..... (7),

where A649/664 = absorbance at 649 and 664 nm, respectively, and a factor of 10 is used to account for the dilution factor.

4.3 Results

4.3.1 Root and shoot growth traits of barley lines under water stress

We measured barley seedlings' root and shoot growth traits under well-watered (WW) and water stress (WS) treatments 17 days after the stress onset. Shoot fresh weight (g) differed significantly among treatments but not between genotypes or genotype x treatment interaction (Table 4.1). *Barke* shoot fresh weight (g) of 1.28 was the largest, while 0.9 recorded for *Scarlett* was the smallest under WW (Table 4.1). Under WS, a marginal increase in shoot fresh weights was detected for *Barke* and *NIL 143* compared to *Scarlett* (Table 4.1). Shoot dry weight (g) also was significantly different ($P \leq 0.001$) between treatments, but not between genotypes or in terms of interaction (Table 4.1). *NIL 143* and *Barke* shoot dry weight of 0.14 were the largest, while 0.10 recorded for *Scarlett* was the smallest genotype under WW (Table 4.1). Under WS, *Barke* shoot dry weight (g) of 0.07 was the largest, while 0.05 recorded for *NIL 143* was the smallest (Table 4.1). Root dry weight (g), on the other hand, significantly differed ($P \leq 0.05$) between treatments as well as genotypes and in terms of interaction (Table 4.1). *NIL 143* root dry weight (g) was the largest 0.04, while *Scarlett* was the smallest 0.02, under WW (Table 4.1). *Barke* root dry weight (g) of 0.02 was the largest, while *Scarlett* and *NIL 143* were the smallest 0.01 under WS (Table 4.1). The root/shoot ratio was significantly different ($P \leq 0.001$) between treatments but not between genotypes or in terms of interaction (Table 4.1). Under WW, *NIL 143* and *Barke* root/shoot ratio were the largest 0.25, while 0.23 recorded for *Scarlett* was the smallest (Table 4.1). Under WS, *Barke* root/shoot ratio was the largest 0.32, with a larger percentage change variation of 28%, while that of *NIL 143* and *Scarlett* was the smallest 0.28, compared to WW (Table 4.1). Except for the treatment effect, no significant genotypic or interaction effect was observed for shoot height (cm), leaf number, and leaf length (cm) under both WW and WS (Table 4.1). *Barke* had the largest

maximum leaf width, 0.7 cm, under WW and WS. Leaf area (cm^2) was different ($P \leq 0.001$) between treatments but not genotypes or the interaction (Table 4.1). *NIL 143* had the largest leaf area, 25.0, while *Scarlett* had the smallest, 16.8, under WW (Table 4.1). *Barke* leaf area (cm^2) was the largest, 13.3, while *NIL 143* had the smallest, 8.9, under WS (Table 4.1).

Table 4.1 Root and shoot traits among the different barley genotypes 17 days after the onset of water stress in the rhizoboxes experiment.

Trait	**Treatment**				
	Genotype	**WW**	**WS**	**P-Values**	**% change**
Shoot height (cm)	*Barke*	22.8 ± 1.8^{ab}	16.3 ± 1.3^{c}	Genotype^{NS}	-29
	Scarlett	20.8 ± 0.9^{abc}	17.6 ± 1.3^{bc}	Treatment***	-9
	NIL 143	25.8 ± 1.6^{a}	16.2 ± 1.6^{c}	G×T^{NS}	-30
Leaf number	*Barke*	3.2 ± 0.2^{ab}	2.5 ± 0.2^{b}	Genotype^{NS}	-21
	Scarlett	3.5 ± 0.2^{ab}	2.7 ± 0.2^{b}	Treatment ***	-24
	NIL 143	4.0 ± 0.3^{a}	2.8 ± 0.3^{b}	G×T^{NS}	-30
Leaf length (cm)	*Barke*	11.4 ± 0.9^{a}	8.8 ± 0.3^{ab}	Genotype^{NS}	-23
	Scarlett	9.4 ± 1.0^{ab}	9.35 ± 0.4^{ab}	Treatment ^{NS}	-5
	NIL 143	8.8 ± 1.7^{ab}	8.8 ± 0.9^{b}	G×T^{NS}	-27
Max-Leaf width (cm)	*Barke*	0.73 ± 0.1^{a}	0.66 ± 0.01^{bc}	Genotype***	-9
	Scarlett	0.57 ± 0.01^{ab}	0.52 ± 0.02^{c}	Treatment *	-10
	NIL 143	0.62 ± 0.01^{abc}	0.53 ± 0.03^{c}	G×T^{NS}	-16
Leaf area (cm^2)	*Barke*	23.9 ± 2.5^{a}	13.3 ± 2.8^{bc}	Genotype^{NS}	-45
	Scarlett	16.8 ± 2.5^{ab}	11.1 ± 2.5^{c}	Treatment ***	-34
	NIL 143	25.0 ± 2.5^{a}	8.9 ± 2.5^{c}	G×T^{NS}	-64
SFW (g)	*Barke*	1.28 ± 0.1^{a}	0.48 ± 0.1^{b}	Genotype^{NS}	-60
	Scarlett	0.90 ± 0.1^{a}	0.45 ± 0.1^{b}	Treatment ***	-46
	NIL 143	1.33 ± 0.2^{ab}	0.48 ± 0.1^{b}	G×T^{NS}	-57
SDW (g)	*Barke*	0.14 ± 0.01^{a}	0.07 ± 0.001^{bc}	Genotype^{NS}	-49
	Scarlett	0.10 ± 0.01^{ab}	0.06 ± 0.001^{bc}	Treatment ***	-40
	NIL 143	0.14 ± 0.02^{a}	0.05 ± 0.001^{c}	G×T^{NS}	-60
RDW (g)	*Barke*	0.035 ± 0.002^{ab}	0.020 ± 0.01^{c}	Genotype**	-75
	Scarlett	0.023 ± 0.002^{c}	0.018 ± 0.01^{c}	Treatment ***	-28
	NIL 143	0.041 ± 0.002^{a}	0.018 ± 0.01^{c}	G×T*	-128
Root/Shoot ratio	*Barke*	0.25 ± 0.021^{ab}	0.32 ± 0.02^{a}	Genotype^{NS}	+28
	Scarlett	0.22 ± 0.021^{b}	0.28 ± 0.02^{ab}	Treatment ***	+27
	NIL 143	0.25 ± 0.01^{ab}	0.28 ± 0.003^{ab}	G×T^{NS}	+12

SF*W: shoot fresh weight. SDW: shoot dry weight. RDW: root dry weight. G×T: genotype x treatment interaction, NS: No significance. Data are means ± standard error (n=6) after the two-way ANOVA. Significant differences between the genotypes and treatment based on the Tukey test (α = 0.05) are indicated with different letters. Asterisks: *, **, *** follows the standard probability values of 0.05, 0.01, and 0.001, respectively. Genotypes were compared within and between treatments. The % change was calculated as the mean difference between drought and control conditions expressed as a percentage. The table was taken from Frimpong et al., 2021b.*

4.3.2 Effect of water stress on barley seedlings physiological traits

Chlorophyll-a (µg mL^{-1}) under WW was not different among the genotypes (Table 4.2). Under WS, Chlorophyll-a content differed significantly among the genotypes and between treatments and the interaction was significant (Table 4.2). Under WS, *NIL 143* had the highest chlorophyll content of 2.7, while 1.17 recorded for *Scarlett* was the lowest (Table 4.2). Chlorophyll-a significantly ($P \leq 0.05$) correlated positively with stomatal conductance (0.46), % relative leaf water content (0.46), leaf area (0.46), root length density (0.53) and lateral root length (0.48, Appendix 4.3). Plant water potential (Ψ_{plant}, MPa) of all genotypes under WW treatment varied only marginally, and there were no significant differences between the genotypes (Table 4.2). Ψ_{plant} of -0.17 recorded for *NIL 143* was the highest, while *Barke* was the lowest -0.39, under WW. Water stress significantly ($P < 0.001$) decreased the Ψ_{plant} of all the genotypes (Table 4.2). However, the Ψ_{plant} between the genotypes varied significantly ($P < 0.05$), with *Barke* and *Scarlett* exhibiting the lowest values of -1.2 compared with -0.17 for *NIL 143*, with no significant interaction under WS (Table 4.2). Significant differences in treatment, genotypes, and interaction effects were found in RWC. WS significantly decreased RWC ($P < 0.001$; Table 4.2), with *NIL 143* showing higher RWC compared to *Barke* and *Scarlett*. All genotypes maintained RWC above 85% under WW treatment, with no significant differences (Table 4.2). Percentage reductions in leaf RWC were minimal for *NIL 143* (41 %) compared with 51-53 % for *Barke* and *Scarlett* (Table 4.2). The relative leaf water content correlated significantly and positively ($P \leq 0.05$) with root length density (0.72), lateral root length (0.70), and total root length (0.66, Appendix 4.3).

Net CO_2 assimilation rate (µmol m^{-2} s^{-1}) under WW was not different among the genotypes (Table 4.2). Under WS, the net CO_2 assimilation rate was significantly different between the genotypes, treatment and the interaction were significant (Table 4.2). Under WS, *NIL 143* had the highest (19) net CO_2 assimilation rate, while *Barke* had the lowest (12) and a more considerable percentage change (63%, Table 4.2). Under WW, stomatal conductance (mol m^{-2} s^{-1}) was not different among the genotypes averaging at 0.5 (Table 4.2). Under WS, stomatal conductance was

significantly different among the genotypes, treatment and the interaction were significant (Table 4.2). Under WS, *NIL 143* had the highest (0.18) stomatal conductance, while *Barke* had the lowest (0.09). Stomatal conductance significantly ($P \leq 0.01$) correlated positively with RWC (0.86), root length density (0.63), lateral root length (0.83), and total root length (0.73). Under WW, transpiration rate (mol m^{-2} s^{-1}) was not different among the genotypes averaging at 7.7×10^{-3} (Table 4.2). Under WS, the transpiration rate was significantly different among the genotypes, treatment and the interaction were significant (Table 4.2). Under WS, *NIL 143* had the highest (3.7×10^{-3}) transpiration rate, while *Barke* had the lowest (1.9×10^{-3}) and a more considerable percentage change (77%, Table 4.2).

Table 4.2 Physiological plant traits of different barley genotypes 17 days after onset of water stress in the rhizoboxes experiment.

Parameter	Treatment				
	Genotype	WW	WS	P-Values	% change
Chlorophyll-a (μgmL^{-1})	*Barke*	2.37 ± 0.3^{a}	1.07 ± 0.1^{b}	Genotype***	-24
	Scarlett	2.14 ± 0.01^{a}	1.17 ± 0.01^{b}	Treatment***	-19
	NIL 143	2.89 ± 0.2^{a}	2.69 ± 0.01^{a}	G×T *	-7
Fv/Fm	*Barke*	0.8 ± 0.01^{a}	0.81 ± 0.01^{a}	Genotype ^{NS}	0
	Scarlett	0.81 ± 0.01^{a}	0.81 ± 0.01^{a}	Treatment ^{NS}	0
	NIL 143	0.81 ± 0.01^{a}	0.81 ± 0.01^{a}	G×T^{NS}	0
A ($\mu mol\ m^{-2}\ s^{-1}$)	*Barke*	32.3 ± 0.3^{a}	12.0 ± 0.6^{d}	Genotype ***	-63
	Scarlett	27.5 ± 1.9^{b}	14.4 ± 0.3^{d}	Treatment***	-48
	NIL 143	30.4 ± 0.9^{ab}	19.4 ± 0.4^{c}	G×T***	-36
gsw ($mol\ m^{-2}\ s^{-1}$)	*Barke*	0.6 ± 0.06^{a}	0.086 ± 0.01^{c}	Genotype *	-86
	Scarlett	0.5 ± 0.02^{a}	0.105 ± 0.02^{c}	Treatment***	-80
	NIL 143	0.5 ± 0.02^{a}	0.183 ± 0.02^{b}	G×T***	-65
E ($mol\ m^{-2}\ s^{-1}$)	*Barke*	$8.2\times10^{-3} \pm 1.7\times10^{-4a}$	$1.9 \times10^{-3} \pm 2.3\times10^{-4c}$	Genotype **	-77
	Scarlett	$7.2\times10^{-3} \pm 1.5\times10^{-4a}$	$2.2\times10^{-3} \pm 4.9\times10^{-4c}$	Treatment ***	-69
	NIL 143	$7.8\times10^{-3} \pm 2.3\times10^{-4a}$	$3.7\times10^{-3} \pm 1.7\times10^{-4b}$	G×T***	-53
iWUE ($\mu mol\ CO_2\ mmol^{-1}\ H_2O$)	*Barke*	52.6 ± 3.14^{c}	134.41 ± 3.14^{a}	Genotype **	-155
	Scarlett	54.5 ± 3.14^{c}	122.5 ± 3.14^{a}	Treatment***	-125
	NIL 143	56.4 ± 3.44^{c}	104.2 ± 3.14^{b}	G×T***	-85
Plant water potential, Ψ (Mpa)	*Barke*	-0.394 ± 0.2^{ab}	-1.23 ± 0.11^{c}	Genotype **	-75
	Scarlett	-0.293 ± 0.2^{ab}	-1.26 ± 0.11^{c}	Treatment***	-121
	NIL 143	-0.170 ± 0.2^{a}	-0.17 ± 0.11^{bc}	G×T^{NS}	-78
% RWC	*Barke*	98 ± 2.0^{a}	46 ± 1.8^{c}	Genotype *	-51
	Scarlett	88 ± 2.0^{ab}	41 ± 1.8^{c}	Treatment***	-53
	NIL 143	95 ± 2.2^{a}	59 ± 1.7^{b}	G×T*	-41

*Fv/Fm: maximum quantum efficiency of PSII, A: Net CO_2 assimilation, E: transpiration, gsw: stomatal conductance, iWUE (A/gsw): intrinsic water use efficiency, % RWC: percentage relative leaf water content, G×T: genotype x treatment interaction, NS: no significance. Data are means ± standard error (n=6) after the two-way ANOVA. Significant differences between the genotypes and treatment based on Tukey's post hoc test (α = 0.05) are indicated with different letters. Asterisks: *, **, *** follows the standard probability values of 0.05, 0.01, and 0.001, respectively. The % change was calculated as the mean difference between drought and control conditions expressed as a percentage. The table was taken from Frimpong et al., 2021b.*

4.3.3 Effect of water stress on proline content in barley seedlings shoots and roots

We characterized proline accumulation in leaf, stem, and roots under WW and WS conditions by measuring concentrations in the shoot (leaf and stem) and root tissues at the seedlings stage 17 days after stress. Under WW, the leaf, stem, and root proline concentration (FW, µg/g) were very low (~35) and not significantly different among all the genotypes (Figure 4.1). Under WS, root proline concentration was significantly higher ($P < 0.001$, +40%) for *NIL 143* compared to the elite lines (Figure 4.1A). Root proline significantly and negatively ($P \leq 0.01$) correlated with chlorophyll-a (0.47), stomatal conductance (0.64), % relative leaf water content (0.62), leaf area (0.62), root length density (0.60), lateral root length (0.65), and total root length (0.71, Appendix 4.3). Leaf proline significantly ($P \leq 0.05$) correlated negatively with plant water potential (0.50, Appendix 4.3). A significant interaction ($P < 0.01$) effect was detected for the leaf and root proline concentrations of the barley seedlings. However, the elite lines accumulated more proline in the stem compared to *NIL 143* under WS, even though no significant differences ($P > 0.05$) were detected (Figure 4.1B). Significant differences ($P < 0.001$) in treatment but not genotype and no significant interaction effect were found for stem proline concentration. Quantification of leaf proline concentration (FW, µg/g) in the *NIL 143* together with the elite lines showed a significant increase ($P < 0.001$) in proline accumulation in *NIL 143* up to 906 compared with 600 and 544 for *Scarlett* and *Barke*, respectively under WS (Figure 4.1C).

4.3.4 Barley seedlings root architectural traits under water stress

The growth of all the root system traits (total root length, root max width, depth, laterals, seminal roots, and convex hull area) was strongly reduced over time after 14 days of onset of WS (Figure 4.2 A-F). WS significantly decreased ($P < 0.001$, -20%) the length of the visible root system for all the genotypes (Figure 4.2 A-F). Again, for none of the visible root system traits we found significant genotype × treatment interaction (Figure 4.2). However, we observed genotypic differences in root system depth, width, lateral root length, convex hull area, but not in total and seminal root lengths over time (Figure 4.2 A-F). Under WW, genotypic differences in lateral roots, depth and convex hull area were evident early, 14 days after WS start and lasted until the 17th day of harvest (Figure 4.2 A-F). *NIL 143* exhibited considerable lateral root length relative to the shoots compared to *Barke* and *Scarlett* under WW (Table 4.1, Figures 4.2A, 4.2D and 4.2F). *NIL 143* had the highest total root length (274 cm), depth (51 cm), width (15 cm), lateral root length (22 cm),

convex hull area (548 cm^2), and seminal root length (252 cm, Figure 4.2A-F) after 17 days under WW. *Scarlett* had the lowest total (226 cm), lateral (10 cm), and seminal root lengths (225 cm, Figures 4.2A, 4.2D, and 4.2F) after 17 days under WW.

Under WS, we found significant differences among the genotypes in maximum root width, depth, lateral root length, convex hull area but not in total root length and seminal root length (Figure 4.2A-F). Under WS, genotypic differences in lateral roots, width and convex hull area became evident early, 16 days after WS start and lasted until harvest (Figure 4.2 A-F). WS *Barke* had the longest total root length (130 cm) and seminal root length (125 cm, Figure 4.2A and F). WS *NIL 143* had the biggest root system width (34 cm), deeper depth (11 cm), longer laterals (8 cm), largest convex hull area (211 cm^2, Figures 4.2 B-E) 17 days after onset of stress.

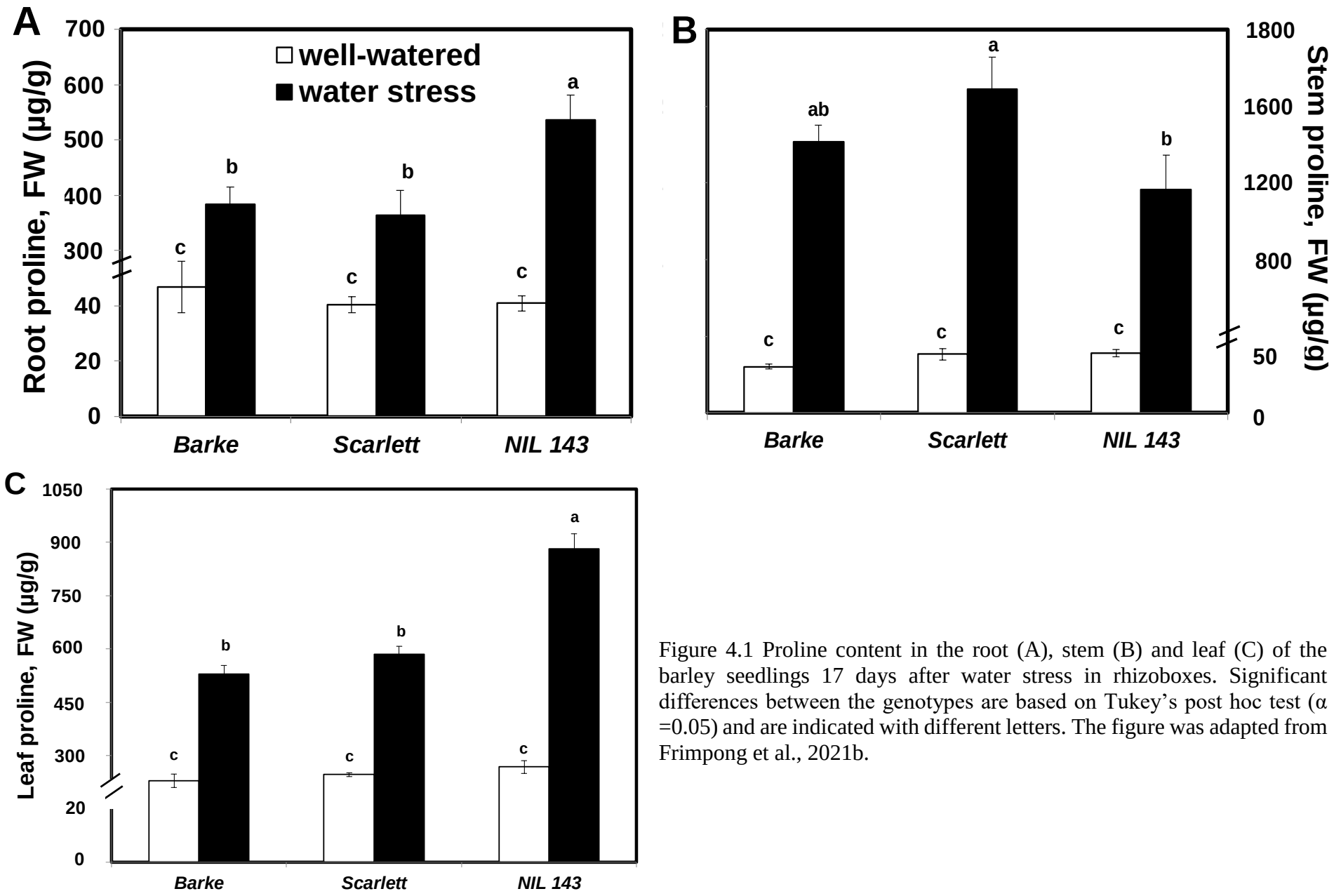

Figure 4.1 Proline content in the root (A), stem (B) and leaf (C) of the barley seedlings 17 days after water stress in rhizoboxes. Significant differences between the genotypes are based on Tukey's post hoc test (α =0.05) and are indicated with different letters. The figure was adapted from Frimpong et al., 2021b.

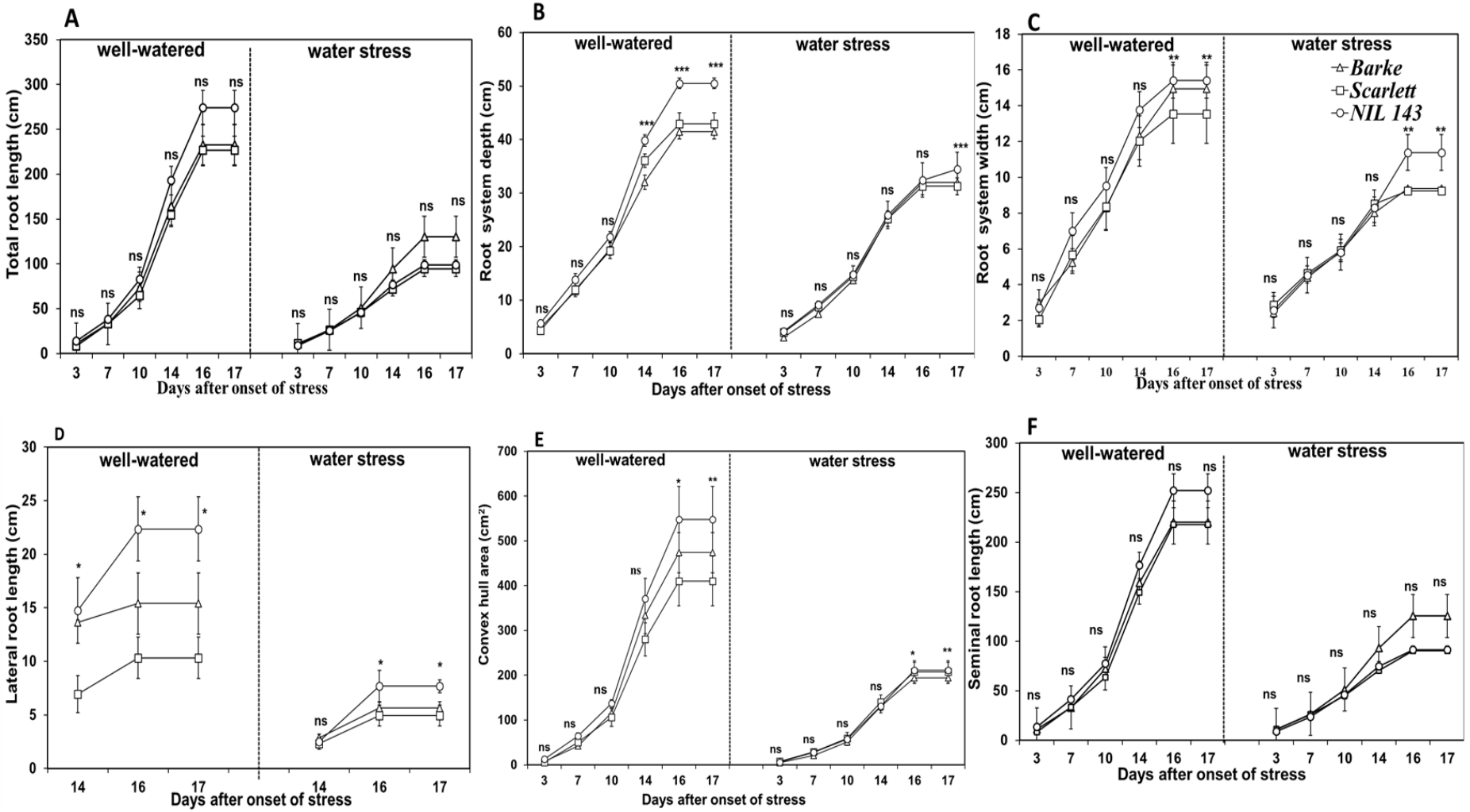

Figure 4.2 Visible root system growth at seedlings stage over time among the different barley genotypes under well-watered and water stress conditions in rhizoboxes. Plotted are the means fitted with the standard error, n=6. Significant differences ($\alpha = 0.05$) among genotypes and treatments at specific days after stress are indicated with asterisks *, **, *** which follow the standard probability values of 0.05, 0.01, and 0.001, respectively. Shown are total root length (A), root system depth (B), root system width (C), lateral root length (D), convex hull area (E) and seminal root length (F). The figure was taken from Frimpong et al., 2021b

Under WS, we found significant differences among the genotypes in maximum root width, depth, lateral root length, convex hull area but not in total root length and seminal root length (Figure 4.2 A-F). Under WS, genotypic differences in lateral roots, width and convex hull area became evident early, 16 days after WS start and lasted until harvest (Figure 4.2 A-F). WS *Barke* had the longest total root length (130 cm) and seminal root length (125 cm, Figure 4.2 A and F). WS *NIL 143* had the biggest root system width (34 cm), deeper depth (11 cm), longer laterals (8 cm), largest convex hull area (211 cm^2, Figure 4.2 B-E) 17 days after onset of stress.

We evaluated the different barley seedlings' root placement (root positioning within the substrate profile) under limited water conditions. *NIL 143* had the longest and deepest root system, as shown by total root length, seminal root length and lateral root length under WW (Figure 4.3 A, C and E). *Scarlett* had the shortest and most shallow lateral roots (Figure 4.3E), even under WW conditions, compared with the other two genotypes. This trend was, however, different under WS. Under WS, *Barke* had the longest and deepest root system, as shown by total root length and seminal root length values (Figure 4.3 B and D), but not the lateral roots. Under WS, *NIL 143* had significantly deeper and longer lateral roots among the genotypes (+33%, Figure 4.3F).

Overall, non-destructive root measurements could estimate approximately 30% of the total root system compared with the root scanned after destructive harvest (Figure 4.2A and 4.4A). WinRHIZO scans of the barley seedlings root system 17 days after onset of WS showed a significant ($P < 0.001$) reduction in total root length, total root length density, average max root diameter, and seminal root number (-20%, Figures 4.4 A, C, E & F). The root architectural traits analyzed included total root length (cm), root volume (root diameter × length, cm^3), total root length density (root length/volume, cm cm^{-3}), root distribution homogeneity ratio (root convex hull area/volume, cm^{-1}), the average diameter (mm), and seminal root number 17 days after onset of WS (Figure 4.4 A-F). We observed significant genotype x treatment interaction only in the root volume, total root length density and cumulative fine root length. Under WW, total root length was not significantly different among the genotypes (Figure 4.4A). Under WW, *NIL 143* had the highest total root length (1209, Figure 4.4A). Under WS, *NIL 143* (438), *Barke* (450), and *Scarlett* (433) recorded no significant differences in total root length (Figure 4.4A). Under WW, root volume (cm^3) was significantly different among genotypes (Figure 4.4B). Under WW, *NIL 143* (0.44) had the highest root volume compared to the elite lines (0.30, Figure 4.4B). We observed genotypic

differences in the root volume under WS (Figure 4.4B). Under WS, *Barke* (0.27) had the highest root volume compared to *NIL 143* (0.18) and *Scarlett* (0.19), respectively (Figure 4.4B).

Under WW, the seminal root number was not different among the genotypes (Figure 4.4F). *Barke* had the highest seminal root number (12), compared to (11) and (10) counted for *NIL 143* and *Scarlett*, respectively. (Figure 4.4F) under WW. We observed no genotypic differences in the seminal root number under WS, with an average of ~8 for all the genotypes (Figure 4.4F). Under WW, total root length density (cm cm^{-3}) was significantly different among the genotypes (Figure 4.4C). *NIL 143* had the highest root length density (3064, Figure 4.4C) under WW. We observed genotypic differences in the root length density under WS (Figure 4.4C). *NIL 143* had the highest total root length density (2446), while *Barke* had the lowest (1646, Figure 4.4C) under WS. Under WW, root homogeneity (cm^{-1}) was not different among the genotypes (Figure 4.4D). *Barke* showed the poorest root homogeneity (182, Figure 4.4D) under WW. Genotypic differences were observed in the distribution of root homogeneity ratio (cm^{-1}) under WS (Figure 4.4D). *NIL 143* showed a better root homogeneity ratio (175), while *Barke* had the worst (144, Figure 4.4D) under WS. Under WW, the average max root diameter (mm) was not different among the genotypes (Figure 4.4D). *NIL 143* had the largest average max root diameter (0.4, Figure 4.4E) under WW. All genotypes under WS had a similar average max root diameter (~0.3) with no differences (Figure 4.4E). No differences were observed under both WW and WS in the total root length by diameter distribution between 0 to 1.65 mm (Figure 4.5A-B). However, in our study, *NIL 143* produced more lateral roots (diameter <0.35 mm) under WS. *NIL 143* cumulative fine root length within the first seven diameter classes up to 0.35 mm was higher compared to *Barke* (+22%) and *Scarlett* (+6%) under WS (Figure 4.5C). Lateral root length significantly ($P \leq 0.001$) correlated positively with total root length (0.80, Appendix 4.3).

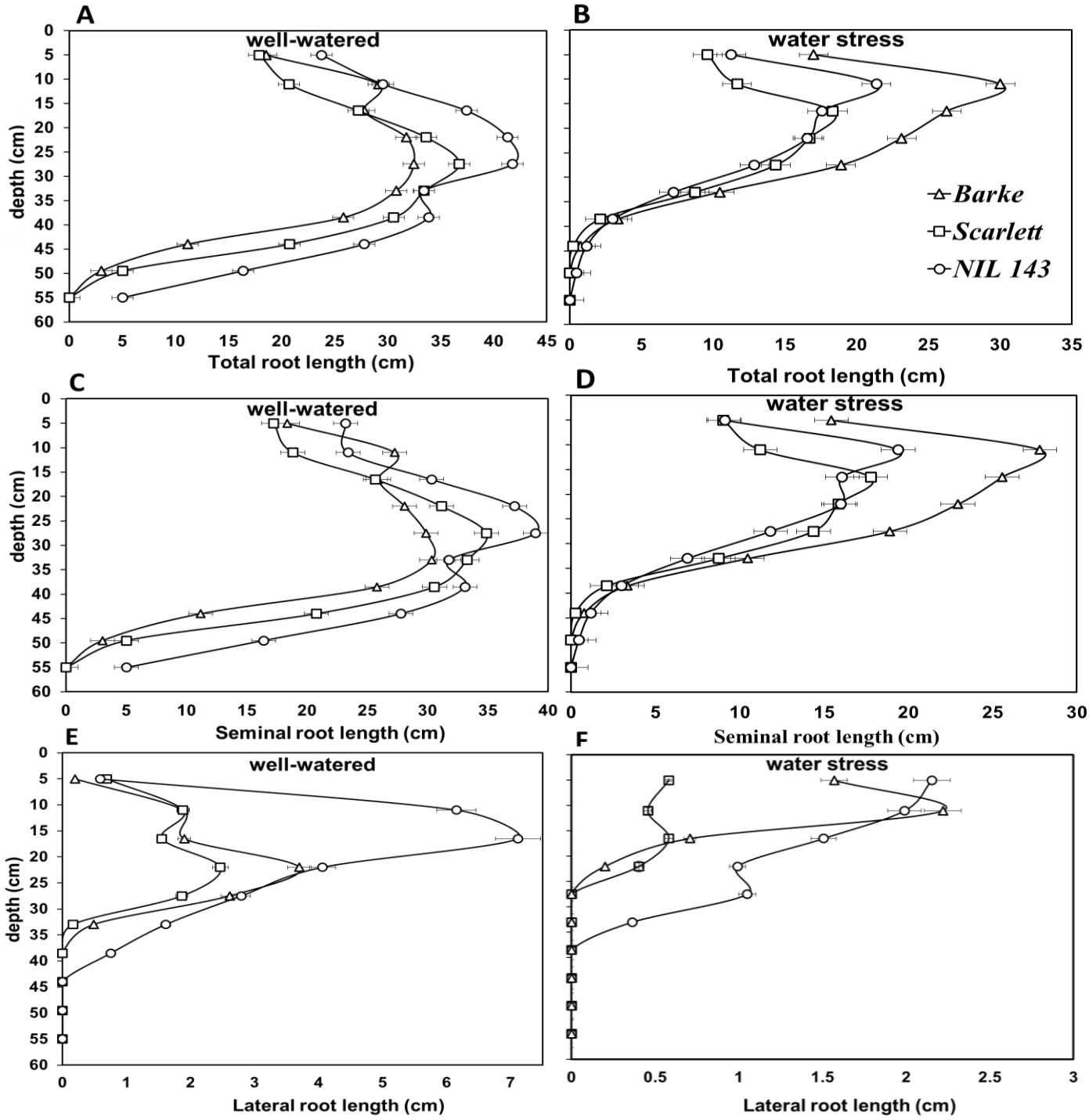

Figure 4.3 Visible root system placement along the soil profile (0-55 cm) in rhizoboxes for the different genotypes under WW and WS conditions 17 days after onset of stress. Shown are visible total root length under WW conditions (A), visible total root length under WS conditions (B), visible seminal root length under WW conditions (C), visible seminal root length under WS conditions (D), visible lateral root length under WW conditions (E), and visible lateral root length under WS conditions (F). Each point represents root growth averaged among six rhizoboxes per treatment (n=6). Bars on top are standard errors. The figure was taken from Frimpong et al., 2021b.

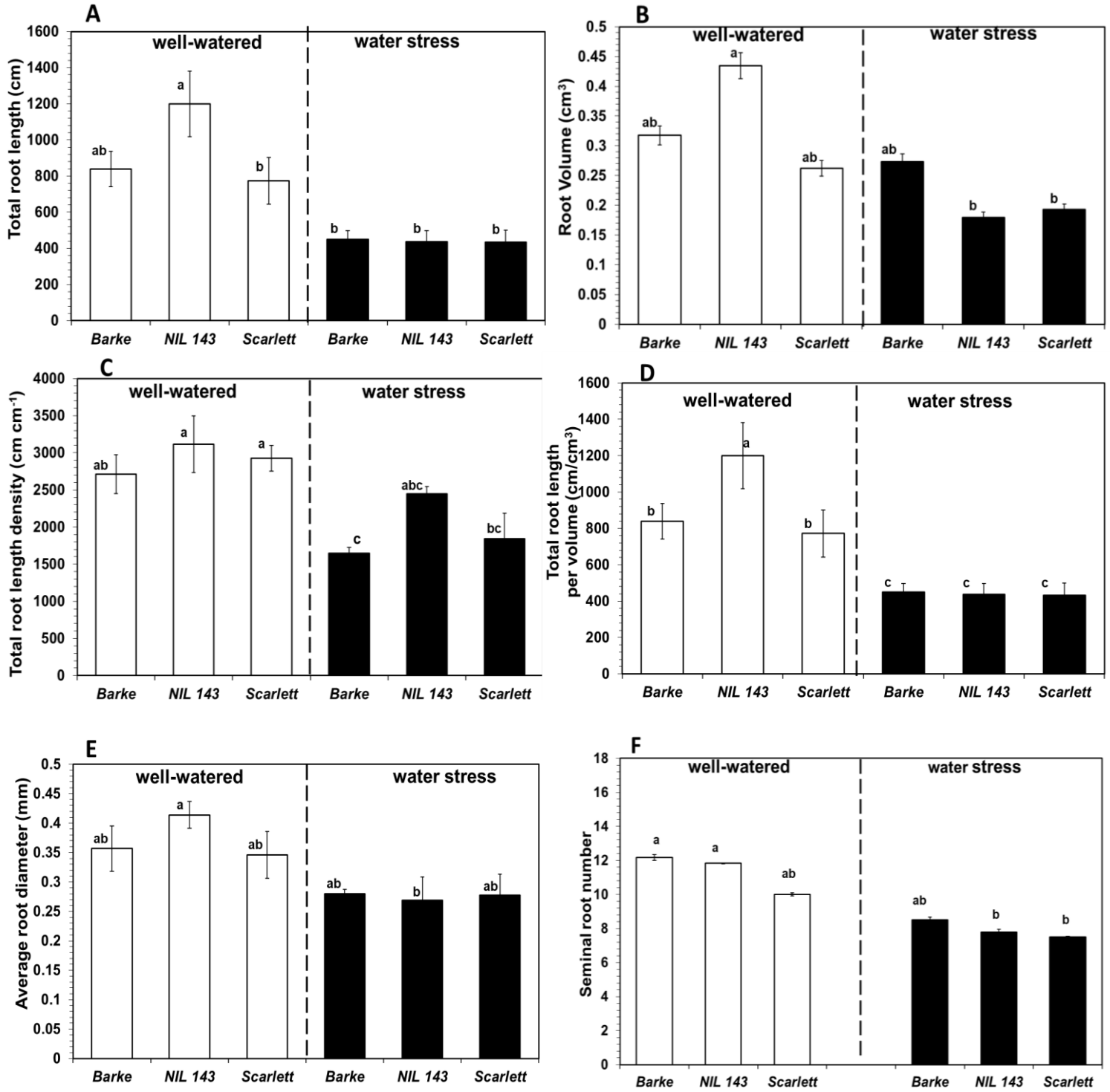

Figure 4.4 Root architectural traits of the different barley genotypes 17 days after the start of the experiment under well-watered and water stress treatments in rhizoboxes. In the panels are: (A) total root length, (B) root volume, (C) total root length density, (D) root distribution homogeneity ratio, (E) average root diameter, and (F) seminal root number. Plotted are the means and their respective standard error. Letters on the bars denote significant differences ($\alpha = 0.05$) based on Tukey's *post hoc* test for pair-wise comparison, n=6. The figure was taken from Frimpong et al., 2021b.

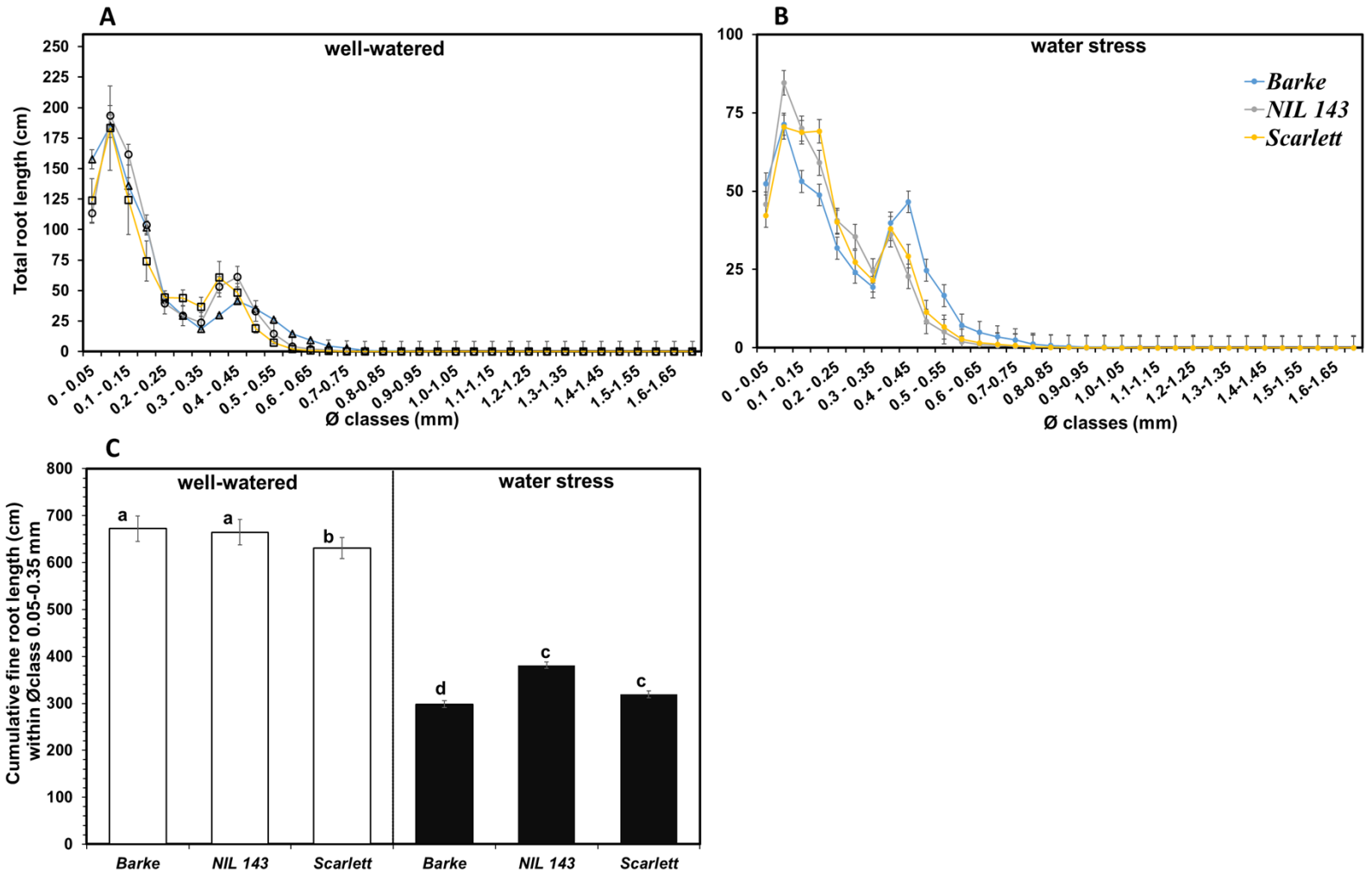

Figure 4.5 Total root length distribution of all diameter classes of the barley seedlings under WW (A) and WS conditions (B). Cumulative fine root length, i.e. the mean sum of total root length (cm) within seven diameter classes from 0.05 mm up to 0.35 mm, is shown in panel (C). Letters on the bars denote significant differences ($\alpha = 0.05$) based on Tukey's *post hoc* test for pair-wise comparison, n=6. The figure was taken from Frimpong et al., 2021b.

4.4 Discussion

Several studies reported that variations in fine root structures and deep roots are linked to differences in whole-plant productivity under water limitations (Lynch, 1995; Fry et al., 2018; Wasson et al., 2020). The current study investigated the hypothesis that proline accumulation contributes to barley root growth under water stress. We characterized root system architectural traits and root placement among contrasting barley genotypes, including the breeding line that harbour the wild allele at the *P5cs1* locus under water stress. From our results, *P5cs1*-isogenic barley line accumulated higher concentrations of root and leaf proline. Further, *NIL 143* had a higher leaf gas exchange, chlorophyll-a content, RWC, root vigour and less severe dehydration under WS compared with *Barke*, and *Scarlett*. The evidence we highlight demonstrates a strong association between organ proline accumulation and lateral root growth under WS in barley at the early seedlings stage.

4.4.1 Barley seedlings root system and root placement in response to water stress

We found that *NIL 143* showed less severe symptoms of drought at the shoot level compared with the more severe symptoms exhibited by the other three genotypes. *NIL 143* also showed differences in root system development and placement under reduced water availability. Under WS, *NIL 143* produced longer lateral roots and more lateral roots and placed the roots deeper (+11%) in the substrate compared with *Barke* and *Scarlett* (Figure 4.3 E-F). Compared to the other genotypes, *NIL 143* had a higher proportion of lateral roots (+30%) placed at deeper substrate horizons under WS (Figures 4.2D, 4.3F, and 4.5). We also found that *NIL 143* had a comparatively larger root maximum width, root length density, and convex hull area than *Barke* and *Scarlett* under reduced water availability conditions. The wild parental barley accession (*ISR42-8*), from which *NIL 143* was derived, also showed the ability to develop an extensive and deep rooting system (Naz et al., 2014).

Faye et al. (2019) distinguished drought resistance or tolerance among different pearl millet (*Pennisetum glaucum* L.) based on root length density (total length of roots per unit of soil volume) and presence of deep lateral roots and fine roots. The reason for choosing this classification is that deeper fine roots and higher root length density define how well plants can

take up water and nutrients from available lower layers of the soil (Palta & Watt, 2009; Placido et al., 2013). Fine roots and root hairs have a larger surface area due to their long combined lengths and are in direct contact with soil water molecules facilitating water extraction (Carvalho & Foulkes, 2018; McCully, 1999). In our study, *NIL 143* had a significantly higher (26%) root length density compared with *Barke* and *Scarlett* (Figure 4.4C) under WS. This was mainly due to differences in root growth of specific diameter classes accounting for a larger lateral root of *NIL 143* under WS.

Similarly, Boudiar et al. (2020) reported a remarkable growth (+20%) in lateral roots compared with seminal roots resulting in better performing modern and landrace barley types grown under low water availability conditions. Under WS, *NIL 143* showed higher root vigour (higher growth of lateral roots, root length density, and fine roots, Figures 4.2D, 4.3F, and 4.5C), which likely contribute to capturing water from deeper waters soil layers. Han et al., 2016; Pierret et al., 2016; Carvalho & Foulkes, 2018 reinforced these suggestions on root vigour (root length density and deep fine roots) of barley seedlings as an important trait under water deficit. Our data confirm that a more vigorous root system might attenuate the effects of drought at the shoot level.

4.4.2 Organ-dependent proline accumulation in barley seedlings promotes water stress tolerance.

We characterized proline accumulation in the leaf, stem, and roots at the seedlings stage of the different barley genotypes and how their root traits responded when exposed to WS. To adapt to moisture gradients in the soil, plants alter their physiology, modify root growth and architecture, and exhibit tissue-specific responses (Gupta et al., 2020). In our study, the genotypes showed varying proline concentrations in the different plant organ tissues under WS (Figure 4.1 A-C). For example, the WS leaf and root tissues (but not the stem tissues) mean proline concentration was higher in *NIL 143* (+1216 and +650%, respectively) compared to *Barke* and *Scarlett* (Figure 4.1 A-C). *NIL 143* showed a 2-fold higher root and leaf proline concentration and less negative plant water potentials than *Barke* and *Scarlett*. The increased proline concentration by the *NIL 143* in the leaf contributed to less severe dehydration and better turgor, higher performance in net CO_2 assimilation rate, stomatal conductance, and transpiration rate compared with *Barke* and *Scarlett* (Table 4.2 and Figure 4.1). This agrees well with the findings of (Quilambo 2004; Mirza et al.,

2019; Mattioli et al., 2020), who suggested that proline accumulation in the roots and leaves improve the whole-plant cell membrane integrity and photosynthesis. Generally, proline concentration was at least 30% higher in the shoot (leaf and stem) than in the roots (Figure 4.1 A-C). This might be caused by the fact that *P5cs1* expression is most highly induced in shoot tissues (Székely et al., 2008; Sharma et al., 2011).

Root proline concentration under WS was at least 40% higher in *NIL 143* than in *Barke* and *Scarlett* (Figure 4.1A). Osmotic adjustment due to proline accumulation has been shown to play an essential role in maintaining root elongation at low water potentials (Voetberg and Sharp, 1991; Ogawa & Yamauchi, 2006). A key observation in the peanut nodules (N2-fixing organs in the legume's root) of the WS-tolerant cultivar (EC-98) was a significant accumulation of osmolytes, including proline (Furlan et al., 2017; Furlan et al., 2020). However, as an indicator of plants experiencing WS, root proline accumulation negatively correlated with root growth in our study (Appendix 4.3). Earlier reports have interpreted such relationships (Bandurska et al., 2017; Boussora et al., 2019) to indicate drought and not the proline effect.

Verslues & Sharp (1999) showed that free proline accumulation in maize roots under water deficit occurred in the root tips. Under WS, *NIL 143* demonstrated a higher capacity to accumulate proline compared with *Barke* and *Scarlett*, both in the roots and leaves but not in the stem. The above results show that *NIL 143* proline accumulation was targeted at specific plant organs during WS. Bandurska & Stroiński (2003) reported on a resistant wild accession of *Hordeum spontaneum* grown under water-limited conditions associated with its higher constitutive ABA and proline concentrations in the roots and leaves compared with the modern barley cultivar *Maresi*. Their wild *Hordeum spontaneum* genotype further showed a higher capacity to accumulate proline compared with their elite barley, both under mild and severe water deficit conditions (Bandurska & Stroiński, 2003). Forde (2014); Forde et al. (2013) attributed their large-scale changes elicited in the root architecture of Arabidopsis mutants to glutamate signalling, a precursor for proline biosynthesis in higher plants. Our data agree with these observations and lend further evidence to the suggestion that drought-inducible proline accumulation in barley is targeted at specific organs, i.e. the roots and leaves.

4.4.3 Proline led to changes in morpho-physiological traits of barley under water stress.

It is well established that proline accumulation and metabolism is a measure adopted by several cereal crops to withstand abiotic stresses. Proline protects cells during osmotic stress by scavenging radical oxygen species, decreasing photo-damage, lipid peroxidation, buffer redox potential, reducing dehydration, and contributing to signalling plant defence machinery come alive (Ahmed et al., 2015; Iqbal & Nazar, 2015). In our study, *NIL 143* accumulation of root and leaf proline was associated with the maintenance of leaf gas exchange, higher chlorophyll-a content, less severe dehydration (RWC and Ψ_{plant}), and the establishment of deep and long lateral roots under WS. Under WS, *NIL 143* had a higher root proline concentration and more lateral roots and fine roots. In root systems, fine roots and root hairs are the most active portions of the root system in terms of water extraction, with many root tips and intense chemical activity (McCully, 1999). As a compatible solute, proline accumulation contributes to maintaining the plant cell water potential equilibrium during WS. An increase in proline causes changes in osmotic potential and cell turgor pressure to elicit matching accumulation of potassium and other solutes in the larger cell vacuole (Verslues & Sharma, 2010). Several other studies indicate that higher leaf and root proline concentrations are associated with greener leaves, cell turgor, cell membrane stability, and improved whole-plant performance in many crops species, including barley (Samarah et al., 2009; Mafakheri et al., 2010; Szabados & Savouré, 2010; Hayat et al., 2012).

A more than 5-fold in spike and leaf proline accumulation has been found to occur in barley introgressions bearing the wild allele of *pyrroline-5-carboxylate synthase1,* which contributed to improved seed yield and whole-plant performance under reduced water availability (Frimpong et al., 2021). In the current study, water stress caused more than a 2-fold increase in leaf and root proline concentration in *NIL 143* compared with *Barke* and *Scarlett* (Table 4.1 and Figure 4.1). The increase in shoot and root proline accumulation was accompanied by higher leaf chlorophyll-*a*, turgor, and photosynthesis in *NIL 143* compared with *Barke* and *Scarlett* (Table 4.1 and Figure 4.1). Proline has been implicated in the scavenging of reactive oxygen species that may damage chloroplast membranes under drought (Hayat et al., 2012; Verslues & Sharma, 2010), which might explain the high chlorophyll-*a* content maintained by *NIL 143* under water stress. The

drought inducible *P5cs1* allele from the wild barley introgression into the *NIL 143* might have conferred an enhanced higher proline accumulation under water stress. Considerable reductions in chlorophyll content under water stress has been demonstrated in most crop species (Nikolaeva et al., 2010; Parkash & Singh, 2020). The decrease in chlorophyll under water stress was mainly caused by active oxygen species damaging chloroplasts (Mafakheri et al., 2010). It has been reported that decreases in chlorophyll-a content in barley plants under water stress were lower in drought tolerant than in susceptible genotypes (Gupta, 2019; Nikolaeva et al., 2010; Wang et al., 2018). Our observation that the proline accumulators *NIL 143* maintained a high chlorophyll-*a* content under water stress agrees well with these findings.

All the measured physiological traits of all our genotypes were strongly reduced upon WS. Regarding morpho-physiological shoot differences for the genotypes, *NIL 143* showed a smaller shoot size compared with the roots under WS (Table 4.1). Higher proline concentration was found in the *NIL 143* root tissues under WS compared with the elite lines. The leaves of *NIL 143* were also greener and showed less negative plant water potential (+35%) and less dehydration (+10%, RWC) than *Barke* and *Scarlett* (Table 4.2). This genotype thus showed fewer symptoms of drought and improved tolerance to WS.

In contrast to *Barke* and *Scarlett*, under WS, *NIL 143* did not fully close their stomata but were able to keep transpiring and photosynthesizing. An improved RWC and active photosynthesis (optimal rate of net CO_2, transpiration, stomatal conductance and other gas exchange parameters) were also reported for related barley breeding lines harbouring the same *P5cs1* allele from wild relatives (Muzammil et al., 2018; Frimpong et al., 2021). Accordingly, *NIL 143* showed a good ability to replenish and retain water and fewer drought symptoms from the measurements of whole-plant water potential and iWUE under WS (Table 4.2 and Appendix 4.4 A-C). Arguably, the root proline accumulation might have contributed to the improved water retention and turgor of *NIL 143* and resulted in deeper roots, longer lateral roots, and fine root growth under WS (Table 4.1, Figures 4.2, 4.3, 4.4). In relative terms, *NIL 143* showed less pronounced reductions in lateral root growth (-77%) at harvest under WS compared with *Barke* and *Scarlett* (approximately -80%, Figure 4.2D and 4.3F). Therefore, our results suggest that under

WS, proline accumulation in *NIL 143* contributed to better shoot stomatal conductance, net CO_2 assimilation, RWC, Ψ_{plant} and root length density compared with *Barke* and *Scarlett*.

We found that shoot proline (leaf and stem) concentration was 30% higher than root proline concentration for all genotypes under WS and that these differences were significant. These results indicate that proline accumulates preferentially in developing root systems (Figure 4.1 A-C). Under WS, *NIL 143* had the highest root and leaf proline concentration. *NIL 143* produced the highest growth in lateral roots and fine roots under WS and WW conditions (Figures 4.2D, 4.3 E-F, and 4.5 A-C). Evidence that root growth is stimulated by proline is provided by Biancucci et al. (2015), who reported that exogenous proline stimulated root elongation in Arabidopsis during germination. Under WS, *NIL 143* roots were placed deeper in the soil, indicating a potentially higher ability to take up water from deeper layers. Similar to earlier reports, our results support the argument that proline accumulation under WS increases cell water stability, promoting growth and metabolism (Maggio et al., 2002; Signorelli, 2016). Earlier studies suggested that the cyclic amino acid, proline, has been implicated in root elongation since the discovery of *rolD*, a gene from *Agrobacterium rhizogenes* necessary for hairy roots elongation (Biancucci et al., 2015; White et al., 1985). In summary, water stress may induce higher shoot and root proline accumulation in specific barley genotypes at the seedling stage, and that this effect is associated with a response in root morphology such as pronounced root vigour. We suggest future studies explore how proline accumulation and metabolism might promote root water uptake under drought by acting as an osmolyte.

4.5 Conclusion

The total root system of all genotypes under water stress at the seedlings stage was considerably reduced (-20%) relative to well-watered plants. We observed varying organ proline concentrations for all genotypes as it increased by more than 30% in the shoot compared to the roots under WS. *NIL 143* accumulated higher root, leaf, and not stem proline and showed a comparatively better net CO_2 assimilation, transpiration, stomatal conductance, plant water potential, and RWC compared with *Barke* and *Scarlett. NIL 143* reduced its seminal roots but increased fine and lateral roots (+30%), improving tolerance under reduced water conditions at the seedlings stage. Root growth was therefore enhanced *NIL 143* because it could maintain its water status under WS. The results suggest that water stress may induce higher shoot or root proline accumulation in *NIL 143* at the seedlings stage to stimulate fine or lateral root growth. Future studies would explore the variations in root-shoot growth observed for *NIL 143* in the field to test its performance under a water-limited environment. Further studies will be required to explore how proline accumulation promotes barley root water uptake under water stress.

CHAPTER 5

In vivo visualization of barley (*Hordeum vulgare* L.) grain development by MRI

Felix Frimpong [12], Dagmar van Dusschoten[1], Fabio Fiorani[1], Daniel Pflugfelder[1], Carel W. Windt[1]*

[1] Institute of Bio- and Geosciences, IBG-2: Plant Sciences, Forschungszentrum Jülich, Jülich, Germany
[2] CSIR-Crops Research Institute of Ghana, P. O. Box 3785, Kumasi

***Correspondence:** Carel W. Windt, c.windt@fz-juelich.de

Abstract

In cereals, grain size and number mainly determine the final harvestable yield of the crop. Abortion of grain number is influenced by biotic and abiotic factors, including heat and drought. However, to invasively monitor the number of florets that abort or develop under the influence of abiotic stress is very time-intensive. Additionally, precise examination of functional physiological traits of florets or seeds may require a large plant population. One technique, magnetic resonance imaging (MRI), generates substantial information from a single plant *in vivo*. Therefore, we test if it is possible to use the non-invasive potential of MRI with only a moderate resolution (0.3750 × 0.1875 mm) to achieve maximum throughput and visualize seed development or abortion. We use MRI to quickly visualize seed initiation and development to understand seed abortion of future abiotic stress studies in cereals. To this end, genotypic variations in floret development among three elite genotypes of 2-row spring barley (*Barke, Olve,* and *Sissi*) were grown until maturity. Developing inflorescences from the early booting phase onwards were scanned using a 4.7 Tesla MRI instrument. We analyzed MRI images of floral developmental stages of barley's whole spikes revealing the floret fertility dynamics of our different spring barley 2-row genotypes. Images of the whole spike of seeds were subsequently analyzed destructively under a stereomicroscope. MRI showed internal florets, seed initiation and seed abortion, seed structures, spike architecture, and temporal growth of the grain on intact spikes of the spring barley genotypes. We found that MRI visualized differential genotypic seed initiation, seed growth and development, or abortion. MRI highlighted genotypic variations in a-synchronicity of floret initiation, seed set, and filling along the different spike axis. In comparison to dissection under the microscope, MRI facilitated seed development or abortion monitoring faster and on fewer intact spikes.

Keywords: Barley, cereals, floret fertility, spike phenology, microscopy, Magnetic Resonance Imaging, seed development.

5.1 Background

Understanding floret development is vital for successful cereal breeding. It usually requires phenotyping of several hundreds of genotypes, involving several repeated trials and a high plant population (Gol et al., 2017; Lobos et al., 2017). However, plant histological studies of floret development are slow and, therefore, lack throughput and do not allow an analysis of high spatial and temporal resolution (Bhandari et al., 2015; Glidewell, 2006). Most of the phenotyping methods used to date are destructive and time-consuming (Ruchi Bansal et al., 2016). Gol et al. (2017) argue that studying floret development in wheat or barley can be challenging because the shoot apex develops inside the whorl of leaf sheaths and can only be accessed upon careful microscopic dissection. Fortunately, new avenues are opened in plant sciences by the development of imaging tools which has added advantages of reduced measurement time and generation of high-quality data (Borisjuk et al., 2012; Millet et al., 2019).

The early floral development of the complex barley spike begins from the maximum primordia (stem elongation phase), where spikelet initiation is complete (Kirby, E. J. M., Appleyard, 1984). Floral development continues to the active growth stage of the spike at booting (flag leaf sheath extended and swollen). The spike further develops to the heading stage, i.e. the last stage of pre-anthesis development, where the spike is pushed out of the flag leaf sheath. It then progresses to the anthesis stage, often characterized by spikelets having more than 50% matured anthers. Later spike developmental stages involve grain filling (flowering already completed and first grains have reached half their final size) and physiological maturity stages before ripening (Feng et al., 2017; Ochagavía et al., 2018; Zadoks et al., 1974). By dissecting the flowering period into growth phases, one can assess the actual timing of events to determine the sub-phase in which the plants are most sensitive to stress and the most crucial for floret fertility and seed abortion (Guo et al., 2018). Biological processes and environmental cues of cereal development's pre and post-anthesis phases are crucial for floret survival or abortion (Guo et al., 2016; Slafer, 2003). An alteration in any environmental factor (temperature, photoperiod, water, nutrients, etc.) during the active spike growth stages may cause a significant reduction in the final grain yield (Cattivelli et al., 2011; Cuesta-Marcos et al., 2016). For example, the heading stage was more sensitive to heat

stress than the booting stage, primarily due to the larger decrease in the average seed number in wheat (Balla et al., 2021).

A lack of vascular coordination during seed set and filling may also cause asynchronous spikelet development along the spike in barley or wheat (Hay & Kirby, 1991). Mechanisms leading to the failure of coordinated synchronous development of spikelets and florets in cereals are poorly understood (Hay & Kirby, 1991; Shitsukawa et al., 2009). Several investigations have further shown that the time course of spikelet development can vary between cultivars (González-Navarro et al., 2015; Guo et al., 2018; Hay & Kirby, 1991). However, such investigations often involve large plant populations and genotypes for plant characterization and involve a considerable number of repeated trials of careful dissection of several hundreds of plant apices spanning over a couple of days (González et al., 2003; Guo et al., 2017; Guo et al., 2018). Also, the typical time quoted for stereo microscopic dissections per barley seed sample is 15 minutes Kovacik et al. (2020), which may be too long when studying dynamic plant biological processes.

Non-invasive approaches for plant measurements, including MRI, have the advantage of requiring fewer plants, less time, generating substantial information (Borisjuk et al., 2012). MRI can project a map of protons of mobile molecules containing hydrogen when the organic sample is placed in a strong magnet equipped with an imaging gradient set. In most fresh plant materials, water contributes most of the signal (Glidewell, 2006). The relative intensity of different regions of an image depends not only on the total concentration of mobile protons but also on the rate at which they relax after excitation, as a function of the experimental parameters used (Glidewell, 2006; van As et al., 2013). For a detailed revision on the mechanism of MRI, Borisjuk et al. (2012) explained its advantages and a wide range of possible applications for solving outstanding issues in plant science. Some examples of MRI of plants reproductive structures include; non-invasive acquisition of three-dimensional images of developing shoot apex of maize (van der Weerd et al., 2013) and cherry ripening/vessel bursting (Grimm et al., 2017). Glidewell (2006) also used MRI to study developing barley grains from anthesis to maturity, generating 3D images of caryopses. Frimpong et al. (2021a) distinguished seed abortion of control vs water stress treated spikes in barley using MRI. Other examples include long-term greenhouse experiments, monitoring a beech tree's stem (*Fagus sylvatica*) during bud flushing, leaf development, and leaf maturation (Meixner

et al., 2021). Pielot et al. (2015) demonstrated hormone-mediated growth dynamics of the barley pericarp using MRI with further correlation analysis revealing that MRI signals and growth rates of barley growth in length are mediated by dorsal also lateral rather than ventral regions. Despite these studies, the broader use of MRI is often limited due to the high procurement and maintenance cost (Ruchi Bansal et al., 2016).

Nonetheless, the opportunity MRI offers to visualize spike development continuously and non-invasively cannot be overemphasized. MRI has proven to be possible to image cereal spikes in great detail (Borisjuk et al., 2012), but this requires long measurement times, specialized micro MRI equipment and, in most cases, cannot be done with intact living plants. In our work, we explore if it is possible to image entire spikes sufficiently quick to make the method applicable for applications in plant breeding. For this purpose, we propose that the method: i) Should be suitable; to visualize seed development and seed abortion in the living plant, and ii) do so faster than would be possible by conventional invasive microscopic methods. Many challenges are associated with whole imaging spikes using MRI. Generally, one challenge has to do with the low signal to noise ratio obtained when scanning live plants. The ability to speed up measurement time per spike in a semi-automated fashion and generate images of acceptable resolution is another challenge. Therefore, we test if the various flowering stages, seed set, and seed filling can be distinguished for an intact spike and if florets or grains can be visualized and quantified. We explored if it is possible to study seed setting and the dynamics of seed filling by MRI. Our target was to determine the extent to which MRI can be used to study reproductive development on intact spikes. Specifically, we test the use of MRI to visualize seed development or abortion *in vivo*.

5.2 Materials and methods

5.2.1 Plant cultivation

Seeds of three cultivated two-row spring barley types (*Hordeum vulgare* L.) (*Barke, Olve, and Sissi*) were sown and arranged in a completely randomized design in the greenhouse at Institute of Biogeosciences 2, Plant Sciences, Jülich, Germany. Sowing was done in peat soil under temperature conditions of 25/20 ˚C ± 2, day/night, supplemental light (350 µmol photons m^{-2} s^{-1}, 16/8h photoperiod) and day/night air humidity 60%/50%. Thirty plants per genotype were transplanted six days after germination from a 50-well tray, selecting plants of equal height. All plants were transplanted into 3.5 L plastic pots (20 cm ×16 cm). Each plant received three tablets of slow-release fertilizer (15% N, 8% P_2O_5, and 15% K_2O, plus trace elements) applied at 20 days interval three times through the season, starting ten days after transplanting and placed 2-3 cm deep and away from the plant into the soil. Pests and diseases were chemically controlled.

5.2.2 Flowering stages and floret scores.

The time course for reproductive development of barley genotypes was studied by dissecting the shoot apices (developing main spike) under a stereomicroscope (using surgical knife/blades) of each plant, randomly sampled every week. Three replicates per genotype were used for the phenological staging. Specific floral stages were determined following the Zadoks scale for cereal development (Kirby, E. J. M., Appleyard, 1984; Zadoks et al., 1974). The stages (Figure 2.6) were determined from the maximum number of primordia (MNP) or terminal spikelet (TS) (completion of spikelet initiation); white anther (WA) stage (lemmas of F1 and F2 completely enclose stamens and other structures); green anther (GA) stage (glumes cover all but the tips of florets); yellow anther (YA) stage (glumes are fully formed and the lemmas of the first three florets are visible); tipping (TP) stage (DC49, first awns visible); heading (HD) stage (DC55, 50% of spikes visible); and anthesis (AN) stage (DC65, 50% of spikes with anthers), the onset of grain filling (OGF) DC71 and physiological maturity (PM) (DC89).

The number of days to booting, heading, anthesis, and the onset of grain filling were recorded for all barley genotypes after dissection under the microscope. According to the cereals scales (Zadoks et al., 1974; Waddington et al., 1983; Steinfort et al., 2017), the duration of floral developmental stages was calculated daily based on the thermal time from one-time point to the

other. Thermal time was calculated to represent the duration of each phenological stage (calculated as the sum of the daily mean temperature- [(Tmax + Tmin)/2]°C days) assuming the base temperature to be 0°C (Arisnabarreta & Miralles, 2006) by monitoring plant apices and recording the date at each flowering stage. Data on the maximum number of primordia and fertile florets at anthesis after dissection under the microscope was taken using six plants per genotype (n=6) of main shoot spikes. At the booting stage, main shoots were tagged for easier identification. Following (Appendix 5.1, Waddington et al., 1983; Steinfort et al., 2017), the floret determination scale was used to score the stage of each floret. A floret was considered fertile when it reached stage W9.5-10 (fertile floret-style curves outwards and stigmatic branches spread wide; pollen grains present on well-developed stigmatic branches as well as having healthy turgid anthers.

5.2.3 Growth and yield parameters

The following plant growth parameters were recorded per plant per genotype (n=6): plant height (from the base of the shoot to the spike apex), tiller number, number of leaves at physiological maturity in February and April. For both experiments, shoot dry weight (g), and other yield parameters were recorded on a per plant basis, i.e., number of spikes, the weight of spikes (g), number of grains per main spike at physiological maturity (n=6). Percentage floret survival (the number of fertile florets per spike divided by the maximum number of floret primordia) and grain setting (ratio between spike grain number and fertile florets per spike) and % was calculated as established by (Arisnabarreta & Miralles, 2006) using the main shoot spike.

5.2.4 MRI and light microscopy

The MRI studies were carried out at the Forschungszentrum Jülich GmbH, Institute of Biogeosciences, IBG-2, using a 4.7 T vertical wide-bore MRI system (Varian Inc., USA and MR Solutions, UK) and a 1.5 T wide bore system (MR solutions, UK). The 4.7 T system was equipped with a quadrature transmit/receive coil with an inner diameter of 100 mm and a 400 mT/m gradient system. The main spikes at the dough stage (BBCH- scale, 83) were collected together with a section of the stalk (>20 mm). The cut spikes were placed in a vial with tap water directly after excision. A robotic system (MiniLiner 3.0, Geiger Handling GmbH and Co. Kg, Jülich, Germany) was used to carefully lower and centre the specimen into the MRI scanner. Two-dimensional (2D) images of developing spikes were acquired with an in-plane spatial resolution of 0.3750 and 0.1875

mm, using a multi-spin- echo sequence using the following settings; 32 echoes, 1.5 s repetition time, echo time of n × 8 ms, two averages, 512 × 256 image matrix, a field of view of 100 (read direction) by 50 mm (phase direction), at a slice thickness of 50 mm. The acquired datasets show amplitude images of water content per pixel (Edzes et al., 1998). Each spike was imaged for 12 min. An additional 10 min of preparation and setting the sample to the centre of the magnet were required. For all spikes, the MRI images presented are amplitude parameter maps of a single echo image in grey values in their sagittal orientation after analyzing, using image reconstruction set scripts from Spyder, scientific programming in Python 3.6. All MRI images are presented as amplitude grey values for all figures in their sagittal orientation.

The 1.5 T magnet (Magnex, Oxford, UK) was equipped with an MRS console (MR Solutions, Guildford, UK). We used a solenoid rf-coil with an inner diameter of 25 mm and a length of 50 mm for the spike image acquisition. Spike images were acquired with a field of view of 45 mm. Spikes in their sagittal orientation were scanned for alternate three-dimensional (3D) images, using a 3D gradient echo sequence with an isotropic resolution of 130 μm; eight averages were used at a scan time of approximately 60 mins. The raw data files were later analyzed with the medical image processing and visualization software "MeVisLab" (https://www.mevislab.de/) version 3.0.2 using built-in packages "PhenoVein", "Spike_analyses" and "ImageViewer" to analyze and display the 3D images. The spike scans from the 1.5 T were performed noninvasively and at regular time points from the same main tiller to assess alternate imaging options.

The stereomicroscope (Leica MZ12 stereo microscope, Germany) was equipped with a 1.0 × planochromatic objective, and 10 × eyepieces, a numerical aperture of 0.125 and a resolution of 375 line pairs / mm and was used to dissect florets as stated previously under section 3.2.4 of this thesis. Targeted whole spike imaging of ontogenetic stages from stem elongation, booting, heading, anthesis, and the onset of grain filling was done with the microscope for all genotypes. At each chosen phenological stage, at least three spikes per genotype (including the main spike) were sampled for both MRI and microscopic imaging. A subset of florets (i.e., three each from the proximal (1, 2 & 3), central (7, 8 & 9) and distal sections (13, 14 & 15) along the spike (Appendix 5.1) of the same spikes that were used for MRI scans were then dissected under a microscope and later compared and analyzed side by side to determine temporal development. An average of 15

mins estimated was used to carefully dissect a floret or 330 mins per spike of 22 florets or seeds and image it under the stereomicroscope. Sequences of image maps of developing ears for all genotypes were generated after analysis and processing.

5.2.5 Statistics

Data on growth, yield parameters, and thermal time of flowering duration were subjected to a one-way analysis of variance in 'R' studio after the Shapiro Wilk and Levene test's determination of normality and homogeneity test, respectively (R Core Team, 2020). Six replicates per genotype were used for analysis. Tukey's HSD (honestly significant difference) test was used to separate means where treatment means were significant ($P < 0.05$). Calculations on the grain setting rate and survival rate were done based on the maximum number of floret primordia differentiated per the main spike (MNP) ± (SE), the number of fertile florets per the main spike (FF) ± (SE), the survival rate of florets primordia ($FF \cdot MNP^{-1}$) × 100 ± SE) and grain setting rate ($GN \cdot FF^{-1}$) × 100 ± SE); GN-grain number. The floret fertility, survival, and abortion rate were calculated and adapted (Arisnabarreta & Miralles, 2006).

5.3 Results

We aimed to image entire spikes sufficiently quick to make the method applicable for plant abiotic studies on a temporal scale. Therefore, we determined the spike growth stages for subsequent *in vivo* MRI at those specific floral developmental stages by first characterizing the time to flowering of our spring barley genotypes (*Olve*, *Barke*, and *Sissi*). We dissected the spikes under a stereomicroscope and determined the number of primordia, floret fertility, grain number, survival and grain setting rate of the different barley genotypes. Finally, compared to the light microscopy, we analyzed these destructive measurements versus the *in vivo* MRI of seed set and filling by the three genotypes to answer whether we can see and recognize the various stages of seed development non-destructively.

5.3.1 Duration in floral transitions among the three genotypes

To predict when a specific flowering stage will occur and subsequently image it under MRI, we used the thermal time to calculate the developmental stages of our barley types by assigning a heat value to each day (Miller et al., 2001). The three barley genotypes revealed significant differences in their duration to reach specific flowering stages of booting, heading, anthesis, and the onset of grain filling (Table 5.1). *Olve* was the earliest (797, 841 and 991 °C days) to reach booting, heading, and anthesis stages, respectively (Table 5.1). *Barke* or *Sissi* was slower with a difference of more than 150 °C days (Table 5.1). No significant differences were found between *Barke and Sissi* regarding their time taken to boot, head, reach anthesis, and set grains (Table 5.1). However, there were differences among the three genotypes in their transition time to grain set and filling phase after anthesis. *Olve* took the longest (a minimum of about 132 °C days and a maximum of 163 °C days) to set grains after anthesis. *Barke* and *Sissi* were faster (approximately a minimum of 75 and 55 °C days and a maximum of 75 and 98 °C days, respectively (Table 5.1). There were no significant differences between *Barke* and *Sissi* regarding their transition time from one stage to another (Table 5.1). *Olve* was also significantly slower (~70 °C days) to transit from the anthesis stage to the grain filling stage than the other two genotypes in our study (Table 5.1). A significantly lower final grain number in *Olve* might be due to a higher abortion rate compared to *Barke* and *Sissi* (Table 5.2). Most of *Olves'* florets failed to advance to grain filling (Table 5.2). We observed a longer time duration to the grain setting stage and a reduced final grain number of more than -30% in *Olve* compared with *Barke* and *Sissi* (Tables 5.1 & 5.2).

5.3.2 Fertility, survival and grain setting of the three genotypes

Generally, the maximum number of primordia ranged between 36 - 44 florets, while fertile florets ranged between 25 – 32 florets and grain number ranged between 13 – 26 grains per the main spike of all the three genotypes, determined destructively (Table 5.2). However, the maximum number of primordia was significantly higher ($P < 0.01$) in *Barke* or *Sissi,* i.e. 40 – 44 florets, compared to *Olve,* which was 36-37 florets per main spike (Table 5.2). Consequently, grain number was also significantly higher ($P < 0.01$) in *Barke* or *Sissi,* which ranged from 22 – 26 compared to *Olve,* which ranged from 13 – 14 per the main spike (Table 5.2). There were, however, no significant differences between *Barke* and *Sissi* in terms of their maximum numbers of

primordia, fertile florets, and grain number (Table 5.2). The number of fertile florets was significantly higher ($P < 0.01$) in *Olve*, *i.e.* 32 florets compared to either *Barke* or *Sissi*, which ranged from 25 – 28 florets (Table 5.2) per the main spike. Even though the survival of florets after fertilization was lower in *Barke* and *Sissi*, their grain setting rate after anthesis was about 45% higher than *Olve* (Table 5.2). We found a significantly higher final grain number in *Barke* and *Sissi* than in *Olve* (Table 5.2).

Table 5.1 Duration of developmental stages expressed in thermal time (°C days).

Genotype	Booting	Heading	Anthesis	Onset of grain filling
Barke	941.57 ± 5ab	1013.21 ± 0.02ab	1154.91 ± 0.03a	1229.09 ± 0.09ab
Olve	796.77 ± 11.7c	840.56 ± 0.03c	991.13 ± 0.03c	1154.91 ± 0.08b
Sissi	969.79 ± 9a	1036.51 ± 0.01a	1191.69 ± 0.04ab	1289.68 ± 0.02a

Thermal time was estimated with the formula; [(max°C – min°C temp) ÷ 2; assuming base °C = 0], following Miller et al. (2001). Values presented as mean ± se, n= 12.

Table 5.2 Floret fertility, grain number, survival and grain setting rate per main tiller

Genotype	MNP (maximum number of primordia)	FF (Fertile florets)	GN (Grain Number)	Survival (%) [$(FF \cdot MNP^{-1}) \times 100 \pm SE$]	Grain setting (%) [$(GN \cdot FF^{-1}) \times 100 \pm SE$]
Barke	44 ± 0.54a	28 ± 1.15b	26 ± 1.52a	65 ± 2.67b	93 ± 2.67a
Olve	37 ± 0.48b	32 ± 0.21a	14 ± 3.31b	85 ± 0.69a	45 ± 3.52b
Sissi	42 ± 0.26a	28 ± 0.7b	25 ± 2.5a	64 ± 0.86b	93 ± 3.2a

MNP=Maximum number of floret primordia, FF =fertile florets per spike in three elite barley genotypes (Olve, Barke, and Sissi), GN= grain number, n=12. Letters (a–d) indicate significant differences between means (P < 0.05) within a given experiment based on Tukey's HSD test of comparison of means at 95% confidence.

5.3.3 Seed set and grain filling stages visualized microscopically and by MRI

Intact spike scans from the MRI revealed internal floret development (Figure 5.1). To increase throughput and shorten image acquisition time, the field of view was chosen as large as possible (to encompass the entire spike in one go) and the number of acquired pixels as low as necessary for sufficient image quality. The MRI of the barley spikes acquisition time was 12 minutes, while the microscopic image acquisition time was approximately 45 minutes per spike. The MRI studies were from early booting, tipping, heading, anthesis, and the onset of grain filling stages until the physiological maturity of *Olve, Barke,* and *Sissi.* A comparison between the proton density image (2D) of an intact two-row spring-barley (Olve) spike four days after anthesis and its developing seeds after excision and imaged with a stereomicroscope showed either no development (abortions) or ongoing cell differentiation and expansion of the individual seeds (Figure 5.1). The proton density image was acquired with a slice thickness much larger than the thickness of the spike with all enclosed tissues (awns, glumes, lemma, palea, leaf sheath etc.), giving rise to some intensity, reducing the contrast with which the developing seeds appear (Figure 5.1). In essence, neither leaf bundle sheaths nor the awns of the immature spikes obstructed or caused noise during visualizing internal spike structures. The MRI were sufficiently accurate enough to recognize whole spike or seed development (Figure 5.1). We found undifferentiated ovaries, anthers, and expanding embryos of individual seeds at various growth levels from the MRI of the spikes (Figures 5.1 and 5.2). In our study, microscopic imaging invasively produced higher resolution than the MRI of specific spikelets from basal/proximal, central, and apical/distal sections (Figure 5.1).

From the MRI, we can observe that grain filling initiation begins from the lower mid-section of the spike, and later on, the distal sections (apical and basal) are filled (Figure 5.2). Images of individual seeds at the central region of the spikes show that seeds appear larger and farther in development compared to those at the proximal and distal ends for all three genotypes (Figure 5.2). Selected florets or seeds from the basal (1, 2 & 3), central (8, 9 & 10), and apical (14, 15 & 16) positions along the spike dissected under microscope affirmed the overall degree of a-synchronicity within individual spikes irrespective of the genotype (Figure 5.2). In all the three genotypes (whether main/side spike) scanned, the MRI images clearly showed an overall a-synchronicity in floret initiation, seed set, and filling along the axis of the barley spikes (Figure 5.2). In terms of

grain filling, both the MRI and microscopic images showed acropetal seed filling from the proximal part of the spike to the distal end in all three barley genotypes (Figure 5.2). On grain architecture or the seed forms, MRI visibly differentiated the three barley genotypes from one another (Figures 5.2 and 5.3). Optically and from the MRI images, the three genotypes differed in seed shape (Figures 5.2 and 5.3). *Olve* seeds tended to be more oblong-round, while *Sissi* was slightly slenderer than the other genotypes (Figure 5.3). *Barke* seed shape was more intermediate compared to the other two genotypes (Figure 5.3). Other genotypic differences in grain or seed traits such as length, width, or axial variations were also visible in the MRI images. Such traits may later be necessary to characterise seed traits important for physiology studies related to germination and vigour under abiotic stress. Our study recognized grain architecture, seed set and seed abortion from the MRI (Figures 5.1 to 5.4).

We visualized *in vivo* barley spikes in all three genotypes (Figures 5.3 & 5.4). We recognized when seeds abort from the MRI images (Figure 5.3). Seed abortion was typically recognizable from the beginning of grain filling stages until physiological maturity in all the three barley genotypes (Figure 5.3). The challenge we faced in our study of the whole spikes MRI was distinguishing fertilization from the abortion of a floret before or during the anthesis stage. Low image intensity was one reason, particularly of very young spikes at early booting stages of the white, green & yellow anther and tipping stages (Figure 5.3). The low water amounts of such young spikes (yellow anther, tipping and heading stages) resulted in a low contrast image in all the three barley genotypes (Figure 5.3). However, clearer MRI images were attained after anthesis, initiation, or onset of grain filling stages up to maturity. We tested alternative methods to observe the spikes using the 3D approach. However, the 3D image acquisition time of whole barley spikes was much slower, requiring an additional 48 mins compared to the 2D imaging (Figure 5.4). The MRI detected the onset of grain filling or seed abortion during filling and confirmed the extent of a-synchronicity in seed filling along a spike (Figures 5.1 to 5.4).

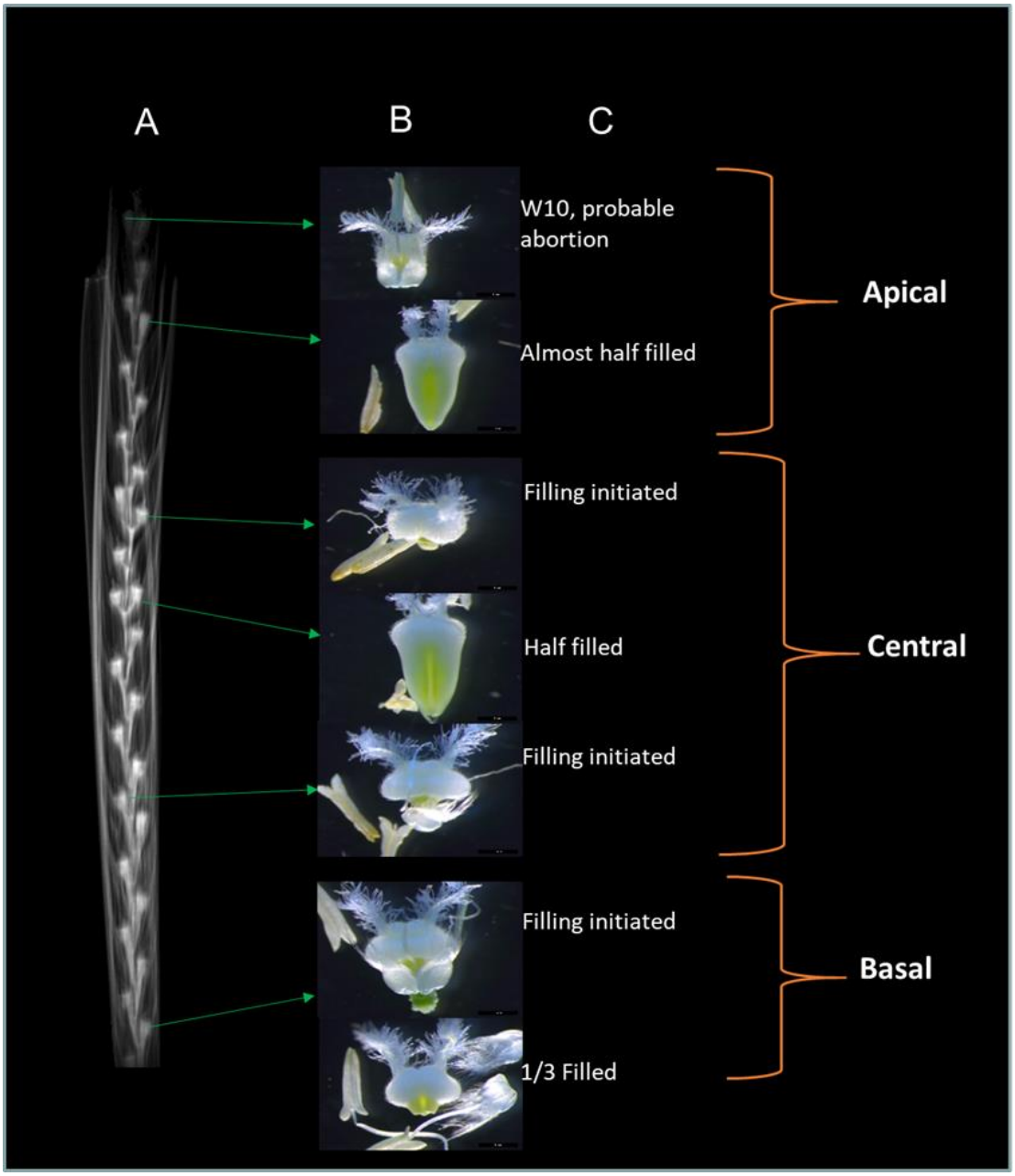

Figure 5.1 Comparison between the proton density image (2D projection) of an intact two-row spring-barley spike of variety *Olve* (A), imaged by means of MRI four days after anthesis, and its developing seeds as imaged with a stereomicroscope after excision (B). MRI image acquisition time was 12 minutes. In column C the corresponding floret/spikelet scores as based on the Waddington scale are shown (Waddington et al., 1983; Steinfort et al., 2017).

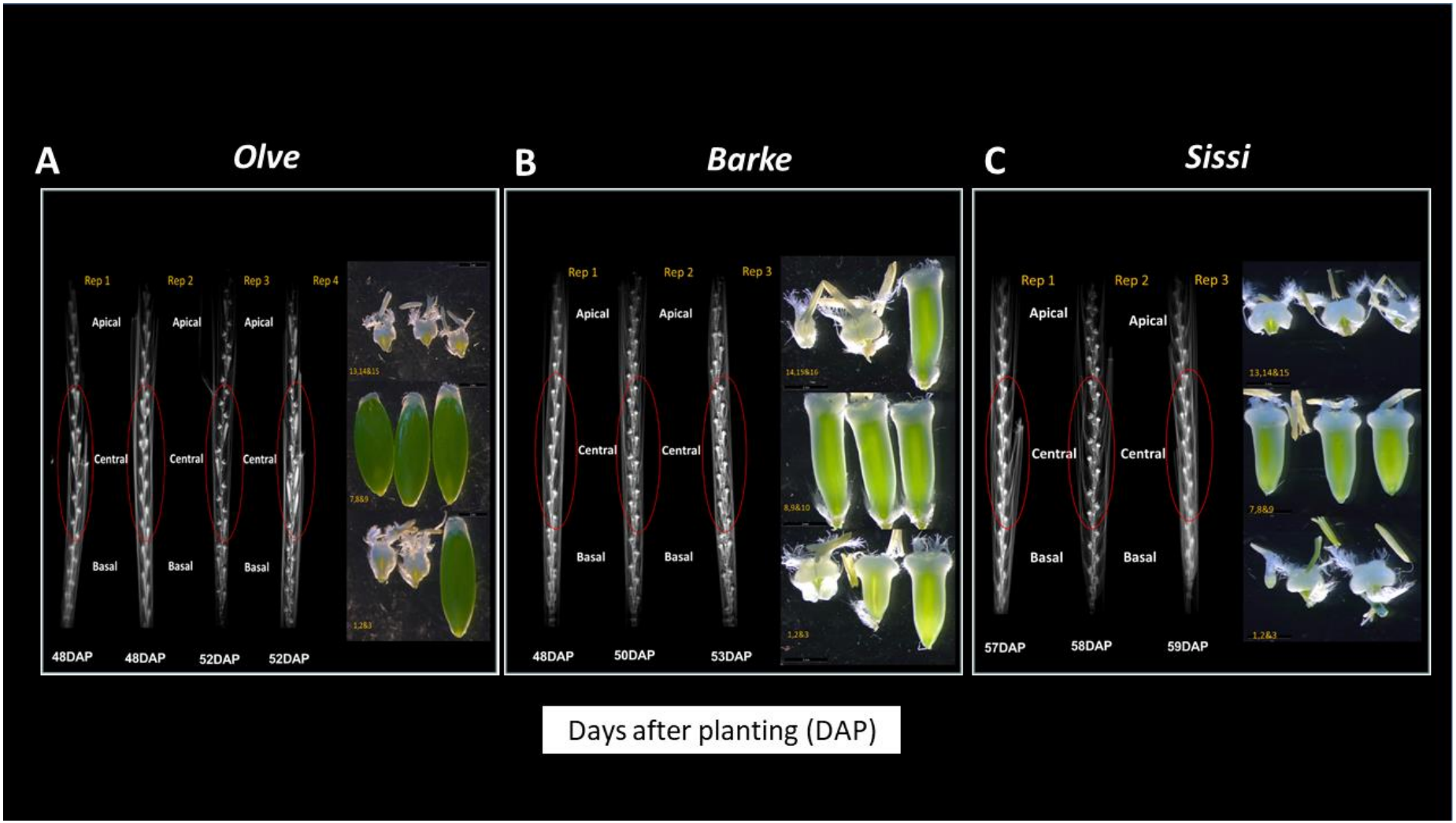

Figure 5.2 MRI and microscopic images of barley spikes at grain filling stage. Shown are barley genotypes *Olve* (A), *Barke* (B) and *Sissi* (C). On the left of each panel MRI amplitude images are displayed. On the right side of each panel microscopic images of selected florets from basal (1, 2 & 3), central (7, 8 & 9) and apical (13, 14 & 15) spikelet positions are shown. Red ovals on each spike highlight the onset of seed initiation and filling beginning from the lower-mid section of the spike. The results of both MRI and microscopy suggest a degree of a-synchronicity during grain filling along the spike, with somewhat better synchrony at the central floret positions than distal positions.

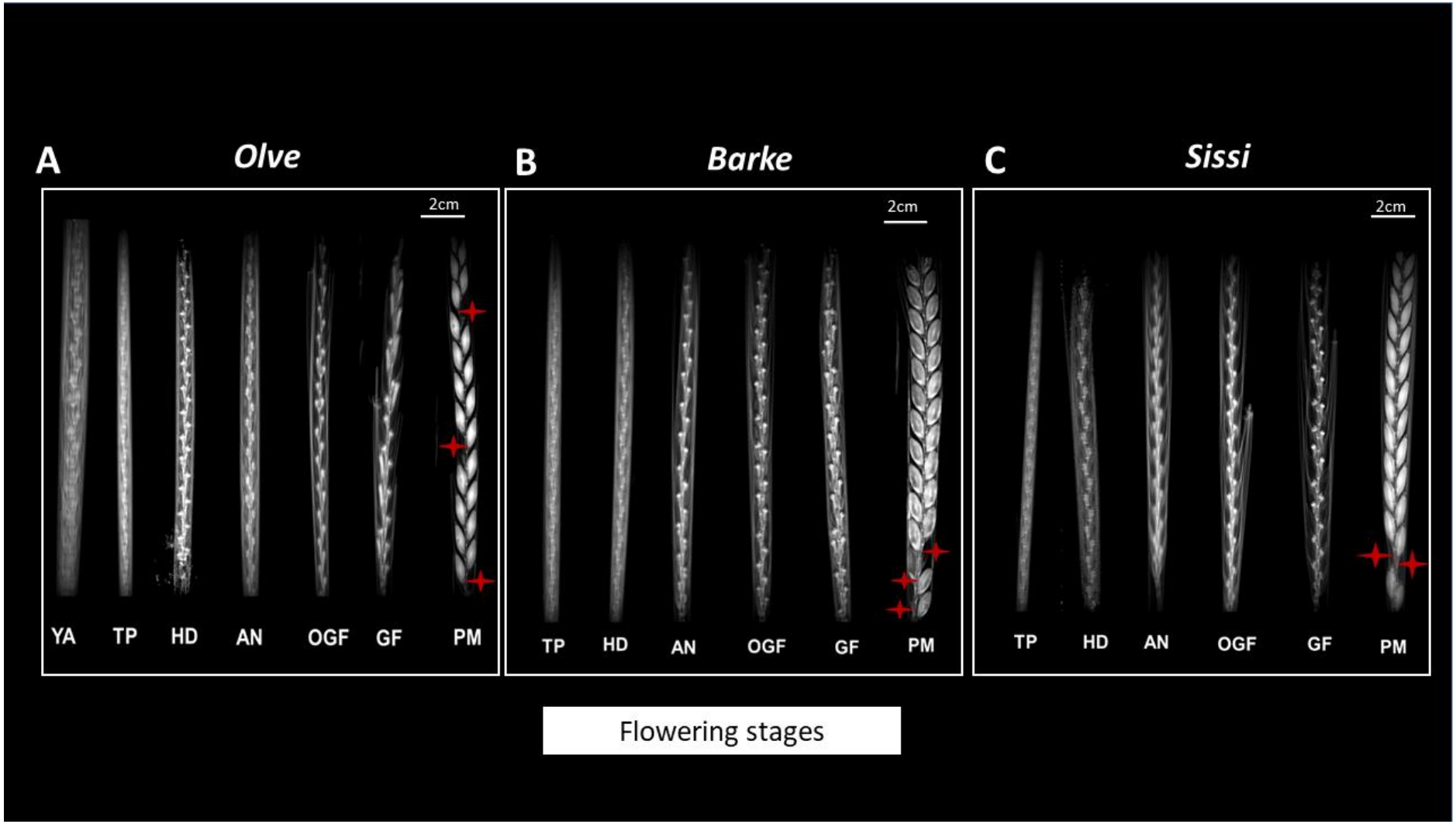

Figure 5.3 *In vivo* barley spike ontogenetic development visualized with MRI. The MRI images are from different tillers at yellow anther stage (YA), tipping (TP), heading (HD), anthesis (AN), the onset of grain filling (OGF) & physiological maturity (PM). Starting from left to right are shown genotype "Olve" (A), "Barke" in the middle (B), and "Sissi" (C). In each genotype, ✦ denotes sterility/aborted grains due to infertility at anthesis. Image acquisition time 12 minutes per spike.

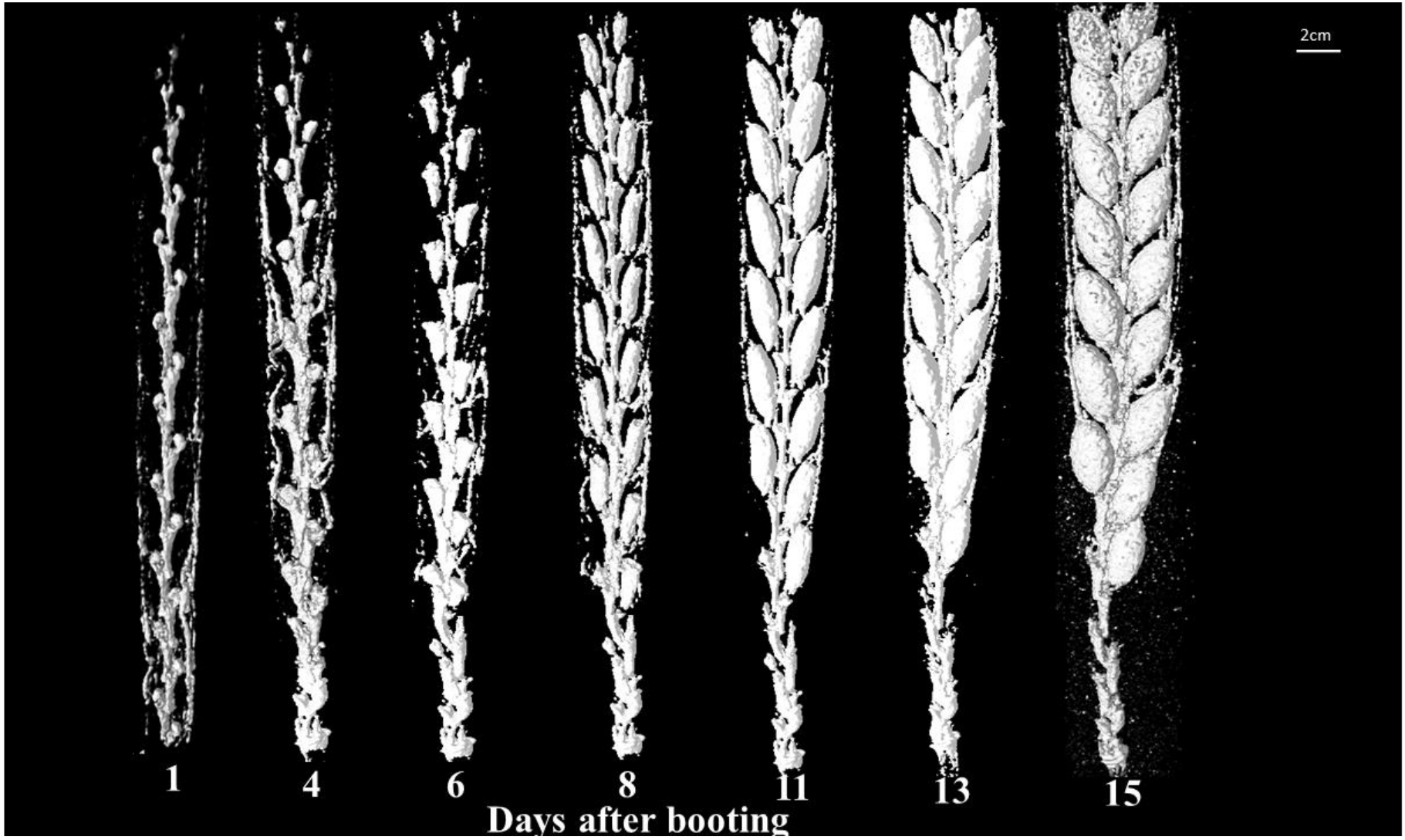

Figure 5.4 Surface rendering of non-invasive three-dimensional MRI images of an intact two-row spring barley (Barke) spike from early booting to physiological maturity, imaged continuously and in a 1.5 T MR imager. Image acquisition time was 60 minutes.

5.4 Discussion

Our study aimed to non-invasively image entire spikes sufficiently quick to make the method applicable for plant abiotic studies on a temporal scale. MRI proved to be a helpful technique visualizing seed set and filling on intact spikes at a shorter measurement time of 12 mins per spike (2D images) versus 330 mins from our timer to dissect a whole spike under the microscope requiring fewer spikes in our study. We were within the typically quoted barley seed dissection time of 15 mins (Kovacik et al., 2020), yet nowhere near the high throughput the 2D MRI offered (~0.5 mins per seed), on estimations of an average of 22 seeds per spike. Similar NMR barley imaging was reported previously on the non-destructive acquisition of three-dimensional images of developing single grains from anthesis to maturity, 40 days after anthesis (Glidewell 2006). However, the alternative MRI approach, full 3D imaging in our study, was much slower at 60 mins per spike.

In our study, the 2D and 3D MRI of whole-intact barley spikes recognized the onset of grain filling and filling stages or otherwise, i.e. seed abortion (Figures 5.1 to 5.4). At the onset of the grain filling stage, we recognized seed abortion (sterile florets) from the MRI images in all three barley types (Figure 5.3). Similarly, Frimpong et al. (2021a) examined and identified the effect of water stress on seed abortion and filling early in the reproductive development phase (before grain maturation) of barley using MRI to scan immature spikes at the soft milky dough stage. MRI of the barley spike further visualized the acropetal nature of seed set and filling and the extent of a-synchronicity. MRI of whole-intact barley spikes again showed the various stages of seed development, even though we are looking at a projection of all tissues in the spike, including the awns, lemma, glumes and covering leaves (Figures 5.1 to 5.4). We recognized the various ontogenetic cereal developmental stages in the three barley genotypes and seed abortion from the MRI (Figure 5.3). Researchers underscore that seeds are of high agronomic importance. An appreciation of the developmental processes that determine potential seed numbers could enhance breeding programs' efficiency to improve barley yield (Gol et al., 2017).

5.4.1 MRI visualized seed abortion, asynchrony in seed set and filling

The onset of grain filling or seed abortion through MRI could be visualized and the degree of a-synchronicity in seed filling along the different barley spikes. It is established that in barley or wheat, floret initiation does not begin from the basal spikelets of the ear but the lower mid-part, progressing later both towards the tip and the base (Hay & Kirby, 1991). Whole intact spike scans using MRI complemented with microscopic imaging (Figures 5.1 & 5.2) in our study confirmed the existence of a-synchronous filling, beginning from the lower-mid section. Our results agree well with the findings by Schmidt et al. (2020) that the central region of their wheat ears contained larger seeds (seed size > 2.0 mm) than the top and bottom when visualized with computed tomography. It has been suggested that most of the failures to set grains observed in the distal spikelets positions within the spike (also reported in our current study) was a consequence of an increased asynchrony in the floret primordia initiation between central and distal spikelets (Arisnabarreta & Miralles, 2006). The lack of synchrony at the more distal positions of the spike is attributed to the impedance of the movement of resources due to poor vascular connectivity (Hay & Kirby, 1991). Similarly, in our study, the lack of synchrony between the first initiated primordia in the middle part of the spike and those initiated on the top and basal positions (Figure 5.2) also resulted in differences in floret survival (Table 5.2) between our barley types. The increased floret survival in two-row cultivars is related to a higher ability to reduce the asynchrony of floret development between the primordia initiated in the top and those placed in the basal or central position within the spike (Arisnabarreta & Miralles, 2006). We, however, recommend further studies as to why the initiation of grain filling begins from the lower mid-section and to unravel the mystery of lowering the level of a-synchronicity, which could lead to a higher final grain number.

5.4.2 Variations in seed set and filling among the three genotypes

Several studies have shown that an increase in temperature decreases the time to-heading both in wheat or barley (Hay & Kirby, 1991; Kirby, E. J. M., Appleyard, 1984; Zadoks et al., 1974). The time taken to transit into grain filling after fertilization played a critical role in determining the yields of the different genotypes. This highlights the critical role of post-anthesis processes as determinants of final grain yield due to the maximum number of primordia at earlier stages of spike initiation and later transitional stages of seed setting to understand genotypic variations of cereals reproductive development (Guo et al., 2016). In terms of the production of potential grains, the growth habit of barley, where each spikelet has only one floret (unlike wheat with several florets

per spikelet) and no terminal spikelet is formed, up to about 40 spikelets are initiated during the maximum number of primordia stage and around 15 of the latest-formed die (Hay & Kirby, 1991). This is in agreement with studies that found that for barley and wheat floret mortality ($\sim \frac{1}{3}$) occurs naturally (González, Slafer, & Miralles, 2003; Guo et al., 2015a) and varies within and among genotypes as well as with the time of occurrence (Guo & Schnurbusch, 2015b; Hay & Kirby, 1991; Kirby, E. J. M., Appleyard, 1984). In the current study, we observed a similar trend among the genotypes, with *Olve* having fewer grains due to delay in transition (of at least ~70+°C days) to set grains. This confirms the hypothesis that floret initiation was far less relevant than the subsequent process of primordia degeneration to determine the number of fertile florets and consequently the final grain number (Arisnabarreta & Miralles, 2006; Gol et al., 2017). This is because *Barke and Sissi,* having a higher maximum number of primordia than *Olve,* achieved a higher final grain number. According to previous studies by Cockram et al. (2015), this is mainly due to the ability to initiate grain setting much earlier. This may suggest that grain set/abortion post-anthesis processes are also crucial for determining genotypic variation in grain number. Yet, in contrast with the view that the number of grains per spike is mainly determined by floret initiation and degradation of fertile florets (Kirby, 1988).

5.5 Conclusion

MRI of whole intact spikes recognized the various ontogenetic stages of seed development in all three barley genotypes. MRI also recognized when seeds are aborting from the onset of grain filling stages onwards. We demonstrated that MRI has the potential over optical microscopy to visualize seed development or abortion on intact spikes faster, less invasively and can be helpful during pre-selection in cereal breeding and abiotic stress studies. MRI of whole intact developing spikes showed acropetal seed filling and the level of a-synchronicity in all three of our 2-row spring barley types. Our method further highlighted the initiation of seed set and filling to be the lower mid-section of the spike. Our study provided insights about genotypic differences among some 2-row spring barley genotypes in their flowering duration from the anthesis stage to the time of grain setting and filling stages. In our case, a long time to transit from one stage to the other in some barley genotypes negatively led to a significant reduction in the final grain number. Future MRI studies could integrate algorithmic tools and machine learning models to explore different functional seed traits and physiological behaviour even beyond our photographing. Furthermore, MRI offers the possibility to measure several spikes simultaneously with no or a small-time penalty, which would allow it to measure about 25 spikes per hour.

CHAPTER 6

Quantifying spike filling rate, dry matter and water content of two-row barley genotypes non-invasively with a multiplexed NMR sensor

Felix Frimpong [12], Dagmar van Dusschoten[1], Johannes Kochs[1], Carel W. Windt*[1]

[1] Institute of Bio- and Geosciences, IBG-2: Plant Sciences, Forschungszentrum Jülich, Germany

[2]CSIR-Crops Research Institute of Ghana, P. O. Box 3785, Kumasi, Ghana

***Correspondence:** Carel W. Windt, c.windt@fz-juelich.de

Abstract

Seed filling parameters such as spike fresh weight, dry matter accumulation and water content are critical agronomic traits in barley breeding. However, to measure the dynamics of seed filling by conventional destructive methods is laborious and requires large numbers of samples. It has been shown that Nuclear Magnetic Resonance (NMR) relaxometry can be used to monitor grain filling non-invasively, in terms of fresh weight (FW), dry weight (DW) and water weight (WW). In this work, we test the utility of a multiplexed NMR sensor with 6 probe heads to monitor and compare developmental traits of the barley spike, such as seed filling duration, maximum filling rate, average filling rate, the diurnal fresh weight gain, dry matter gain, and water influx. To this end, three barley genotypes (*Olve*, *Sissi* and *Barke*) were grown under controlled conditions in a climate chamber. The multiplexed NMR sensor readily allowed to distinguish differences in spike filling rate among the three barley genotypes. Compared to *Olve* and *Sissi, Barke* was projected to produce the highest seed yield due to its rapid and a higher spike or seed filling depositions of fresh weight, water and dry matter content even before maturation, matching what was measured destructively. *Barke* showed at least 5% higher seed filling rate and the highest average peak deposition rate of FW, DW and WW (40, 13 and 29 mg/day) compared to *Olve* (25, 6 and 19 mg/day) and *Sissi* (32, 9 and 25 mg/day, respectively). The multiplexed NMR sensor and relaxometric method thus presents a unique phenotyping modality to monitor and characterize spike development in cereals.

Keywords: dry matter content, grain filling rate, multiplexed NMR sensor, non-invasive phenotyping, peak influx, spring barley, spike growth,

6.1 Background

Researchers continue to breed superior barley (*Hordeum vulgare* L.) cultivars to close the yield gap of more than 50 % (Taner et al., 2004; Schils et al., 2018; FAOSTAT, 2021). However, one daunting task they face is destructively phenotyping several thousands of plants to estimate seed filling duration, filling rate, and subsequent seed yield. The seed filling process is complex and directly affects the setting rate and grain weight, thus influencing the yield (Jing Zhang et al., 2021). Additionally, flowering and grain filling stages are susceptible to heat and drought stress exposure, leading to a significant loss in crop yields (Hein et al., 2021). Therefore, phenotyping to enhance resilience to these abiotic stresses is critical for sustaining genetic gains in crop improvement programs (Hein et al., 2021). In wheat and barley, the shoot apex harbouring the seed reproductive structure develops inside the whorl of leaf sheaths (Gol, 2020). Thus, studies on seed development and subsequent filling in barley and wheat are only possible upon careful microscopic dissection (Gol et al., 2017). However, traditional screening methods (manual harvesting, dissection, counting and weighing plants) of studying seed developmental traits related to abiotic stresses are destructive, slow, laborious, and often expensive (Ruchi Bansal et al., 2016; Hein et al., 2021). Cereal seed development is understudied because of the difficulty of quantifying *in vivo* grain traits using the traditional hand methods (Dreccer et al., 2019; Hughes et al., 2019).

The seed filling process, a part of seed development in cereals, begins after fertilization of the ovule, which involves two male nuclei (Emes et al., 2003). One nucleus fuses with the egg, forming a diploid zygote and giving rise to the embryo; the other merges with two polar nuclei to produce a triploid nucleus, further dividing and producing the endosperm (Emes et al., 2003). The grain seed is a fruit that consists of a seed coat, or testa, which surrounds the endosperm (the largest organ of the seed) and embryo. Grain development (seed setting and filling) can be sub-divided into three stages. The early pre-storage phase (or cell division or morphogenesis), the storage (or maturation), and later the desiccation phase or late grain maturation (Gubatz & Weschke, 2016; Sreenivasulu et al., 2010). The first stage of cereal grain enlargement involves early, rapid division of the zygote and triploid nucleus (Bradford, 1995; Emes et al., 2003). Cell division is accompanied by the influx of water, which drives cell extension (Bradford, 1995). This stage generally occurs approximately 3-20 days after anthesis (Emes et al., 2003). During the next stage (grain filling), cell division slows and then ceases while storage products are accumulated, beginning at around

ten days after anthesis until maturity when the endosperm functions as a carbohydrate store (Bradford, 1995; Emes et al., 2003). During the grain filling process, photosynthetic products are transported from the effective leaf (source) to grain (sink) through the stem, and starch is synthesized and accumulated in the grain as well (Zhong et al., 2003). Generally, for cereals like barley, the grain after filling comprises 15% protein, 1.5-2% fats, 1.5-2% minerals, vitamins and 60-80% carbohydrate portion of the grain attributed to starch (Emes et al., 2003; Zhiqin Wang et al., 2015). Grain filling is therefore heavily dependent on starch biosynthesis i.e. series of enzyme-catalyzed reactions in the grain (Lv et al., 2021; Zhiqin Wang et al., 2015).

Previous reports showing seed filling curves in barley and wheat under field or controlled conditions relied on destructive harvesting of spikes and seeds. For example, (Brenchley and Hall, 1909; Jenner & Rathjen, 1972; Schnyder and Baum, 1992) showed seed filling curves based on spikes harvested at regular intervals throughout seed development, or fitted the curves directly to the mean values of grain weight averaged over several experiments and replicates (Gooding et al., 2003). Changes in barley kernel growth and maturation have been previously reported either as linear plots (Schnyder and Baum, 1992) or as smooth curves (MacGregor et al., 1971), often drawn and extrapolated on the basis on only a few data points that were actually measured, to describe the various phases of seed development. MacGregor et al. (1971) reported on changes in the components (starch, fibre, sugars, fat, protein, ash, moisture content and dry matter) of barley seed growth up to maturation. They found major components, protein and starch, reached their maximum values 32 to 36 days after ear emergence at a moisture content of about 70% within the first 14 days, while seeds reached maximum size after 36 days at a moisture content of 27% by which time the dry matter had ceased.

Arguably, so far only limited progress has been achieved in employing sensor-based technologies to measure seed filling and yield development in vivo. However, nuclear magnet resonance (NMR) based non-invasive sensors have now opened new avenues to evaluate these hard to quantify and time-sensitive traits. Windt et al. (2021) introduced a simple NMR relaxometric method that can be run on even the most basic NMR setups to study seed filling dynamics. Their method was demonstrated using a mobile NMR sensor to monitor the water content of rice leaves as affected by salinity, as well as by measuring the dynamics of seed filling in a developing wheat-ear. The NMR sensor enables the non-invasive determination of dry matter accumulation rate

continuously during the entire cereal seed filling phase (Windt et al., 2021). A drawback of the method is that it allows only a single plant to be measured at any given time, limiting throughput.

In this study, we demonstrate for the first time a multiplexed version of the mobile NMR plant sensor, the NMR multiplex. The NMR multiplex allows for the simultaneous measurement of multiple plant replicates. To this end the NMR multiplex is equipped with six sensor heads, each consisting of a C-shaped small permanent magnet and rf coil assembly, driven by a single spectrometer. The spectrometer is the most expensive component in the NMR multiplex. Multiplexing the NMR sensor heads thus significantly reduces the cost per NMR sensor while allowing six plants to be measured simultaneously and under the same environmental conditions.

Windt et al. (2021) observed that in wheat most dry matter is deposited in the grain during the night and not during the day. We test if such night time deposition of solids also occurs during barley grain filling, and if variations in grain filling characteristics can be detected among genotypes. We explore how non-invasive monitoring of deposition rates of dry matter and water in the barley spike, as made possible by the NMR sensor or NMR multiplex, can be used to characterize seed development and seed filling on a temporal scale. To do so we establish new metrics that can be derived from the acquired seed filling data, such as the day and night time fresh weight gain, dry matter gain and water influx; as well as specific periods in seed filling that can now easily be recognized, such as peak fresh weight increase and peak dry matter deposition.

6.2 Materials and Methods

6.2.1 Barley cultivation and destructive yield determination

Two German elite spring barley (*Hordeum vulgare* L.) genotypes, *Barke, Sissi,* and a Norwegian type, *Olve*, were grown (series of repeated experiments) in a climate chamber and arranged in a completely randomized design in 1.5 L pots of 13×13×13 cm at the Institute of Bio and Geosciences 2, Plant Science, Forschungszentrum Jülich, Germany. Sowing was done in peat soil (ED 73, Stangenberg GmbH, Germany), after which the seeds were left to germinate in a growth chamber under 25/20 ± 2˚C, day/night temperature conditions. In the growth chamber, plants were subjected to photosynthetic active radiation (PAR) of approximately 500 µmol photons m^{-2} s^{-1}, under 16/8hrs photoperiod day/night and relative humidity 65/50%, respectively. All plants

were irrigated to field capacity twice daily with an automatic watering system from germination to harvest. Each plant received three tablets of slow-release fertilizer (15% N, 8% P_2O5, and 15% K_2O, plus trace elements) applied at 20 days interval three times through the growing season, starting ten days after transplanting and placed 2-3 cm deep and away from the plant into the soil. Pests and diseases were chemically controlled according to the standard greenhouse practice of the research centre.

6.2.1.2 Growth and yield parameters

Measures of the following plant growth parameters were taken per plant per genotype (n=6) several days after sowing: plant height (cm, from the base of the shoot to the spike apex), tiller number, number of leaves, SPAD, estimated single leaf area (cm^2, Leaf area =Width × Length × k, where k is the shape factor, which is 0.69 for barley leaves, Boudiar et al., 2020). Yield parameters were recorded on a per plant basis, i.e., shoot dry weight (g), number of spikes, the weight of spikes (g), number of grains per main spike at physiological maturity (n=6). Biomass harvest index (HI) was calculated per plant basis as a ratio of total grain weight divided by total dry biomass weight at harvest (n=6).

6.2.2 Light response and CO_2 response measurements

Leaf-level net CO_2 assimilation of the second youngest fully expanded leaf from the top was measured at late booting (BBCH46) and grain filling stages (BBCH74) with a portable gas exchange system (LI6800; Li-Cor, Lincoln, NE, USA). All measurements were done in the growth chamber between 11:00 – 15:00 CET. Light levels (µmol m^{-2} s^{-1}): 2000, 1500, 1250, 1000, 750, 500, 250, 100, 75, 50, 25, 10, 0, relative humidity: 50 – 65%, airflow rate: 400 µmol s^{-1}, CO_2 Level: ambient (400 µmol mol^{-1}), vapor pressure deficit in the leaf (VPDleaf): 2.11 ± 0.01, O_2 level: ambient (~21%), block temperature was set at 28 °C were used during the measurement. Each measurement was later corrected for diffusive leaks between the cuvette and external environment (Bernacchi et al., 2001) before fitting the curves with the Excel solver spreadsheet (Bernacchi et al., 2001; Lobo et al., 2013; Sharkey et al., 2007).

Parameters such as dark respiration (R-dark), light compensation point (LCP), maximum assimilation rate (Amax), apparent quantum yield (q) were obtained after fitting the light response curves. In terms of the response of leaf net CO_2 uptake to intracellular CO_2 concentration (A/Ci curves), measurements were done after steady-state from initial saturation light intensity of 1500

µmol m^{-2} s^{-1} (90% red and 10% blue light) and a CO_2 concentration of 400 µmol mol^{-1} inside the cuvette. The chamber inlet CO_2 was varied according to the following sequence: 5, 50, 75, 100, 150, 270, 400, 600, 800, 1100, 1500, 2000 µmol mol^{-1}. The following parameters were obtained after fitting the A/Ci curves in Excel solver; apparent maximum of rubisco carboxylation rate (*Vcmax*), regeneration of ribulose-1, 5-biphosphate expressed as electron transport rate (*Jmax*) and triose phosphate utilization (TPU). The calculated parameters were then analyzed for significance ($\alpha \leq 0.05$).

6.2.3 The multiplexed NMR Sensor

The multiplexed Nuclear Magnetic Resonance (NMR) sensor is an upgraded version of the single mobile NMR sensor previously developed by Windt et al. (2021). It comprised six C-shaped movable NMR magnets, each fitted with rf coil. The six NMR sensors were driven by a single spectrometer (Kea II spectrometer with a built-in 100W radio-frequency amplifier from Magritek, Wellington, New Zealand, in a climate-controlled housing, Figure 2.5). Further detail on the spectrometer was earlier reported (Windt et al., 2021). All six NMR sensor heads were fitted with solenoidal radio frequency (rf) coils (25 mm long, Ø20 mm wide), wound onto glass formers, allowing light penetration and easy spike inspection. The C-shaped magnets enabled access from the sides providing easy spike insertion and height adjustment. At any given time, six spikelets or later grains were counted (three on each side of our two-row spikes) inside the coil during the NMR sensor measurements. We included only spikes (all genotypes) data that did not show seed abortion in the measured lower-mid section.

6.2.3.1 NMR measurement principle and relaxometric method

The best-known application of Nuclear Magnetic Resonance (NMR) is magnetic resonance imaging (MRI). Like MRI, the NMR sensor uses the fact that protons (^1H) are present in every water and organic molecule and that these protons possess a magnetic moment. When water or organic samples are placed in a strong magnetic field, the protons begin to spin along the direction of the field. They then process with a Larmor frequency which scales linearly with the field strength. These moving protons (spins) can be brought out of equilibrium by a radio pulse with this specific resonance frequency. In the rf coil of the NMR scanner, these exciting spins stimulate an rf signal, whose maximum displacement (amplitude) is directly proportional to the number of spins

within that sample. After excitation, the NMR signal of the spins relaxes exponentially, with a constant time characteristic for their physicochemical environment.

As described by Windt et al. (2021), two types of signal relaxation can be distinguished in NMR: spin-lattice relaxation (T_1) and spin-spin relaxation (T_2). The T_1 relaxation occurs due to the carry-over of energy from spins to the lattice molecules. For the type of NMR sensing employed in our study, T_2 is the most useful relaxation mechanism. It is faster and more straightforward to detect and is much more sensitive to changes in proton mobility than T_1. This property of T_2 can be exploited to distinguish between solid and liquid protons possessed by any matter. For example, protons in liquid water have very long T_2 relaxation times with values of up to 2 s. In liquids that are more viscous, or in water that is enclosed in small cells or narrow pores, T_2 becomes shorter. The T_2 relaxation times of oils are in the tens of milliseconds. Protons in solids exhibit shorter T_2 values still, with values in the microsecond range. Based on these relaxation differences, time-domain NMR (TD-NMR) can quantitatively distinguish the signal of protons in solids from that of protons in liquids (Windt et al., 2021).

6.2.3.2 Data processing, Sequences and NMR routines

All NMR relaxometry and data evaluation was done as previously described by Windt et al. (2021), and summarized below. Prospa (Prospa, Magritek, New Zealand), a spectrometer proprietary software, was used for all the NMR measurements. Two NMR sequences, one pulse free induction decay (FID) and Carr-Purcell-Meiboom-Gill (CPMG) (Edzes et al., 1998), were combined to acquire the signal. The FID sequence was used to acquire the signal of total proton density (PD_{tot}) in the plant sample. The FID data points between 0 and 75 µs were fitted with a single exponential. Fitting signal amplitude against time, PD_{tot} was given by the Y-intercept. Note that this approximation only holds if it can be assumed that the sample does not contain a significant fraction of crystalline or glassy proton bearing solids. This condition may be violated when seeds senesce or dry down to moisture contents below 15%.

To estimate the proton density of all liquids in a sample (PD_{liq}), the CPMG curve data points between 0 and 25 ms of the echo train were averaged. This interval was empirically found to provide a linear relationship with water content for a variety of plant tissues, including cereal

spikes. The difference between PD_{tot} and PD_{liq} then becomes the measure for the proton density of all solids in the sample (PD_{sol}) (Windt et al., 2021).

The following NMR settings and sequences (FID and CPMG, respectively) were used in our study. Repetition time: 5 s, echo time: 500 µs, number of echoes: 50, spectral width: 2 MHz, averages: 64, dead time 12 µs, 90-degree pulses: 3 µs and amplitudes (in dB): -8.5, -9.25, -9.5, -8.5, -8.75, -8.5 for sensors 1-6, respectively. 180 pulses 12 µs and amplitudes (in dB): -16.25, -17, -17, -16, -16.25, -16.0 for sensors 1-6, respectively.

6.2.3.3 Barley spike handling

All NMR spike measurements were done inside the climate chamber where the multiplexed NMR sensor was placed. For all genotypes, a 20 mm long section of the lower-mid region of the spike was marked out and measured (20 mm long as allowed by the rf coil size). At the start of the measurement, a 10 to 15 cm extended non-ferromagnetic lab jack was placed underneath the plants, allowing easy height adjustment. The NMR sensor heads were placed at a sufficient height to slip the live barley spikes into the sample holder without bending or causing any harm to the main rachis or any part of the plant. To prevent the spikes from shifting upwards through the coil, a small copper rod (Ø 0.20 mm) was threaded through the bottom of the spike between the pedicels of the spikelets, perpendicular to the axis and directly underneath the rf coil. As the stem grew, the spikes fixed themselves relative to the rf coil. The lab jack was lowered during the growth period whenever needed to prevent buckling of the stem.

6.2.3.4 NMR reference curves

To gather enough material for the reference curves, barley plants were sown each week for six weeks. Spikes at various ages and stages from early booting till physiological maturity were harvested. Sections of 20 mm were excised from the lower-mid of the spike. The samples were placed inside the NMR sensor with the aid of a non-magnetic holder without touching the coil assembly. At any given time, six spikelets or later grains were counted (three on each side of our two-row spikes) inside the coil during the reference measurements. We included only data from spikes (all genotypes) that did not show seed abortion in the measured lower-mid section. The spike sections were weighed first, then measured in the NMR plant sensor, and dried overnight in an oven at 70°C for three days to obtain the dry weight. The spike biomass FW, DW and WW were

subsequently determined. In this manner, samples were produced that mimicked what the sensor would measure, namely the entire bulk of the 20 mm high section of the spike, including its awns, palea, lemma, chaff and rachis materials. Total proton density (PD_{tot}), solid proton density (PD_{sol}) and liquid protons (PD_{liq}) were measured from the booting stage onwards to maturity using the NMR sensor.

Regression plots between the NMR sensor and the gravimetric results were generated for all the traits (PD_{tot}, PD_{sol}, PD_{liq}, FW, DW, WW) in all three genotypes to determine the tightness of the relationships. The slope of the parameters of the linear fits (FW vs PD_{tot}, DW vs PD_{liq}, WW vs PD_{liq}) was used to calculate WC % in subsequent measurements according to equation (8),

$$WC\% = a \times (PD_{liq}/ PD_{tot}) + c \quad \ldots\ldots\ldots\ldots \quad (8),$$

where a is the slope and c is the offset of the linear regression (Windt *et al*., 2021).

6.2.3.5 Barley seed filling metrics

To measure seed filling continuously and non-invasively allows to describe spike growth in much greater detail than was possible with earlier conventional methods. Established conventional grain filling parameters as reported and discussed in the results section by MacGregor et al. (1971) were extracted or calculated from our growth curves over the whole growth period, including the mean FW, DW and, peak or maximum influx, FW and DW. The various durations in filling rate, i.e. length of FW, DW and WW, time to reach maximum FW, DW and WW, and the maximum filling rate length were estimated. The diurnal rates of seed filling at peak DW (net deposition per day) in terms of FW, DW and WW, ten up to fifteen days after anthesis depending on the genotype, were also calculated. Additionally, we present the shape of the growth curve of barley spike or seed filling after defining the specific phases of seed development (non-invasive) using the existing destructive seed filling curves as a benchmark.

6.2.4 Statistical analysis

Differences between genotypes were tested with one-way analysis of variance (ANOVA), equation 4 of this thesis using the “Agricolae package” installed in “R” statistical software version 4.0.2 for agricultural research (R Core Team, 2020). Normality and homoscedasticity were tested using the Shapiro–Wilk’s and Levene’s tests for all measured traits. All the data met the criteria

for normality and homoscedasticity assumptions for ANOVA. The statistical significance was set at $\alpha \leq 0.05$. A *post hoc* test, Tukey's HSD, was used to separate the means.

6.3 Results

6.3.1 Destructive measurements of barley growth and seed yield

Olve, Barke, and *Sissi* were similar in growth in terms of their individual leaf area (36 cm^2) and SPAD values (55, Appendix 6.1). After 88 days of sowing *Barke* had the highest plant height (92 cm; significant, $P < 0.05$), and number of leaves (137) and tillers (28) of the three genotypes (Appendix 6.1). *Olve, Barke,* and *Sissi* differed significantly ($P < 0.01$) in terms of main tiller spike grain number, total spike dry weight, total grain number, total grain weight (Table 6.1). After harvest, *Barke* and *Sissi* had the highest main tiller spike grain number (19) compared to *Olve* (14, Table 6.1). *Barke* had the highest total spike dry weight (44 g) compared to *Sissi* and *Olve* (22 and 18 g, Table 6.1), respectively. *Barke* had the highest total grain number (989) compared to *Sissi* and *Olve* (521 and 297, respectively, Table 6.1). *Barke* also had the highest total grain weight (35 g) compared to *Sissi* and *Olve* (17 and 12 g, respectively, Table 6.1). Overall, *Barke* showed a significantly higher seed yield than *Olve* or *Sissi* (Table 6.1).

However, the different genotypes were similar in terms of the main tiller spike weight (1.1g), main tiller spike length (11.5 cm) and 100 seed weight (3.5 g, Table 6.1). Tukey's HSD test revealed, *Olve, Barke,* and *Sissi* differed significantly ($P < 0.05$) in fresh shoot weight (g) and shoot dry weight (Table 6.1). Shoot fresh weight of *Olve* was the highest (49 g) compared to *Barke* and *Sissi* (45 and 34 g, respectively, Table 6.1). Shoot dry weight of *Barke* was the highest (36 g) compared to *Olve* and *Sissi* (26 and 22 g, respectively Table 6.1). After harvest, the HI (harvest index) of *Barke* was much higher compared to *Olve* and *Sissi* (0.5, 0.4 and 0.3, respectively, Table 6.1).

6.3.2 Light response at booting and grain filling

Maximum net CO_2 assimilation rate (A_{max}) showed significant ($P \leq 0.05$) differences at booting, grain filling stages and between the genotypes (Table 6.2, Figure 6.1 A and B). *Olve* had the highest A_{max} at the booting (34 µmol m^{-2} s^{-1}) stage, with *Barke* and *Sissi* recording the lowest

(25 µmol m^{-2} s^{-1}, Table 6.2). *Barke* had the highest A_{max} at grain filling (42 µmol m^{-2} s^{-1}), whereas *Olve* had the lowest assimilation rate (37 µmol m^{-2} s^{-1}, Table 6.2). Light compensation point (LCP, µmol m^{-2} s^{-1}) showed significant ($P \leq 0.05$) differences at booting, grain filling stages and between the genotypes (Table 6.2). *Barke* and *Sissi* had the highest LCP at booting (28,37), and grain filling stages (17, 20) compared to *Olve* (24, 14), respectively (Table 6.2). Dark respiration (R-dark), quantum yield efficiency, and apparent quantum yield (q) did not significantly differ ($P \geq 0.05$) among the genotypes at booting and grain filling growth stages (Table 6.2).

6.3.3 CO_2 response of the different barley at booting and grain filling

The apparent maximum of rubisco carboxylation rate (µmol CO_2 $m^{-2}s^{-1}$, VC_{max}), regeneration of ribulose-1, 5-biphosphate expressed as electron transport rate (µmol e^- $m^{-2}s^{-1}$, J_{max}), and triose phosphate utilization (µmol CO_2 $m^{-2}s^{-1}$, TPU) also showed significant differences ($P \leq 0.05$) at booting and grain filling stage, as well as between genotypes (Table 6.3, Figure 6.1 C&D). *Olve* had the highest VC_{max} (124 µmol CO_2 $m^{-2}s^{-1}$) at booting, while *Barke* had the lowest (110 µmol CO_2 $m^{-2}s^{-1}$, Table 6.3). However, *Barke* had the highest VC_{max} (174 µmol CO_2 $m^{-2}s^{-1}$) at grain filling, while *Olve* had the lowest (140 µmol CO_2 $m^{-2}s^{-1}$, Table 6.3). *Olve* had the highest J_{max} (187) at booting, while *Sissi* had the lowest (142, Table 6.3). However, *Barke* had the highest J_{max} (325) at grain filling, while *Olve* had the lowest (253, Table 6.3). There were no significant differences ($P \geq 0.05$) between genotypes in terms of dark respiration (Rd) and mesophyll conductance (gm, Table 6.3).

Table 6.1 Biomass and seed yield-related traits of barley after destructive harvest.

Genotype	Shoot fresh weight (g)/plant	Shoot dry weight (g)/plant	Total spike dry weight (g)/plant	Total grain number/plant	Main tiller spike length (cm)	Main tiller spike grain number	Main tiller spike weight (g)	Total grain weight (g)/plant	100 Seed Weight (g)	HI
Barke	45 ± 1.3ab	36 ± 2a	44 ± 1.3a	989 ± 37a	11.3 ± 0.3a	19 ± 1.5a	1.28 ± 0.10a	35 ± 1a	3.6 ± 0.13a	0.5 ± 0.01 a
Olve	49 ± 2a	26 ± 1b	18 ± 1bc	297 ± 34c	11 ± 0.4a	14 ± 2b	0.8 ± 0.10ab	12 ± 1c	3.8 ± 0.1a	0.44 ± 0.02 ab
Sissi	34 ± 5b	22 ± 3.5bc	22 ± 2b	521 ± 45b	12.2 ± 0.3a	19 ± 2a	1.1 ± 0.14ab	17 ± 2b	3.3 ± 0.17a	0.30 ± 0.02 b

Different letters denote Tukey's HSD Test of significance. Data are means, n=6 ± standard deviation.

Table 6.2 Leaf-level light response measurements of the different barley genotypes after fitting with the Sharkey et al., 2007 model.

Growth stage	Genotype	R-dark	Quantum yield	LCP	*Amax*	q	SSD	r^2
Booting BBCH 46	*Barke*	1.2 ± 0.2ab	0.04 ± 0.001a	28 ± 3.0ab	25 ± 5.0b	0.79 ± 0.1a	1.1 ± 0.9ab	0.993
	Olve	1.6 ± 0.2a	0.07 ± 0.002a	24 ± 2.0b	34 ± 6.0a	0.74 ± 0.2a	1.5 ± 0.6a	0.951
	Sissi	1.5 ± 0.2a	0.04 ± 0.002a	37 ± 3.0a	26 ± 3.0b	0.79 ± 0.1a	0.3 ± 0.1b	0.926
Grain filling BBCH 74	*Barke*	1.5 ± 0.2ab	0.09 ± 0.01a	17.2 ± 2.2ab	42.3 ± 6.0a	0.92 ± 0.04a	3.51±0.96ab	0.987
	Olve	1.3 ± 0.2ab	0.10 ± 0.01a	13.4 ± 1.3b	37 ± 4.0b	0.89 ± 0.03a	6.21 ±1.45a	0.981
	Sissi	2 ± 0.1a	0.10 ± 0.01a	20.5 ± 1.2a	39 ± 5.0ab	0.82 ± 0.04a	6.29±1.81a	0.992

Different letters denote Tukey's HSD Test of significance. R-dark: dark respiration, LCP: light compensation point (µmol m^{-2} s^{-1}), A_{max}: maximum assimilation rate (µmol m^{-2} s^{-1}), q: apparent quantum yield (mol/mol). Data are means, n=6 ± standard deviation.

Table 6.3 Leaf-level CO_2 response measurements of the different barley genotypes after fitting with the Sharkey et al., 2007 model.

Growth stage	Genotype	*Vcmax*	*Jmax*	TPU	Rd	gm
Booting BBCH 46	*Barke*	110 ± 5ab	158 ± 16ab	11.6 ± 1.1ab	0.91 ± 0.1a	28.1 ± 2.2ab
	Olve	124 ± 16a	187 ± 25a	12.9 ± 1.5a	0.88 ± 0.3a	29.9 ± 0.17a
	Sissi	100 ± 8b	142 ± 21b	9.9 ± 1.6b	1.02 ± 0.5a	30.3 ± 0.19a
Grain filling BBCH 74	*Barke*	174 ± 22a	325.1 ± 31a	23.3 ± 2a	0.5 ± 0.3ab	29.995±0.03a
	Olve	140.6 ± 10b	253.4 ± 15b	18.4 ± 1.2b	0.7 ± 0.2ab	29.837±0.14a
	Sissi	155.5 ± 19ab	288.3 ± 26ab	20.9 ± 1.7ab	0.8 ± 0.4a	29.715±0.17a

Different letters denote Tukey's HSD Test of significance. VC_{max}: apparent maximum of rubisco carboxylation rate, J_{max}: regeneration of ribulose-1, 5-biphosphate expressed as electron transport rate, TPU: triose phosphate utilization, Rd: dark respiration, gm: mesophyll conductance. Data are means, n=6 ± standard deviation.

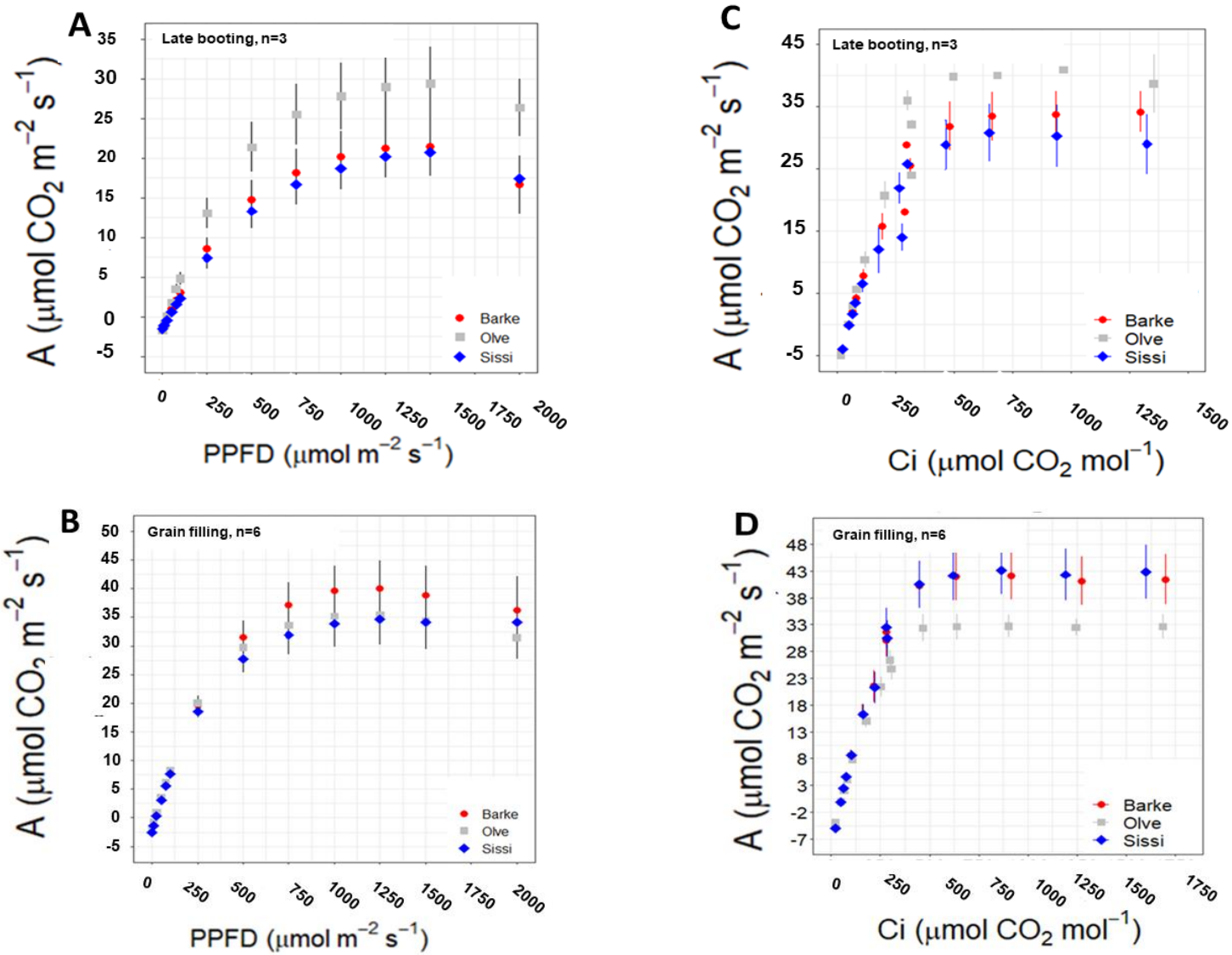

Figure 6.1 Light response curves of barley genotypes *Olve*, *Sissi* and *Barke*, measured at late booting (A) and grain filling stage (B). CO_2 response curves of barley leaf carbon assimilation at the booting and grain filling stages are shown in panels (C) and (D), respectively. PPFD: Photosynthetic photon flux density, A: net CO_2 assimilation rate, Ci: Intracellular CO_2.

6.3.4 Reference curves of barley spike filling

Reference curves were constructed based on spike samples collected from the booting stage until maturity (Figure 6.2 A-D). Regression plots between the destructive and non-destructive results showed strong linearity, correlation, and good fit for all four parameters, irrespective of genotype or spike age. The R^2 of the linear fits from figures 6.2A to 6.2D varied between 0.84 and 0.97 (Figure 6.2 A-D). The reference curves of all spikes showed a robust linear relationship between the water content and PD_{liq}/PD_{tot} (Figure 6.2D).

6.3.5 Seed filling curve of barley spike

A pronounced bell shape can be distinguished in the FW and WW seed filling curves. Four phases (exponential, plateau, desiccation and ripe) can be observed for FW and WW curves (Figure 6.3). First, an initial steady filling phase gives way to a steep exponential phase that reaches a maximum (Figure 6.3, FW and WW, exponential phase). For all genotypes, in this phase a maximum filling rate was reached and maintained for some days and transitioning into a plateau phase (Figure 6.3, FW and WW, plateau phase). The final stage of spike development was the desiccation phase, at which water is lost, DW deposition stagnates, and finally decrease gradually (Figure 6.3, DW, desiccation phase) before reaching ripe (Figure 6.3, DW, ripe phase).

We observed a rapid influx of water into the spike or seed for all studied barley genotypes during the early 3 to 5 days after anthesis. However, water influx was reduced strongly around the peak filling rate (peak DW deposition, Figure 6.3). All barley genotypes showed similar DW spike filling curves (Figures 6.3 and 6.4 A-I). DW increased progressively to peak DW (20 days after anthesis) from the initial seed filling stages. Peak DW growth rate continued for about a week in all genotypes before it started to decrease (Figure 6.4 A-I). For all genotypes, the DW spike filling continued longer than the net influx of water, giving rise to an elongated wave-like curve instead of a bell shape (Figures 6.3 and 6.4 A-I). A comparison of filling rates between the three genotypes suggests that a higher influx of water into the spike was associated with a concomitant higher deposition in terms of DW.

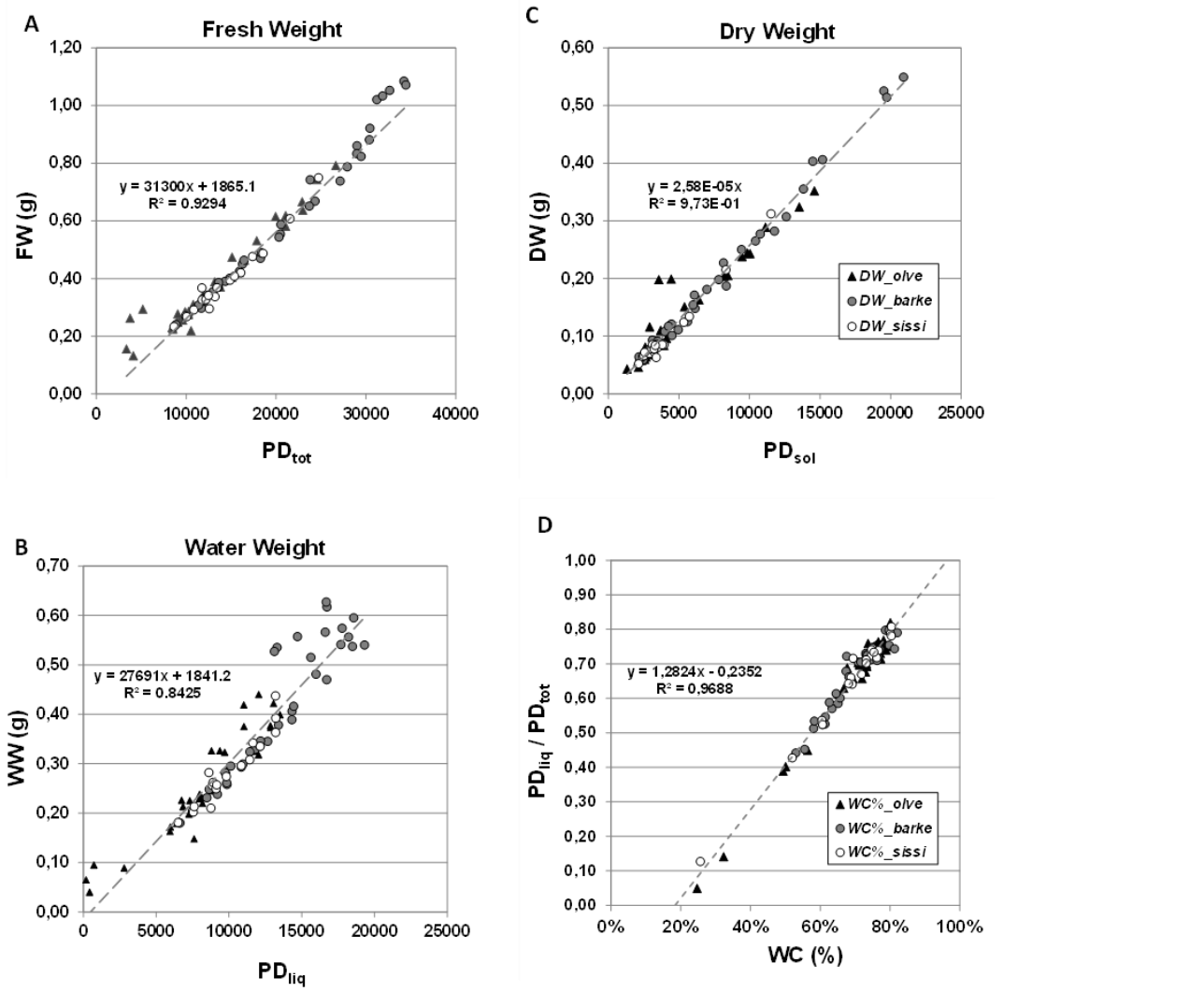

Figure 6.2 Reference curves for excised 20 mm long spike sections of barley genotypes *Olve*, *Sissi* and *Barke*, harvested in a period from booting stage onwards to ripening. In panel (A) fresh weight (FW) is plotted against total proton density (PD_{tot}); in panel (B) water weight (WW) is plotted against liquid proton density (PD_{liq}); in panel (C) dry weight (DW) is plotted against PD_{sol}; in panel (D) PD_{tot}/ PD_{liq} is plotted against water content (WC). n=40.

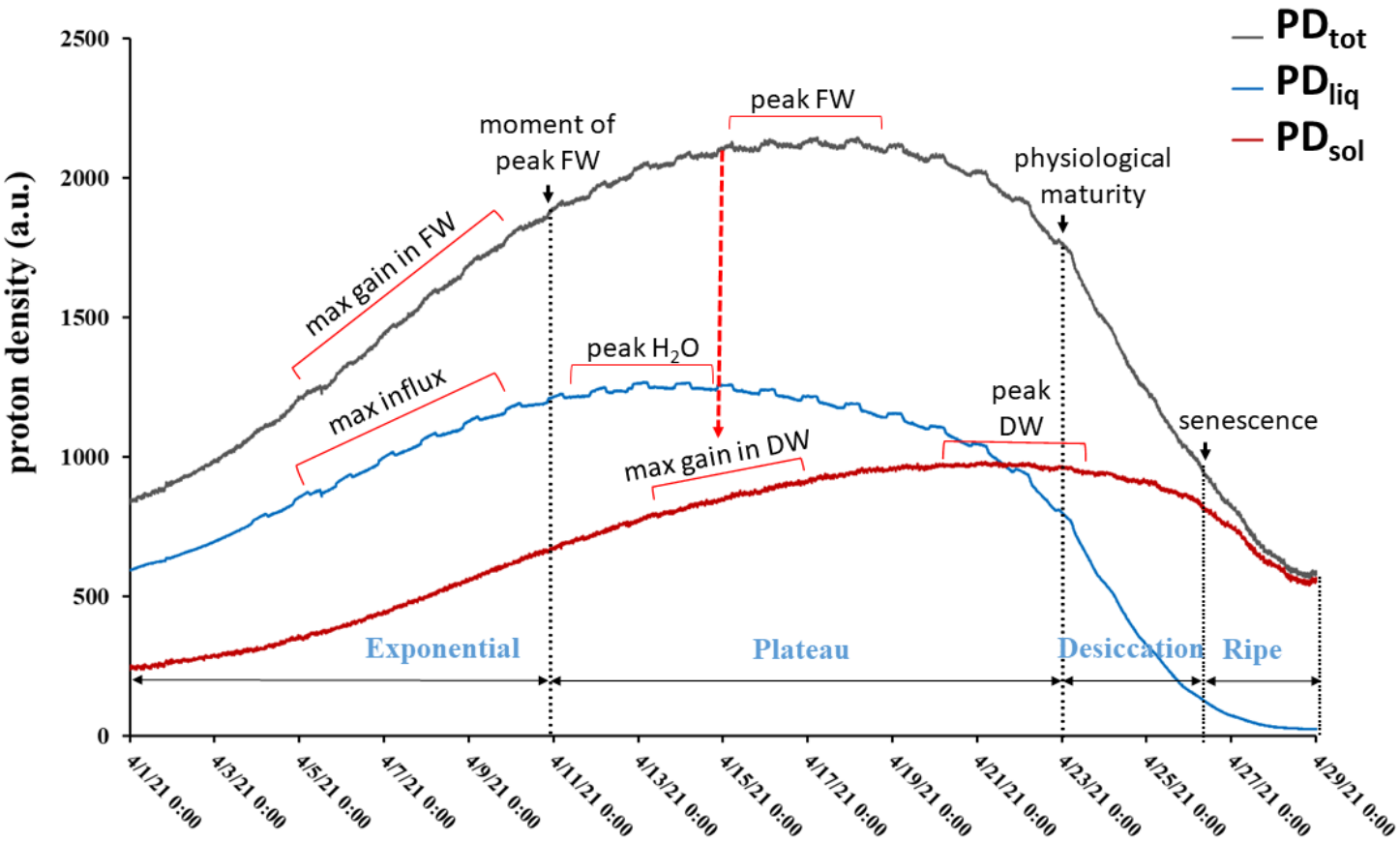

Figure 6.3 Typical seed filling curve of two-row spring barley (*Barke*) from seed initiation till seed ripe, as acquired non-invasively by the multiplexed NMR sensor. The seed filling curves could be categorized into four phases. First, an initial exponential growth phase (rapid growth) can be distinguished, characterized by grain cell expansion. It is driven by a fast influx of water (PD_{liq}, blue line) and dry matter (PD_{sol}, red line), which together give rise to a fast increase in fresh weight (PD_{tot}, dark grey line). In the second phase (plateau), both maximum filling rate in terms of DW occurs, as well as peak FW. The plateau phase ends when physical maturity, as well as peak DW, is reached. Hereafter, PD_{liq} (WW) reduces sharply until senescence sets in and finally, the grains ripen.

6.3.6 Maximum fresh weight, water and dry matter content of the spikes

Biomass FW, WW and DW (Figures 6.5 A-I) were calculated from the raw NMR proton densities (Appendix 6.2 and 6.3) based on the reference measurements (Figure 6.2) to simplify comparison of the rate of filling to gravimetric measurements. *Barke* had the highest ($P < 0.05$) mean peak FW and mean peak DW (36 and 14 mg, respectively) compared to *Olve* or *Sissi* (28, 31 and 10.6, 11 mg, respectively, Table 6.4). The dry matter deposition rate was highest at the late mid-stages of the growth curve and showed a similar pattern or shape for all three barley genotypes (Figure 6.4 A- I). At the initial spike filling stages, water content for all the genotypes studied was very high compared to the late filling stage both in the calculated weights (Figures 6.5 A-I) and the raw NMR proton densities (Appendix 6.2 and 6.3). The mean water content (62%) was not significantly different among the three genotypes at the peak filling of FW (Tables 6.4, Appendix 6.2, and Figure 6.5 A-I).

6.3.7 Seed filling duration

The average number of days after anthesis (DAA) until completion of seed ripening was 27 for *Barke*, 26 for *Olve* and 26 for *Sissi*, which was not significantly different ($P \geq 0.05$) among the three barley genotypes (Table 6.5). *Barke* took 11 days (DAA) to reach peak FW or peak filling rate, faster than *Olve* and *Sissi* (13 and 14 DAA, respectively, Table 6.5). The number of days for *Barke* to reach peak WW also were lower (9 DAA) than for *Olve* and *Sissi* (10 and 11 DAA respectively, Table 6.5). All three genotypes maintained their respective peak FW for a similar number of days, ~10 DAA (Table 6.5). The number of days to reach peak WW was lower for *Sissi* (7 DAA) compared to *Barke* and *Olve* (10 DAA, Table 6.5). However, *Barke* showed an earlier decrease in FW, after ~22 DAA, than *Olve* and *Sissi* (at ~25 and ~24 DAA, respectively; Table 6.5). After reaching its peak, WW started to decrease after ~19 DAA in all three genotypes (Table 6.5). No differences in total DW filling duration were observed in the three genotypes. In all three genotypes, the number of days to reach peak DW averaged about 20 DAA (Figure 6.4). After that, DW stagnated for about ~7 days in all three genotypes (Figure 6.4). DW subsequently decreased after about 27 DAA in all three genotypes, when the non-seed biomass in the spike started to senesce (Figure 6.4).

6.3.8 Day and night time seed filling

We observed marginal variations in deposition of FW, WW and DW by the different barley genotypes at night and during the day (Figure 6.6). The average rate of seed filling in terms of WW at maximum influx, 3-7 DAA and the net deposition at a maximum gain in DW, 10-15 DAA, of the three barley genotypes showed significant differences (Figure 6.6). *Barke* had the highest deposition rates of FW, WW and DW (40, 29 and 13 mg/day, respectively) in the period between 3-7 DAA, compared to *Olve* (25, 19 and 6 mg/day) and *Sissi* (32, 25 and 9 mg/day) (Figure 6.6). The average rate of seed filling at peak filling, 10-15 DAA, also differed significantly among the genotypes (Figure 6.6). In this period *Barke* had the highest filling rates in terms of FW, DW and WW (53, 33 and 20 mg/day) compared to *Olve* (37, 21 and 16 mg/day) and *Sissi* (47, 30 and 17 mg/day), respectively (Figure 6.6). Generally, the filling rate in FW, WW, and DW at night was marginally higher in all three barley genotypes than during the day (Figure 6.6).

Table 6.4 FW DW and WC at the moment of peak FW of the different barley spike sections (20 mm) measured with the multiplexed NMR sensor from anthesis stage to seed maturity.

Genotypes	Mean FW (mg)	Mean DW (mg)	Mean WC %
Barke	36.43 ± 1.5a	13.6 ± 0.59a	62.33 ± 0.33a
Olve	28.34 ± 1.1b	10.56 ± 0.43b	61.17 ± 0.17a
Sissi	31.15 ± 1.6ab	11.18 ± 0.65b	64.83 ± 0.48a

Different letters denote Tukey's HSD Test of significance. FW-fresh weight, DW-dry weight, WC-water content. Data are means, n=6 ± standard deviation.

Table 6.5 Duration (days after anthesis) of biomass accumulation into the different barley spike sections (20 mm) measured with the multiplexed NMR sensor over time.

Genotypes	Days to ripening (days)	Time to reach peak FW (days)	Length of the peak FW (days)	Time after which peak FW decline (days)	Time to reach Peak WW (days)	Length of the Peak WW (days)	Time after which Peak WW decline (days)
Barke	27 ± 0.01a	10.5 ± 0.56b	11.17 ± 0.16ab	21.67 ± 0.56b	8.67 ± 0.33ab	10.33 ± 0.56a	19 ± 0.45ab
Olve	26.33 ± 0.42a	12.83 ± 0.95ab	12 ± 0.57a	24.83 ± 1.05a	10.16 ± 0.17a	9.83 ± 1.45a	20 ± 1.46a
Sissi	26.5 ± 0.62a	14.33 ± 0.56a	9.17 ± 0.40ab	23.83 ± 0.60ab	10.83 ± 0.48a	7 ± 0.36b	17.67 ± 0.76ab

Different letters denote Tukey's HSD Test of significance. FW-fresh weight, DW-dry weight, WW-water weight. Data are means, n=6 ± standard deviation.

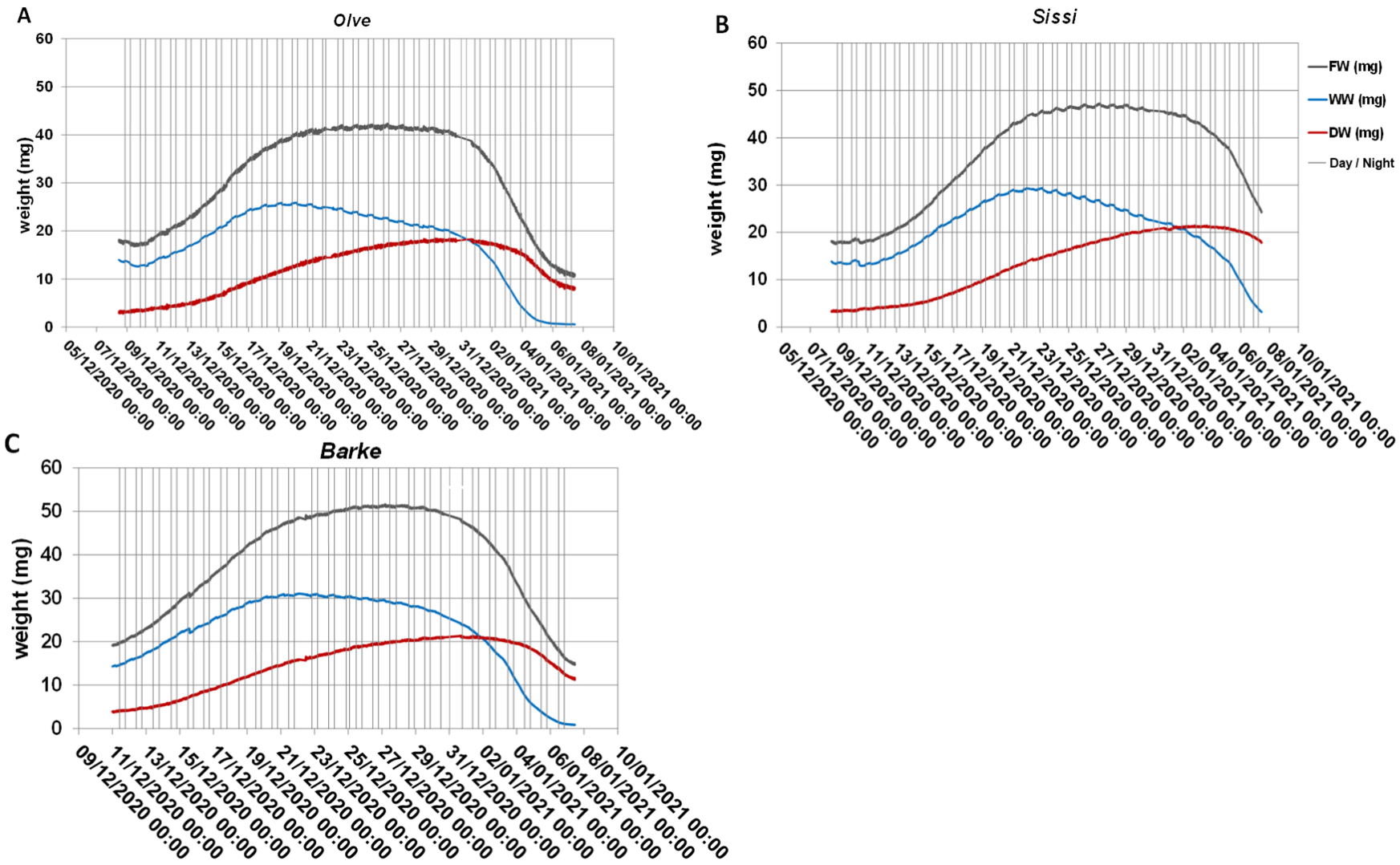

Figure 6.4 Dry and liquid matter deposition in terms of fresh weight (FW, grey line), water weight (WW, blue line), and dry weight (DW, red line) in the main tiller spikes of barley genotypes *Olve* (A), *Sissi* (B), and *Barke* (C) during 20 days of reproductive development after anthesis until maturity, as measured non-invasively by the multiplexed NMR sensor. The figure shows representative measurements of individual main spikes of each genotype.

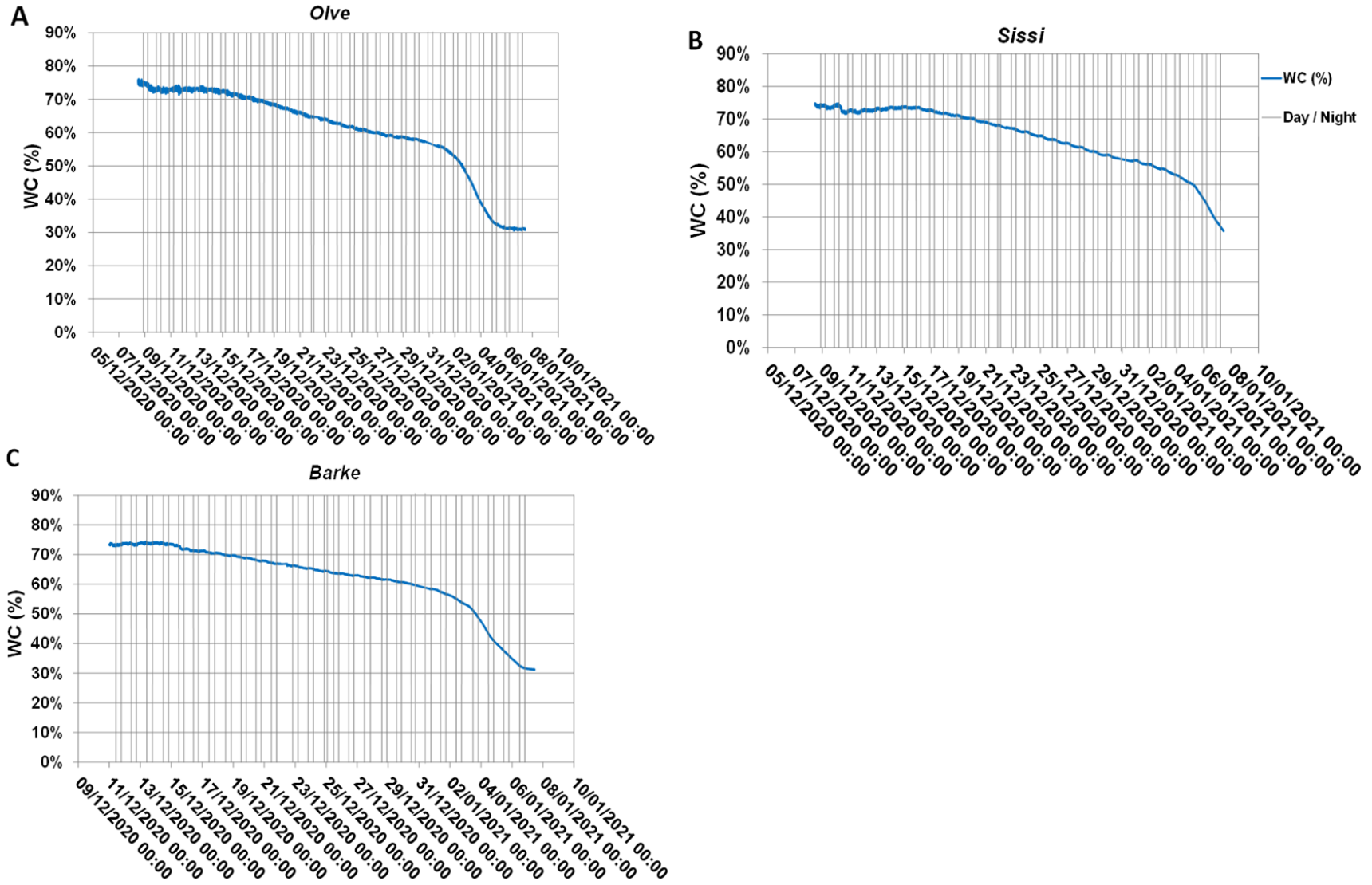

Figure 6.5 Relative water content of the main spikes of barley genotypes *Olve* (A), *Sissi* (B), and *Barke* (C) during 20 days of reproductive development from anthesis till maturity. Plotted are relative water content (WC, %, blue line), the vertical light ash grid lines indicate day/night intervals. Shown are representative measurements of individual main spikes for each genotype.

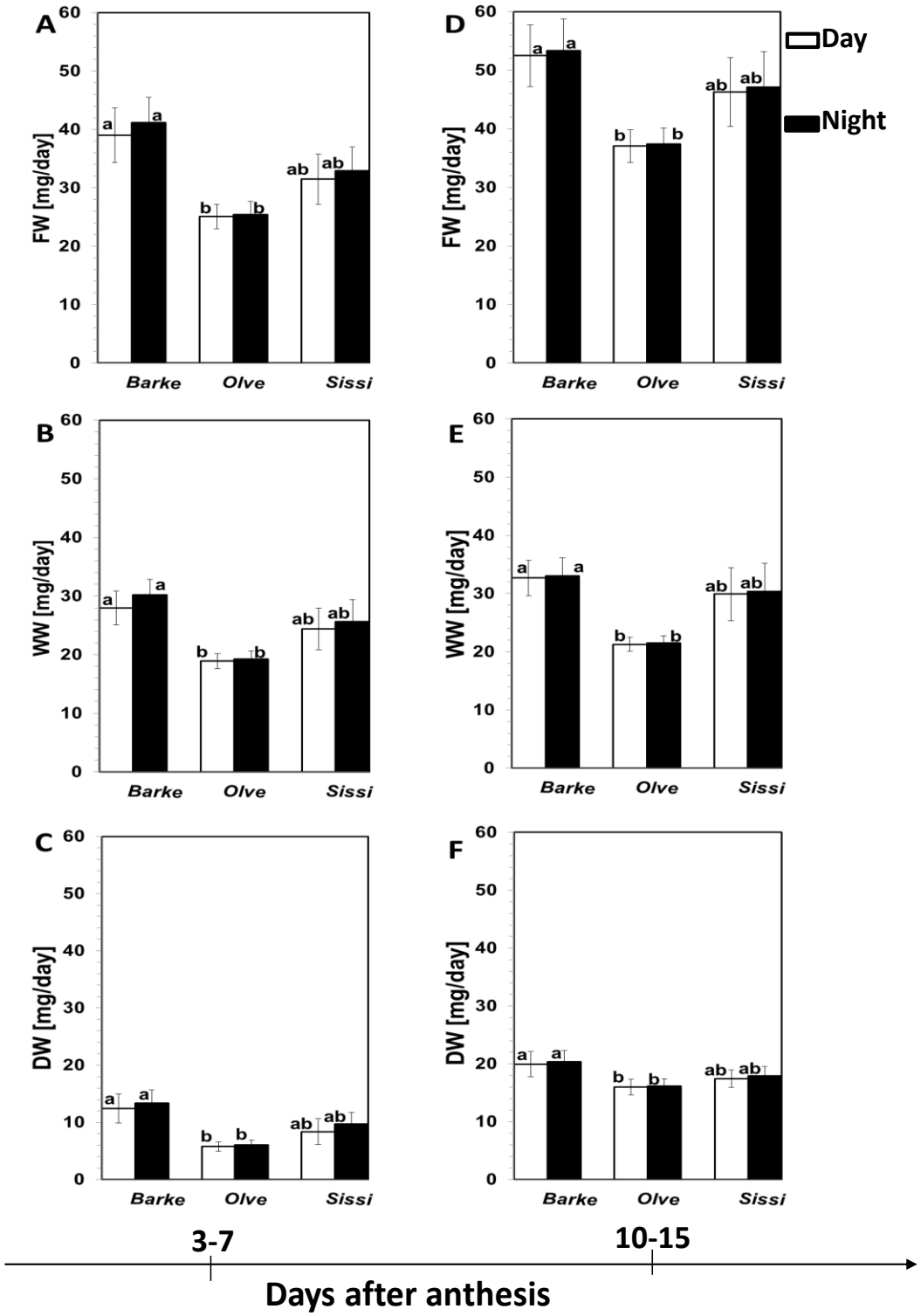

Figure 6.6 Average day and night time increment in fresh weight (FW), panels (A) and (D), water weight (WW), panels (B) and (E) and dry weight (DW), panels (C) and (F) in main spikes of barley genotypes *Barke*, *Olve* and *Sissi*, as determined during the period of maximum FW increase, 3-7 days after anthesis (DAA; left column of graphs) and during the period of maximum DW increase (10-15 DAA; right column of graphs). n=6.

6.4 Discussion

A unique benefit of the NMR sensor is that it allows non-invasive measurements of FW, DW and WW of the developing spike. Measuring multiple plants with one sensor, however, is slow and undesirable. Changing samples is laborious, and the instrument is most likely to detect small dynamic changes if the plant under observation is not moved or changed between readings. Multiplexing the NMR sensor made it possible to measure six plants simultaneously, grown on the same table and under the same environmental conditions. Multiplexing has been demonstrated before in magnetic resonance imaging, using many small rf coils to measure multiple objects simultaneously inside a large MR scanner. In this work, we instead drove multiple NMR magnets, each with their rf coils and together making up six sensor heads, utilizing a single spectrometer. Since the spectrometer is the most expensive part of an NMR sensor, this approach can significantly reduce the technique's cost per plant measured. This would especially hold true if the magnets, rf coils and associated tuning apparatus were built in larger series.

By means of the multiplexed NMR sensor, we were able to study seed filling in our three barley genotypes with an unprecedented time resolution. One data point was recorded every 5.5 minutes per spike. This translates to ~262 data points per day or 5240 data points for 20 days of seed filling post-anthesis. In contrast, in the most detailed temporal analysis of seed filling done on a barley using the destructive gravimetric method, a one-time weight or data point could be collected per day per spike (Goudriaan & Laar, 1994). Goudriaan & Laar (1994) reported on growth curves of barley where they sampled and measured ~100 spikes per m^2 per day (which translates to 700 data points a week). A drawback of the NMR sensor relative to gravimetric analysis is that all tissues and organs inside the rf coil (aside from on average 6 developing spikelets, also the leaf sheath, awns, glumes, palea, lemma, palea, awns, rachis, chaff) contribute to the measured signal. A second drawback is the limited sensitive region of the NMR sensors, 20 mm as limited by the rf coil size. This could be improved in future versions to cover the entire length of the spike.

The NMR sensors allowed us to monitor barley seed filling dynamics in more detail than was possible before. On the basis of non-destructive NMR measurements, the grain filling rate, water accumulation rate, fresh weight, and dry matter content of the main spikes of three spring barley genotypes could readily be determined (Table 6.4 and Figures 6.5 and 6.6). The shape of the

growth curve of our barley spikes (20 mm of the lower-mid section) during grain filling was similar to earlier reports on seed filling of wheat (Lv et al., 2021; Takahashi et al., 2001; Wardlaw et al., 2000; Windt et al., 2021) and rice (Wang et al., 2015). Previously, studies of seed filling in barley and wheat, however, depicted the growth phases very differently, often with straight lines delineating each phase of seed development (exponential, linear and senescence phases, Goudriaan and van Laar 1994), drawn on the basis of only a few measured data points (Brenchley and Hall, 1909; Gooding et al., 2003; Schnyder and Baum, 1992). Smooth spline curves have been drawn as well (MacGregor et al., 1971), but again with only a few measured data points. Our study shows that the transitions between the phases, in fact, are smooth, and the whole curve looks more like a stretched-out bell curve than the square-ish boxcar-like plots previously reported. The ability to obtain seed filling characteristics of genotypes on the basis of only a few plants may be of great interest to breeders, for example, identifying plants with seed that fill and mature faster. Such genotypes may have an advantage in climates where abiotic stresses are likely to occur later in the growing season (Shavrukov et al., 2017). The detailed seed filling curves further allowed us to derive new seed filling metrics such as the period of maximum influx of water during seed filling (in our three genotypes occurring 3-7 DAA), and the period of maximum DW gain (in our genotypes occurring 10-15 DAA).

In our study, barley seed filling began with approximately 10 days of a rapid influx of water, synchronized later with fast deposition of the dry matter content of mainly starch and carbohydrates, proteins, and other solid materials in the first 10 up to 15 days of cell expansion. Growth stabilized at peak filling rate for about 5 to 10 days before seed desiccation kicked in at the final seed maturity phase (Figure 6.3 and Table 6.5) for all our genotypes. The spike or seed filling durations described above agree well with (MacGregor et al., 1971) as they defined the growth phases in the same manner, where barley grain filling was studied in detail destructively. We monitored the spikes of all three barley genotypes continued growth and expansion until 27 days after anthesis (Table 6.5). The period of cell division ends between 16 and 20 days after anthesis; cell volume, however, according to literature, continues to increase until 35 days after anthesis (Briarty et al., 1979). The seed filling determines the final seed weight (seed size), a primary component of total seed yield (Sehgal et al., 2018). In our study, taking into consideration the whole seed reproductive cycle, *Barke* had the highest average peak deposition rate of FW, DW and WW (40, 13 and 29 mg/day) compared to *Olve* (25, 6 and 19 mg/day) and *Sissi* (32, 9 and 25 mg/day),

respectively (Figure 6.6). *Barke* was faster to reach peak filling rate of water content by ~8 days and maximum gain in FW, by 10 days (Tables 6.5) compared to the other genotypes. The difference in time to reach peak water and dry matter filling rate compared to *Olve* and *Sissi* was about 2 and 4 days, respectively (Table 6.5). The mean peak FW and peak DW during seed filling of all the barley types ranged between 28 – 37 mg and 10 – 14 mg, respectively (Table 6.4). These results above agree with Wardlaw et al. (2000), who reported similar values on wheat kernel filling under non-limiting conditions. Grain filling occurred both during the day and the night in all four phases of seed development. Our three barley types showed a similar magnitude of filling during day and night (Figure 6.6). This in contrasts strongly with earlier findings by Windt et al. (2021), who found that in wheat, most dry matter was deposited in the seed at night, not during the day.

HI is a carbon-centric metric to estimate plant efficiency in agricultural systems (partitioning of biomass as a whole), and selection for high HI in plant breeding has successfully improved yield production, e.g. wheat (Broberg et al., 2021). Among the three barley genotypes, *Barke* had the highest harvest index (HI) of 0.5 (Table 6.1). HI, the ratio of grain yield to total biomass is considered a measure of biological efficiency in partitioning assimilated photosynthates to the harvestable product. HI is an integrative measure representing the cumulative biological processes during crop growth, such as remobilization, transporting and depositing photoassimilates and nutrients from vegetative plant tissues into the seeds (Smith et al., 2018). Therefore, *Barke* had higher assimilate partitioning, deposition of carbon, and starch remobilization into the grains compared with *Olve* and *Sissi*. *Barke's* higher HI and seed yield might be due to its higher capacity for photosynthesis, particularly at the critical seed filling stage. Prins et al. (2016) reported that Rubisco and maximum carboxylation rate efficiency are major targets for improving crop photosynthesis and yield. Increasing the efficiency of CO_2 fixation by Rubisco will increase the synthesis of carbohydrates required for plant growth and yield (Sharwood, 2017). In our study, we found that *Barke* showed superior leaf-level photosynthetic efficiency than *Olve* and *Sissi* during the grain filling stage. The high photosynthetic capacity of *Barke* in our study may have allowed for a higher source strength and, therefore, a faster seed filling rate than the other barley genotypes.

6.5 Conclusion

By means of the multiplexed NMR sensor we were able to monitor spike filling with high temporal resolution, in terms of fresh weight, dry weight and water content, from the onset of grain filling till seed maturity. We found that seed filling in all three barley genotypes occurs night and day, and that day and night time deposition rates were similar. The detailed seed filling curves allowed us to easily derive new seed filling metrics such as the period of maximum influx of water during seed filling (in our three genotypes occurring 3-7 DAA), and the period of maximum DW gain (in our genotypes occurring 10-15 DAA). We could determine that *Barke* had an at least 5% higher DW seed filling rate, having had the highest average peak deposition rates of FW, DW and WW (40, 13 and 29 mg/day) compared to *Olve* (25, 6 and 19 mg/day) and *Sissi* (32, 9 and 25 mg/day, respectively). We propose that these derived metrics can be used to characterize and compare the seed filling dynamics in cereals and other grain crops. Comparative to *Olve* and *Sissi*, *Barke* showed superior leaf-level photosynthesis and overall morpho-physiological performance during seed filling, which may explain its higher seed filling rate. Destructive gravimetric analysis after harvest confirmed that *Barke* had higher assimilate partitioning, deposition of carbon, and starch remobilization into the grains than *Olve* and *Sissi*. We envisage that breeders could reduce labour and save time using the multiplexed NMR sensor at the preselection phase to characterize and determine seed filling traits in genotypes using only a few plants, which would otherwise require large numbers of plants when measured destructively.

CHAPTER 7

Most parts of this chapter were adapted from Frimpong et al., (2021a & b) of this thesis.

7 GENERAL DISCUSSION

So far, we characterized a panel of contrasting elite barley genotypes and *P5cs1*-introgression lines and monitored their morpho-physiological responses after water withdrawal during reproductive development. Several morpho-physiological traits had significant genotypes by treatment interaction and reduction under WS (Frimpong et al., 2021a). We further characterized the isogenic line of *P5cs1*-introgressions root architectural traits and root placement (roots positioning within the substrate profile) under water stress and control conditions in barley genotypes (Frimpong et al., 2021b). Finally, we used NMR's (multiplexed NMR sensor and MRI) to study the reproductive development of barley on intact barley spikes and identified the variations in different barley genotypes during spike growth non-destructively, continuous and simultaneously.

Arguably, differential plant organ proline is not extensively researched. We addressed this gap by elucidating whether barley introgression lines harbouring a wild allele at *Pyrroline-5-carboxylate synthase1-P5cs1* locus are comparatively more drought-tolerant at the reproductive stage by inducing proline accumulation in their immature spikes. We gave insights into the differential spike and leaf proline accumulation among these genotypes and their photosynthetic and intrinsic water use efficiency responses. The possible physiological mechanisms and root architectural traits that lead to comparatively improved tolerance to water stress of barley introgression lines bearing a wild allele at *P5cs1* locus were discussed.

We found varying levels of genotypic proline accumulation, and differences in WS tolerance were observed. Spike proline accumulation was higher than leaf proline accumulation for all genotypes under WS (Frimpong et al., 2021a). Also, introgression lines carrying a wild allele at the *P5cs1* locus had a markedly higher spike and leaf proline content compared with the other genotypes (Frimpong et al., 2021a). These introgression lines showed milder drought symptoms compared with elite genotypes, remained photosynthetically active under WS, and maintained their intrinsic water use efficiency (Frimpong et al., 2021a). These combined responses contributed to

the achievement of higher final seed productivity (Frimpong et al., 2021a). Magnetic resonance imaging (MRI) of whole spikes at the soft dough stage showed an increase in seed abortion among the elite genotypes compared with the introgression lines 15 days after WS treatment. Our results suggest that proline accumulation at the reproductive stage contributes to the maintenance of grain formation under water shortage (Frimpong et al., 2021a).

Moreover, root growth in rhizoboxes under reduced water availability conditions caused a significant reduction in total root length, rooting depth, root maximum width, and root length density of barley. On average, root growth was reduced by more than 20% due to water stress. Differences in organ proline concentrations were observed for all genotypes studied, with shoots grown under water stress exhibiting at least 30% higher concentration than the roots. Drought further induced higher leaf and root proline concentrations in *NIL 143* compared with any of the other genotypes. Under reduced water availability conditions, *NIL 143* showed less severe symptoms of drought, higher lateral root length, rooting depth, maximum root width, root length density, and convex hull area compared with *Barke* and *Scarlett*. Within the same comparison, under water stress, *NIL 143* had a higher proportion of lateral roots (+30%), which were also placed at deeper substrate horizons. In addition, *NIL 143* had a less negative plant water potential and higher relative leaf water content and stomatal conductance compared with the other genotypes under water stress. Under these conditions, this genotype also maintained a net photosynthetic rate and exhibited considerable fine root growth (diameter class 0.05-0.35 mm). These results show that water stress induces increased shoot and root proline accumulation in the *NIL 143* barley genotype at the seedlings stage and that this effect is associated with increased lateral root growth.

7.1 Drought, barley yield and genetic improvement efforts

Reduced water availability leads to crop water shortage. Drought affects metabolism, development and crop habitus. Intense water deficiency most often leads to significant alterations to physiological processes under dehydration, slowing down growth, or even arresting it and reducing yield (Dietz et al., 2021). In barley and most crops, yield losses in the field under drought typically range between 30% and 90%, depending on the species (Dietz et al., 2021). Dietz et al. (2021) emphasized that crop yield sensitivity to water shortage depends on the type of harvested agricultural products, such as taproots, shoots, leaves, fruits or seeds. Drought during specific phases of crop development may have dire consequences on yield, especially during the

reproductive phase of cereals cultivation (Frimpong et al., 2021a). For example, prolonged drought at the booting stage caused a significant reduction of 76% of barley grain weight per plant (Frimpong et al., 2021a). For barley roots, drought led to at least 20 % reduction of the total root development, lateral roots formation and less vigorous fine roots (Frimpong et al., 2021b). Fortunately, there is a growing popularity for crop genotype improvement, through the introduction of exotic genetic introgressions which are important genetic assets for the genetic dissection of complex quantitative traits (Bohra et al., 2021). For instance, Hornsdorf et al. (2014) and Muzammil et al. (2018) reported an enhanced drought tolerance within barley introgression lines of the *S42* library (which we tested and confirm), of progenies of a Meditarranean wild parental allele backcrossing. Therefore, an informed choice of crop wild relatives for genetic studies and breeding can be made by considering the collection sites' environmental variables. We highlight that instead of random sampling, trait-specific crop wild relatives may be selected from areas experiencing natural selection pressure (hot spots) for the specific trait or traits of interest (Bohra et al., 2021).

7.2 Proline accumulation for barley drought tolerance

As a response to drought, heat, salinity, cold and other abiotic stresses, plants including barley may accumulate proline in the chloroplasts after synthesis in the cytosol (Meena et al., 2019). Proline accumulation and its homeostasis in plants defence is a well-documented physiological response to osmotic stress triggered largely by abiotic stress. Proline plays a number of defensive and improvement functions such as osmoprotectant, cell membrane stability, stabilizing enzymatic reactions, regulation of plant improvement, including flowering, pollen, embryo, and leaf enlargement and scavenging for oxygen species, thus keeping a redox balance during stress (Meena et al., 2019). Consistent with the literature, Templer et al. (2017) observed an accumulation of proline, fructose, and glucose in their elite German and Mediterranean barley types under drought and combined heat and drought stress conditions. Furthermore, we found that a wild allele of *pyrroline-5-carboxylate synthase1* leads to proline accumulation in spikes and leaves of barley, contributing to improved performance under reduced water availability (Frimpong et al., 2021a). The reasons are; proline protects cellular structures from dehydration, functions as a molecular chaperone stabilizing the structure of proteins, and proline accumulation buffer cytosolic pH to balance cell redox status (Verbruggen & Hermans, 2008). Finally, proline accumulation partly acts

as a stress signal influencing adaptive responses (Verbruggen & Hermans, 2008). Thus, our results provide an agronomic and physiological basis for further breeding of barley cultivars, focusing on improving proline-mediated drought tolerance mechanisms.

7.3 NMR sensing and MRI for non-invasive barley seed phenotyping

We demonstrated that the multiplexed NMR sensor and MR imaging have the potential over optical microscopy to non-invasively visualize and quantify seed development or abortion on intact spikes faster and can be helpful during pre-selection in cereal breeding and abiotic stress studies. Non-invasive NMR sensor and MRI scans of whole intact developing spikes revealed the overall perspective about the level of a-synchronicity during grain filling in our two-row spring barley types. MRI highlighted the point of initiation of seed set and filling to be the lower mid-section of the spike. Our NMR setup revealed genotypic variations of the two-row spring barley in their loading rates of fresh weight, water and dry mater content depositions into the seed. These variations in loading rates of the different genotypes were similar to the observed manual yield trends, which could mean that the loading capacities considerably explain the variations in grain yield by the different genotypes under control conditions. Additionally, we demonstrated that the NMR sensor is another available through-put non-invasive approach to quantify seed filling in a manner that could facilitate barley pre-breeding selection processes.

7.4 Summary and outlook

First, we have addressed the role of proline in barley spikes as an energy source driving photosynthesis and redox balancing under drought stress (Frimpong et al. 2021a). Drought tolerance was enhanced in the leaves by staying green, showing less drought symptoms and in the roots with the production of deeper and longer lateral/fine roots. The high proline accumulating isogenic line, *NIL 143*, having had the highest RWC and more vigorous roots, showed better osmotic adjustment and capacity than any other barley genotype in our study (Frimpong et al. 2021a & b). The noninvasive approaches (MRI and the NMR- Multiplex) we used provided an option to monitor *in vivo* developing seeds and internal floret structures. From our MR images, we were able to phenotype under drought and select higher seed yield barley genotypes from poor ones by monitoring seed abortion, other seed qualities such as the seed mass, seed shape and architecture in a shorter time frame and less laborious compared to conventional phenotyping. The results of our MRI study have provided the basis for further research. We suggest combining MRI with

artificial intelligence and machine learning to quantitatively characterize seeds from initiation until maturity in abiotic stress studies. To our knowledge and for the first time, the multiplexed NMR approach monitored several live barley spikes simultaneously as the plant photosynthesized while seed loading was taking place. We quantified water influx, the diurnal rate change in fresh and dry matter depositions across the entire timescale of reproductive stage till seed maturity (Chapter 6 of this thesis). Furthermore, by elucidating the role of proline aboveground (leaves) and belowground (lateral roots), we provided the basis for future or additional research in terms of noninvasive monitoring of cereals spike and seed development using MRI and multiplexed NMR sensor. The two NMR approaches showed how internal structures develop on live spikes that could not be conducted under conventional manual counting or weighing to unravel these specific spike phenes during our proline drought studies (Chapters 3-6 of this thesis).

Overall, it is interesting to highlight tissue-specific differences in proline accumulation for tolerance under reduced water conditions in different barley genotypes. Enhanced proline accumulation in some barley genotypes promotes drought tolerance mainly by helping maintain whole-plant water status. Thus, proline-mediated drought tolerance might lead to improved aboveground (better seed yield at the reproductive stage) and belowground (growth of lateral roots at the seedlings stage) phenotypic traits. Our results suggest that proline accumulation in barley spikes under drought plays a significant role in maintaining final seed yield (Frimpong et al., 2021a). Again, our results show that water stress induces increased shoot and root proline accumulation in the isogenic barley line *NIL 143* at the seedlings stage and that this effect is associated with increased lateral root growth.

On the other hand, we quantified and visualized *in vivo* barley seed filling using our multiplexed NMR and MRI during spike development (Chapters 5 & 6 of this thesis). These methods detected variations among barley genotypes during seed filling on intact barley spikes through continuous, simultaneous and in situ measurements. Future studies on the *P5cs1*-introgressions should focus on validating presented physiological variation in field conditions and the effect of elevated proline on grain quality traits. We recommend further studies to explore the variations in root-shoot growth observed for *NIL 143* in the field to test their performance under a water-limited environment. In addition, further studies will be required to explore how proline accumulation promotes barley root water uptake under water stress.

PUBLICATIONS

1. **Frimpong, F.**, Windt, C., van Dusschoten, D., Naz, A., Frei, M., & Fiorani, F. (2021a). A wild allele of *Pyrroline-5-carboxylate synthase1* leads to proline accumulation in spikes and leaves of barley contributing to improved performance under reduced water availability. *Frontiers in Plant Science, 12*(180). https://doi.org/10.3389/fpls.2021.633448

    - Scientific work and development-50%
    - Greenhouse work-95%
    - Proline analysis- 80%
    - Data analysis-85%
    - Publication work-70%

2. **Frimpong, F.**, Anokye, M., Windt, C., van Dusschoten, D., Naz, A., Frei, M., & Fiorani, F. (2021b). Proline mediated drought tolerance in barley (*Hordeum vulgare* L.) isogenic line is associated with lateral root growth at the early seedlings stage. *Plants 10*. https://doi.org/10.3390/plants10102177

    - Scientific work and development-50%
    - Greenhouse work-70%
    - Proline analysis- 65%
    - Data analysis-95%
    - Publication work-70%

3. **Frimpong, F.**, van Dusschoten, D., Fiorani, F., Pflugfelder, D., Windt, C., W. (2021c) *In vivo* visualization of barley (*Hordeum vulgare* L.) grain development by MRI. *Manuscript in preparation. Unpublished.*

    - Scientific work and development-50%
    - Greenhouse work-95%
    - MRI analysis- 60%
    - Data analysis-80%
    - Publication work-80%

4. **Frimpong, F.**, van Dusschoten, D., Kochs J., Windt, C.W. (2021d). Quantifying spike filling rate, dry matter and water content of two-row barley genotypes with the non-invasive multiplexed NMR sensor. *Manuscript in preparation. Unpublished.*

    - Scientific work and development-50%
    - Climate chamber work-75%
    - Multiplex data analysis- 60%
    - Other Data analysis-90%
    - Publication work-70%

APPENDICES

Chapter 3 appendices

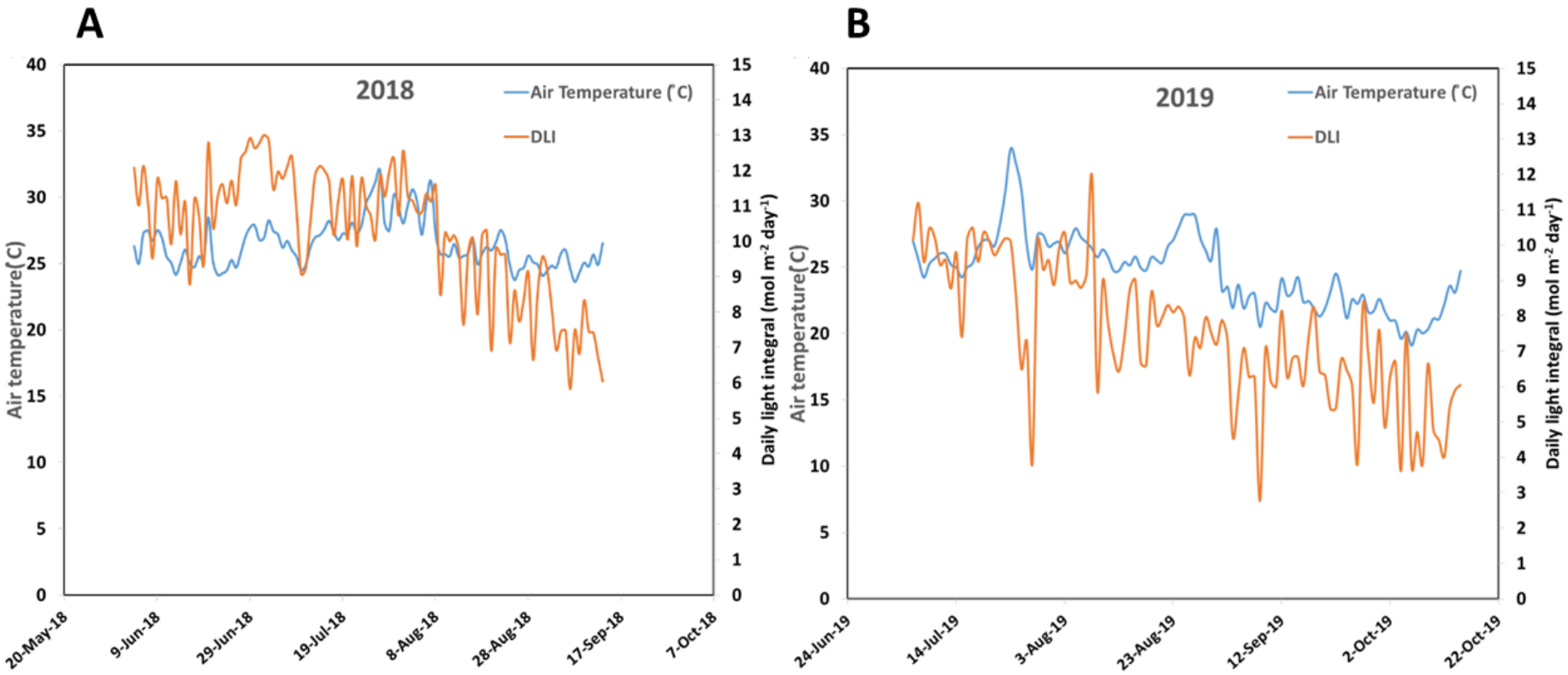

Appendix 3.1 Daily mean air temperature (℃) and daily light integral (mol m^{-2} day^{-1}) recorded at the greenhouse during the experiments in 2018 (a) and 2019 (b). The figure was taken from Frimpong et al., 2021a

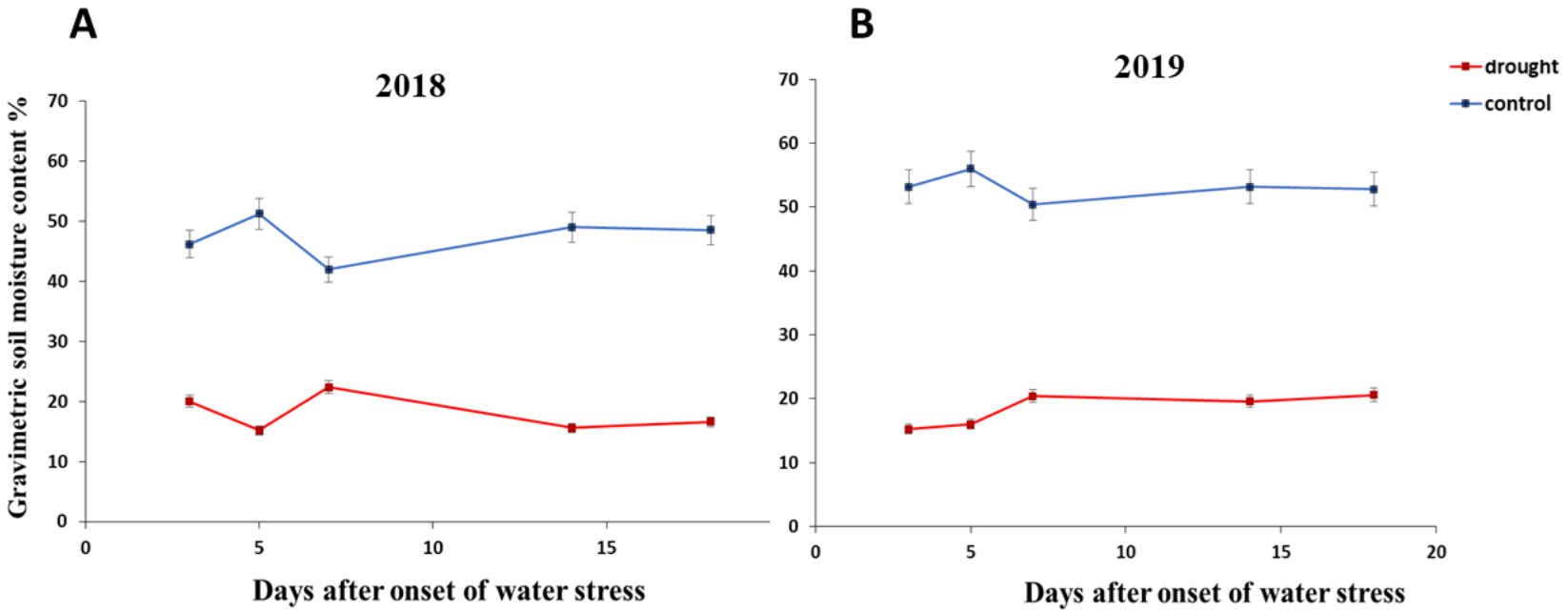

Appendix 3.2 Line graphs of the gravimetric soil moisture content measured with the Theta ML2 probe during the application of the two irrigation regimes for the 2018 (A) and 2019 (B) experiments. The blue line represents the percentage gravimetric moisture content of the well-watered plants (~50% g/g), and the red line is the percentage gravimetric moisture content of the water stressed plants after two days of dry down (water stress ~20% g/g). The figure was taken from Frimpong et al., 2021a.

Appendix 3.3 Results of three-way analysis of variance (Type III, error) of proline tissue type spike data.

```
Anova Table (Type III tests)

Response: sqrt(proline)
                               Sum Sq  Df   F value                  Pr(>F)
(Intercept)                     44235   1 6753.9858 < 0.00000000000000022 ***
treatment                        6321   1  965.1592 < 0.00000000000000022 ***
tissue_type                        24   2    1.7959                0.170201
genotype                         1004   4   38.3405 < 0.00000000000000022 ***
treatment:tissue_type               7   2    0.5024                0.606261
treatment:genotype               1288   4   49.1568 < 0.00000000000000022 ***
tissue_type:genotype              174   8    3.3292                0.001731 **
treatment:tissue_type:genotype    118   8    2.2536                0.027660 *
Residuals                         825 126
---
Signif. codes:  0 ‘***’ 0.001 ‘**’ 0.01 ‘*’ 0.05 ‘.’ 0.1 ‘ ’ 1
                          Effect DFn DFd       F
1                      treatment   1 126 965.159
2                    tissue_type   2 126   1.796
3                       genotype   4 126  38.340
4          treatment:tissue_type   2 126   0.502
5             treatment:genotype   4 126  49.157
6           tissue_type:genotype   8 126   3.329
7 treatment:tissue_type:genotype   8 126   2.254
                                                                  p p<.05   ges
1 0.000000000000000000000000000000000000000000000000000000000000651     * 0.885
2 0.170000000000000012212453270876721944659948348999023437500000000       0.028
3 0.000000000000000000005840000000000002273875532310398739355150 61     * 0.549
4 0.605999999999999983124610025697620585560798645019531250000000000       0.008
5 0.000000000000000000000007420000000000000114561138353508340514 96     * 0.609
6 0.002000000000000000041633363423443370265886187553405761718750000     * 0.174
```

```
simple two-way interaction-----------
data %>% group_by(treatment) %>% anova_test(sqrt(proline) ~ tissue_type * genotype, error = model)
A tibble: 6 x 8
treatment Effect                DFn   DFd      F        p `p<.05`   ges
<fct>     <chr>               <dbl> <dbl>  <dbl>    <dbl> <chr>   <dbl>
control   tissue_type             2   126  0.602 5.49e- 1 ""      0.009
control   genotype                4   126 17.2   2.74e-11 "*"     0.353
control   tissue_type:genotype     8   126  0.216 9.88e- 1 ""      0.014
drought   tissue_type             2   126  1.79  1.71e- 1 ""      0.028
drought   genotype                4   126 71.6   1.58e-31 "*"     0.695
drought   tissue_type:genotype     8   126  5.33  9.01e- 6 "*"     0.253

data %>% group_by(tissue_type) %>% anova_test(sqrt(proline) ~ treatment * genotype, error = model)
A tibble: 9 x 8
tissue_type Effect               DFn   DFd     F        p `p<.05`   ges
<fct>       <chr>              <dbl> <dbl> <dbl>    <dbl> <chr>   <dbl>
apical      treatment              1   126 375.  1.36e-39 *       0.749
apical      genotype               4   126  18.3 7.11e-12 *       0.367
apical      treatment:genotype     4   126  26.5 5.63e-16 *       0.457
basal       treatment              1   126 327.  8.01e-37 *       0.722
basal       genotype               4   126  13.2 4.96e- 9 *       0.296
basal       treatment:genotype     4   126  10.8 1.40e- 7 *       0.256
middle      treatment              1   126 321.  1.91e-36 *       0.718
middle      genotype               4   126  14.5 8.87e-10 *       0.316
middle      treatment:genotype     4   126  16.5 6.64e-11 *       0.344
```

```
#simple simple main effects-----------
treatment.effect <- data %>% group_by(genotype, tissue_type) %>% anova_test(sqrt(proline) ~ treatment, error = model)
treatment.effect %>% filter(tissue_type == "apical")
genotype tissue_type Effect      DFn   DFd     F        p `p<.05`   ges
  <fct>    <fct>       <chr>     <dbl> <dbl> <dbl>    <dbl> <chr>   <dbl>
1 Barke    apical      treatment     1   126  34.3 3.93e- 8 *       0.214
2 HOR10151 apical      treatment     1   126  19.2 2.49e- 5 *       0.132
3 S42IL141 apical      treatment     1   126 269.  4.75e-33 *       0.681
4 S42IL143 apical      treatment     1   126 147.  6.91e-23 *       0.538
5 Scarlett apical      treatment     1   126  12.2 6.72e- 4 *       0.088

treatment.effect %>% filter(tissue_type == "middle")
 genotype tissue_type Effect      DFn   DFd     F        p `p<.05`   ges
  <fct>    <fct>       <chr>     <dbl> <dbl> <dbl>    <dbl> <chr>   <dbl>
1 Barke    middle      treatment     1   126  30.8 1.58e- 7 *       0.197
2 HOR10151 middle      treatment     1   126  32.5 7.92e- 8 *       0.205
3 S42IL141 middle      treatment     1   126 171.  3.42e-25 *       0.575
4 S42IL143 middle      treatment     1   126 141.  2.93e-22 *       0.528
5 Scarlett middle      treatment     1   126  12.1 6.85e- 4 *       0.088

treatment.effect %>% filter(tissue_type == "basal")
genotype tissue_type Effect      DFn   DFd     F        p `p<.05`   ges
  <fct>    <fct>       <chr>     <dbl> <dbl> <dbl>    <dbl> <chr>   <dbl>
1 Barke    basal       treatment     1   126  53.0 3.21e-11 *       0.296
2 HOR10151 basal       treatment     1   126  54.0 2.18e-11 *       0.3
3 S42IL141 basal       treatment     1   126 106.  2.31e-18 *       0.456
4 S42IL143 basal       treatment     1   126 148.  5.91e-23 *       0.539
5 Scarlett basal       treatment     1   126  10.3 2.00e- 3 *       0.075
```

```
#simple simple main effects-----------
treatment.effect <- data %>% group_by(genotype, tissue_type) %>% anova_test(sqrt(proline) ~ treatment, error = model)
treatment.effect %>% filter(tissue_type == "apical")
genotype tissue_type Effect      DFn   DFd     F        p `p<.05`   ges
  <fct>    <fct>       <chr>     <dbl> <dbl> <dbl>    <dbl> <chr>   <dbl>
1 Barke    apical      treatment     1   126  34.3 3.93e- 8 *       0.214
2 HOR10151 apical      treatment     1   126  19.2 2.49e- 5 *       0.132
3 S42IL141 apical      treatment     1   126 269.  4.75e-33 *       0.681
4 S42IL143 apical      treatment     1   126 147.  6.91e-23 *       0.538
5 Scarlett apical      treatment     1   126  12.2 6.72e- 4 *       0.088

treatment.effect %>% filter(tissue_type == "middle")
 genotype tissue_type Effect      DFn   DFd     F        p `p<.05`   ges
  <fct>    <fct>       <chr>     <dbl> <dbl> <dbl>    <dbl> <chr>   <dbl>
1 Barke    middle      treatment     1   126  30.8 1.58e- 7 *       0.197
2 HOR10151 middle      treatment     1   126  32.5 7.92e- 8 *       0.205
3 S42IL141 middle      treatment     1   126 171.  3.42e-25 *       0.575
4 S42IL143 middle      treatment     1   126 141.  2.93e-22 *       0.528
5 Scarlett middle      treatment     1   126  12.1 6.85e- 4 *       0.088

treatment.effect %>% filter(tissue_type == "basal")
genotype tissue_type Effect      DFn   DFd     F        p `p<.05`   ges
  <fct>    <fct>       <chr>     <dbl> <dbl> <dbl>    <dbl> <chr>   <dbl>
1 Barke    basal       treatment     1   126  53.0 3.21e-11 *       0.296
2 HOR10151 basal       treatment     1   126  54.0 2.18e-11 *       0.3
3 S42IL141 basal       treatment     1   126 106.  2.31e-18 *       0.456
4 S42IL143 basal       treatment     1   126 148.  5.91e-23 *       0.539
5 Scarlett basal       treatment     1   126  10.3 2.00e- 3 *       0.075
```

```
genotype.effect <- data %>% group_by(treatment, tissue_type) %>% anova_test(sqrt(proline) ~ genotype, error = model)
genotype.effect %>% filter(tissue_type == "apical")
treatment tissue_type Effect     DFn   DFd     F        p `p<.05`   ges
  <fct>     <fct>       <chr>    <dbl> <dbl> <dbl>    <dbl> <chr>   <dbl>
1 control   apical      genotype     4   126  4.34 3.00e- 3 *       0.121
2 drought   apical      genotype     4   126 40.5  8.73e-22 *       0.563

genotype.effect %>% filter(tissue_type == "middle")
 treatment tissue_type Effect     DFn   DFd     F        p `p<.05`   ges
  <fct>     <fct>       <chr>    <dbl> <dbl> <dbl>    <dbl> <chr>   <dbl>
1 control   middle      genotype     4   126  6.27 1.23e- 4 *       0.166
2 drought   middle      genotype     4   126 24.8  3.87e-15 *       0.44

genotype.effect %>% filter(tissue_type == "basal")
treatment tissue_type Effect     DFn   DFd     F        p `p<.05`   ges
  <fct>     <fct>       <chr>    <dbl> <dbl> <dbl>    <dbl> <chr>   <dbl>
1 control   basal       genotype     4   126  7.04 3.81e- 5 *       0.183
2 drought   basal       genotype     4   126 17.0  3.45e-11 *       0.351

tissue_type.effect %>% filter(treatment == "control")
genotype treatment Effect        DFn   DFd     F     p `p<.05`      ges
  <fct>    <fct>     <chr>       <dbl> <dbl> <dbl> <dbl> <chr>      <dbl>
1 Barke    control   tissue_type     2   126 0.473 0.624 ""      0.007
2 HOR10151 control   tissue_type     2   126 0.373 0.689 ""      0.006
3 S42IL141 control   tissue_type     2   126 0.186 0.83  ""      0.003
4 S42IL143 control   tissue_type     2   126 0.04  0.961 ""      0.000639
5 Scarlett control   tissue_type     2   126 0.394 0.675 ""      0.006
```

```
tissue_type.effect %>% filter(treatment == "control")
genotype treatment Effect        DFn   DFd     F     p `p<.05`      ges
  <fct>    <fct>     <chr>       <dbl> <dbl> <dbl> <dbl> <chr>      <dbl>
1 Barke    control   tissue_type     2   126 0.473 0.624 ""      0.007
2 HOR10151 control   tissue_type     2   126 0.373 0.689 ""      0.006
3 S42IL141 control   tissue_type     2   126 0.186 0.83  ""      0.003
4 S42IL143 control   tissue_type     2   126 0.04  0.961 ""      0.000639
5 Scarlett control   tissue_type     2   126 0.394 0.675 ""      0.006

tissue_type.effect %>% filter(treatment == "drought")
# A tibble: 5 x 9
  genotype treatment Effect        DFn   DFd      F           p `p<.05`   ges
  <fct>    <fct>     <chr>       <dbl> <dbl>  <dbl>       <dbl> <chr>   <dbl>
1 Barke    drought   tissue_type     2   126  0.565 0.570       ""      0.009
2 HOR10151 drought   tissue_type     2   126  4.23  0.017       "*"     0.063 !!! p-correction 0.05/5 -> p needs < 0.01
3 S42IL141 drought   tissue_type     2   126 17.4   0.000000205 "*"     0.217
4 S42IL143 drought   tissue_type     2   126  0.141 0.869       ""      0.002
5 Scarlett drought   tissue_type     2   126  0.73  0.484       ""      0.011

#simple simple comparisons-tissue_type effect in genotype S42IL143 under drought----------
pwc <- data %>% group_by(treatment, genotype) %>%
  emmeans_test(sqrt(proline) ~ tissue_type, p.adjust.method = "bonferroni")
pwc %>% filter(genotype == "S42IL143", treatment == "drought")

treatment genotype term        .y.           group1 group2    df statistic            p
  <chr>     <chr>    <chr>       <chr>         <chr>  <chr>  <dbl>     <dbl>        <dbl>
1 drought   S42IL141 tissue_type sqrt(proline) apical basal    126      5.91 0.0000000304
2 drought   S42IL141 tissue_type sqrt(proline) apical middle   126      2.67 0.00851
3 drought   S42IL141 tissue_type sqrt(proline) basal  middle   126     -3.10 0.00242
         p.adj p.adj.signif
         <dbl> <chr>
```

```
1 0.0000000912 ****
2 0.0255       *
3 0.00725      **

#post-hoc-genotype effect within treatment and tissue type----------
pwc <- data %>% group_by(tissue_type, treatment) %>%
  emmeans_test(sqrt(proline) ~ genotype, p.adjust.method = "bonferroni")

 tissue_type treatment term     .y.           group1   group2      df statistic        p    p.adj p.adj.signif
 * <chr>       <chr>     <chr>    <chr>         <chr>    <chr>    <dbl>     <dbl>    <dbl>    <dbl> <chr>
 1 apical      control   genotype sqrt(proline) Barke    HOR10151   126   -2.96   3.66e- 3 3.66e- 2 *
 2 apical      control   genotype sqrt(proline) Barke    S42IL141   126   -1.12   2.66e- 1 1.00e+ 0 ns
 3 apical      control   genotype sqrt(proline) Barke    S42IL143   126   -0.833  4.06e- 1 1.00e+ 0 ns
 4 apical      control   genotype sqrt(proline) Barke    Scarlett   126   -3.30   1.24e- 3 1.24e- 2 *
 5 apical      control   genotype sqrt(proline) HOR10151 S42IL141   126    2.13   3.54e- 2 3.54e- 1 ns
 6 apical      control   genotype sqrt(proline) HOR10151 S42IL143   126    2.29   2.37e- 2 2.37e- 1 ns
 7 apical      control   genotype sqrt(proline) HOR10151 Scarlett   126   -0.183  8.55e- 1 1.00e+ 0 ns
 8 apical      control   genotype sqrt(proline) S42IL141 S42IL143   126    0.269  7.88e- 1 1.00e+ 0 ns
 9 apical      control   genotype sqrt(proline) S42IL141 Scarlett   126   -2.47   1.49e- 2 1.49e- 1 ns
10 apical      control   genotype sqrt(proline) S42IL143 Scarlett   126   -2.62   9.83e- 3 9.83e- 2 ns
11 apical      drought   genotype sqrt(proline) Barke    HOR10151   126   -1.75   8.30e- 2 8.30e- 1 ns
12 apical      drought   genotype sqrt(proline) Barke    S42IL141   126  -10.3    1.57e-18 1.57e-17 ****
13 apical      drought   genotype sqrt(proline) Barke    S42IL143   126   -6.80   3.85e-10 3.85e- 9 ****
14 apical      drought   genotype sqrt(proline) Barke    Scarlett   126   -0.785  4.34e- 1 1.00e+ 0 ns
15 apical      drought   genotype sqrt(proline) HOR10151 S42IL141   126   -8.52   4.16e-14 4.16e-13 ****
16 apical      drought   genotype sqrt(proline) HOR10151 S42IL143   126   -5.05   1.52e- 6 1.52e- 5 ****
17 apical      drought   genotype sqrt(proline) HOR10151 Scarlett   126    0.962  3.38e- 1 1.00e+ 0 ns
18 apical      drought   genotype sqrt(proline) S42IL141 S42IL143   126    3.25   1.50e- 3 1.50e- 2 *
19 apical      drought   genotype sqrt(proline) S42IL141 Scarlett   126    9.52   1.58e-16 1.58e-15 ****
20 apical      drought   genotype sqrt(proline) S42IL143 Scarlett   126    6.01   1.86e- 8 1.86e- 7 ****
21 basal       control   genotype sqrt(proline) Barke    HOR10151   126   -4.76   5.12e- 6 5.12e- 5 ****
22 basal       control   genotype sqrt(proline) Barke    S42IL141   126   -1.36   1.76e- 1 1.00e+ 0 ns
23 basal       control   genotype sqrt(proline) Barke    S42IL143   126   -1.88   6.23e- 2 6.23e- 1 ns
```

24	basal	control	genotype	sqrt(proline)	Barke	Scarlett	126	-3.38	9.57e- 4	9.57e- 3	**
25	basal	control	genotype	sqrt(proline)	HOR10151	S42IL141	126	3.57	5.09e- 4	5.09e- 3	**
26	basal	control	genotype	sqrt(proline)	HOR10151	S42IL143	126	3.02	3.02e- 3	3.02e- 2	*
27	basal	control	genotype	sqrt(proline)	HOR10151	Scarlett	126	1.23	2.20e- 1	1.00e+ 0	ns
28	basal	control	genotype	sqrt(proline)	S42IL141	S42IL143	126	-0.544	5.87e- 1	1.00e+ 0	ns
29	basal	control	genotype	sqrt(proline)	S42IL141	Scarlett	126	-2.17	3.18e- 2	3.18e- 1	ns
30	basal	control	genotype	sqrt(proline)	S42IL143	Scarlett	126	-1.65	1.01e- 1	1.00e+ 0	ns
31	basal	drought	genotype	sqrt(proline)	Barke	HOR10151	126	-4.17	5.57e- 5	5.57e- 4	***
32	basal	drought	genotype	sqrt(proline)	Barke	S42IL141	126	-3.87	1.77e- 4	1.77e- 3	**
33	basal	drought	genotype	sqrt(proline)	Barke	S42IL143	126	-6.15	9.33e- 9	9.33e- 8	****
34	basal	drought	genotype	sqrt(proline)	Barke	Scarlett	126	0.689	4.92e- 1	1.00e+ 0	ns
35	basal	drought	genotype	sqrt(proline)	HOR10151	S42IL141	126	0.136	8.92e- 1	1.00e+ 0	ns
36	basal	drought	genotype	sqrt(proline)	HOR10151	S42IL143	126	-2.25	2.59e- 2	2.59e- 1	ns
37	basal	drought	genotype	sqrt(proline)	HOR10151	Scarlett	126	4.89	2.99e- 6	2.99e- 5	****
38	basal	drought	genotype	sqrt(proline)	S42IL141	S42IL143	126	-2.29	2.38e- 2	2.38e- 1	ns
39	basal	drought	genotype	sqrt(proline)	S42IL141	Scarlett	126	4.55	1.23e- 5	1.23e- 4	***
40	basal	drought	genotype	sqrt(proline)	S42IL143	Scarlett	126	6.84	3.04e-10	3.04e- 9	****
41	middle	control	genotype	sqrt(proline)	Barke	HOR10151	126	-4.18	5.42e- 5	5.42e- 4	***
42	middle	control	genotype	sqrt(proline)	Barke	S42IL141	126	-0.897	3.71e- 1	1.00e+ 0	ns
43	middle	control	genotype	sqrt(proline)	Barke	S42IL143	126	-0.955	3.41e- 1	1.00e+ 0	ns
44	middle	control	genotype	sqrt(proline)	Barke	Scarlett	126	-3.34	1.12e- 3	1.12e- 2	*
45	middle	control	genotype	sqrt(proline)	HOR10151	S42IL141	126	3.32	1.16e- 3	1.16e- 2	*
46	middle	control	genotype	sqrt(proline)	HOR10151	S42IL143	126	3.09	2.48e- 3	2.48e- 2	*
47	middle	control	genotype	sqrt(proline)	HOR10151	Scarlett	126	0.809	4.20e- 1	1.00e+ 0	ns
48	middle	control	genotype	sqrt(proline)	S42IL141	S42IL143	126	-0.0995	9.21e- 1	1.00e+ 0	ns
49	middle	control	genotype	sqrt(proline)	S42IL141	Scarlett	126	-2.48	1.45e- 2	1.45e- 1	ns
50	middle	control	genotype	sqrt(proline)	S42IL143	Scarlett	126	-2.28	2.44e- 2	2.44e- 1	ns
51	middle	drought	genotype	sqrt(proline)	Barke	HOR10151	126	-4.46	1.77e- 5	1.77e- 4	***
52	middle	drought	genotype	sqrt(proline)	Barke	S42IL141	126	-8.01	6.55e-13	6.55e-12	****
53	middle	drought	genotype	sqrt(proline)	Barke	S42IL143	126	-7.26	3.45e-11	3.45e-10	****
54	middle	drought	genotype	sqrt(proline)	Barke	Scarlett	126	-1.36	1.77e- 1	1.00e+ 0	ns
55	middle	drought	genotype	sqrt(proline)	HOR10151	S42IL141	126	-3.09	2.46e- 3	2.46e- 2	*
56	middle	drought	genotype	sqrt(proline)	HOR10151	S42IL143	126	-2.18	3.14e- 2	3.14e- 1	ns

```
57 middle      drought   genotype sqrt(proline) HOR10151 Scarlett   126    3.18   1.84e- 3 1.84e- 2 *
58 middle      drought   genotype sqrt(proline) S42IL141 S42IL143   126    1.10   2.72e- 1 1.00e+ 0 ns
59 middle      drought   genotype sqrt(proline) S42IL141 Scarlett   126    6.65   7.87e-10 7.87e- 9 ****
60 middle      drought   genotype sqrt(proline) S42IL143 Scarlett   126    5.85   4.06e- 8 4.06e- 7 ****

###ALTERNATIVE####
#Compute estimated marginal means (EMMs) for specified factors or factor combinations in a linear model; and optionally, comparisons or contrasts among them.
#Estimated marginal means (i.e. adjusted means) with 95% confidence interval
proline.emm.s <- emmeans(model, ~ genotype * treatment | tissue_type)
write.table(proline.emm.s, file = 'Proline_EMMs.csv', sep = ',', dec = '.', append = FALSE, row.names = FALSE, col.names = TRUE)
png(filename = 'Proline_emmsPlot_20220120.png', width = 1000, height = 800, units = "px", pointsize = 12, bg = "white")
plot(proline.emm.s, comparisons = TRUE)
dev.off()
pairs <- pairs(proline.emm.s) #pairwise comparisons
write.table(pairs, file = 'proline_pwc.csv', sep = ',', dec = '.', append = FALSE, row.names = FALSE, col.names = TRUE)
```

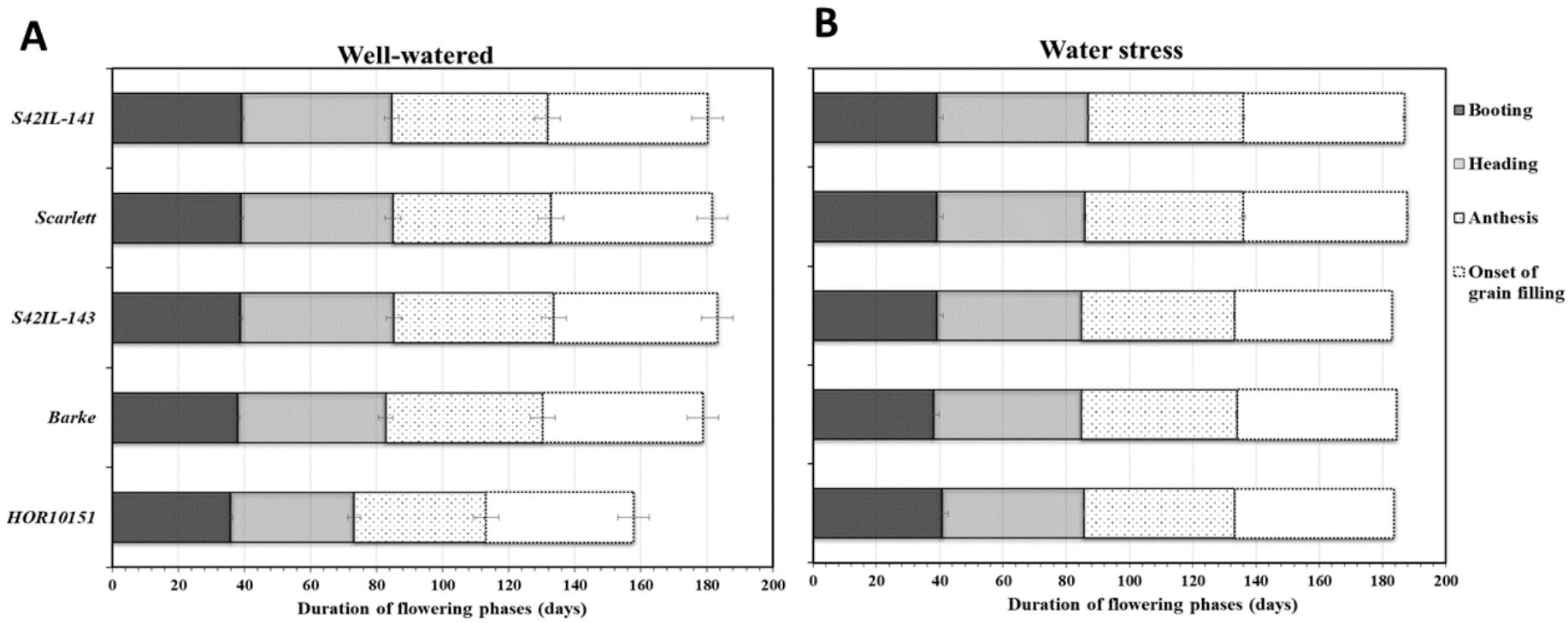

Appendix 3.4 Duration of flowering phases of the spikes under well-watered condition (A) and water stress conditions (B). The legend indicates the various spike developmental stages from booting, heading, anthesis, and on-set of grain filling. The Y-axis shows the different genotypes. The figure was taken from Frimpong et al., 2021a.

Appendix 3.5 Range of variation and relative percentage change of morphological, yield, and physiological traits under well-watered (WW) and water stress (WS) conditions during the 2018 and 2019 experimental years. Morphological and yield traits were measured at harvest, photosynthesis and gas exchange parameters were measured three days after the onset of water stress. The table was taken from Frimpong et al., 2021a.

	Data range (min-max)				Relative percentage change (100 × WS -WW/WW)	
	WW		WS			
Selected plant trait	**2018**	**2019**	**2018**	**2019**	**2018**	**2019**
Plant height (cm)	77-105	79-106	59-88	61-82	-18	-27
Tiller number	14-23	16-25	10-19	6-17	-19	-47
Spike number	16-22	21-30	6-12	11-22	-45	-38
Length of main spike (cm)	6-14	6-13	4-12	3-13	-18	-22
Grain number per main tiller	14-43	15-61	0-28	0-30	-30	-58
Grain weight (g)	7-8	8-18	1-8	0-9	-76	-76
shoot fresh weight (g)	23-95	16-116	16-69	5-28	-18	-44
% Relative leaf water content	82-94	76-97	50-92	14-91	-15	-35
Net CO_2 Assimilation (µmol m^{-2} s^{-1})	20-30	20-22	8-22	3-10	-56	-72
Stomatal conductance (mol m^{-2} s^{-1})	0.33-0.55	0.20-0.40	0.069-0.19	0.02-0.10	-74	-77
iWUE (µmol CO_2 $mmol^{-1}$ H_2O)	55-82	61-94	87-149	69-111	+73	+17
Electron transport rate (µmol m^{-2} s^{-1})	130-194	127-180	70-134	51-152	-31	-28
Transpiration rate (mol m^{-2} s^{-1})	$8.0E^{-3}$-$1.2E^{-2}$	$4.0E^{-3}$-$9.0E^{-3}$	$1.9E^{-3}$-$5.9E^{-3}$	$5.2E^{-4}$-$3.0E^{-3}$	-63	-76

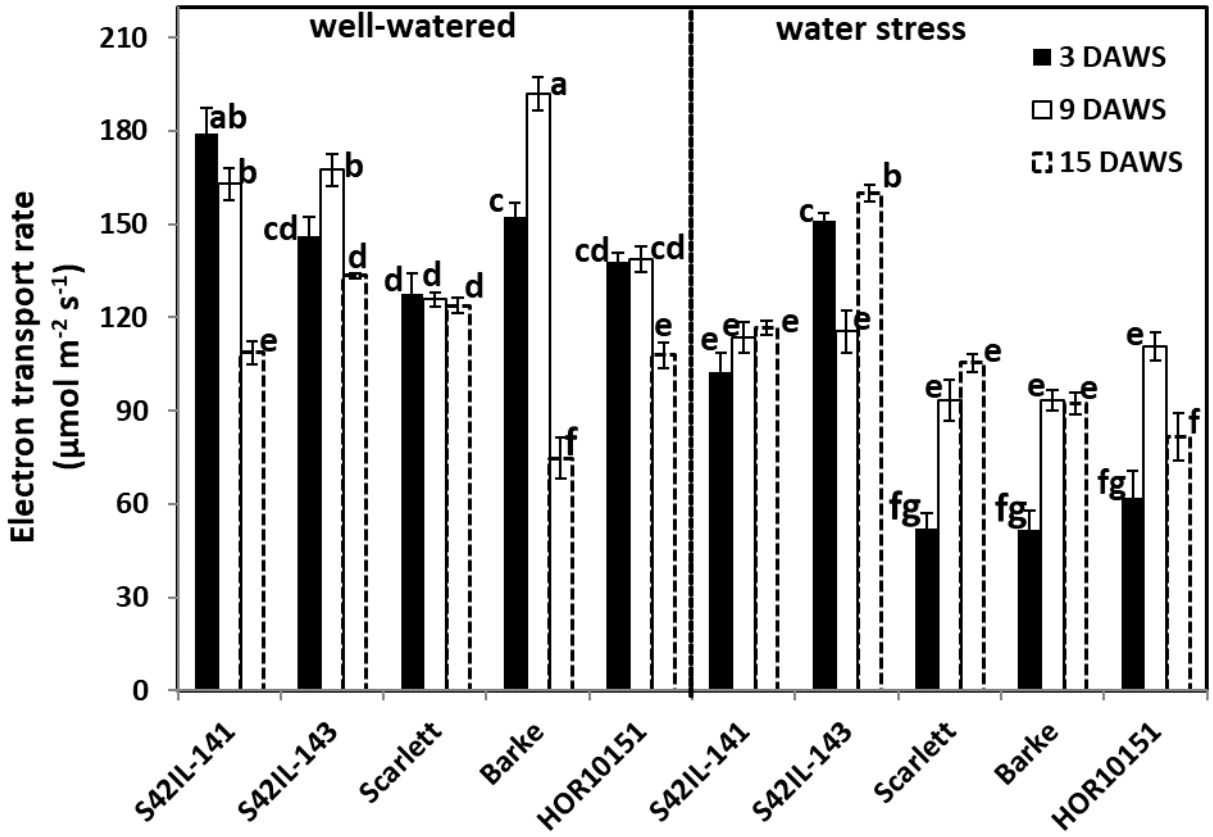

Appendix 3.6 Bar plot of electron transport rate, y-axis, for the different barley genotypes under well-watered and water stress treatments, the x-axis is the different genotypes. The legend represents the measurement days of 3, 9, and 15 days after drought stress (DAWS), *i.e.* at booting, heading, and on-set of grain filling stages of floral development. Different letters on the bars denote significant differences ($P \leq 0.05$) according to Tukey's HSD test. The figure was taken from Frimpong et al., 2021a.

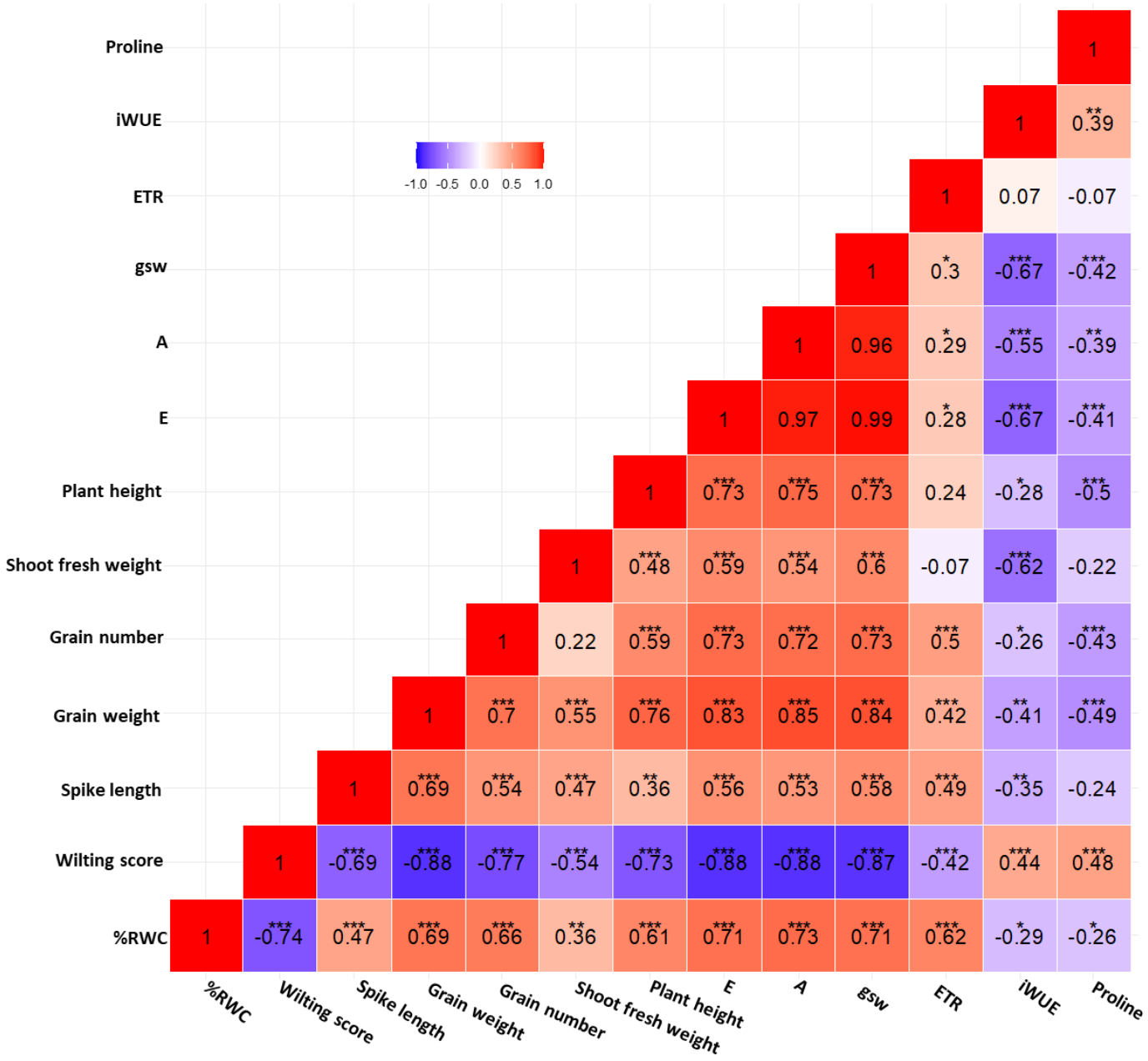

Appendix 3.7 Spearman correlation heat map of selected plant traits for pairwise comparison based on our 2019 data. Significant correlations "*, **, ***" follows the standard probability values ($P \leq 0.05$, $P \leq 0.01$or $P \leq 0.001$). A: Net CO_2 assimilation, E: transpiration, gsw: stomatal conductance, % RWC: percentage relative leaf water content, iWUE: intrinsic water use efficiency (A/gsw), and ETR: electron transport rate. The figure was taken from Frimpong et al., 2021a.

Appendix 3.8 Estimated proline concentration on a dry biomass basis (2019). The table was taken from Frimpong et al., 2021a.

Treatment	Genotype	Shoot dry biomass/ plant (g)	Proline content (amount/plant, µmol/g)
	S42IL-141	14.68	7.63 **d**
	S42IL-143	16.72	5.40 **d**
Well-watered	*Scarlett*	16.06	5.73 **d**
	Barke	26.42	12.17 **c**
	HOR10151	20.58	14.29 **c**
	S42IL-141	11.37	54.70 **b**
	S42IL-143	13.64	81.46 **a**
Water stress	*Scarlett*	10.83	5.39 **d**
	Barke	15.70	15.29 **c**
	HOR10151	9.17	12.29 **c**

The estimated content proline was calculated based on the mean dry biomass multiplied by the metabolite concentration (Podda et al., 2019). The different letters a-d represents Tukey's HSD test of significance (P≤ 0.001).

Appendix 3.9 A drought susceptibility index (DSI) was calculated based on total grain weight per plant (g) at harvest for all genotypes and years. The table was taken from Frimpong et al., 2021a.

Year	***Genotypes***	***DSI***
	Barke	1.2
	HOR10151	1
2018	*Scarlett*	0.6
	S42IL-141	0.26
	S42IL-143	0.25
	Barke	0.7
	HOR10151	0.63
2019	*Scarlett*	0.63
	S42IL-141	0.5
	S42IL-143	0.4

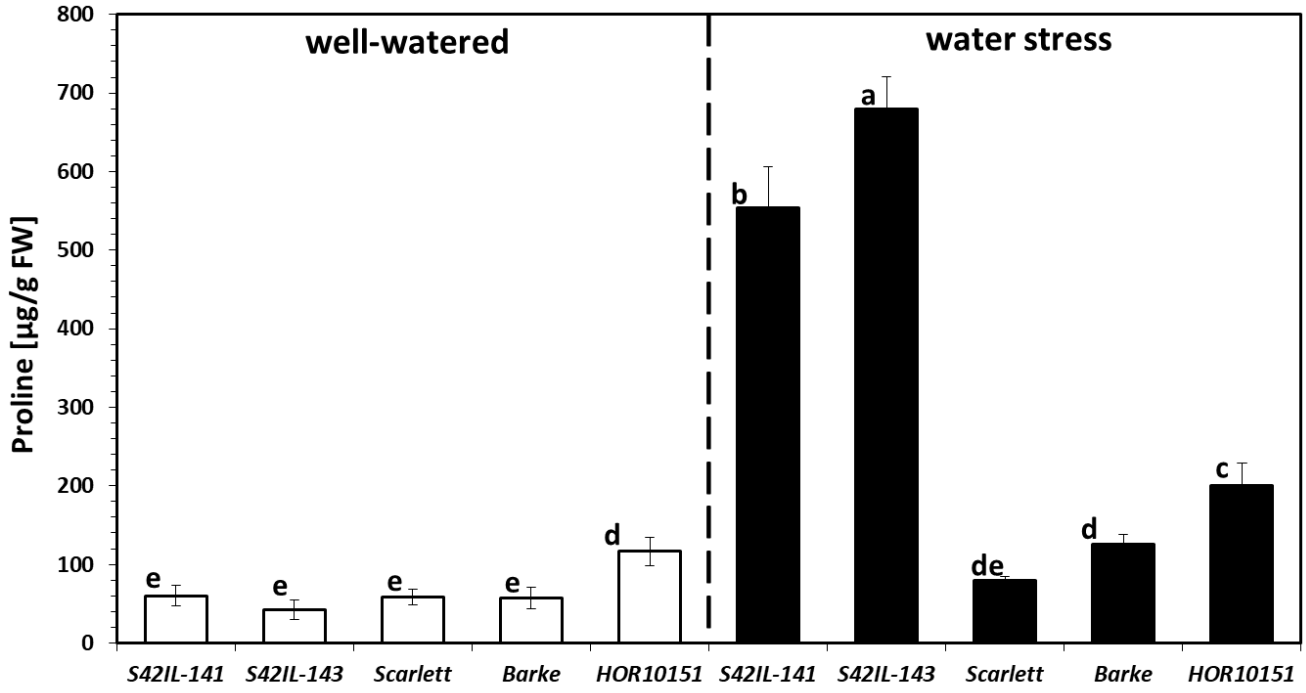

Appendix 3.10 Leaf proline for 2018 under well-watered and water stress conditions for the different barley genotypes. Different letters on the bars denote significant differences ($P < 0.05$) according to Tukey's HSD test. The figure was taken from Frimpong et al., 2021a.

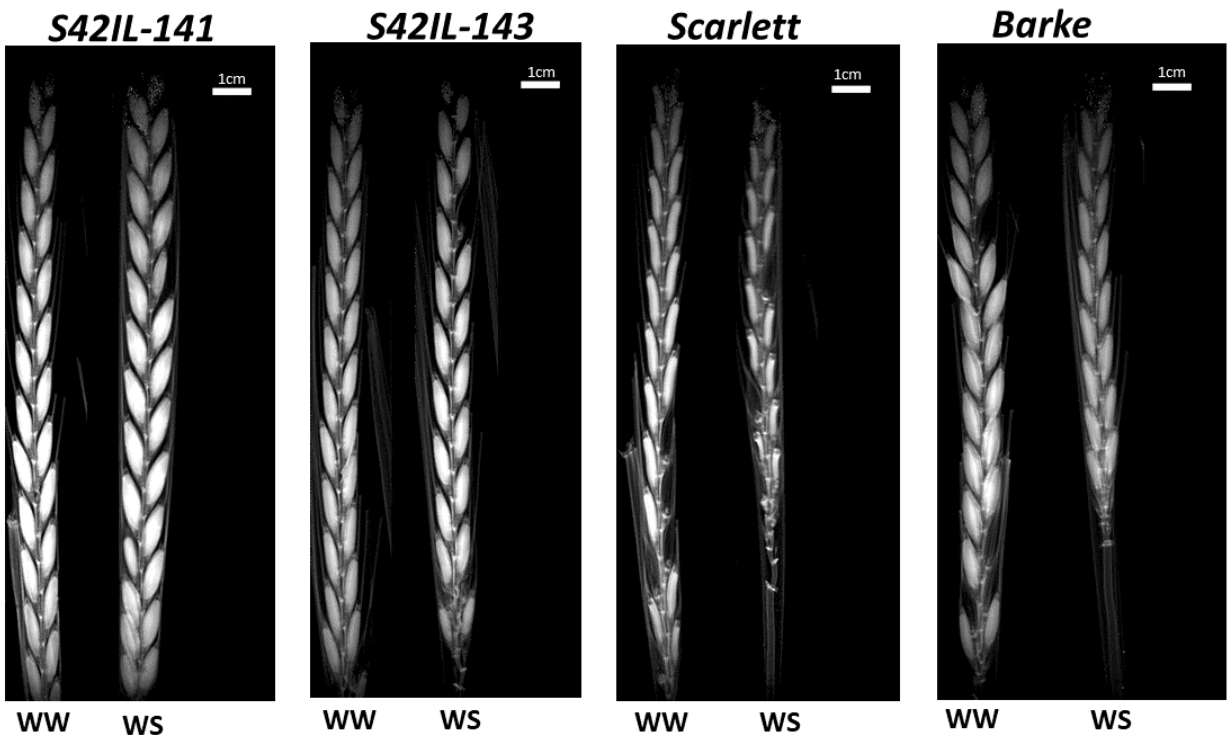

Appendix 3.11 MRI amplitude images of intact main spikes of barley at BBCH 83, 15 days after well-watered (WW) or water stress (WS) treatment, acquired with a multiple spin-echo sequence. n=1, scale bar = 1 cm. The figure was taken from Frimpong et al., 2021a.

Chapter 4 appendices

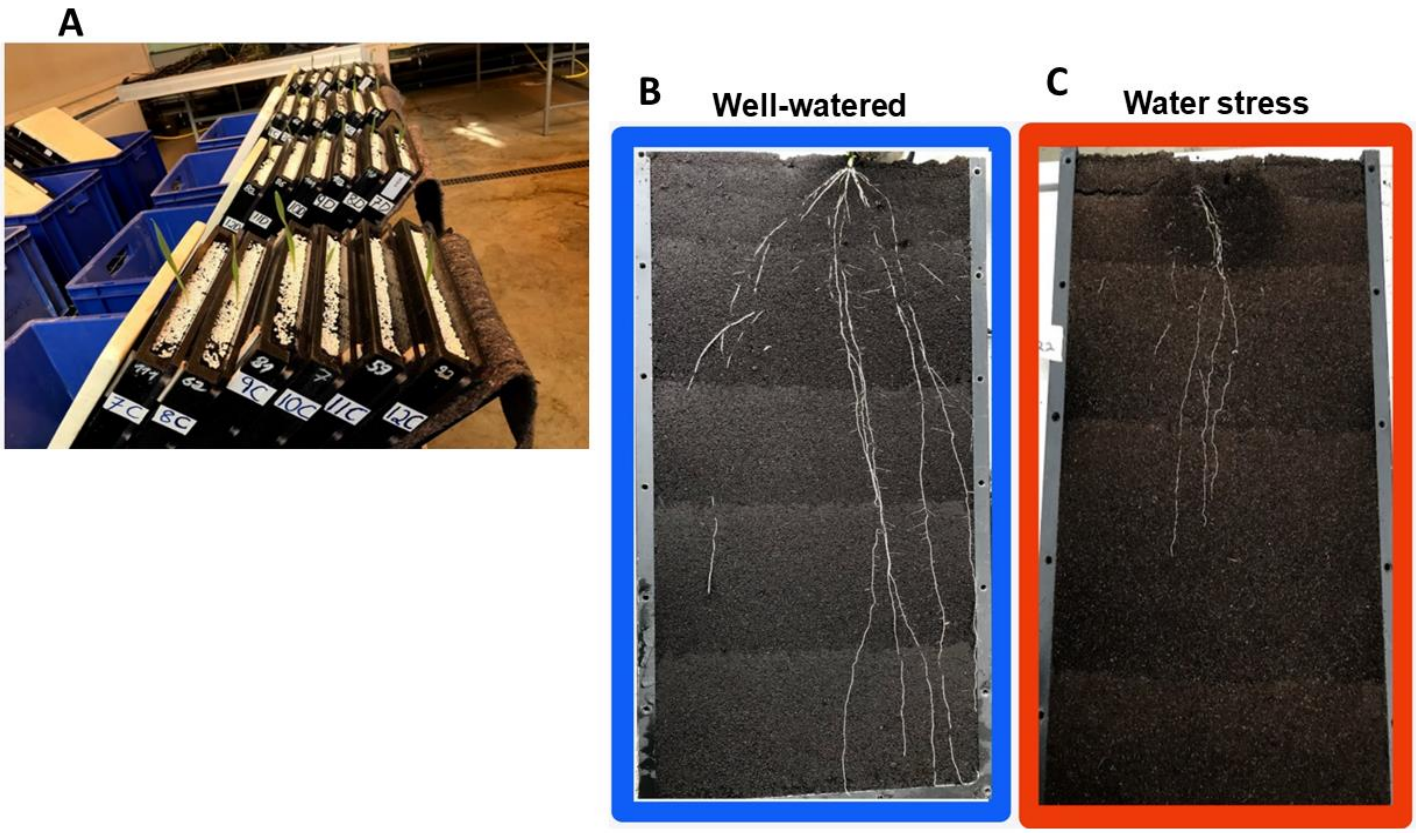

Appendix 4.1 Experimental setup of barley seedlings in rhizoboxes inclined at 45˚C at the greenhouse (A) and an illustration of the root system as grown under well-watered (B) and water stress (C) conditions, 17 days after treatment application. The figure was taken from Frimpong et al., 2021b.

Appendix 4.2 Summary of shoot and root morphological traits, their description, and units. The table was taken from Frimpong et al., 2021b.

Plant trait	Description	Unit
Number of leaves (NL)	The number of leaves/plants were counted at harvest	count
Leaf area (LA)	Destructive using LI-3100C Area Meter (LI-COR, Lincoln, NE, USA) at harvest	cm^2
Light and dark instantaneous leaf-level gas exchange	*A, gsw, E, iWUE(A/gsw) Fv/Fm* (Licor 6800)	µmol $mol^{-1}s^{-2}$
Shoot fresh weight (SFW)	Plants were cut and weighed individually	g
Shoot dry weight (SDW)	Plants were dried in the oven at 65º C for 72 h and weighed	g
Root fresh and dry weight (RFW, RDW)	Root fresh and dry biomass were cut and weighed before and after oven drying (65 º C for 72 h), respectively.	g
Visible root architectural traits	The visible root traits per plant were analyzed with PaintRHIZO software by following the protocol developed by (Nagel et al., 2009)	cm
Root architectural traits	Total root system length and diameter were scanned with WinRHIZO after harvest	cm
% Relative leaf water content (RWC)	$\mathbf{RWC} = \frac{\boldsymbol{fresh\ weight - dry\ weight}}{\boldsymbol{turgid\ weight - dry\ weight}} \times \mathbf{100}$ (Tahara et al., 1990)	%

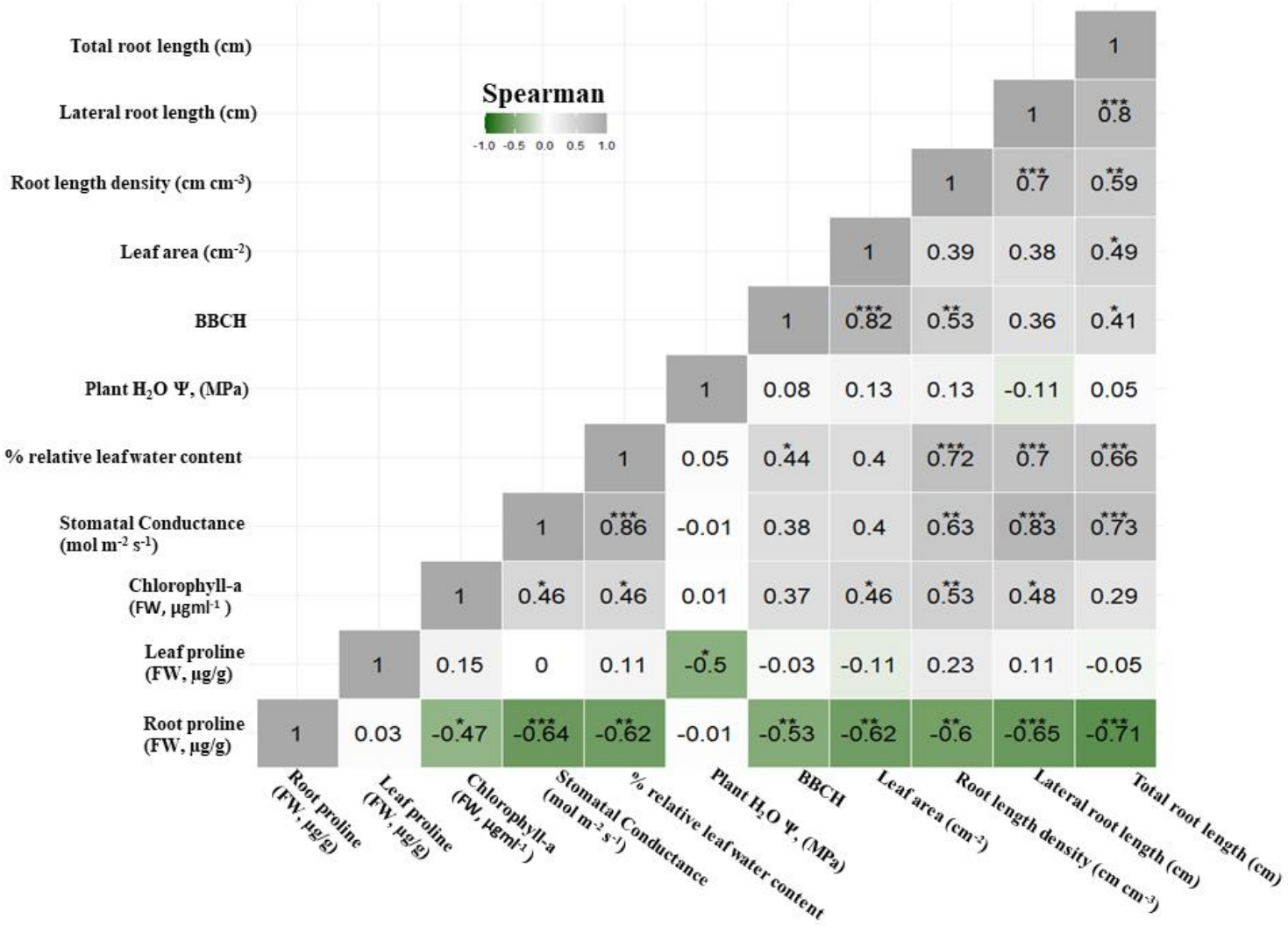

Appendix 4.3 Trait relationships according to the Spearman correlation coefficient of measured roots, shoots and physiological parameters. Significant correlations "*, **, ***" follows the standard probability values ($P \leq 0.05$, $P \leq 0.01$or $P \leq 0.001$). The figure was taken from Frimpong et al., 2021b.

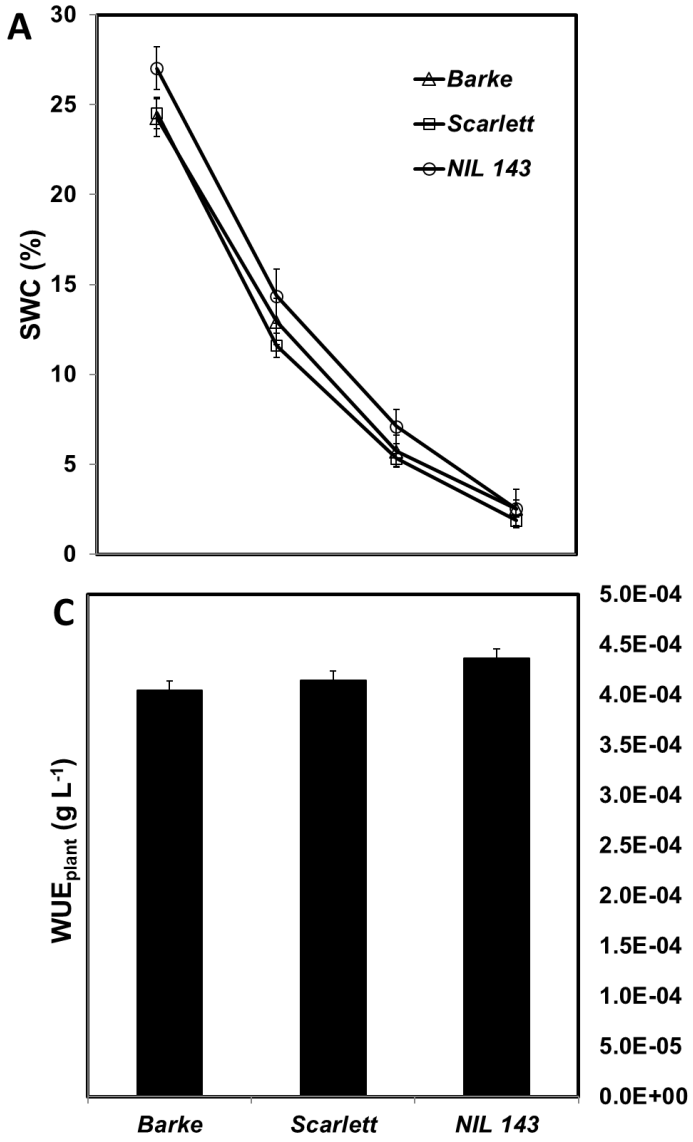

Appendix 4.4 Greenhouse pot (1.5 L) experiment comparing the barley near-isogenic line, NIL 143 and the two elite lines, Scarlett and Barke, under 14 days continuous soil drying conditions. Soil water content (SWC, A) and water use (B) were recorded twice a week until harvesting. Final shoot dry weight was measured at the end of the experiment, and whole-plant water use efficiency (WUEplant, C) was calculated as the ratio between final shoot dry weight and water use. Data are means ± standard error (n=3). The figure was taken from Frimpong et al., 2021b.

Chapter 5 appendices

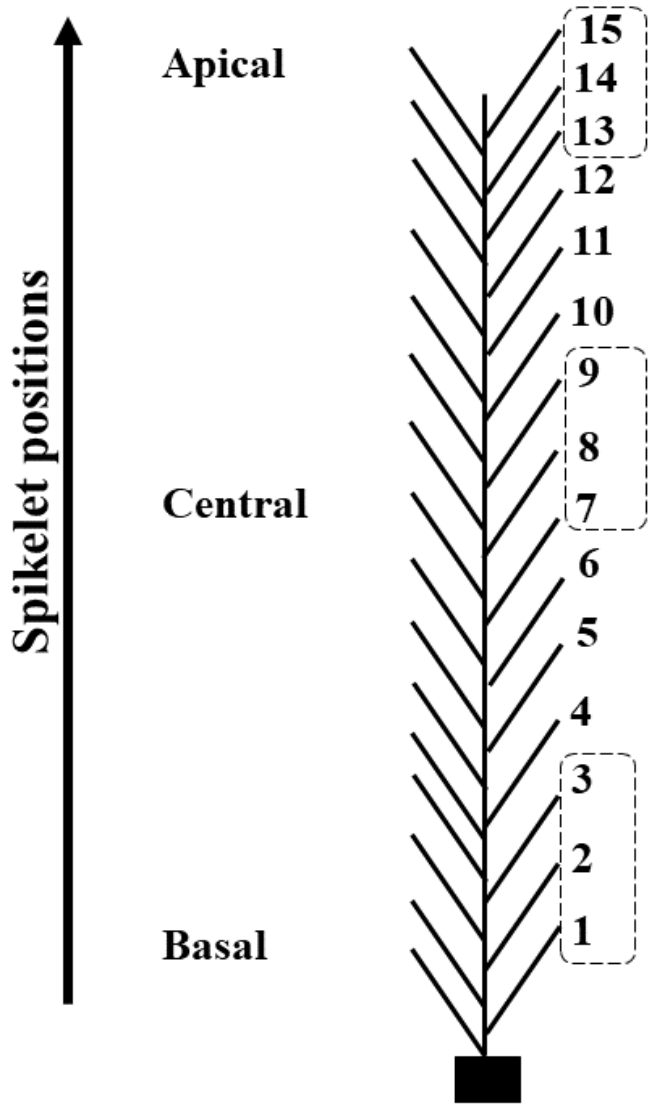

Appendix 5.1 Spikelet positions within a spike in which floral score [based on the scale according to (Waddington et al., 1983) and established for barley (Steinfort et al., 2017)] was determined (marked in dashed lines) throughout the crop cycle for imaging. Adapted from (Arisnabarreta et al., 2006).

Chapter 6 appendices

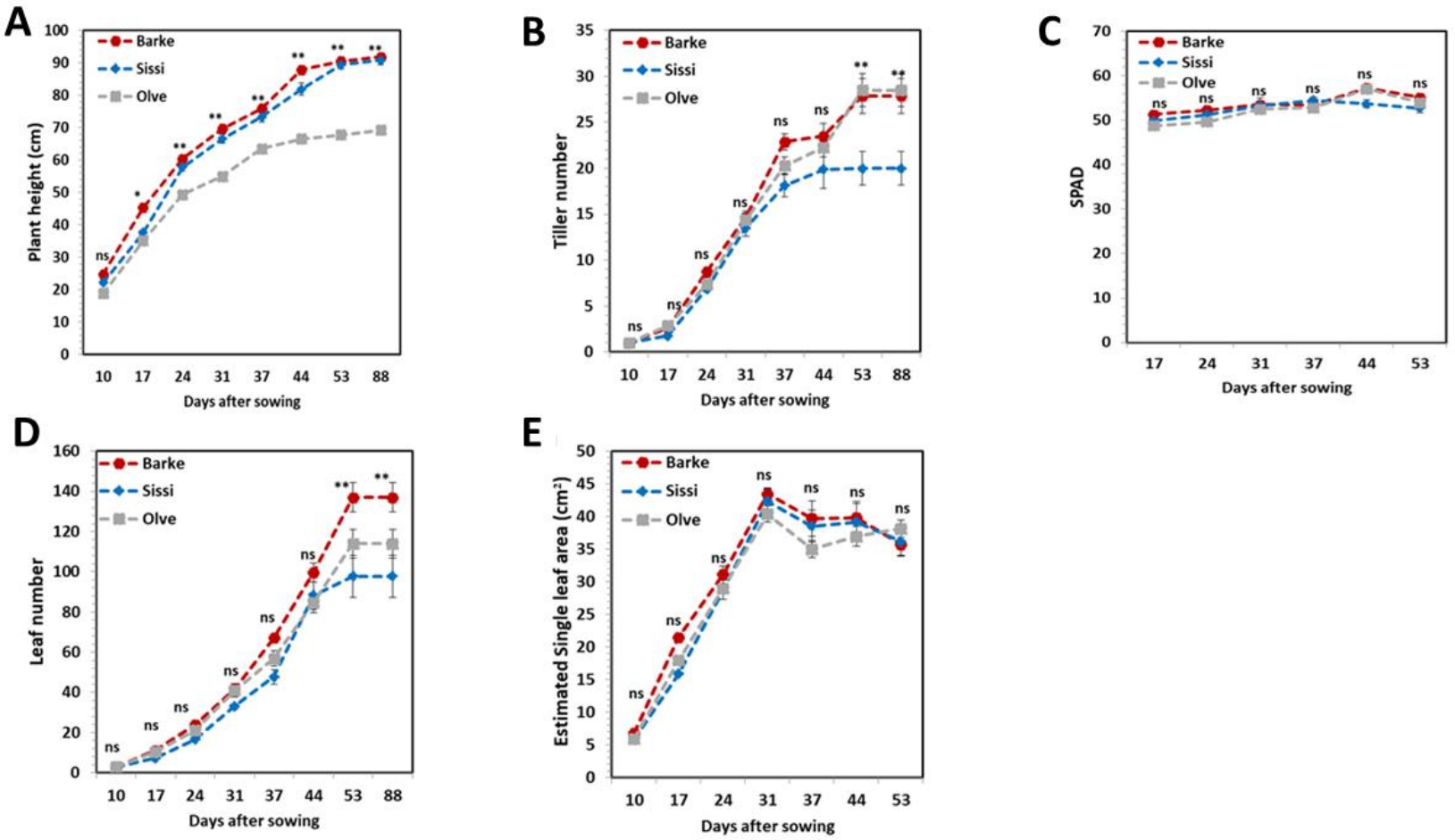

Appendix 6.1 Growth characteristics of spring barley genotypes Olve, Sissi and Barke in the growth chamber. Shown are plant height (A), tiller number (B), SPAD measurements (C), leaf number (D) and estimated single leaf area (E); n=12. Asterisks *, **, *** follows the standard probability values for significance after the one-way ANOVA; ns means no significance.

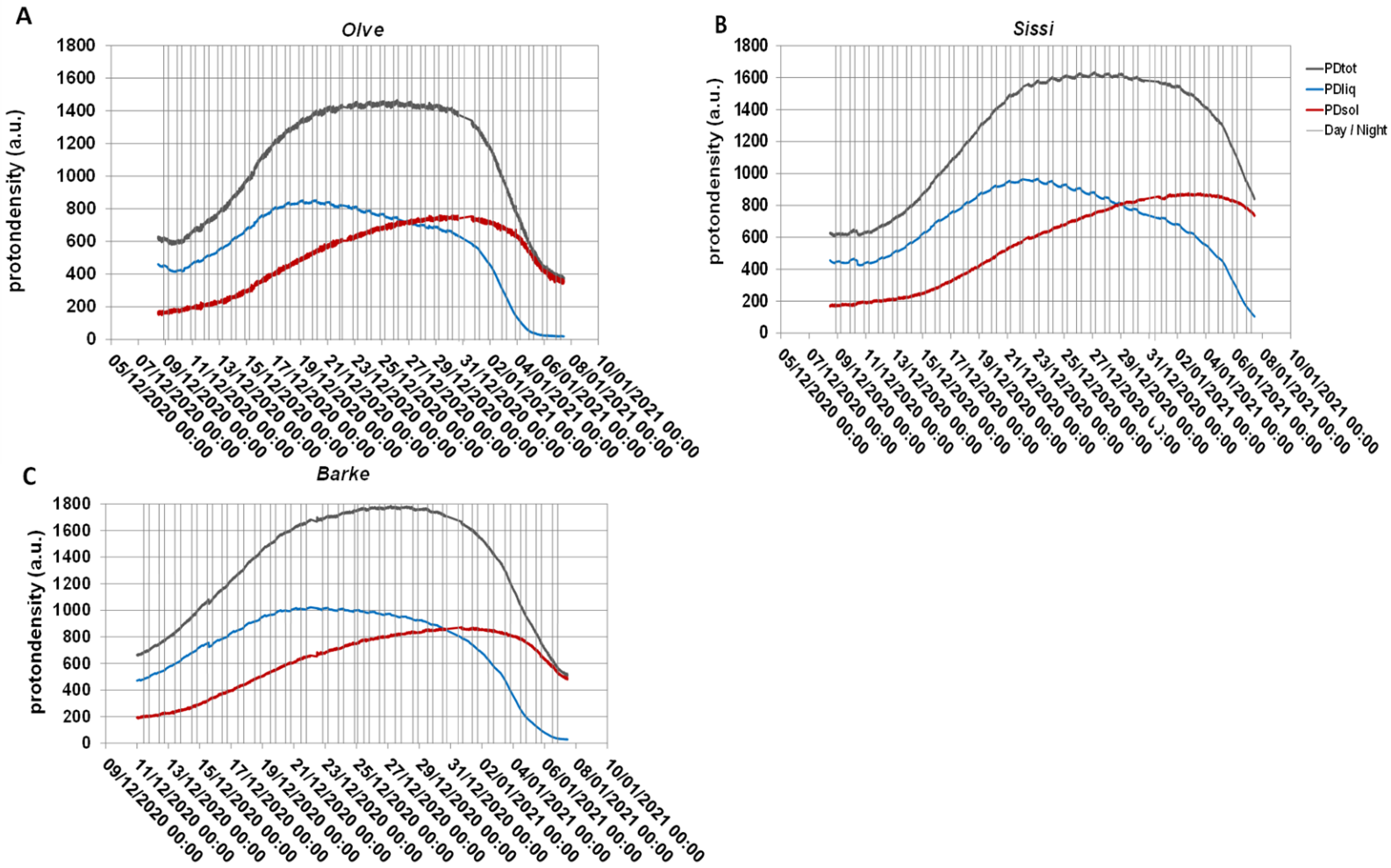

Appendix 6.2 Proton density of spike growth of barley using the multiplexed NMR sensor. Plotted are total proton density (PD_{tot}), liquid proton density (PD_{liq}), solid proton density (PD_{sol}), and diurnal pattern (Day/Night) of developing barley spikes (main tiller) during 20 days of reproductive development by the different genotypes (*Olve*, *Sissi*, and *Barke*). In the panel: (A-C) - proton density for *Olve*, proton density for *Sissi*, and proton density for *Barke*. The figures are representative measurements of individual main spikes for each genotype.

Appendix 6.3 Fresh weight, water weight and dry matter content of 20 mm spike sections of barley, at the moment of peak filling and at the end of seed development, as measured non-invasively by means of the NMR Multiplex.

Genotypes	Peak PD_{tot} (a.u)	PD_{tot}_End (a.u)	Peak FW (mg)	FW_End (mg)	Peak DW (mg)	DW_End (mg)	Peak WC %
Barke	1683 ± 46a	597 ±74a	49 ± 1.5a	13 ± 0.8b	20 ± 0.4 a	11 ± 0.6a	75 ± 0.9a
Olve	1367 ± 53c	393 ± 20b	40 ± 1.5b	12 ± 1.2b	17 ± 0.4ab	7 ± 1.2ab	77 ± 0.6a
Sissi	1450 ± 66ab	667 ± 65a	42 ± 2b	21 ± 3.4a	17 ± 1.2ab	11 ± 1.6a	76 ± 0.6a

Peak PD_{tot}: maximum total proton density, PD_{tot}_End: total proton density at the end of the experiment, Peak FW: maximum fresh weight, FW_End: fresh weight at the end of the experiment, Peak DW: maximum dry weight, DW_End: dry weight at the end of the experiment, Peak WC: maximum water content. Different letters denote Tukey's HSD Test of significance, n=6.

LITERATURE CITED

1. Abdel-Ghani, A. H., Sharma, R., Wabila, C., Dhanagond, S., Owais, S. J., Duwayri, M. A., Al-Dalain, S. A., Klukas, C., Chen, D., Lübberstedt, T., Von Wirén, N., Graner, A., Kilian, B., & Neumann, K. (2019). Genome-wide association mapping in a diverse spring barley collection reveals the presence of QTL hotspots and candidate genes for root and shoot architecture traits at seedling stage. BMC Plant Biology, 19(1), 1–19. https://doi.org/10.1186/s12870-019-1828-5

2. Abdelrahman, M., Burritt, D. J., Gupta, A., Tsujimoto, H., Tran, L. S. P., & Foyer, C. (2020). Heat stress effects on source-sink relationships and metabolome dynamics in wheat. Journal of Experimental Botany, 71(2), 543–554. https://doi.org/10.1093/jxb/erz296

3. Abid, M., Tian, Z., Ata-Ul-Karim, S. T., Cui, Y., Liu, Y., Zahoor, R., Jiang, D., & Dai, T. (2016). Nitrogen nutrition improves the potential of wheat (*Triticum aestivum* L.) to alleviate the effects of drought stress during vegetative growth periods. Frontiers in Plant Science, 7, 1–14. https://doi.org/10.3389/fpls.2016.00981

4. Ahmed, I. M., Bibi, N., Nadira, U. A., & Zhang, G. P. (2015). Tolerance to Combined Stress of Drought and Salinity in Barley. Combined Stresses in Plants: Physiological, Molecular, and Biochemical Aspects. Springer International Publishing. https://doi.org/10.1007/978-3-319-07899-1

5. Allahverdiyev, T. (2015). Effect of Drought Stress on Some Physiological Traits of Durum (*Triticum durum* Desf.) and Bread (*Triticum aestivum* L.) Wheat Genotypes. Journal of Stress Physiology & Biochemistry, 11(1), 29–38.

6. Arai-Sanoh, Y., Takai, T., Yoshinaga, S., Nakano, H., Kojima, M., Sakakibara, H., Kondo, M., & Uga, Y. (2014). Deep rooting conferred by *DEEPER ROOTING 1* enhances rice yield in paddy fields. Scientific Reports, 4(5563), 1–6. https://doi.org/10.1038/srep05563

7. Arisnabarreta, S., & Miralles, D. J. (2006). Floret development and grain setting in near isogenic two- and six-rowed barley lines (*Hordeum vulgare* L.). Field Crops Research, 96(2–3), 466–476. https://doi.org/10.1016/j.fcr.2005.09.004

8. Avramova, V., Nagel, K. A., Abdelgawad, H., Bustos, D., Duplessis, M., Fiorani, F., & Beemster, G. T. S. (2016). Screening for drought tolerance of maize hybrids by multi-scale analysis of root and shoot traits at the seedling stage. Journal of Experimental Botany, 67(8), 2453–2466. https://doi.org/10.1093/jxb/erw055

9. Badr, A., Müller, K., Schäfer-Pregl, R., El Rabey, H., Effgen, S., Ibrahim, H. H., Pozzi, C., Rohde, W., & Salamini, F. (2000). On the origin and domestication history of barley (Hordeum vulgare). Molecular Biology and Evolution, 17(4), 499–510. https://doi.org/10.1093/oxfordjournals.molbev.a026330

10. Balla, K., Karsai, I., Kiss, T., Horváth, Á., Berki, Z., Cseh, A., Bónis, P. T., Árendás, T., & Veisz, O. (2021). Single versus repeated heat stress in wheat: What are the consequences in different developmental phases? PLoS ONE, 16(May 2021), 1–22. https://doi.org/10.1371/journal.pone.0252070

11. Bandurska, H., Niedziela, J., Pietrowska-Borek, M., Nuc, K., Chadzinikolau, T., & Radzikowska, D. (2017). Regulation of proline biosynthesis and resistance to drought stress in two barley (*Hordeum vulgare* L.) genotypes of different origin. Plant Physiology and Biochemistry, 118, 427-437. https://doi.org/10.1016/j.plaphy.2017.07.006

12. Bandurska, H., & Stroiński, A. (2003). ABA and proline accumulation in leaves and roots of wild (*Hordeum spontaneum*) and cultivated (*Hordeum vulgare* 'Maresi') barley genotypes under water deficit conditions. Acta Physiologiae Plantarum, 25(1), 55–61. https://doi.org/10.1007/s11738-003-0036-x

13. Barrs, H., & Weatherley, P. (1962). A Re-Examination of the Relative Turgidity Technique for Estimating Water Deficits in Leaves. Australian Journal of Biological Sciences, 15(3), 413. https://doi.org/10.1071/bi9620413

14. Basu, S., Ramegowda, V., Kumar, A., & Pereira, A. (2016). Plant adaptation to drought stress. F1000Research 2016, 5(F1000 Faculty Rev),1554. https://doi.org/10.12688/F1000RESEARCH.7678.1

15. Bates L, Waldren R, T. I. (1973). Rapid determination of free proline for water-stress studies. Plant Soil, 207(39), 205–207.

16. Becker, S. R., Byrne, P. F., Reid, S. D., Bauerle, W. L., McKay, J. K., & Haley, S. D. (2016). Root traits contributing to drought tolerance of synthetic hexaploid wheat in a greenhouse study. Euphytica, 207(1), 213–224. https://doi.org/10.1007/s10681-015-1574-1

17. Belko, N., Zaman-Allah, M., Cisse, N., Diop, N. N., Zombre, G., Ehlers, J. D., & Vadez, V. (2012). Lower soil moisture threshold for transpiration decline under water deficit correlates with lower canopy conductance and higher transpiration efficiency in drought-tolerant cowpea. Functional Plant Biology, 39(4), 306–322. https://doi.org/10.1071/FP11282

18. Berkeley International. (2021). Barley FAQ's. http://www.berkeleyinternational.net/Barley_introduction.htm. Accessed on 15 December 2021.

19. Bernacchi, C. J., Singsaas, E. L., Pimentel, C., & Long, A. R. P. J. S. P. (2001). Improved temperature response functions for models of Rubisco-limited photosynthesis. Plant Cell and Environment, 24, 253–259. https://doi.org/10.1111/j.1365-3040.2001.00668.x

20. Bhandari, D. R., Wang, Q., Friedt, W., Spengler, B., Gottwald, S., & Römpp, A. (2015). High resolution mass spectrometry imaging of plant tissues: Towards a plant metabolite atlas. Analyst, 140(22), 7696–7709. https://doi.org/10.1039/c5an01065a

21. Bhaskara, G. B., Yang, T.-H. and, & Verslues, P. E. (2015). Dynamic Proline Metabolism: Importance and Regulation in Water-Limited Environments. Frontiers in Plant Science, 6(484). https://doi.org/10.3389/fpls.2015.00484

22. Biancucci, M., Mattioli, R., Moubayidin, L., Sabatini, S., Costantino, P., & Trovato, M. (2015). Proline affects the size of the root meristematic zone in Arabidopsis. BMC Plant Biology, 15(1), 263. https://doi.org/10.1186/s12870-015-0637-8

23. Blum, A. (2005). Drought resistance, water-use efficiency, and yield potential - Are they compatible, dissonant, or mutually exclusive? Australian Journal of Agricultural Research, 56(11), 1159–1168. https://doi.org/10.1071/AR05069

24. Borisjuk, L., Rolletschek, H., & Neuberger, T. (2012). Surveying the plant's world by magnetic resonance imaging. Plant Journal, 70(1), 129–146. https://doi.org/10.1111/j.1365-313X.2012.04927.x

25. Boudiar, R., Casas, A. M., Gioia, T., Fiorani, F., Nagel, K. A., & Igartua, E. (2020). Effects of Low Water Availability on Root Placement and Shoot Development in Landraces and Modern Barley Cultivars. Agronomy, 2020(10), 134. https://doi.org/10.3390/agronomy10010134

26. Boussora, F., Allam, M., Guasmi, F., Ferchichi, A., Rutten, T., Hansson, M., Youssef, H. M., & Börner, A. (2019). Spike developmental stages and ABA role in spikelet primordia abortion contribute to the final yield in barley (*Hordeum vulgare* L.). Botanical Studies, 60(1). https://doi.org/10.1186/s40529-019-0261-2

27. Box, G. E., & Cox, D. R. (1964). An analysis of transformations revisited, rebutted. Journal of the Royal Statistical Society, 26(2), 211–252. https://doi.org/10.1080/01621459.1982.10477788

28. Bradford, K. J. (1995). Seeds: physiology of development and germination. Seed Science Research, 5(2), 127–128. https://doi.org/10.1017/S0960258500002713

29. Brenchley, W. E., and Hall, A. D. (1909). The development of the grain of wheat. Journal of Agriculture Science., 3, 195–217. http://www.epjap.org/10.1051/epjap/2012110475

30. Briarty, L. G., Hughes, C. E., & Evers, A. D. (1979). The developing endosperm of wheat - a stereological analysis. Annals of Botany, 44(6), 641–658. https://doi.org/10.1093/oxfordjournals.aob.a085779

31. Broberg, M. C., Xu, Y., Feng, Z., & Pleijel, H. (2021). Harvest index and remobilization of 13 elements during wheat grain filling: Experiences from ozone experiments in China and Sweden. Field Crops Research, 271, 108259. https://doi.org/10.1016/j.fcr.2021.108259

32. Cai, K., Chen, X., Han, Z., Wu, X., Zhang, S., Li, Q., Mudassir Nazir, M., Zhang, G., Zeng, F., Zhou, M., & Wu, H. (2020). Screening of worldwide barley collection for drought tolerance: The assessment of various physiological measures as the selection criteria. Frontiers in Plant Science, 11. https://doi.org/10.3389/fpls.2020.01159

33. Calleja-Cabrera, J., Boter, M., Oñate-Sánchez, L., & Pernas, M. (2020). Root Growth Adaptation to Climate Change in Crops. Frontiers in Plant Science, 11. https://doi.org/10.3389/fpls.2020.00544

34. Carvalho, P., & Foulkes, M. J. (2018). Roots and Uptake of Water and Nutrients. In R. A. Meyers (Ed.), Encyclopedia of Sustainability Science and Technology, 1–24. Springer New York. https://doi.org/10.1007/978-1-4939-2493-6_195-3

35. Cattivelli, L., Ceccarelli, S., Romagosa, I., & Stanca, M. (2011). Abiotic Stresses in Barley: Problems and Solutions. In Barley: Production, Improvement, and Uses. https://doi.org/10.1002/9780470958636.ch10

36. Challinor, A. J., Watson, J., Lobell, D. B., Howden, S. M., Smith, D. R., & Chhetri, N. (2014). A meta-analysis of crop yield under climate change and adaptation. Nature Climate Change, 4(4), 287–291. https://doi.org/10.1038/nclimate2153

37. Chiang, H.-H., & Dandekar, A. M. (1995). Regulation of proline accumulation in *Arabidopsis thaliana* (L.) Heynh during development and in response to desiccation. Plant, Cell & Environment, 18(11), 1280–1290. https://doi.org/10.1111/j.1365-3040.1995.tb00187.x

38. Chimungu, J. G., Brown, K. M., & Lynch, J. P. (2014). Large root cortical cell size improves drought tolerance in maize. Plant Physiology, 166(4), 2166–2178. https://doi.org/10.1104/pp.114.250449

39. Choudhury, F. K., Rivero, R. M., Blumwald, E., & Mittler, R. (2017). Reactive oxygen species, abiotic stress and stress combination. Plant Journal, 90(5), 856–867. https://doi.org/10.1111/tpj.13299

40. Cockram, J., Horsnell, R., Soh, E. hee, Norris, C., & O'Sullivan, D. M. (2015). Molecular and phenotypic characterization of the alternative seasonal growth habit and flowering time in barley (*Hordeum vulgare ssp. vulgare* L.). Molecular Breeding, 35(8), 1–11. https://doi.org/10.1007/s11032-015-0359-5

41. Comas, L. H., Becker, S. R., Cruz, V. M. V., Byrne, P. F., & Dierig, D. A. (2013). Root traits contributing to plant productivity under drought. Frontiers in Plant Science, 4, 1–16. https://doi.org/10.3389/fpls.2013.00442

42. Cuesta-Marcos, A., Kling, J. G., Belcher, A. R., Filichkin, T., Fisk, S. P., Graebner, R., Helgerson, L., Herb, D., Meints, B., Ross, A. S., Hayes, P. M., & Ulrich, S. E. (2016). Barley: Genetics and Breeding. Encyclopedia of Food Grains (Second), 287–295. https://doi.org/10.1016/B978-0-12-394437-5.00208-4

43. Dar M.I., Naikoo M.I., Rehman F., Naushin F., K. F. A. (2016). Proline Accumulation in Plants: Roles in Stress Tolerance and Plant Development. In Osmolytes and Plants Acclimation to Changing Environment: Emerging Omics Technologies. Springer. https://doi.org/https://doi.org/10.1007/978-81-322-2616-1_9

44. De Datta, S. K., Malabuyoc, J. A., & Aragon, E. L. (1988). A field screening technique for evaluating rice germplasm for drought tolerance during the vegetative stage. Field Crops Research, 19(2), 123–134. https://doi.org/10.1016/0378-4290(88)90050-0

45. Delauney, A. J., & Verma, D. P. S. (1993). Proline biosynthesis and osmoregulation in plants. The Plant Journal, 4(2), 215–223. https://doi.org/10.1046/j.1365-313X.1993.04020215.x

46. Deng, G., Liang, J., Xu, D., Long, H., Pan, Z., & Yu, M. (2013). The relationship between proline content, the expression level of P5CS (*Δ1-pyrroline-5-carboxylate synthetase*), and drought tolerance in Tibetan hulless barley (Hordeum vulgare var. nudum). Russian Journal of Plant Physiology, 60(5), 693–700. https://doi.org/10.1134/S1021443713050038

47. Dien, D. C., Mochizuki, T., & Yamakawa, T. (2019). Effect of various drought stresses and subsequent recovery on proline, total soluble sugar and starch metabolisms in Rice (*Oryza sativa* L.) varieties. Plant Production Science, 22(4), 530–545. https://doi.org/10.1080/1343943X.2019.1647787

48. Dolferus, R. (2014). To grow or not to grow: A stressful decision for plants. In Plant Science, 229 (2014), 247–261.http://dx.doi.org/10.1016/j.plantsci.2014.10.002

49. Dolferus, R., Ji, X., & Richards, R. A. (2011). Abiotic stress and control of grain number in cereals. Plant Science : An International Journal of Experimental Plant Biology, 181(4), 331–341. https://doi.org/10.1016/j.plantsci.2011.05.015

50. Dreccer, M. F., Molero, G., Rivera-Amado, C., John-Bejai, C., & Wilson, Z. (2019). Yielding to the image: How phenotyping reproductive growth can assist crop improvement and production. Plant Science, 282, 73–82. https://doi.org/https://doi.org/10.1016/j.plantsci.2018.06.008

51. Edzes, H. T., van Dusschoten, D., & Van As, H. (1998). Quantitative T_2 Imaging of Plant Tissues By Means Of Multi-Echo MRI Microscopy. Magnetic Resonance Imaging, 16(2), 185–196. https://doi.org/https://doi.org/10.1016/S0730-725X(97)00274-9

52. Emes, M. J., Bowsher, C. G., Hedley, C., Burrell, M. M., Scrase-Field, E. S. F., & Tetlow, I. J. (2003). Starch synthesis and carbon partitioning in developing endosperm. Journal of Experimental Botany, 54(382), 569–575. https://doi.org/10.1093/jxb/erg089

53. Fahad, S., Bajwa, A. A., Nazir, U., Anjum, S. A., Farooq, A., Zohaib, A., Sadia, S., Nasim, W., Adkins, S., Saud, S., Ihsan, M. Z., Alharby, H., Wu, C., Wang, D., & Huang, J. (2017). Crop Production under Drought and Heat Stress: Plant Responses and Management Options. Frontiers in Plant Science, 8. https://doi.org/10.3389/fpls.2017.01147

54. FAOSTAT. (2021). Production quantities of Barley by country. http://www.fao.org/faostat/en/#data/QC/visualize. Accessed on 16th November, 2021.

55. Faye, A., Sine, B., Chopart, J. L., Grondin, A., Lucas, M., Diedhiou, A. G., Gantet, P., Cournac, L., Min, D., Audebert, A., Kane, A., & Laplaze, L. (2019). Development of a model estimating root length density from root impacts on a soil profile in pearl millet (*Pennisetum glaucum* (L.) R. Br). Application to measure root system response to water stress in field conditions. PLoS ONE, 14(7), 1–18. https://doi.org/10.1371/journal.pone.0214182

56. Feng, N., Song, G., Guan, J., Chen, K., Jia, M., Huang, D., Wu, J., Zhang, L., Kong, X., Geng, S., Liu, J., Li, A., & Mao, L. (2017). Transcriptome Profiling of Wheat Inflorescence Development from Spikelet Initiation to Floral Patterning Identified Stage-Specific Regulatory Genes. Plant Physiology, 174(3), 1779–1794. https://doi.org/10.1104/pp.17.00310

57. Feng, W., Lindner, H., Robbins, N. E., & Dinneny, J. R. (2016). Growing out of stress: The role of cell- and organ-scale growth control in plant water-stress responses. Plant Cell, 28(8), 1769–1782. https://doi.org/10.1105/tpc.16.00182

58. Ferguson, J. N. (2019). Climate change and abiotic stress mechanisms in plants. Emerging Topics in Life Sciences, 3(2), 165–181. https://doi.org/10.1042/etls20180105

59. Forde, B. G. (2014). Glutamate signalling in roots. Journal of Experimental Botany, 65(3), 779–787. https://doi.org/10.1093/jxb/ert335

60. Forde, B. G., Cutler, S. R., Zaman, N., & Krysan, P. J. (2013). Glutamate signalling via a *MEKK1 kinase*-dependent pathway induces changes in Arabidopsis root architecture. Plant Journal, 75(1), 1–10. https://doi.org/10.1111/tpj.12201

61. Forlani, G., Bertazzini, M., Zarattini, M., Funck, D., Ruszkowski, M., & Nocek, B. (2015). Functional properties and structural characterization of rice *δ1-pyrroline-5-carboxylate reductase*. Frontiers in Plant Science, 6, 1–13. https://doi.org/10.3389/fpls.2015.00565

62. Frimpong, F., Windt, C., van Dusschoten, D., Naz, A., Frei, M., & Fiorani, F. (2021a). A wild allele of *Pyrroline-5-carboxylate synthase1* leads to proline accumulation in spikes and leaves of barley contributing to improved performance under reduced water availability. Frontiers in Plant Science, 12, 180. https://doi.org/10.3389/fpls.2021.633448

63. Frimpong, F., Anokye, M.,Windt, C., van Dusschoten, D., Naz, A., Frei, M., & Fiorani, F. (2021b). Proline mediated drought tolerance in the barley (*Hordeum vulgare* L.) isogenic line is associated with lateral root growth at the early seedlings stage. Plants, 10(2177). https://doi.org/https://doi.org/10.3390/plants 10102177

64. Fry, E. L., Evans, A. L., Sturrock, C. J., Bullock, J. M., & Bardgett, R. D. (2018). Root architecture governs plasticity in response to drought. Plant and Soil, 433(1–2), 189–200. https://doi.org/10.1007/s11104-018-3824-1

65. Furlan, A. L., Bianucci, E., Castro, S., & Dietz, K.-J. (2017). Metabolic features involved in drought stress tolerance mechanisms in peanut nodules and their contribution to biological

nitrogen fixation. Plant Science, 263, 12–22. https://doi.org/https://doi.org/10.1016/j.plantsci.2017.06.009

66. Furlan, A. L., Bianucci, E., Giordano, W., Castro, S., & Becker, D. F. (2020). Proline metabolic dynamics and implications in drought tolerance of peanut plants. Plant Physiology and Biochemistry, 151, 566–578. https://doi.org/10.1016/j.plaphy.2020.04.010

67. Genuchten, V. (1980). A Closed-form Equation for Predicting the Hydraulic Conductivity of Unsaturated Soils. Soil Science Society of America Journal, 44, 892–898.

68. Ghaffari, H., Tadayon, M. R., Nadeem, M., Cheema, M., & Razmjoo, J. (2019). Proline-mediated changes in antioxidant enzymatic activities and the physiology of sugar beet under drought stress. Acta Physiologiae Plantarum, 41(2), 1–13. https://doi.org/10.1007/s11738-019-2815-z

69. Glidewell, S. M. (2006). NMR imaging of developing barley grains. Journal of Cereal Science, 43(1), 70–78. https://doi.org/10.1016/j.jcs.2005.07.003

70. Gol, L. (2020). Influence of drought on the reproductive development of barley. Heinrich Heine Universität Düsseldorf Library repository. https://docserv.uni-duesseldorf.de/servlets/DerivateServlet/Derivate-58261/PhD_Thesis_Leonard_Gol_Abgabeversion_Bibliothek_PDFA2b.pdf

71. Gol, L., Tomé, F., & Von Korff, M. (2017). Floral transitions in wheat and barley: Interactions between photoperiod, abiotic stresses, and nutrient status. Journal of Experimental Botany, 68(7), 1399–1410. https://doi.org/10.1093/jxb/erx055

72. González-Navarro, O. E., Griffiths, S., Molero, G., Reynolds, M. P., & Slafer, G. A. (2015). Dynamics of floret development determining differences in spike fertility in an elite population of wheat. Field Crops Research, 172, 21–31. https://doi.org/10.1016/j.fcr.2014.12.001

73. González, F. G., Slafer, G. A., & Miralles, D. J. (2003). Floret development and spike growth as affected by photoperiod during stem elongation in wheat. Field Crops Research, 81(1), 29–38. https://doi.org/10.1016/S0378-4290(02)00196-X

74. Gooding, M. J., Ellis, R. H., Shewry, P. R., & Schofield, J. D. (2003). Effects of restricted water availability and increased temperature on the grain filling, drying and quality of winter wheat. Journal of Cereal Science, 37(3), 295–309. https://doi.org/10.1006/jcrs.2002.0501

75. Goudriaan J., H.H. van Laar (1994). Modelling potential crop growth processes: textbook with exercises. Kluwer Academic Publishers (Current issues in production ecology 2). 140, Laboratorium voor Theoretische Productie Ecologie en Agronomie, ISBN: 9780792332190 - 238

76. Grando, S. and H. G. M. (2005). Food Barley: Importance, Uses and Local Knowledge. Proceedings of the International Workshop on Food Barley Improvement. In Barley-based Food in Southern Morocco.

77. Grimm, E., Pflugfelder, D., van Dusschoten, D., Winkler, A., & Knoche, M. (2017). Physical rupture of the xylem in developing sweet cherry fruit causes progressive decline in xylem sap inflow rate. Planta, 246(4), 659–672. https://doi.org/10.1007/s00425-017-2719-3

78. Guan, C., Cui, X., Liu, H., Li, X., Li, M., & Zhang, Y. (2020). Proline Biosynthesis Enzyme Genes Confer Salt Tolerance to Switchgrass (*Panicum virgatum* L.) in Cooperation With Polyamines Metabolism. Frontiers in Plant Science, 11, 1–14. https://doi.org/10.3389/fpls.2020.00046

79. Gubatz, S., & Weschke, W. (2016). Barley Grain: Development and Structure. In Barley: Chemistry and Technology, Second Edition, 11–53. AACC International Press, Washinton DC, USA. https://doi.org/10.1016/B978-1-891127-79-3.50002-0

80. Guo, Z., Chen, D., Alqudah, A. M., Röder, M. S., Ganal, M. W., & Schnurbusch, T. (2017). Genome-wide association analyses of 54 traits identified multiple loci for the determination of floret fertility in wheat. New Phytologist, 214(1), 257–270. https://doi.org/10.1111/nph.14342

81. Guo, Z., Chen, D., Röder, M. S., Ganal, M. W., & Schnurbusch, T. (2018). Genetic dissection of pre-anthesis sub-phase durations during the reproductive spike development of wheat. Plant Journal, 95(5), 909–918. https://doi.org/10.1111/tpj.13998

82. Guo, Z., Chen, D., & Schnurbusch, T. (2015). Variance components, heritability and correlation analysis of anther and ovary size during the floral development of bread wheat. Journal of Experimental Botany, 66(11), 3099–3111. https://doi.org/10.1093/jxb/erv117

83. Guo, Z., Chen, D., & Schnurbusch, T. (2018). Plant and Floret Growth at Distinct Developmental Stages During the Stem Elongation Phase in Wheat. Frontiers in Plant Science, 9, 1–14. https://doi.org/10.3389/fpls.2018.00330

84. Guo, Z., & Schnurbusch, T. (2015). Variation of floret fertility in hexaploid wheat revealed by tiller removal. Journal of Experimental Botany, 66(19), 5945–5958. https://doi.org/10.1093/jxb/erv303

85. Guo, Z., Slafer, G. A., & Schnurbusch, T. (2016). Genotypic variation in spike fertility traits and ovary size as determinants of floret and grain survival rate in wheat. Journal of Experimental Botany, 67(14), 4221–4230. https://doi.org/10.1093/jxb/erw200

86. Gupta, A., Rico-Medina, A. A., Caño-Delgado, A. I., & Cano-Delgado, A. I. (2020). The physiology of plant responses to drought. Science, 368, 266–269. https://doi.org/10.1126/science.aaz7614

87. Gupta, U. S. (2019). Drought Tolerance. Physiology of Stressed Crops, First edition, 62–104. CRC Press. https://doi.org/10.1201/9780367813635-3

88. Haddadin, M. F. (2015). Assessment of drought tolerant barley varieties under water stress. International Journal of Agriculture and Forestry, 5(2), 131–137. https://doi.org/10.5923/j.ijaf.20150502.06

89. Hajjar, G., Quellec, S., Pépin, J., Challois, S., Joly, G., Deleu, C., Leport, L., & Musse, M. (2021). MRI investigation of internal defects in potato tubers with particular attention to rust spots induced by water stress. Postharvest Biology and Technology, 180, 111600. https://doi.org/10.1016/J.POSTHARVBIO.2021.111600

90. Han, E., Kautz, T., & Köpke, U. (2016). Precrop root system determines root diameter of subsequent crop. Biology and Fertility of Soils, 52(1), 113–118. https://doi.org/10.1007/s00374-015-1049-5

91. Hay, R. K. M., & Kirby, E. J. M. (1991). Convergence and Synchrony- a Review of the Coordination of Development in Wheat. Australian Journal of Agricultural Research, 42, 661–700.

92. Hayat, S., Hayat, Q., Alyemeni, M. N., Wani, A. S., Pichtel, J., & Ahmad, A. (2012). Role of proline under changing environments: A review. Plant Signaling and Behavior, 7(11), 1456–1466. https://doi.org/10.4161/psb.21949

93. Hecht, V. L., Temperton, V. M., Nagel, K. A., Rascher, U., Pude, R., & Postma, J. A. (2019). Plant density modifies root system architecture in spring barley (*Hordeum vulgare* L.) through a change in nodal root number. Plant and Soil, 439(1–2), 179–200. https://doi.org/10.1007/s11104-018-3764-9

94. Hein, N. T., Ciampitti, I. A., & Jagadish, S. V. K. (2021). Bottlenecks and opportunities in field-based high-throughput phenotyping for heat and drought stress. Journal of Experimental Botany, 72(14), 5102–5116. https://doi.org/10.1093/jxb/erab021

95. Hernández-Sánchez, N., Barreiro, P., & Ruiz-Cabello, J. (2006). On-line Identification of Seeds in Mandarins with Magnetic Resonance Imaging. Biosystems Engineering, 95(4), 529–536. https://doi.org/10.1016/j.biosystemseng.2006.08.011

96. Hernández-Sánchez, N., Hills, B. P., Barreiro, P., & Marigheto, N. (2007). An NMR study on internal browning in pears. Postharvest Biology and Technology, 44(3), 260–270. https://doi.org/10.1016/j.postharvbio.2007.01.002

97. Hernandez, J., Meints, B., & Hayes, P. (2020). Introgression Breeding in Barley: Perspectives and Case Studies. Frontiers in Plant Science, 11, 1–15. https://doi.org/10.3389/fpls.2020.00761

98. Heuer, B. (2016). Role of proline in plant response to drought and salinity. Handbook of Plant and Crop Stress, Third Edition (November 2010), 213–238. https://doi.org/10.1201/b10329-12

99. Hoffmann, T., Bleisteiner, M., Sappa, P. K., Steil, L., M€ader, U., Völker, U., & Bremer, E. (2017). Synthesis of the compatible solute proline by *Bacillus subtilis* : point mutations rendering the osmotically controlled proHJ promoter hyperactive. Environmental Microbiology, 19(9), 3700–3720. https://doi.org/10.1111/1462-2920.13870

100. Honsdorf, N., March, T. J., Berger, B., Tester, M., & Pillen, K. (2014). High-throughput phenotyping to detect drought tolerance QTL in wild barley introgression lines. PLoS ONE, 9(5). https://doi.org/10.1371/journal.pone.0097047

101. Honsdorf, N., March, T. J., & Pillen, K. (2017). QTL controlling grain filling under terminal drought stress in a set of wild barley introgression lines. PLoS ONE, 12(10), 1–18. https://doi.org/10.1371/journal.pone.0185983

102. Hughes, N., Askew, K., Scotson, C. P., Williams, K., Sauze, C., Corke, F., Doonan, J. H., & Nibau, C. (2017). Non-Destructive, high-Content analysis of wheat grain traits using X-ray micro computed tomography. Plant Methods, 13(1), 1–16. https://doi.org/10.1186/s13007-017-0229-8

103. Hughes, N., Oliveira, H. R., Fradgley, N., Corke, F. M. K., Cockram, J., Doonan, J. H., & Candida, N. (2019). μCT trait analysis reveals morphometric differences between domesticated temperate small grain cereals and their wild relatives. The Plant Journal, 99, 98–111. https://doi.org/10.1111/tpj.14312

104. Iqbal, N., & Nazar, R. (2015). Osmolytes and plants acclimation to changing environment: Emerging omics technologies. Osmolytes and Plants Acclimation to Changing Environment: Emerging Omics Technologies, 1–170. https://doi.org/10.1007/978-81-322-2616-1

105. Jenner, C. F., & Rathjen, A. J. (1972). Factors limiting the supply of sucrose to the developing wheat grain. Annals of Botany, 36(4), 729–741. https://doi.org/10.1093/oxfordjournals.aob.a084629

106. Jia, Z., Liu, Y., Gruber, B. D., Neumann, K., Kilian, B., Graner, A., & von Wirén, N. (2019). Genetic dissection of root system architectural traits in spring barley. Frontiers in Plant Science, 10, 1–14. https://doi.org/10.3389/fpls.2019.00400

107. Jiménez-Donaire, M. D. P., Giráldez, J. V., & Vanwalleghem, T. (2020). Impact of climate change on agricultural droughts in Spain. Water, 12(11), 1–13. https://doi.org/10.3390/w12113214

108. Kamal, N. M., Gorafi, Y. S. A., Abdelrahman, M., Abdellatef, E., & Tsujimoto, H. (2019). Stay-green trait: A prospective approach for yield potential, and drought and heat stress adaptation in globally important cereals. International Journal of Molecular Sciences, 20(23). https://doi.org/10.3390/ijms20235837

109. Kavi Kishor, P. B., & Sreenivasulu, N. (2014). Is proline accumulation per se correlated with stress tolerance or is proline homeostasis a more critical issue? Plant, Cell and Environment, 37(2), 300–311. https://doi.org/10.1111/pce.12157

110. Kebede, A., Kang, M. S., & Bekele, E. (2019). Advances in mechanisms of drought tolerance in crops, with emphasis on barley. Advances in Agronomy, 156, 265–314. https://doi.org/10.1016/bs.agron.2019.01.008

111. Kelly, P. (2019). The EU cereals sector: Main features, challenges and prospects. European Parliamentary Research Service, September 2019. https://www.europarl.europa.eu/RegData/etudes/BRIE/2019/640143/EPRS_BRI(2019)640143_EN.pdf

112. Kirby, E. J. M., Appleyard, M. (1984). Cereal Development Guide (2nd ed.). Arable Unit, National Agricultural Centre, Stoneleigh, Kenilworth.

113. Kirby, E. J. M. (1988). Analysis of leaf, stem and ear growth in wheat from terminal spikelet stage to anthesis. Field Crops Research, 18(2–3), 127–140. https://doi.org/10.1016/0378-4290(88)90004-4

114. Kishor, K., B, P., & Sreenivasulu, N. (2014). Is proline accumulation per se correlated with stress tolerance or is proline homeostasis a more critical issue? Plant Cell and Environment, 37, 300–311. https://doi.org/10.1111/pce.12157

115. Koenigshofer, H., & Loeppert, H. G. (2019). The up-regulation of proline synthesis in the meristematic tissues of wheat seedlings upon short-term exposure to osmotic stress. Journal of Plant Physiology, 237, 21–29. https://doi.org/10.1016/j.jplph.2019.03.010

116. Kovacik, M., Nowicka, A., & Pecinka, A. (2020). Isolation of High Purity Tissues from Developing Barley Seeds. Scientific video journal, 164. https://doi.org/doi:10.3791/61681

117. Kuromori, T., Seo, M., & Shinozaki, K. (2018). ABA Transport and Plant Water Stress Responses. Trends in Plant Science, 23(6), 513–522. https://doi.org/10.1016/j.tplants.2018.04.001

118. Lee, B. R., Jin, Y. L., Avice, J. C., Cliquet, J. B., Ourry, A., & Kim, T. H. (2009). Increased proline loading to phloem and its effects on nitrogen uptake and assimilation in water-stressed white clover (*Trifolium repens*). New Phytologist, 182(3), 654–663. https://doi.org/10.1111/j.1469-8137.2009.02795.x

119. Li, Y., Li, H., Li, Y., & Zhang, S. (2017). Improving water-use efficiency by decreasing stomatal conductance and transpiration rate to maintain higher ear photosynthetic rate in drought-resistant wheat. Crop Journal, 5(3), 231–239. https://doi.org/10.1016/j.cj.2017.01.001

120. Liu, L., & Basso, B. (2020). Impacts of climate variability and adaptation strategies on crop yields and soil organic carbon in the US Midwest. PLoS ONE, 15(1), 1–20. https://doi.org/10.1371/journal.pone.0225433

121. Lobo, F. de A., de Barros, M. P., Dalmagro, H. J., Dalmolin, Â. C., Pereira, W. E., de Souza, É. C., Vourlitis, G. L., & Rodríguez Ortíz, C. E. (2013). Fitting net photosynthetic light-response curves with Microsoft Excel - a critical look at the models. Photosynthetica, 51(3), 445–456. https://doi.org/10.1007/s11099-013-0045-y

122. Lobos, G. A., Camargo, A. V., del Pozo, A., Araus, J. L., Ortiz, R., & Doonan, J. H. (2017). Editorial: Plant Phenotyping and Phenomics for Plant Breeding. Frontiers in Plant Science, 8, 1–3. https://doi.org/10.3389/fpls.2017.02181

123. Lovarelli, D., Garcia, L. R., Sánchez-Girón, V., & Bacenetti, J. (2020). Barley production in Spain and Italy: Environmental comparison between different cultivation practices. Science of the Total Environment, 707, 135982. https://doi.org/10.1016/j.scitotenv.2019.135982

124. Lozano, Y. M., Aguilar-Trigueros, C. A., Flaig, I. C., & Rillig, M. C. (2020). Root trait responses to drought are more heterogeneous than leaf trait responses. Functional Ecology, 34(11), 2224–2235. https://doi.org/10.1111/1365-2435.13656

125. Luo, X., Ma, C., Yue, Y., Hu, K., Li, Y., Duan, Z., Wu, M., Tu, J., Shen, J., Yi, B., & Fu, T. (2015). Unravelling the complex trait of harvest index in rapeseed (Brassica napus L.) with association mapping. BMC Genomics, 16(1), 1–10. https://doi.org/10.1186/s12864-015-1607-0

126. Lv, X., Ding, Y., Long, M., Liang, W., Gu, X., Liu, Y., & Wen, X. (2021). Effect of Foliar Application of Various Nitrogen Forms on Starch Accumulation and Grain Filling of Wheat (*Triticum aestivum* L.) Under Drought Stress. Frontiers in Plant Science, 12(3), 1–17. https://doi.org/10.3389/fpls.2021.645379

127. Lynch, J. (1995). Root architecture and plant productivity. Plant Physiology, 109(1), 7–13. https://doi.org/10.1104/pp.109.1.7

128. Lynch, J. P., & Wojciechowski, T. (2015). Opportunities and challenges in the subsoil: Pathways to deeper rooted crops. Journal of Experimental Botany, 66(8), 2199–2210. https://doi.org/10.1093/jxb/eru508

129. Lynch, & P., J. (2013). Steep, cheap and deep: An ideotype to optimize water and N acquisition by maize root systems. Annals of Botany, 112(2), 347–357. https://doi.org/10.1093/aob/mcs293

130. MacGregor, A., LaBerge, D., & Meredith, W. S. (1971). Changes in barley kernels during growth and maturation. Cereal Chem, 48, 255–269.

131. Maeght, J. L., Rewald, B., & Pierret, A. (2013). How to study deep roots-and why it matters. Frontiers in Plant Science, 4, 1–14. https://doi.org/10.3389/fpls.2013.00299

132. Mafakheri, A., Siosemardeh, A., Bahramnejad, B., Struik, P. C., & Sohrabi, E. (2010). Effect of drought stress on yield, proline and chlorophyll contents in three chickpea cultivars. Australian Journal of Crop Science, 4(8), 580–585.

133. Markwell, J. P., Danko, S. J., Bauwe, H., Osterman, J., Gorz, H. J., & Haskins, F. A. (1986). A Temperature-Sensitive Chlorophyll b -Deficient Mutant of Sweetclover (*Melilotus alba*). Plant Physiology, 81(2), 329–334. https://doi.org/10.1104/pp.81.2.329

134. Marok, M. A., Tarrago, L., Ksas, B., Henri, P., Abrous-Belbachir, O., Havaux, M., & Rey, P. (2013). A drought-sensitive barley variety displays oxidative stress and strongly increased contents in low-molecular weight antioxidant compounds during water deficit compared to a tolerant variety. Journal of Plant Physiology, 170(7), 633–645. https://doi.org/10.1016/j.jplph.2012.12.008

135. Matin, M. A., Brown, J. H., & Ferguson, H. (1989). Leaf Water Potential, Relative Water Content, and Diffusive Resistance as Screening Techniques for Drought Resistance in Barley. Agronomy Journal, 81(1), 100. https://doi.org/10.2134/agronj1989.00021962008100010018x

136. Mattioli, R., Palombi, N., Funck, D., & Trovato, M. (2020). Proline Accumulation in Pollen Grains as Potential Target for Improved Yield Stability Under Salt Stress. Frontiers in Plant Science, 11, 1–8. https://doi.org/10.3389/fpls.2020.582877

137. McCully, M. E. (1999). Roots in soil: Unearthing the complexities of roots and their rhizospheres. Annual Review of Plant Biology, 50, 695–718. https://doi.org/10.1146/annurev.arplant.50.1.695

138. Meena, M., Divyanshu, K., Kumar, S., Swapnil, P., Zehra, A., Shukla, V., Yadav, M., & Upadhyay, R. S. (2019). Regulation of L-proline biosynthesis, signal transduction, transport, accumulation and its vital role in plants during variable environmental conditions. Heliyon, 5(12), e02952. https://doi.org/10.1016/j.heliyon.2019.e02952

139. Meier, U. (2001). Growth stages of mono-and dicotyledonous plants : BBCH Monograph, 2nd Edition. German Federal Biological Research Centre for Agriculture and Forestry, BBCH-Monograph, BlackwellScience.

140. Meixner, M., Kochs, J., Foerst, P., & Windt, C. W. (2021). An integrated magnetic resonance plant imager for mobile use in greenhouse and field. Journal of Magnetic Resonance, 323, 106879. https://doi.org/10.1016/j.jmr.2020.106879

141. Mickky, B., Aldesuquy, H., & Elnajar, M. (2019). Drought-induced change in yield capacity of ten wheat cultivars in relation to their vegetative characteristics at heading stage. Physiology and Molecular Biology of Plants, 25(5), 1137–1148. https://doi.org/10.1007/s12298-019-00705-0

142. Miller, P., Lanier, W., & Brandt, S. (2001). Using Growing Degree Days to Predict Plant Stages. Montana State University Extension Service, 9, MT00103 AG 7/2001.

143. Millet, E. J., Kruijer, W., Coupel-ledru, A., Prado, S. A., Cabrera-bosquet, L., Lacube, S., Charcosset, A., Welcker, C., Eeuwijk, F. Van, & Tardieu, F. (2019). Genomic prediction of maize yield across European environmental conditions. Nature Genetics, 51, 952–956. https://doi.org/10.1038/s41588-019-0414-y

144. Mirza, H., Kamrun, N., Masayuki, F., Hirosuke, O., Islam, T. M., Shahzad, B., Fahad, S., Tanveer, M., Saud, S., & Khan, I. A. (2019). Plant Responses and Tolerance to Salt Stress. Approaches for Enhancing Abiotic Stress Tolerance in Plants, 61–78. https://doi.org/10.1201/9781351104722-3

145. Mohamed, N. E. M., Naz, A. A., Bauer, A., Schumann, H., & Léon, J. (2014). Association Mapping for Shoot Traits Related to Drought Tolerance in Barley. International Journal of Agriculture Innovations and Research, 3(1), 68–79.

146. Munns, R., James, R. A., Sirault, X. R. R., Furbank, R. T., & Jones, H. G. (2010). New phenotyping methods for screening wheat and barley for beneficial responses to water deficit. Journal of Experimental Botany, 61(13), 3499–3507. https://doi.org/10.1093/jxb/erq199

147. Muñoz-Amatriaín, M., Hernandez, J., Herb, D., Baenziger, P. S., Bochard, A. M., Capettini, F., Casas, A., Cuesta-Marcos, A., Einfeldt, C., Fisk, S., Genty, A., Helgerson, L., Herz, M., Hu, G., Igartua, E., Karsai, I., Nakamura, T., Sato, K., Smith, K., … Hayes, P. (2020). Perspectives on Low Temperature Tolerance and Vernalization Sensitivity in Barley: Prospects for Facultative Growth Habit. Frontiers in Plant Science, 11, 1–15. https://doi.org/10.3389/fpls.2020.585927

148. Muzammil, S., Shrestha, A., Dadshani, S., Pillen, K., Siddique, S., Léon, J., & Naz, A. A. (2018). An Ancestral Allele of *Pyrroline-5-carboxylate synthase1* Promotes Proline Accumulation and Drought Adaptation in Cultivated Barley. Plant Physiology, 178(2), 771–782. https://doi.org/10.1104/pp.18.00169

149. Nagel, K. A., Kastenholz, B., Jahnke, S., Van Dusschoten, D., Aach, T., Mühlich, M., Truhn, D., Scharr, H., Terjung, S., Walter, A., & Schurr, U. (2009). Temperature responses of roots: Impact on growth, root system architecture and implications for phenotyping. Functional Plant Biology, 36(11), 947–959. https://doi.org/10.1071/FP09184

150. Nakashima, K., Fujita, Y., Kanamori, N., Katagiri, T., Umezawa, T., Kidokoro, S., Maruyama, K., Yoshida, T., Ishiyama, K., Kobayashi, M., Shinozaki, K., & Yamaguchi-Shinozaki, K. (2009). Three arabidopsis *SnRK2* protein kinases, *SRK2D/SnRK2.2*, *SRK2E/SnRK2.6/OST1* and *SRK2I/SnRK2.3*, involved in ABA signaling are essential for the control of seed development and dormancy. Plant and Cell Physiology, 50(7), 1345–1363. https://doi.org/10.1093/pcp/pcp083

151. Naz, A. A., Arifuzzaman, M., Muzammil, S., Pillen, K., & Leon, J. (2014). Wild barley introgression lines revealed novel QTL alleles for root and related shoot traits in the cultivated barley (*Hordeum vulgare* L.). BMC Genetics, 15(107), 1471-2156. https://doi.org/10.1186/s12863-014-0107-6

152. Nieves-Cordones, M., García-sánchez, F., Pérez-pérez, J. G., Colmenero-Flores, M. J., Rubio, F., & Rosales, A. M. (2019). Coping With Water Shortage : An Update on the Role of

K + , Cl - , and Water Membrane Transport Mechanisms on Drought Resistance. Frontiers in Plant Science, 10(1619), 1–9. https://doi.org/10.3389/fpls.2019.01619

153. Nikolaeva, M. K., Maevskaya, S. N., Shugaev, A. G., & Bukhov, N. G. (2010). Effect of drought on chlorophyll content and antioxidant enzyme activities in leaves of three wheat cultivars varying in productivity. Russian Journal of Plant Physiology, 57(1), 87–95. https://doi.org/10.1134/S1021443710010127

154. Ochagavía, H., Prieto, P., Savin, R., Griffiths, S., & Slafer, G. A. (2018). Dynamics of leaf and spikelet primodia initiation in wheat as affected by *Ppd-1a* alleles under field conditions. Journal of Experimental Botany, 69(10), 2633–2645. https://doi.org/10.1093/jxb/ery105

155. Ochieng, J., Kirimi, L., & Mathenge, M. (2016). Effects of climate variability and change on agricultural production: The case of small scale farmers in Kenya. NJAS - Wageningen Journal of Life Sciences, 77(2016), 71–78. https://doi.org/10.1016/j.njas.2016.03.005

156. Ogawa, A., & Yamauchi, A. (2006). Root Osmotic Adjustment under Osmotic Stress in Maize Seedlings 1. Transient Change of Growth and Water Relations in Roots in Response to Osmotic Stress. Plant Production Science, 9(1), 27–38. https://doi.org/10.1626/pps.9.27

157. Ostonen, I., Püttsepp, Ü., Biel, C., Alberton, O., Bakker, M. R., Lõhmus, K., Majdi, H., Metcalfe, D., Olsthoorn, A. F. M., Pronk, A., Vanguelova, E., Weih, M., & Brunner, I. (2007). Specific root length as an indicator of environmental change. Plant Biosystems, 141(3), 426–442. https://doi.org/10.1080/11263500701626069

158. Oyiga, B. C., Palczak, J., Wojciechowski, T., Lynch, J. P., Naz, A. A., Léon, J., & Ballvora, A. (2020). Genetic components of root architecture and anatomy adjustments to water-deficit stress in spring barley. Plant Cell and Environment, 43(3), 692–711. https://doi.org/10.1111/pce.13683

159. Palta, J., & Watt, M. (2009). Chapter 13 - Vigorous Crop Root Systems: Form and Function for Improving the Capture of Water and Nutrients. In V. Sadras & D. Calderini (Eds.), Crop Physiology,309–325. Academic Press, San Diego, USA. https://doi.org/https://doi.org/10.1016/B978-0-12-374431-9.00013-X

160. Parkash, V., & Singh, S. (2020). A review on potential plant-basedwater stress indicators for vegetable crops. Sustainability, 12(10), 3945. https://doi.org/10.3390/SU12103945

161. Pflugfelder, D., Metzner, R., van Dusschoten, D., Reichel, R., Jahnke, S., & Koller, R. (2017). Non-invasive imaging of plant roots in different soils using magnetic resonance imaging (MRI). Plant Methods, 13(1), 102. https://doi.org/10.1186/s13007-017-0252-9

162. Pielot, R., Kohl, S., Manz, B., Rutten, T., Weier, D., Tarkowská, D., Rolčík, J., Strnad, M., Volke, F., Weber, H., & Weschke, W. (2015). Hormone-mediated growth dynamics of the barley pericarp as revealed by magnetic resonance imaging and transcript profiling. Journal of Experimental Botany, 66(21), 6927–6943. https://doi.org/10.1093/jxb/erv397

163. Pierret, A., Maeght, J. L., Clément, C., Montoroi, J. P., Hartmann, C., & Gonkhamdee, S. (2016). Understanding deep roots and their functions in ecosystems: An advocacy for more unconventional research. Annals of Botany, 118(4), 621–635. https://doi.org/10.1093/aob/mcw130

164. Placido, D. F., Campbell, M. T., Folsom, J. J., Cui, X., Kruger, G. R., Baenziger, P. S., & Walia, H. (2013). Introgression of novel traits from a wild wheat relative improves drought adaptation in wheat. Plant Physiology, 161(4), 1806–1819. https://doi.org/10.1104/pp.113.214262

165. Podda, A., Pollastri, S., Bartolini, P., Pisuttu, C., Pellegrini, E., Nali, C., Cencetti, G., Michelozzi, M., Frassinetti, S., Giorgetti, L., Fineschi, S., Del Carratore, R., & Maserti, B. (2019). Drought stress modulates secondary metabolites in *Brassica oleracea L. convar. acephala* (DC) *Alef, var. sabellica* L. Journal of the Science of Food and Agriculture, 99(12), 5533–5540. https://doi.org/10.1002/jsfa.9816

166. Poole, N. (2005). Cereal Growth Stages - The link to crop management. Grains Research & Development Corporation. (Issue 2). https://grdc.com.au/__data/assets/pdf_file/0031/364594/Cereal-growth-stages.pdf%0Ahttps://grdc.com.au/uploads/documents/GRDC Cereal Growth Stages Guide1.pdf VN - readcube.com

167. Porra, R. J., Thompson, W. A., & Kriedemann, P. E. (1989). Determination of accurate extinction coefficients and simultaneous equations for assaying chlorophylls a and b extracted with four different solvents: verification of the concentration of chlorophyll standards by atomic absorption spectroscopy. Biochimica et Biophysica Acta, 3(975), 384–394.

168. Prins, A., Orr, D. J., Andralojc, P. J., Reynolds, M. P., Carmo-Silva, E., & Parry, M. A. J. (2016). Rubisco catalytic properties of wild and domesticated relatives provide scope for improving wheat photosynthesis. Journal of Experimental Botany, 67(6), 1827–1838. https://doi.org/10.1093/jxb/erv574

169. Qamar, A., Mysore, K. S., & Senthil-Kumar, M. (2015). Role of proline and *pyrroline-5-carboxylate* metabolism in plant defense against invading pathogens. Frontiers in Plant Science, 6, 1–9. https://doi.org/10.3389/fpls.2015.00503

170. Quilambo, O. A. (2004). Proline content, water retention capability and cell membrane integrity as parameters for drought tolerance in two peanut cultivars. South African Journal of Botany, 70(2), 227–234. https://doi.org/10.1016/S0254-6299(15)30239-8

171. R Core Team. (2020). R: A language and environment for statistical computing. http://www.r-project.org/.

172. Rady, M. M., Taha, R. S., & Mahdi, A. H. A. (2016). Proline enhances growth, productivity and anatomy of two varieties of *Lupinus termis* L. grown under salt stress. South African Journal of Botany, 102, 221–227. https://doi.org/10.1016/j.sajb.2015.07.007

173. Rani, S., & Chaudhary, A. (2018). Management strategies for abiotic stresses in barley. Wheat and Barley Research. Journal of Cereal Research, 10(3), 151–165. https://doi.org/10.25174/2249-4065/2018-85229

174. Rascher, U., Blossfeld, S., Fiorani, F., Jahnke, S., Jansen, M., Kuhn, A. J., Matsubara, S., Mrtin, L. L. A., Merchant, A., Metzner, R., Mller-Linow, M., Nagel, K. A., Pieruschka, R., Pinto, F., Schreiber, C. M., Temperton, V. M., Thorpe, M. R., Van Dusschoten, D., Van Volkenburgh, E., … Schurr, U. (2011). Non-invasive approaches for phenotyping of enhanced performance traits in bean. Functional Plant Biology, 38(12), 968–983. https://doi.org/10.1071/FP11164

175. Raza, A., Razzaq, A., Mehmood, S. S., Zou, X., Zhang, X., Lv, Y., & Xu, J. (2019). Impact of climate change on crops adaptation and strategies to tackle its outcome: A review. Plants, 8(2), 34. https://doi.org/10.3390/plants8020034

176. Rekowski, A., Wimmer, M. A., Tahmasebi, S., Dier, M., Kalmbach, S., Hitzmann, B., & Zörb, C. (2021). Drought Stress during Anthesis Alters Grain Protein Composition and Improves Bread Quality in Field-Grown Iranian and German Wheat Genotypes. Applied Sciences, 11(21). https://doi.org/10.3390/app11219782

177. Rodrigues, J., Inzé, D., Nelissen, H., & Saibo, N. J. M. (2019). Source–Sink Regulation in Crops under Water Deficit. Trends in Plant Science. https://doi.org/10.1016/J.TPLANTS.2019.04.005

178. Ruchi Bansal, Jyoti Kumari, Vikender Kaur, Sundeep Kumar, V. S. (2016). High-throughput phenotyping for abiotic stress tolerance. Plant Stress Tolerance Physiological & Molecular Strategies. Scientific Publishers, Delhi, India. www.scientificpub.com

179. Sallam, A., Alqudah, A., Börner, A., Dawood, M., & Baenziger, P. (2019). Drought stress tolerance in wheat and barley: Advances in physiology, breeding and genetics research. International Journal of Molecular Sciences, 20(13), 3137. https://doi.org/10.3390/ijms20133137

180. Samarah, N. H., Alqudah, A. M., Amayreh, J. A., & McAndrews, G. M. (2009). The effect of late-terminal drought stress on yield components of four barley cultivars. Journal of Agronomy and Crop Science, 195(6), 427–441. https://doi.org/10.1111/j.1439-037X.2009.00387.x

181. Sayed, M. A., Schumann, H., Pillen, K., Naz, A. A., & Leon, J. (2012). AB-QTL analysis reveals new alleles associated to proline accumulation and leaf wilting under drought stress conditions in barley (*Hordeum vulgare* L.). BMC Genetics, 13 (61). https://doi.org/10.1186/1471-2156-13-61

182. Schils, R., Olesen, J. E., Kersebaum, K. C., Rijk, B., Oberforster, M., Kalyada, V., Khitrykau, M., Gobin, A., Kirchev, H., Manolova, V., Manolov, I., Trnka, M., Hlavinka, P., Paluoso, T., Peltonen-Sainio, P., Jauhiainen, L., Lorgeou, J., Marrou, H., Danalatos, N., … van

Ittersum, M. K. (2018). Cereal yield gaps across Europe. European Journal of Agronomy, 101, 109–120. https://doi.org/10.1016/j.eja.2018.09.003

183. Schmalenbach, I., Körber, N., & Pillen, K. (2008). Selecting a set of wild barley introgression lines and verification of QTL effects for resistance to powdery mildew and leaf rust. Theoretical and Applied Genetics, 117(7), 1093–1106. https://doi.org/10.1007/s00122-008-0847-7

184. Schmidt, J., Claussen, J., Wörlein, N., Eggert, A., Fleury, D., Garnett, T., & Gerth, S. (2020). Drought and heat stress tolerance screening in wheat using computed tomography. Plant Methods, 16(1), 1–12. https://doi.org/10.1186/s13007-020-00565-w

185. Schmidt, R., Stransky, H., & Koch, W. (2007). The amino acid permease AAP8 is important for early seed development in *Arabidopsis thaliana.* Planta, 226(4), 805–813. https://doi.org/10.1007/s00425-007-0527-x

186. Schnyder, H., and Baum, U. (1992). Growth of the grain of wheat (*Triticum aestivum* L.). The relationship between water content and dry matter accumulation. European Journal of Agronomy, 2(1), 51–57. https://doi.org/10.1016/s1161-0301(14)80001-4

187. Scholander, P. F., Hammel, H. T., Hemmingsen, E. A., & Bradstreet, E. D. (1964). Hydrostatic pressure and osmotic potential in leaves of mangroves and some other plants. Proceedings of the National Academy of Sciences, 52(1), 119–125. https://doi.org/10.1073/pnas.52.1.119

188. Sehgal, A., , Kumari Sita, K. H. M. S., Kumar, R., Bhogireddy, S., Varshney, R. K., HanumanthaRao, B., Ramakrishnan M. Nair, Prasad, P. V. V., & Nayyar, and H. (2018). Drought or/and heat-stress effects on seed filling in food crops: Impacts on functional biochemistry, seed yields, and nutritional quality. Frontiers in Plant Science, 871. https://doi.org/10.3389/fpls.2018.01705

189. Sharkey, T. D., Bernacchi, C. J., Farquhar, G. D., & Singsaas, E. L. (2007). Fitting photosynthetic carbon dioxide response curves for C3 leaves. Plant, Cell and Environment, 30(9), 1035–1040. https://doi.org/10.1111/j.1365-3040.2007.01710.x

190. Sharma, S., & Verslues, P. E. (2010). Mechanisms independent of abscisic acid (ABA) or proline feedback have a predominant role in transcriptional regulation of proline metabolism during low water potential and stress recovery. Plant, Cell and Environment, 33(11), 1838–1851. https://doi.org/10.1111/j.1365-3040.2010.02188.x

191. Sharma, S., Villamor, J. G., & Verslues, P. E. (2011). Essential role of tissue-specific proline synthesis and catabolism in growth and redox balance at low water potential. Plant Physiology, 157(1), 292–304. https://doi.org/10.1104/pp.111.183210

192. Sharp, R. E., Hsiao, T. C., & Silk, W. K. (1990). Growth of the maize primary root at low water potentials: II. Role of growth and deposition of hexose and potassium in osmotic adjustment. Plant Physiology, 93(4), 1337–1346. https://doi.org/10.1104/pp.93.4.1337

193. Sharwood, R. E. (2017). Engineering chloroplasts to improve Rubisco catalysis: prospects for translating improvements into food and fiber crops. New Phytologist, 213(2), 494–510. https://doi.org/10.1111/nph.14351

194. Shavrukov, Y., Kurishbayev, A., Jatayev, S., Shvidchenko, V., Zotova, L., Koekemoer, F., de Groot, S., Soole, K., & Langridge, P. (2017). Early flowering as a drought escape mechanism in plants: How can it aid wheat production? Frontiers in Plant Science, 8, 1–8. https://doi.org/10.3389/fpls.2017.01950

195. Shinde, S., Villamor, J. G., Lin, W., Sharma, S., & Verslues, P. E. (2016). Proline coordination with fatty acid synthesis and redox metabolism of chloroplast and mitochondria. Plant Physiology, 172(2), 1074–1088. https://doi.org/10.1104/pp.16.01097

196. Shitsukawa, N., Kinjo, H., Takumi, S., & Murai, K. (2009). Heterochronic development of the floret meristem determines grain number per spikelet in diploid, tetraploid and hexaploid wheats. Annals of Botany, 104(2), 243–251. https://doi.org/10.1093/aob/mcp129

197. Shrestha, A. (2020). Genetic and molecular analysis of drought stress adaptation in cultivated and wild barley. University of Bonn, library repository. https://bonndoc.ulb.uni-bonn.de/xmlui/bitstream/handle/20.500.11811/8648/5980.pdf?sequence=5&isAllowed=y

198. Slafer, G. A. (2003). Genetic basis of yield as viewed from a crop physiologist's perspective. Annals of Applied Biology, 142(2), 117–128. https://doi.org/10.1111/j.1744-7348.2003.tb00237.x

199. Smith, M. R., Rao, I. M., & Merchant, A. (2018). Source-sink relationships in crop plants and their influence on yield development and nutritional quality. Frontiers in Plant Science, 871, 1–10. https://doi.org/10.3389/fpls.2018.01889

200. Sreenivasulu, N., Borisjuk, L., Junker, B. H., Mock, H. P., Rolletschek, H., Seiffert, U., Weschke, W., & Wobus, U. (2010). Barley grain development: Toward an integrative view. International Review of Cell and Molecular Biology, 281st edition, 281(Issue C). https://doi.org/10.1016/S1937-6448(10)81002-0

201. Strange, H., Zwiggelaar, R., Sturrock, C., Mooney, S. J., & Doonan, J. H. (2015). Automatic estimation of wheat grain morphometry from computed tomography data. Functional Plant Biology, 42(5), 452–459. https://doi.org/10.1071/FP14068

202. Sucre, B., & Suárez, N. (2011). Effect of salinity and PEG-induced water stress on water status, gas exchange, solute accumulation, and leaf growth in Ipomoea pes-caprae. Environmental and Experimental Botany, 70(2–3), 192–203. https://doi.org/10.1016/j.envexpbot.2010.09.004

203. Szabados, L., & Savouré, A. (2010). Proline: a multifunctional amino acid. Trends in Plant Science, 15(2), 89–97. https://doi.org/10.1016/j.tplants.2009.11.009

204. Székely, G., Ábrahám, E., Cséplo, Á., Rigó, G., Zsigmond, L., Csiszár, J., Ayaydin, F., Strizhov, N., Jásik, J., Schmelzer, E., Koncz, C., & Szabados, L. (2008). Duplicated P5CS genes of Arabidopsis play distinct roles in stress regulation and developmental control of proline biosynthesis. Plant Journal, 53(1), 11–28. https://doi.org/10.1111/j.1365-313X.2007.03318.x

205. Tahara, M., Carver, B. F., Johnson, R. C., & Smith, E. L. (1990). Relationship between relative water content during reproductive development and winter wheat grain yield. Euphytica, 49(3), 255–262. https://doi.org/10.1007/BF00036297

206. Takahashi, F., Kuromori, T., Urano, K., Yamaguchi-Shinozaki, K., & Shinozaki, K. (2020). Drought Stress Responses and Resistance in Plants: From Cellular Responses to Long-Distance Intercellular Communication. Frontiers in Plant Science, 11, 1–14. https://doi.org/10.3389/fpls.2020.556972

207. Takahashi, T., Chevalier, P. M., & Rupp, R. A. (2001). Storage and remobilization of soluble carbohydrates after heading in different plant parts of a winter wheat cultivar. Plant Production Science, 4(3), 160–165. https://doi.org/10.1626/pps.4.160

208. Taner, A., Muzaffer, A., & Fazil, D. (2004). Barley: Post-harvest Operations. Food and Agriculture Organization of the United Nations, 1–64. http://www.fao.org/3/a-au997e.pdf

209. Tardieu, F., Simonneau, T., & Muller, B. (2018). The Physiological Basis of Drought Tolerance in Crop Plants: A Scenario-Dependent Probabilistic Approach. Annual Review of Plant Biology, 69, 733–759. https://doi.org/10.1146/annurev-arplant-042817-040218

210. Teixeira, W. F., Soares, L. H., Fagan, E. B., da Costa Mello, S., Reichardt, K., & Dourado-Neto, D. (2020). Amino Acids as Stress Reducers in Soybean Plant Growth Under Different Water-Deficit Conditions. Journal of Plant Growth Regulation, 39(2), 905–919. https://doi.org/10.1007/s00344-019-10032-z

211. Templer, S. E., Ammon, A., Pscheidt, D., Ciobotea, O., Schuy, C., McCollum, C., Sonnewald, U., Hanemann, A., Förster, J., Ordon, F., Von Korff, M., & Voll, L. M. (2017). Metabolite profiling of barley flag leaves under drought and combined heat and drought stress reveals metabolic QTLs for metabolites associated with antioxidant defense. Journal of Experimental Botany, 68(7), 1697–1713. https://doi.org/10.1093/jxb/erx038

212. Tracy, S. R., Gómez, J. F., Sturrock, C. J., Wilson, Z. A., & Ferguson, A. C. (2017). Non-destructive determination of floral staging in cereals using X-ray micro computed tomography (μCT). Plant Methods, 13(1), 1–12. https://doi.org/10.1186/s13007-017-0162-x

213. Trovato, M., Forlani, G., Signorelli, S., & Funck, D. (2019). Proline Metabolism and Its Functions in Development and Stress Tolerance. Osmoprotectant-Mediated Abiotic Stress Tolerance in Plants: Recent Advances and Future Perspectives. 41–72. Springer International Publishing, Cham, Switzerland . https://doi.org/10.1007/978-3-030-27423-8_2

214. Uga, Y., Sugimoto, K., Ogawa, S., Rane, J., Ishitani, M., Hara, N., Kitomi, Y., Inukai, Y., Ono, K., Kanno, N., Inoue, H., Takehisa, H., Motoyama, R., Nagamura, Y., Wu, J., Matsumoto, T., Takai, T., Okuno, K., & Yano, M. (2013). Control of root system architecture by *DEEPER ROOTING 1* increases rice yield under drought conditions. Nature Genetics, 45(9), 1097–1102. https://doi.org/10.1038/ng.2725

215. Ugarte, C., Calderini, D. F., & Slafer, G. A. (2007). Grain weight and grain number responsiveness to pre-anthesis temperature in wheat, barley and triticale. Field Crops Research, 100(2–3), 240–248. https://doi.org/10.1016/j.fcr.2006.07.010

216. Vadez, V., Kholova, J., Medina, S., Kakkera, A., & Anderberg, H. (2014). Transpiration efficiency: New insights into an old story. Journal of Experimental Botany, 65(21), 6141–6153. https://doi.org/10.1093/jxb/eru040

217. Van As, H., & Van Duynhoven, J. (2013). MRI of plants and foods. Journal of Magnetic Resonance, 229, 25–34. https://doi.org/10.1016/j.jmr.2012.12.019

218. van der Weerd, L., Ruttink, T., van Dusschoten, D., Vergeldt, F. J., de Jager, P. A., & Van As, H. (2013). Plant Growth Studies Using Low Field NMR. Spatially Resolved Magnetic Resonance. https://doi.org/10.1002/9783527611843.ch45

219. van Dusschoten, D., Metzner, R., Kochs, J., Postma, J. A., Pflugfelder, D., Buehler, J., Schurr, U., & Jahnke, S. (2016). Quantitative 3D Analysis of Plant Roots growing in Soil using Magnetic Resonance Imaging. Plant Physiology, 170, pp.01388.2015. https://doi.org/10.1104/pp.15.01388

220. Venekamp, J. H., & Koot, J. T. M. (1984). The Distribution of Free Amino Acids, Especially of Proline, in the Organs of Field Bean Plants, Vicia faba L., during Development in the Field. Journal of Plant Physiology, 116(4), 343–349. https://doi.org/https://doi.org/10.1016/S0176-1617(84)80113-3

221. Verbruggen, N., & Hermans, C. (2008). Proline accumulation in plants: A review. Amino Acids, 35(4), 753–759. https://doi.org/10.1007/s00726-008-0061-6

222. Verslues, P. E., & Sharma, S. (2010). Proline Metabolism and Its Implications for Plant-Environment Interaction. The Arabidopsis Book, 8, e0140–e0140. https://doi.org/10.1199/tab.0140

223. Verslues, P. E., & Sharp, R. E. (1999). Proline accumulation in maize (Zea mays L.) primary roots at low water potentials. II. Metabolic source of increased proline deposition in the elongation zone. Plant Physiology, 119(4), 1349–1360. https://doi.org/10.1104/pp.119.4.1349

224. Verstegen, H., Köneke, O., Korzun, V., & von Broock, R. (2014). The World Importance of Barley and Challenges to Further Improvements. Biotechnological Approaches to Barley Improvement, 3–19. Springer, Berlin, Heidelberg, Germany. https://doi.org/10.1007/978-3-662-44406-1_1

225. Voetberg, G. S., & Sharp, R. E. (1991). Growth of the maize primary root at low water potentials: III. Role of increased proline deposition in osmotic adjustment. Plant Physiology, 96(4), 1125–1130. https://doi.org/10.1104/pp.96.4.1125

226. Wang, Zhibo, Li, G., Sun, H., Ma, L., Guo, Y., Zhao, Z., Gao, H., & Mei, L. (2018). Effects of drought stress on photosynthesis and photosynthetic electron transport chain in young apple tree leaves. Biology Open, 7(11), 1–9. https://doi.org/10.1242/bio.035279

227. Wang, Zhiqin, Xu, Y., Chen, T., Zhang, H., Yang, J., & Zhang, J. (2015). Abscisic acid and the key enzymes and genes in sucrose-to-starch conversion in rice spikelets in response to soil drying during grain filling. Planta, 241(5), 1091–1107. https://doi.org/10.1007/s00425-015-2245-0

228. Wardlaw, I. F., & Willenbrink, J. (2000). Mobilization of fructan reserves and changes in enzyme activities in wheat stems correlate with water stress during kernel filling. New Phytologist, 148(3), 413–422. https://doi.org/10.1046/j.1469-8137.2000.00777.x

229. Wasaya, A., Zhang, X., Fang, Q., & Yan, Z. (2018). Root phenotyping for drought tolerance: A review. Agronomy, 8(11), 1–19. https://doi.org/10.3390/agronomy8110241

230. Wasson, A. P., Nagel, K. A., Tracy, S., & Watt, M. (2020). Beyond Digging: Noninvasive Root and Rhizosphere Phenotyping. Trends in Plant Science, 25(1), 119–120. https://doi.org/10.1016/j.tplants.2019.10.011

231. Weemstra, M., Kiorapostolou, N., van Ruijven, J., Mommer, L., de Vries, J., & Sterck, F. (2020). The role of fine-root mass, specific root length and life span in tree performance: A whole-tree exploration. Functional Ecology, 34(3), 575–585. https://doi.org/10.1111/1365-2435.13520

232. White, F. F., Taylor, B. H., Huffman, G. A., Gordon, M. P., & Nester, E. W. (1985). Molecular and genetic analysis of the transferred DNA regions of the root-inducing plasmid of Agrobacterium rhizogenes. Journal of Bacteriology, 164(1), 33–44. https://doi.org/10.1128/jb.164.1.33-44.1985

233. Windt, C. W., Nabel, M., Kochs, J., Jahnke, S., & Schurr, U. (2021). A Mobile NMR Sensor and Relaxometric Method to Non-destructively Monitor Water and Dry Matter Content in Plants. Frontiers in Plant Science, 12, 1–17. https://doi.org/10.3389/fpls.2021.617768

234. Yamauchi, T., Pedersen, O., Nakazono, M., & Tsutsumi, N. (2021). Key root traits of Poaceae for adaptation to soil water gradients. New Phytologist, 229(6), 3133–3140. https://doi.org/10.1111/nph.17093

235. Yang, X., Wang, B., Chen, L., Li, P., & Cao, C. (2019). The different influences of drought stress at the flowering stage on rice physiological traits, grain yield, and quality. Scientific Reports, 9(1). https://doi.org/10.1038/s41598-019-40161-0

236. Zadoks, J., Chang, T., & Konzak, C. (1974). A decimal growth code for the growth stages of cereals. Weed Research, 14(14), 415–421.

237. Zhang, Jing, Zhang, Y. yan, Song, N. yuan, Chen, Q. li, Sun, H. zheng, Peng, T., Huang, S., & Zhao, Q. zhi. (2021). Response of grain-filling rate and grain quality of mid-season indica rice to nitrogen application. Journal of Integrative Agriculture, 20(6), 1465–1473. https://doi.org/10.1016/S2095-3119(20)63311-1

238. Zhang, Jinmeng, Zhang, S., Cheng, M., Jiang, H., Zhang, X., Peng, C., Lu, X., Zhang, M., & Jin, J. (2018). Effect of drought on agronomic traits of rice and wheat: A meta-analysis. International Journal of Environmental Research and Public Health, 15(5), 839. https://doi.org/10.3390/ijerph15050839

239. Zhong, W., Yunjie, G., Gang, C., Fei, X., & Yunxiang, L. (2003). Rice quality and its affecting factors. Molecular Plant Breeding.1(2), 231—241. http://europepmc.org/abstract/CBA/482215

240. Zhou M.X. (2009) Barley Production and Consumption. Genetics and Improvement of Barley Malt Quality. Advanced Topics in Science and Technology in China. Springer, Berlin, Heidelberg, Germany. https://doi.org/10.1007/978-3-642-01279-2_1